Rates of natural climate change : a study of speleothems

Thesis

Rates of Natural Climate Change – A Study of Speleothems

A thesis submitted for the degree of Doctor of Philosophy

Stephen E.J. Swabey
M.A. (Oxon.)

Department of Earth Sciences
The Open University

October 1996

BRITISH LIBRARY

IMAGING SERVICES NORTH

Boston Spa, Wetherby
West Yorkshire, LS23 7BQ
www.bl.uk

NO CD/DVD ATTACHED

PLEASE APPLY TO THE UNIVERSITY

MISSING PAGE/PAGES HAVE NO CONTENT

Abstract

Speleothems (cave calcite) provide many different proxy indicators for palaeoclimatic changes during the Quaternary era. Generally, the occurrence of growing speleothems is a strong proxy for global palaeoclimate, both geographically and through time. A database of speleothem U-Th ages shows some evidence for an early transition from the penultimate glacial to the last interglacial at ~140 Ka BP. The database suggests an age of 63 Ka BP for the maximum cold period within isotope stage 4. Isotope stage 3 contains three periods of increased number of growing speleothems, at 40, 50 and 56 Ka BP mainly in low latitude caves. The start of growth, growth rate, oxygen isotopes, carbon isotopes and luminescence intensity in two speleothems from southern Ireland provide high-resolution records of rapid palaeoclimate changes in that region during the Late Glacial. Several of these palaeoclimate proxies appear to be linked. The Younger Dryas (YD) cold event is dated at between 12.5 and 11.4 Ka BP in both speleothem records. The dominant agent of palaeoclimatic variation during the YD is probably changes in North Atlantic ocean circulation. A Microsoft Excel spreadsheet is developed as a means of rapidly converting between ^{14}C and calendar years and *vice versa*.

Table of Contents

List of Equations

List of Tables

List of Figures

Chapter 1: Introduction

Palaeoclimatology is concerned with the nature of climate change in the geological past. Palaeoclimate change is of great interest to many other sciences as climate affects many different Earth systems, from the weathering of continental sediments (Büdel, 1982) to the adaptation of species to their environment (Darwin, 1859). The climate of the Earth has varied enormously from the Pre-Cambrian to the present. Indeed, our present climate cannot be considered 'normal' at all (Nairn, 1961). If our present climate is not 'normal', in the future climatic changes must be expected as a matter of course, whether due to natural or human influences. Some baseline data is required to anticipate what magnitude and rate of change should be expected during either natural or human-induced climate change. Currently, the only reliable data available is palaeoclimate change due to natural causes. Examined here are some of the most recent palaeoclimate changes with large magnitude and high rates of change – rates which may be similar to those expected in the future. These changes took place during the period of geological time known as the Quaternary.

1.1. The Quaternary Period

The Quaternary is the period of geological time immediately following the Pliocene and is divided into Pleistocene and Recent epochs. The lower boundary of the Quaternary is placed at approximately 1.65 Ma (million years before present) (Haq *et al.*, 1977), although it is increasingly clear that this is an arbitrary boundary (Kukla, 1989). The Quaternary is also the period when the first example of the genus Homo (humans) becomes widespread in the archaeological record (McDermott *et al.*, 1993; Roberts *et al.*, 1994), although hominids are also known from the Pliocene (Clarke and Tobias, 1995; White *et al.*, 1994). Another characteristic of the Quaternary is long periods of cold global climate – the 'ice ages', interrupted by short-lived, warm 'interglacial' conditions similar to today's climate. The brief interglacial periods which interrupt the ice ages (figure 1.7) recur in the geological past as far back as 2.5 million years (Kukla, 1989). During the Pleistocene the Earth has been subject to a number of ice ages, the last glacial maximum (LGM) occurring just 18,000 years before present (BP) (Broecker *et al.*, 1988). In the Recent (or Holocene) period following the LGM, global climate conditions have been relatively stable in comparison to the last complete interglacial–glacial cycle (130,000 years). The difference in mean temperature between the maximum cold of the LGM and the Holocene was up to 15°C at high latitudes (Cuffey *et al.*, 1995) and 4°C - 6°C at mid- to low latitudes (Broecker and Denton, 1989; Stute *et al.*, 1995). The primary cause of the recurrent ice ages is variations in the amount and distribution of solar radiation received at the Earth's surface through time – the Milankovitch variations in orbital paramaters (Berger, 1988).

1.2. Milankovitch variations

Perturbations in the Earth's orbit around the sun are caused by the gravitational effects of other planets in our solar system (Berger, 1988). Through these perturbations the amount of solar radiation received at the Earth's outer atmosphere varies through time (figure 1.1 & 1.2). The history of the study of these perturbations is a long one. The importance of orbital precession of the equinoxes to the volume of ice present on the Earth was first suggested by (Adhémar, 1842). James Croll extended this hypothesis to include other variations in Earth's orbital parameters (Croll, 1875). This work was expanded on by the Serbian mathematician Milankovitch (Milankovitch, 1941).

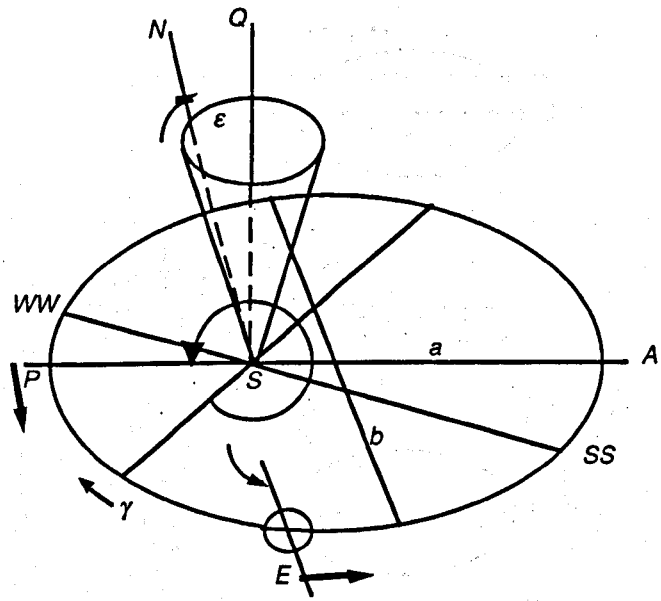

Figure 1.1. Elements of the Earth's orbit. The orbit of the Earth, E, around the sun, S, is represented by the ellipse PγEA with P the perihelion (closest approch of Earth to the sun during a calender year) and A the aphelion (furthest orbital approach). WW and SS are the winter and summer solstices, respectively. γ is the vernal equinox and WW, SS and γ are located at their present day position. SQ is perpendicular to the ecliptic, and the obliquity, ε, is the inclination of the equator on the ecliptic. Figure 8 from Berger (1988).

Milankovitch placed precise figures on the recurrence intervals of the orbital perturbations. There are many periods associated with each of the several orbital perturbations:

i) *Variations in the distance between Earth and the sun during the solar year, or eccentricity of the Earth's orbit.* The value of orbital eccentricity (e) is defined in equation 1.1.

$$e = \frac{\sqrt{(a^2 - b^2)}}{a}$$

Equation 1.1. The value of e (eccentricity of the Earth's orbit). a is the length of the semi-major axis and b the length of the semi-minor axis of the orbital plane (figure 1.1).

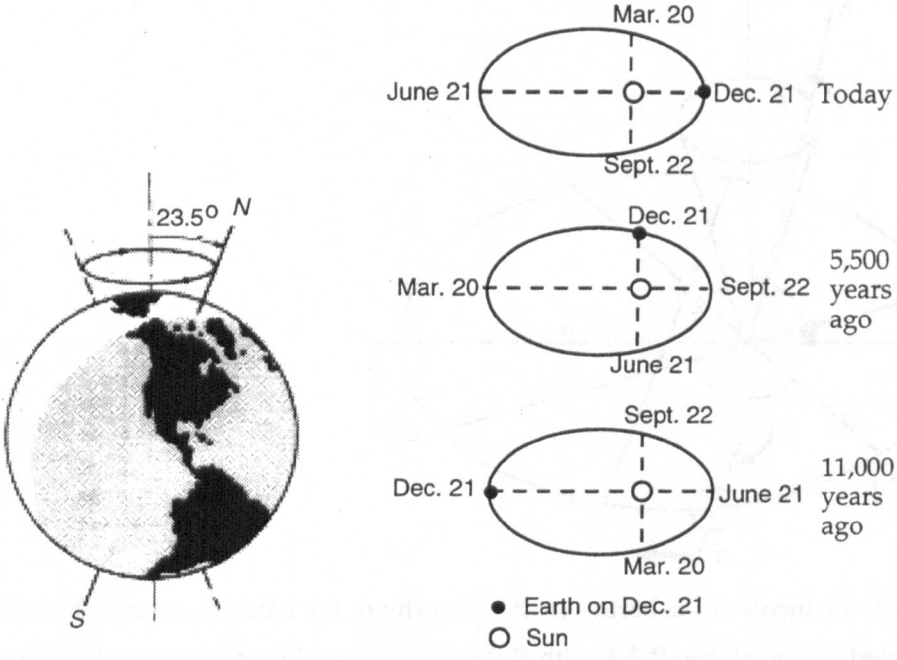

Figure 1.2. The orbit of the Earth round the sun showing the obliquity of axial tilt (on left) and the precession of the equinoxes (on right). The present orbital configuration is shown at the top on the right, with perihelion occuring during the northern hemisphere winter and aphelion during southern hemisphere winter. The situation 5,500 yrs BP is at central right and the situation 11,000 yrs BP at bottom right, from Imbrie and Imbrie (1979).

The calculated value of *e* varies between 0 and 0.0607. The present value of *e* is 0.016 (Berger, 1988) and at present the Earth is 4.8 million km closer to the sun in perihelion than in aphelion (figure 1.2) (Barry and Chorley, 1987). The average quasi-period for a full cycle of values of *e* is 94,945 years (Berger, 1988). When *e* is large, insolation is received in varying amounts depending on the season – the value of *e* reflects the seasonality of total solar radiation received at the Earth's surface. The time of year at which Earth receives the maximum insolation (perihelion) varies through this cycle (see point iii) below). This is the only orbital perturbation that alters the total amount of solar radiation received during the year, although the variation is only 0.2% of the total annual insolation (Berger, 1988).

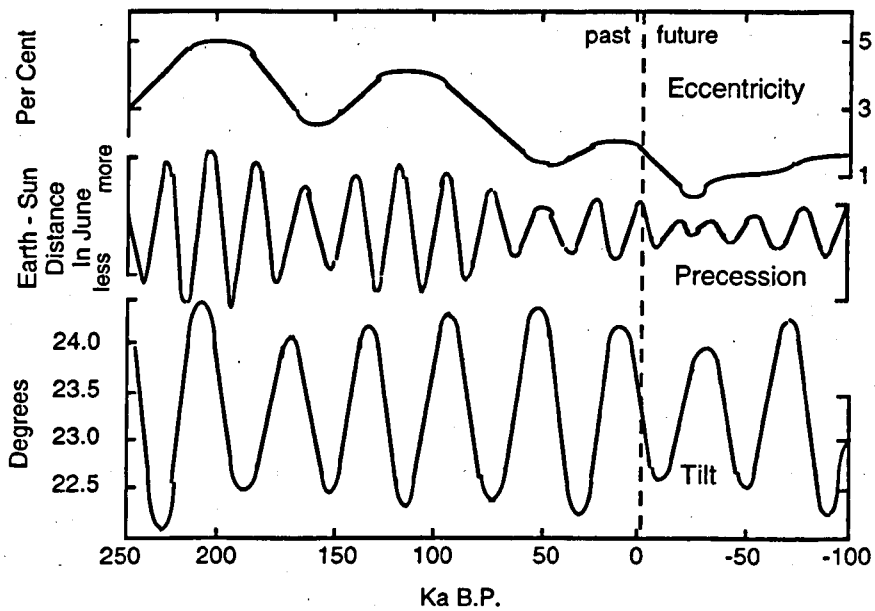

Figure 1.3. Long-term variations of Earth orbital eccentricity, precession, and obliquity of axis (tilt) from 250 Ka BP to 100 Ka AP (after present). Fig. 11 from Berger (1988).

ii) *The obliquity of axial tilt of the Earth away from a position perpendicular to the elliptic through time.* At the moment the Earth is tilted towards the sun at an angle of 23.27° (Berger, 1988), but in the past 5 million years this angle has varied between 22° and 24.5° (figure 1.3,

bottom curve) with a mean of 23.30° (Laskar and Robutel, 1993). The most important period of this orbital variation is 41,000 years. A second period of 39,730 years is also observed with an amplitude approximately one third of the 41,000 year period (Berger, 1988). Seasonal variations in solar insolation are stronger when the Earth's axial tilt is high than during periods of low axial tilt. The Earth's climate systems are sensitive to Milankovitch forcing partly because the geographical position at which solar radiation is received affects Earth climate due to the differing albedo of land, sea and ice (Berger, 1990).

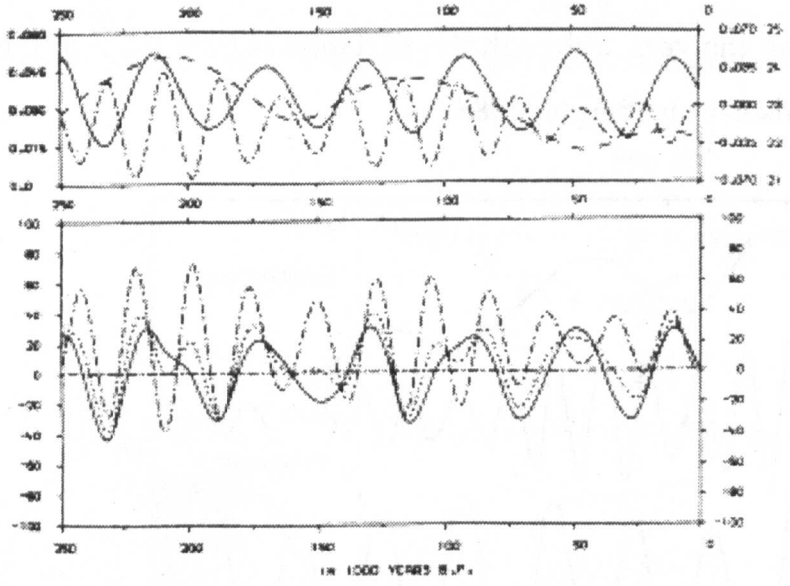

Figure 1.4. Variation of orbital parameters over the last 250,000 years Eccentricity (– – – –), precession (– · – · –) and obliquity (———) (upper diagram) and northern hemisphere summer solar radiation at 80 (———), 65 (·····) and 10°N (– · – · –) latitude (expressed as departures from 1950 values) (lower diagram). The radiation signal at high latitudes (80°N curve) is dominated by the ~41,000 year obliquity cycle (solid line) while the ~23,000 year precessional cycle (pecked and dotted line) is dominant at lower latitudes (10°N curve) (Bradley, 1985).

iii) *The time of perihelion measures the time of year at which the Earth is in perihelion.* At present the Earth is closest to the sun at the northern hemisphere winter solstice, but in the past closest approach has been at any time of the calender year. The dominant period for

precession of the equinoxes (full cycle from northern hemisphere perihelion at midsummer to southern hemisphere perihelion at midsummer and back again) has a recurrence interval of 23,716 years with the next most important quasi-period being 22,428 years (Berger, 1988).

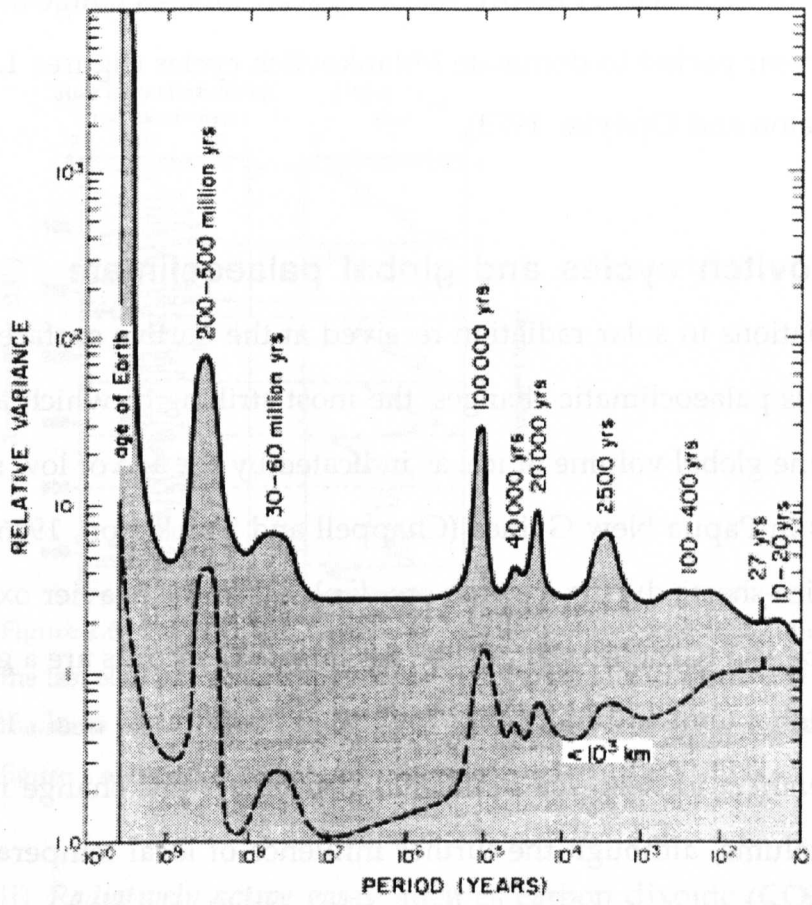

Figure 1.5. Estimate of the relative variance of climate from the age of the Earth to a decade. The Milankovitch orbital variations appear as the central three peak of relative variance, with their multiple-periods averaged, from (Bradley (1985).

Together the Milankovitch orbital variations (figure 1.5) cause the total amount of solar radiation received at the Earth's surface to vary by 0.2% (due to changes in eccentricity – top curve, figure 1.3). The relative importance of the various Milankovitch variations in solar radiation received varies according to location on the Earth. At high latitudes the obliquity (~41,000 year) cycle dominates the solar radiation signal

whilst at lower latitudes the precession (~23,000 year) cycle is more important (figure 1.4) (Berger, 1978).

Although all Milankovitch insolation variations have effects on global palaeoclimate, palaeoclimatic records show that the small variation in total insolation received (*e*) is sufficient to 'pace' climate change and for the 100,000 year period to dominate Milankovitch cycles (figures 1.5 & 1.7) (Shackleton and Opdyke, 1973).

1.3. Milankovitch cycles and global palaeoclimate

Long-term variations in solar radiation received at the Earth's surface cause various palaeoclimatic changes, the most striking of which are changes in the global volume of ice, as indicated by the age of low sea-level stands in Papua New Guinea (Chappell and Shackleton, 1986). Expanding ice-sheets during ice ages are depleted in the heavier oxygen stable isotope ^{18}O (Grootes *et al.*, 1993). Ice core $\delta^{18}O$ records are a good proxy for global temperature change for this reason (Jouzel *et al.*, 1987). Fossil *foraminifera* in deep-sea sediments also reflect this change in global ice volume, although the further influence of local temperature on the $\delta^{18}O$ of *foraminifera* means the relationship between *foraminifera* $\delta^{18}O$ and ice volume is difficult to interpret (Emiliani, 1955).

The Earth's climate systems do not respond in a linear manner to insolation forcing (figure 1.6). Increases in global ice volume (reflected by $\delta^{18}O$ records in deep-sea cores) generally proceed slowly and melt events occur rapidly, usually at the end of a long period of cold conditions (figure 1.7). These non-linear responses are the result of feedback systems in the distribution of received solar energy to the

Earth's climate system. These non-linear responses are the result of feedback systems in the distribution of received solar energy to the Earth's climate system. These feedbacks are complicated and a full examination is beyond the scope of this discussion, but they include:

i) *Changes in deep ocean circulation* which affect the distribution of energy around the globe (Weaver and Hughes, 1994).

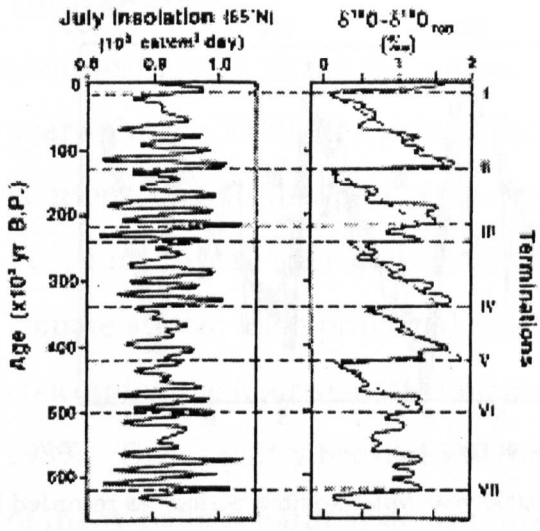

Figure 1.6. Left section- Long-term variations of July mid-month insolation at 65°N for the last 600,000 years. Right section- Long-term $\delta^{18}O$ variations in deep-sea cores over the same period. The 'terminations' marked are the end of individual ice ages. From figure 1 of Broecker & Denton (1990).

ii) *Radiatively active gases*, such as carbon dixoide (CO_2) and methane (CH_4), which affect the total amount of solar energy which is retained by the Earth's atmosphere (the Greenhouse effect) (Barnola *et al.*, 1987; Berger *et al.*, 1993).

iii) *Physical effects of ice sheets*, including *ice albedo feedbacks* (Sirocko *et al.*, 1993), because ice sheets reflect a greater amount of received insolation than other types of land cover; and *isostastic response*, because bedrock responds slowly to change in ice sheet volumes (Pollard, 1982).

Berger (1988) estimated that 60 ± 10% of palaeoclimatic change in the 10–100 kyr (thousand years) range was due to linear astronomical forcing, implying 40 ± 10% of palaeoclimatic change was a result of non-linear feedbacks within the Earth–atmosphere system. Given the influence of the presence of ice on climate systems, one of the main feedbacks is changes in the total volume of ice on the Earth.

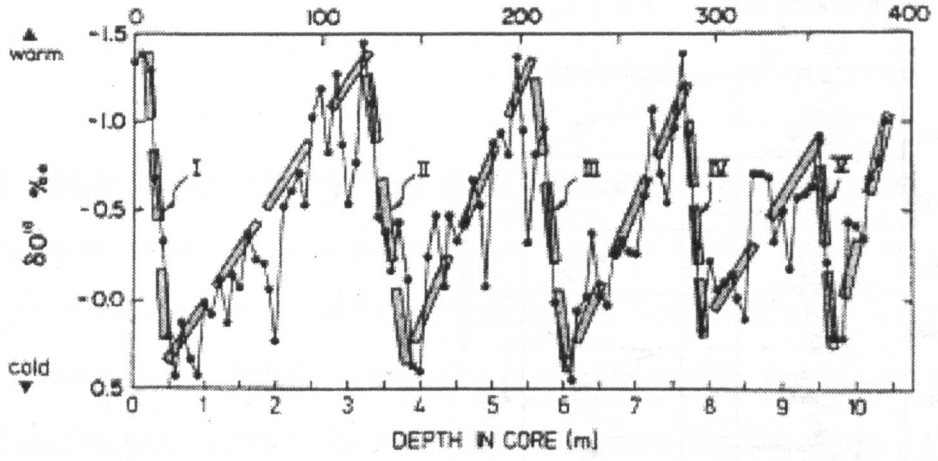

Figure 1.7. Five full cycles of the ~100,000 year Milankovitch periods as recorded by $\delta^{18}O$ in deep-sea cores. Note the general saw-tooth shape of the curve which reflects slow cooling and fast warming present in all these ~100,000 year cycles. The warm periods which punctuate each ~100,000 year cycle are caused either by other periods in the Milankovitch orbital variations or sub-Milankovitch palaeoclimate variations. Figure from Seibold and Berger (1982).

Various strands of geological evidence show that cooling towards maximum cold periods (ice ages) is slow and punctuated by short periods of warmer climate, although warming is rapid following the maximum cold of the 'ice-age' (figure 1.7). Cooling as a result of Milankovitch variations increases the volume of the Earth's water frozen into ice caps (Broecker and van Donk, 1970). Large masses of ice act as thermal sinks and their size means they are able to persist during periods of increased insolation. Increased insolation eventually passes a threshold when the thermal inertia of the large ice masses is

overcome and net ice ablation begins. Once melting is initiated, large volumes of meltwater and thermal expansion of the oceans create a positive feedback where rising sea-levels assist in the break up of ocean-marginal ice sheets (Peltier, 1988).

1.4. Palaeoclimate change on sub-Milankovitch timescales

The shortest period in the main Milankovitch variations is close to 19,000 years (Berger, 1980). If a palaeoclimate change occurs on a timescale shorter than half that period, it may be considered as sub-Milankovitch in nature. These short-term, sub-Milankovitch responses of the Earth's climate system have provoked much debate in Quaternary science concerning the operation of climatic feedbacks (CLIMAP, 1976; Ghil, 1989). This is partly because non-linear response is a common feature of many natural Earth systems (Lovelock, 1979) and elucidating the causes of sub-Milankovitch climate changes may assist us in examining aspects of future climate change. A particular concern has been the period since the most recent ice-age, or Last Glacial Maximum (LGM).

The significance of the LGM is that it lies at the time when humans began to develop complex social structures and move from being controlled by the environment to a position of adapting and even controlling the local environment (Goudie, 1981). It has been argued that a stimulus for these innovations may have been the need to adapt to the severe palaeoclimate changes which took place during the place during the deglaciation of the LGM (Sauer, 1956).

Today human society exists within the latest warm period of the continuing Milankovitch cycles (figure 1.6). If human society in the

past was forced into a period of exceptional innovation (Sauer, 1956) and even evolutionally selected by ancient climate changes (Potts, 1996), the possibility of future natural climate change (Dickinson and Cicerone, 1986) must also concern us, particularly as our population is now vastly inflated by comparison with palaeolithic society (Goudie, 1981) (figure 1.8). Astronomically-forced climate change is not of immediate concern to our society because our time-frame of reference does not extend to the length of Milankovitch cycles. However, future climate change due to human influence on global systems is becoming increasingly important for two reasons: 1) The driving mechanism (population) is increasing in size (figure 1.8); and 2) The ability of population to influence the climate system through industrial change is also increasing. This influence takes the form of production of gases that increase the greenhouse effect (Manabe and Stouffer, 1993; Nisbet, 1992) , such as carbon dioxide (CO_2), methane (CH_4), ozone (O_3) and chlorofluorocarbons (Dickinson and Cicerone, 1986). Of particular concern has been the estimated rate of anthropogenically forced climate change, which has been predicted to increase global temperature by between 1°C and >5°C by the year 2050 (Dickinson and Cicerone, 1986). An important aspect of this future climate change is that it may be difficult to predict local expression of general global changes (Crowley, 1989). However, despite some concern that all climate change is necessarily detrimental, there is the possibility that future climate change may benefit human society. For example, palaeoclimate records indicate that in the past Saharan Africa was less arid than the present day (Rognon, 1987; Rossignol-Strick, 1982).

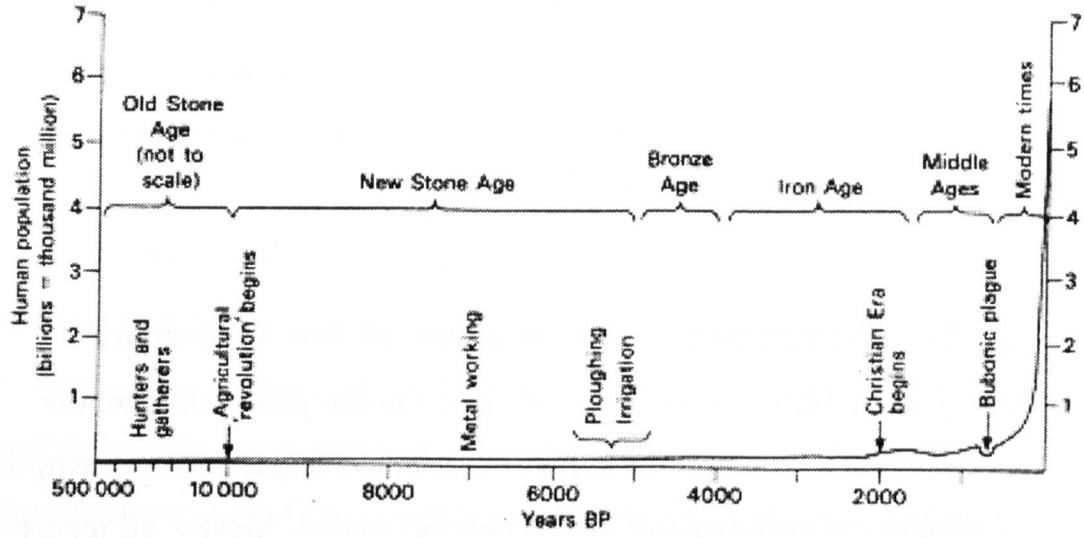

Figure 1.8. Estimated global population from 500,000 years ago to the present day. Figure from Goudie (1981).

In the recent geological past humans have successfully adapted (Allen and Anderson, 1993; Goede *et al.*, 1978) to rapid natural changes in global climate (Hughen *et al.*, 1996; Lehman and Keigwin, 1992). Certain of these palaeoclimate changes occur on sub-Milankovitch timescales and may therefore provide some indication of the results of future anthropogenic climate change. These rapid palaeoclimatic changes may provide a suitable model for the nature of future changes in climate. To appreciate the nature of these climate changes it is preferable to examine one well-documented palaeoclimatic event. The rationale for the choice of the palaeoclimatic event selected for detailed study (the Younger Dryas) is presented in the following sections.

1.5. The Quaternary in the geological record

The nature of the geological record is such that the more ancient geological events often leave less evidence from which to reconstruct the conditions of that environment. The Quaternary is no exception. Most work in Quaternary science has concentrated on the last Glacial and

palaeoenviornmental changes associated with the transition from that Glacial to the present Interglacial. As this work concentrates on palaeoclimate changes of the Late Glacial, some terminological definitions are required.

1.5.1. Stratigraphic nomenclature of the Quaternary

In any comparative examination of Late Glacial palaeoclimate it is desirable to compare local palaeoclimatic changes with contemporary changes in regional and global palaeoclimates. Ideally, all reporting of palaeoclimatic changes would be in years to a common absolute sidereal timescale. However, there are few palaeoclimatic records that are dated with sufficient accuracy to satisfy this condition and the majority of published records are based on radiocarbon chronologies, which are not sidereal in nature. In addition, the regional nature of palaeoclimatic change as expressed in reconstructions from palaeoclimatic proxies, together with a tendency towards self-contained national research groups has meant that a variety of regional and national chronological frameworks have been developed around the world. The stratigraphic subdivisions employed are also determined by the nature of the topic of interest. Thus, chronostratigraphy examines stratigraphic units according to age, but lithostratigraphy classifies local sediment units or rock successions according to lithology, whilst biostratigraphy examines changes in fossil content and morphostratigraphy looks at the relative ages of landforms (Dawson, 1992). This wide variety of chronological schemes makes inter-regional palaeoclimatic comparisons difficult without some overarching chronological framework. One widely-accepted scheme used for global palaeoclimate comparison is the oxygen isotope stages derived from deep-sea core studies (Martinson *et al.*, 1987). However, the isotope

stage system is insufficiently detailed to distinguish between short-lived events during the Late Glacial. Because this chapter will examine palaeoclimate change in several regions of the globe, an alternative comparative framework to which the reader may refer is provided here. As this thesis describes work in Ireland, the framework described here will concentrate on chronostratigraphic divisions in that country. However, the terminology employed in describing Late Glacial events will follow the more detailed chronostratigraphic description of the Scandanavian Late Glacial, since insufficient detail exists in currently-published Irish chronostratigraphies to describe adequately all features of the present work, and two speleothem palaeoclimate records form an inadequate base for the definition of new Irish chronostratigraphic divisions. For completeness, some reference will be made to major events in European chronologies. As the scope of this work does not extend before the penultimate glaciation, the framework will be restricted to the last 20,000 years of time.

Chronostratigraphical subdivison of the Quaternary has proceeded at two levels, with cooler and warmer periods typically given one set of adjectival descriptions, whilst the actual glaciations are given a further set of names. Thus, the Devensian Stage is a cool period of the English Pleistocene containing the Dimlington glacial event (table 1.1). In Ireland the equivalent terms are the Midlandian Stage and Glenavy glacial event (Bowen *et al.*, 1986), although there is some discussion over the use of terms such as the Fenitian Stage for the same period (Warren, 1985).

Several attempts have been made to provide a definitive relationship between the different types of chronologies of various countries and

regions. The last glacial-interglacial transition in NW Europe is traditionally divided into the Oldest Dryas-, Bølling-, Older Dryas-, Allerød-, Younger Dryas-, and Preboreal (Mangerud *et al.*, 1974; Wohlfarth, 1996) on a chronostratigraphic basis. These terms have some local equivalents in the British Isles, and it is desirable to examine the relationship between the main (originally Scandanavian) NW European terms and their local equivalents.

Climate period	Event	British name	European name		Stage
Littletonian		Flandrian	Holocene	W	1
	Nahanaghan	Loch Lomond	Younger Dryas	S	
	Woodgrange	Windermere	Bølling-Allerød	IS	
	Glenavy	Dimlington	Weichselian	S	
Midlandian		Devensian	Weichselian	C	2

Table 1.1. Irish palaeoclimate stages and glacial events with British and European equivalents. W denotes a warm period; C cool period; IS, interstadial; S, stadial.

The precise timing of these supposedly equivalent periods of time is the subject of much discussion in the literature. Argument centres around the precision of ages used to distinguish the boundaries of events in various regions and the global or regional nature of certain (less-marked) palaeoclimatic changes (Wohlfarth, 1996). The majority of age determinations on palaeoecological samples are performed using radiocarbon techniques, which are subject to several uncertainties in measurement and interpretation (Bard, 1988; Bard *et al.*, 1993). The less-marked palaeoclimate events which are not recorded in all locations include short-lived changes such as the Older Dryas (200 years), which is experienced in Scotland (Gray and Lowe, 1977) , but not apparently seen in Ireland, and weak palaeoclimate signals like the

Intra-Allerød (Walker *et al.*, 1991) and Preboreal (also known as YDII) oscillations (Koç Karpuz and Jansen, 1992).

1.5.2 The Last Glacial Maximum

In the geological record of the Quaternary, the deposits of the Last Glacial Maximum (LGM) provide far more evidence for the nature of astronomically-forced palaeoclimate change than any earlier ice age. This is due to the unconsolidated nature of the majority of Quaternary sediments and the fact that subsequent glaciations tend to remove physical evidence for their predecessors. For this reason the LGM is the best studied of all Quaternary glaciations. LGM sediments are also the most superficial of recent Quaternary glaciations and are more physically accessible for that reason.

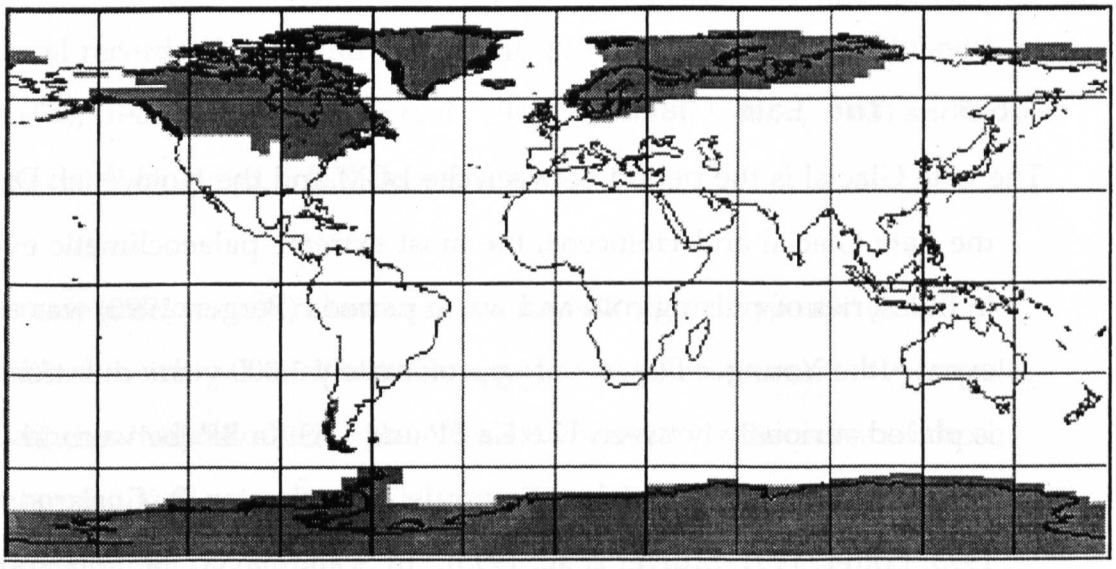

Figure 1.9. Global ice sheets 18,000 years ago reconstructed using various proxies, including pollen, glacial and fluvoglacial deposits (CLIMAP, 1976).

The LGM represents a global cooling from the level of the interglacials of an average 6°C (Broecker and Denton, 1990) with the most severe cooling experienced in the northern hemisphere continents of Europe and North America at higher latitudes (Cuffey *et al.*, 1995). Here the ice

sheets advanced southwards to cover large areas of the continental land mass (figure 1.9). On average, sea levels were 120 m lower during the LGM (Chappell and Shackleton, 1986) due to the large volume of water locked up in ice sheets. At 21 Ka BP (thousand years Before Present) the global ice sheets were at their maximum extent. Shortly after this time a very rapid melting of global ice sheets took place, with the majority of the melting complete by 18 Ka BP (Stein *et al.*, 1994). These palaeoclimate events are predicted by Milankovitch theory and as such do not provide a good test of hypotheses for rates of sub-Milankovitch palaeoclimate change. This significant melt event was followed by a series of warm and cool periods during the Late Glacial (Walker *et al.*, 1994) before more stable warm conditions, with moderate climatic oscillations prevailed after 11.5 Ka BP (Feng and Epstein, 1994; Sejrup *et al.*, 1995).

1.5.3 The Late Glacial

The Late Glacial is the period between the LGM and the Holocene. During the Late Glacial and Holocene, the most extreme palaeoclimatic event in this series of pulsing cold and warm periods (Berger, 1990) was a cold event – the Younger Dryas – of approximately 1,000 years duration that is placed variously between 12.8 Ka BP and 11.3 Ka BP (between 11.0 and 10.0 Ka BP on the radiocarbon timescale – see chapter 5) (Goslar *et al.*, 1993; Lotter, 1991; Stuiver *et al.*, 1995). In Scandinavia, the appearance of the tundra plant, *Dryas octopetela* in pollen records of this age indicates a return to cold conditions (Jensen, 1938), and it is for this plant that the period is named (Peteet, 1995).

1.5.4. The Younger Dryas

The Younger Dryas (YD) cold event is an intriguing global palaeoclimate event because it is not predicted by Milankovitch astronomical theory (Broecker and Denton, 1990), but appears to be due to some other forcing of global palaeoclimate. Evidence for the YD is found in many different locations across the world, including New Zealand (Denton and Hendy, 1994), Australia (Dodson, 1977), North America (Mathewes, 1993), South America (Kuhry *et al.*, 1993), North Africa (Rognon, 1987; Rossignol-Strick, 1982), sub-Saharan Africa (Roberts *et al.*, 1993), the tropical Atlantic (Hughen *et al.*, 1996) and the Pacific (Kennett and Ingram, 1995). However, the strongest evidence for the YD is found in North European records, where an average cooling of 8°C and maximum cooling of 15°C is inferred (Berger, 1990). Evidence for the YD in Europe comes from many palaeoclimate proxies, including sea-level records (Bjorck and Digerfeldt, 1991), pollen (Smith and Goddard, 1991), tree-rings (Oeschger *et al.*, 1980), glacial (Lawson, 1983) and fluvo-glacial (Mangerud, 1987) deposits.

The main concern when examining a non-standard response (sub-Milankovitch palaeoclimate changes) of a system governed by regular features (Milankovitch palaeoclimate changes), is the cause of those non-standard responses. There are several hypotheses for the primary cause of the YD:

i) *Solar insolation.* The YD cold period was a result of short-term (non-Milankovitch) variations in insolation received by the Earth as a result of events such as sunspots (Denton and Karlén, 1973).

ii) *Iceberg calving.* The YD event resulted from an influx of tabular icebergs calving from Arctic ice shelves around the wasting Scandinavian and Siberian ice sheets during the warming after 18 Ka

BP (Mercer, 1969) (figures 1.10, 1.11 and 1.12). This notion may also involve iceberg swarms from surging land-based ice sheets (Andrews and Tedesco, 1992). The episodic presence of large volumes of icebergs in the North Atlantic – occasions known as Heinrich events (Heinrich, 1988) – would have altered oceanic (Broecker, 1994) and atmospheric circulation (Kotilaninen and Shackleton, 1995). In the figures reproduced from (Ruddiman and McIntyre, 1981) the boundary marked as "Polar Front" marks the division between 'polar' and 'non-polar' oceanic water masses. However, the boundary between atmospheric polar air and mid-latitude air (the polar front) was probably also pushed southwards by the presence of the ice (Kotilaninen and Shackleton, 1995).

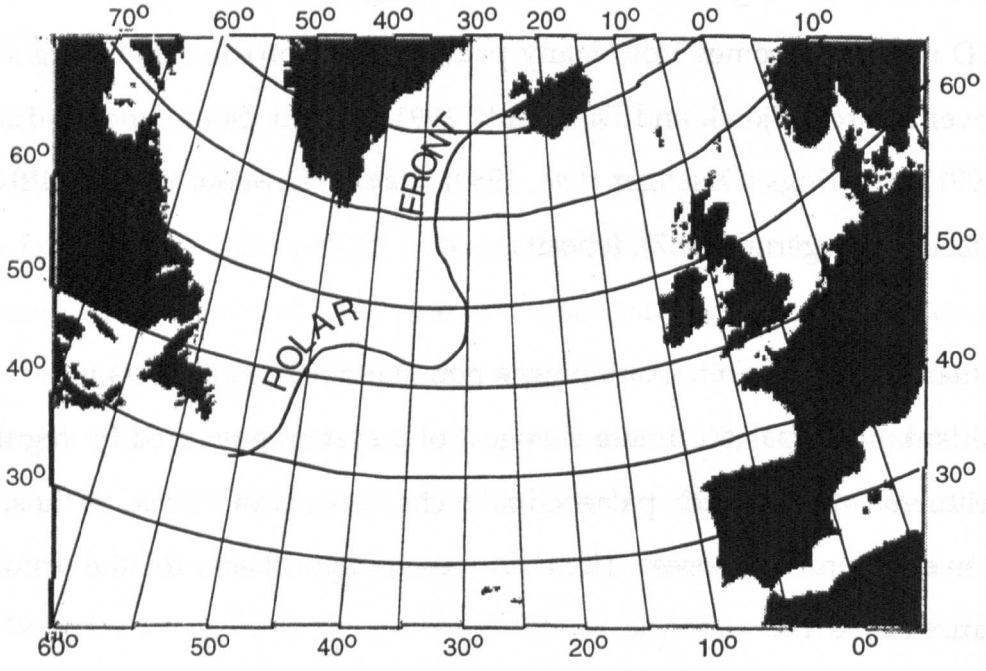

Figure 1.10. Inferred position of the boundary between polar ocean masses and non-polar ocean masses, which probably also marks the division between polar and temperate air in the atmospheric circulation (polar front) in the North Atlantic between 13.0 ^{14}C Ka BP and 11.0 ^{14}C Ka BP (Ka BP – Ka BP). The polar front position is based on the boundary between high and low $CaCO_3$ in deep-sea cores. Dashes indicate a strong thermal gradient in front of the polar front. (Figures 1.10, 1.11 and 1.12 are figs. 21-23 from Ruddiman and McIntyre (1981)).

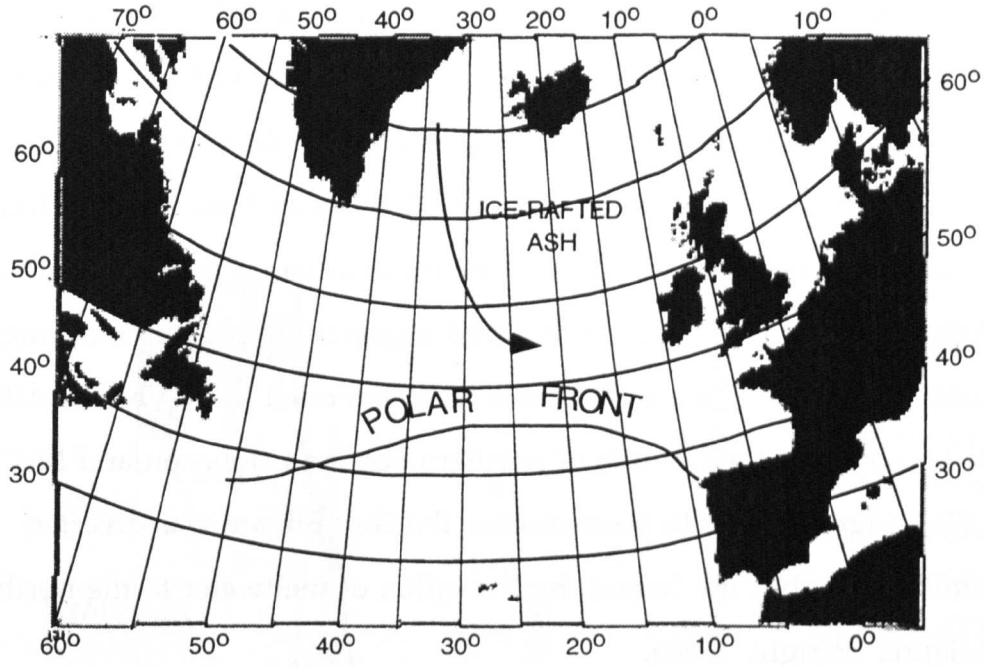

Figure 1.11. North Atlantic polar front during the Younger Dryas (11.0 ^{14}C Ka BP to 10.0 ^{14}C Ka BP, or 12.5 Ka BP to 11.5 Ka BP). The polar front position is based on the boundary between polar and sub-polar planktonic foraminifera. The large arrow marks the path of ash-bearing icebergs at the young boundary of the YD.

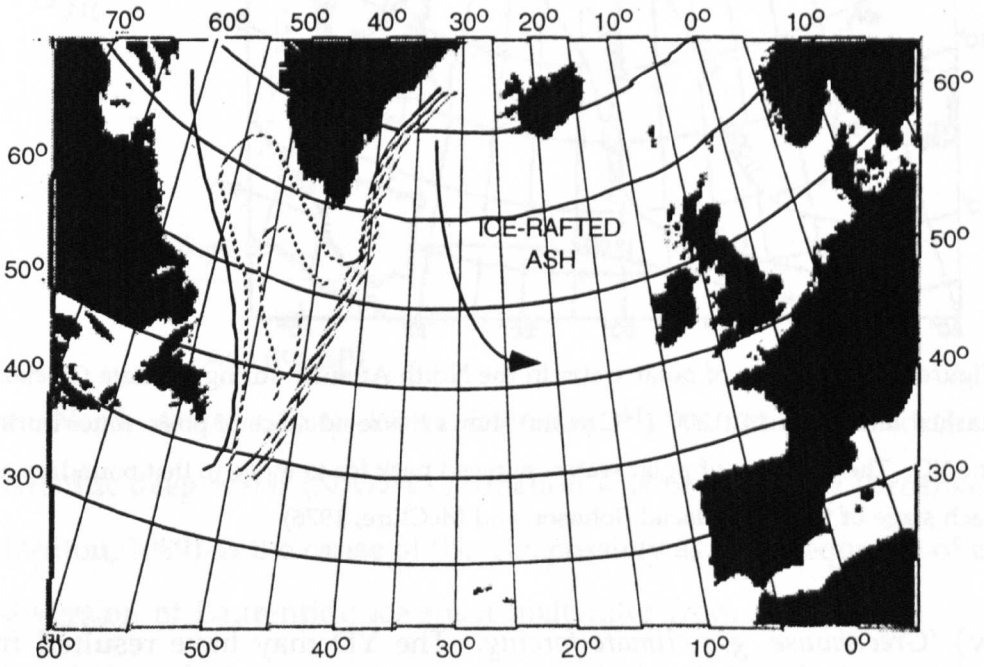

Figure 1.12. North Atlantic polar front during the period following the YD (the Boreal) from 11.0 ^{14}C Ka BP to 9.0 ^{14}C Ka BP. The oceanic polar front position is based on the boundary between moderate foraminiferal productivity and high coccolith productivity levels north-west of the marked polar front and lower levels south-east of the front (Ruddiman and McIntyre, 1981).

iii) *Refreezing of glacial meltwater.* A further hypothesis suggests that commencing around 12.5 Ka BP increased volumes of glacial meltwater from glacial Lake Agassiz draining into the northern Atlantic through the Gulf of St. Lawrence (Bryson *et al.*, 1969) may have lowered local Atlantic salinity and permitted pack-ice to advance into the northern Atlantic. This ice may have lowered regional temperatures during the time of the YD. The pack-ice may have extended in the central Atlantic as far south as the latitude of northern Scotland (Johnson and McClure, 1976) (figure 1.13). In these models the Gulf Stream was diverted southwards (but not halted) by the influx of meltwater to the northern Atlantic (Wright, 1989).

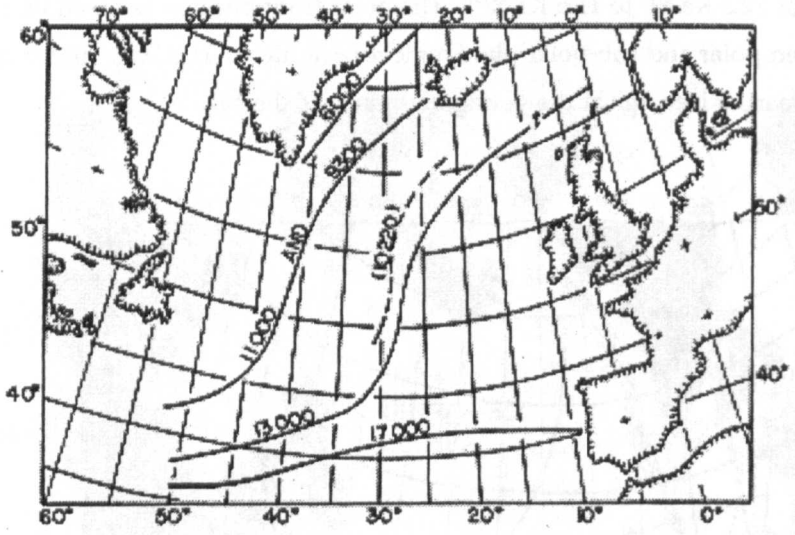

Figure 1.13. Position of polar water in the North Atlantic during the Late Glacial. The dashed line labeled '10,200' (^{14}C years) shows the re-advance of polar water during the YD. The presence of polar waters allowed pack ice to move to that boundary at each stage of the Late Glacial (Johnson and McClure, 1976).

iv) *'Greenhouse' gas climate forcing.* The YD may have resulted from a reduction in the atmospheric concentration of 'greenhouse' gases such as CO_2 (Chappellaz *et al.*, 1993) and/or methane (CH_4) (Nisbet, 1992) following rapid growth of plants in the milder climate following the LGM (figure 1.14). Any reduction in concentration of 'greenhouse'

gases would have the effect of reducing the ability of the Earth to retain received solar insolation and may have led to a period of cooler climate.

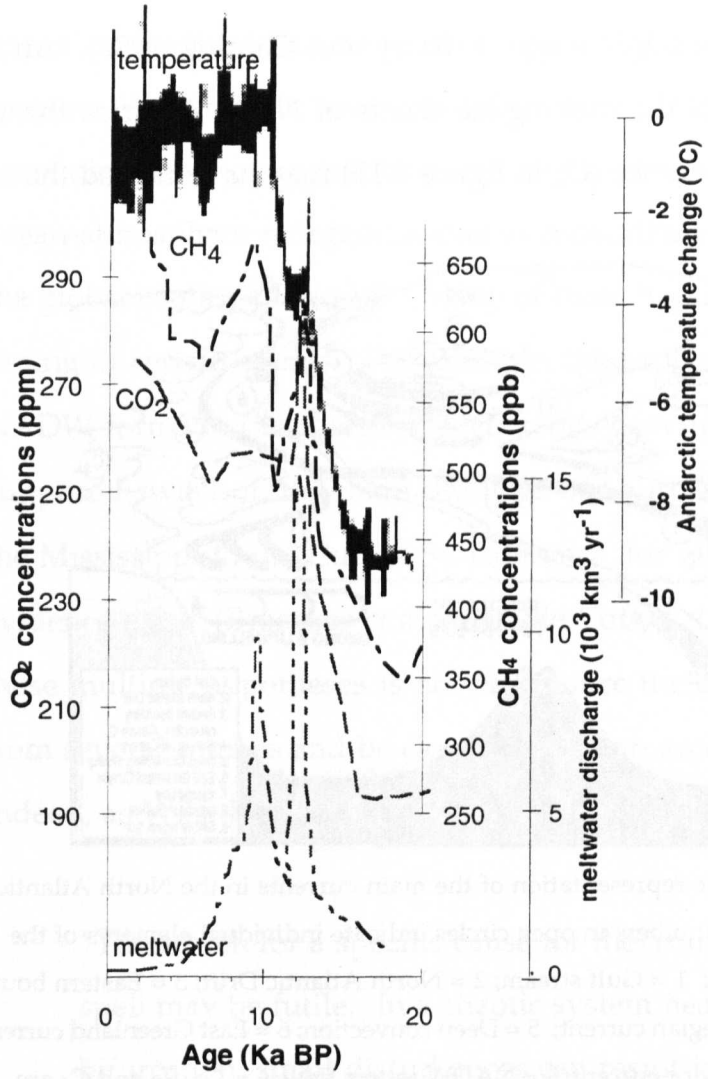

Figure 1.14. Changes in various palaeoclimate proxies at the end of the last glaciation (Nisbet, 1992). Curves are (from bottom): meltwater discharge; CO_2 changes; CH_4 changes; Antarctic temperature at Vostok

v) *North Atlantic Deep Water formation.* A reduction in North Atlantic deep water (NADW) formation was proposed by (Broecker and Denton, 1989) as the cause of the YD, possibly as a consequence of a diversion of Laurentide ice-sheet meltwater from the 'normal' Mississippi drainage route to one through the Gulf of St. Lawrence. At present, the dense salty water of the surface North Atlantic sinks (5 in figure 1.15) to form a south-flowing bottom current, known as NADW return flow (9 in figure 1.15). This sinking water drives the Gulf

Stream (1 in figure 1.15), bringing warm equatorial water to the cold north and making Europe warmer than might be predicted from its latitudinal position. The effect of the Gulf Stream on climate means that the British Isles are some 16°C warmer in winter than the latitudinal average might suggest (Barry and Chorley, 1987). An influx of freshwater from the melting ice sheets of North America through the Gulf of St. Lawrence (C_2 in figure 1.15) may have caused the salinity

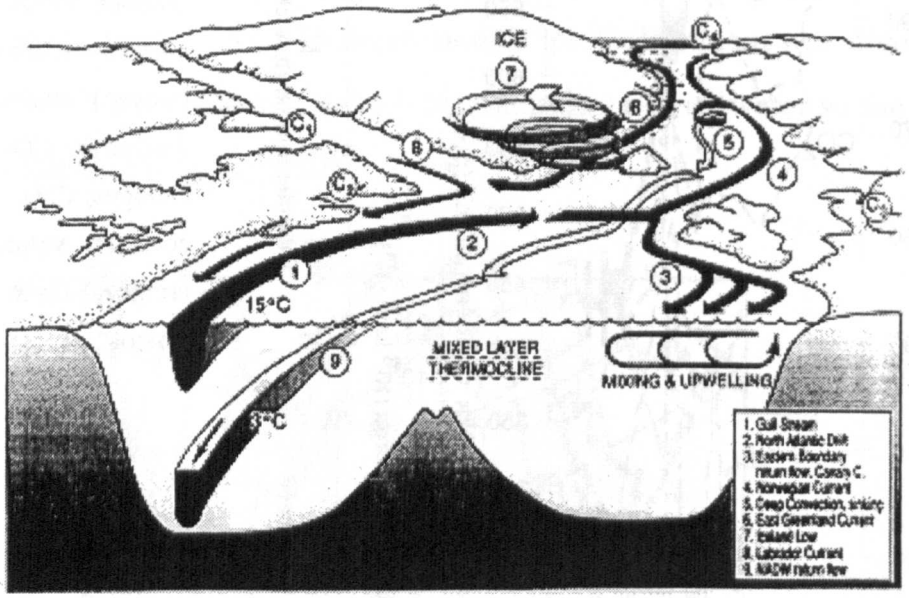

Figure 1.15. Schematic representation of the main currents in the North Atlantic oceanic circulation. Numbers in open circles indicate individual elements of the circulation. These are: 1 = Gulf stream; 2 = North Atlantic Drift; 3 = Eastern boundary return flow; 4 = Norwegian current; 5 = Deep convection; 6 = East Greenland current; 7 = Iceland low; 8 = Labrador current; 9 = NADW return flow; C_1, C_2, C_3 and C_4 are potential points of disruption where meltwater may enter the system (Berger, 1990).

of North Atlantic waters to fall. This reduction of salinity may have slowed NADW formation and reduced the movement of warm water to the northern Atlantic region (Broecker *et al.*, 1990). It has also been suggested that a total shutdown of NADW formation was not required to initiate a 5°C cooling over 10 years (Rahmstorf, 1994). Recent evidence suggests that freshwater exiting through the Gulf of St.

Lawrence was in fact reduced in volume during the YD (de Vernal *et al.*, 1996), and this hypothesis may need reconsideration.

The common feature of all these hypotheses except i) *solar insolation* is an appeal to feedback mechanisms *within* the global ocean-atmosphere system. Variations in solar insolation are external to the Earth, but the remaining theories appeal to purely atmospheric (iv) and coupled ocean-atmosphere reorganizations to redistribute energy and initiate the global cooling of the YD. Many of these hypotheses rely on precise timing of certain events. For example, the proposal that a reduction in NADW formation triggered the YD relies heavily on the timing of a supposed switch in the main drainage of Laurentide meltwater from the Mississippi to the Gulf of St. Lawrence, for which contradictory evidence exists (Broecker *et al.*, 1990; de Vernal *et al.*, 1996). Testing these multiple hypotheses is not easy, since the evidence must come from several sources and be closely tied to an accurate time scale. Indeed, as W.H. Berger notes:

> "The search for a specific cause for the Younger Dryas cold spell may be futile. In a chaotic system near its point of bifurcation, small disturbances can result in large effects, from positive feedback amplification." – (Berger, 1990)

However, as the volume of evidence for global palaeoclimatic change accumulates and the quality of palaeoclimatic reconstructions continues to improve, Berger's observation may yet be disproved. There are several factors to consider when examining the relative value of individual palaeoclimatic records.

1) The first concern is how well the chronology of each proxy record is established. The precision of the chronology must be of the order of a century to examine palaeoclimatic changes that take place over periods as short as several centuries, as during the Late Glacial. To compare and correlate between multiple palaeoclimate records the chronology for each record must also be accurate.

2) If a satisfactory chronology can be established for a palaeoclimate proxy record, the level of information that may be interpreted from the proxy becomes important. The information that may be obtained from a palaeoclimate proxy may vary from simple indication of individual plant species growing at a certain time (pollen records) to a precise record of absolute temperature (detailed stable isotope studies in speleothems and ice cores). The type of information available from proxies to describe the environment of the Quaternary period includes palaeotemperature from speleothems (Gascoyne *et al.*, 1980) and marine shells (Cornu *et al.*, 1993), palaeoprecipitation from speleothems (Rozanski and Dulinski, 1987), palaeohumidity from tree cellulose $\delta^{13}C$ (Becker and Kromer, 1993), palaeoecology from pollen records (Birks *et al.*, 1993; Carrion, 1992; Heijnis *et al.*, 1993) and palaeoclimate from multiple proxies (Imbrie *et al.*, 1973; Markgraf, 1993). The level of information available from palaeoclimate proxies varies from simple description through relative changes to absolute values for climate parameters such as temperature and rainfall.

To examine a short-term event like the Younger Dryas any palaeoclimatic proxy needs to be tied closely to a precise chronology and – to distinguish between the various hypotheses for the event – the proxy detail should ideally be an absolute reconstruction of actual conditions

at the time. The proxy examined in this work is the geochemistry of speleothems from Irish caves, dated with uranium-thorium (U/Th) thermal ionisation mass spectrometry (TIMS). Speleothems are calcium carbonate ($CaCO_3$) secondary deposits found in limestone caves. Speleothems provide several types of palaeoclimatic information, including rates of temperature change, palaeoecology and palaeoprecipitation (see Chapter 3), and speleothems are perhaps unique in terrestrial records in being dateable by U/Th TIMS with time resolutions of less than a century.

1.5.5. Testing hypotheses for the cause of the Younger Dryas

Five different hypotheses for the cause of the Younger Dryas have been introduced above. The type of evidence which might conclusively disprove each hypotheses is listed in the table below (table 1.2).

Hypothesis	Evidence for disproof	Proxies for disproof
Insolation changes	^{14}C and ^{10}Be production	Dual-dated palaeoclimate records
Iceberg swarms	Iceberg drop stones, detrital layers	Ocean cores
Frozen meltwater	Strong NADW & cold continents	Ocean cores & terrestrial records
Greenhouse gases	Gas concentrations in ice cores	Ice core records
NADW changes	Restricted deep-water formation	Ocean cores

Table 1.2. Hypotheses for the cause of the Younger Dryas The first column names the hypothesis for the cause of the YD. The second column indicates what evidence might be expected to disprove the hypothesis. The final column suggests what palaeoclimate proxy might provide this evidence.

i) *Reduction in insolation.* At the time of the Younger Dryas, the Earth was closest to the sun at the northern hemisphere summer solstice (Bradley, 1985), which would have the effect of increasing winter cold (figure 1.2). However, the rate of change of this

Milankovitch orbital variation suggests this factor is not on its own sufficient to cause the rapid and severe cooling of the YD. There is evidence however, for possible further short-term (sub-Milankovitch) variations in solar activity in the past. Variations in ^{10}Be and ^{14}C production rates record changes in the intensity of the magnetic field strength of the solar wind (Neftel *et al.*, 1981; Yiou *et al.*, 1985). When this magnetic shielding is strong (for example during high sunspot activity) galactic cosmic ray flux at the outer edge of the Earth's atmosphere is low and ^{14}C and ^{10}Be production is lower than normal (Stuiver and Quay, 1980). There is limited evidence for a link between sub-Milankovitch climate changes and short-term variations in solar activity (low insolation). The link is low solar activity ≡ high ^{10}Be and ^{14}C production ≡ low global temperatures (Bradley, 1985). One of these short-term variations in solar activity is the 11-year sunspot cycles (Shopov *et al.*, 1994), although unexplained periods of 100 and 200 years are also noted (Neftel *et al.*, 1981). If the YD was caused by a reduction in insolation, the production rate of ^{14}C at the outer atmosphere would be increased. In fact, during the YD it would appear that the rate of ^{14}C production did increase, but this is likely to be the result of changes in the strength of the Earth's magnetic field (Bard *et al.*, 1990) and variations in the global carbon cycle (Bard *et al.*, 1994) caused by major reorganisation of the Earth's atmosphere-ocean system (Broecker and Denton, 1990). However, the evidence for a link between solar activity and climate during the Quaternary is equivocal (Eddy, 1977; Landsberg, 1980; Pittock, 1978). With the lack of evidence for persistent reductions in solar activity on a sub-Milankovitch timescale, it seems unlikely that short-term variations in insolation were a primary trigger for the YD.

ii) *Heinrich events.* At certain times during the Quaternary large volumes of icebergs were present in the North Atlantic. These periods are known as Heinrich events after their discoverer (Broecker, 1994; Heinrich, 1988). The evidence for Heinrich events is layers in ocean cores rich in continental sediments carried by icebergs (Heinrich, 1988). Heinrich (1988) suggested two scenarios for the origin of the iceberg events. The first scenario suggests high summer insolation in the northern hemisphere (due to Milankovitch orbital variations) increased the levels of ice-sheet melting and therefore the volume of sea-ice in winter (Broecker, 1994; Oerlemans, 1993), The second scenario invokes ice-sheet surges due to cold winters, which produce an increased volume of icebergs (Broecker *et al.*, 1992). Heinrich layers are common in the North Atlantic (Broecker *et al.*, 1992), but evidence also exists for Heinrich-type events in the North Pacific (Kotilaninen and Shackleton, 1995). There is some evidence that iceberg production was greater during the YD than at other times of the Late Glacial (Bond *et al.*, 1992) and arguably the YD may be viewed as just another Heinrich event. As the YD appears to be a global event (Kudrass *et al.*, 1991), the key test for this hypothesis is evidence for Heinrich events in oceans besides the North Atlantic, or a mechanism where events in the North Atlantic can influence global climate.

iii) *Refreezing of glacial meltwater.* It has been suggested that the refreezing of a less-saline glacial meltwater layer at the surface of the North Atlantic ocean may have caused the YD period. Although this hypothesis is complex because it involves two separate stages of meltwater output and re-freezing, there is evidence that the ice moving through global oceans at the time of the YD was originally

grounded on a continental land-mass (the Heinrich detritus layers) (Broecker *et al.*, 1992). This makes it unlikely that the origin of this ice was re-freezing of freshwater layers at the surface of the ocean and suggests this hypothesis is untenable.

iv) *'Greenhouse' gas climate forcing.* The timing of changes in atmospheric concentrations of the relevant gases together with any change in temperature is a test for this hypothesis. Deciding whether the YD is a result of changes in gas concentration or gas concentration changes as a result of global climatic change at the YD is hampered by a lack of high resolution palaeoclimate proxy records containing information on both these items.

v) *North Atlantic Deep Water formation.* To disprove this hypothesis evidence is needed that NADW was strong during the YD, rather than being reduced in strength as this hypothesis requires. The best evidence for this comes from ocean cores analysed for Cd/Ca ratios, which are an indicator of the strength of bottom water ventilation. This evidence suggests that during the YD ocean ventilation was equal to (Labeyrie *et al.*, 1992) or greater than (Edwards *et al.*, 1993) normal ventilation rates. In addition, evidence that the oceanic residence time of ^{14}C has varied through time suggests deep-ocean ventilation is not constant in rate (Bard *et al.*, 1994). This information, together with evidence that the supposed trigger for the YD – increased freshwater from the Gulf of St. Lawrence during the time of the YD – is missing, suggests this hypothesis is less acceptable than previously.

Some of the hypotheses proposed above can now be discarded using exisiting evidence. The hypothesis that short-term variations in solar activity (insolation) were the primary cause of the global YD cold event is unlikely given the equivocal evidence for a link between short-term solar activity and climate change. The freezing glacial meltwater hypothesis can be rejected in view of evidence which suggests that ice present in the northern oceans during the YD was depositing detrital material of a continental origin (Heinrich, 1988), which indicates the ice was previously grounded on continental margins. This leaves three main hypotheses for the origin of the Younger Dryas to be examined.

1) Heinrich events.
2) 'Greenhouse' gas climate forcing.
3) Changes in North Atlantic Deep Water formation.

The remainder of this thesis is composed of a series of draft papers complete in themselves. A set of appendices examines data collection and techniques of data analysis and presentation. The structure of the thesis is:

1) *Chapter 2: Palaeoclimate from the frequency of speleothem U-series ages.* This paper discusses the frequency distribution of uranium-series dated speleothems in worldwide caves as a proxy for Quaternary climate change.
2) *Chapter 3: Reconstructing Irish palaeoclimate and environmental conditions during the Late Glacial from speleothems.* This section presents the majority of the data for speleothems collected for this work from Ireland. A discussion of the relationships between speleothem $\delta^{18}O$, $\delta^{13}C$, growth rate, luminescence and palaeoclimate is presented and a reconstruction of palaeoclimate conditions in Ireland during the Late Glacial is discussed.

3) *Chapter 4: Speleothems date the Younger Dryas: U-series ages from the Late Glacial in Ireland.* In this chapter I show why the hypothesis of Heinrich iceberg 'swarm' events is probably the best scenario for the cause of the YD in North-west Europe.

4) *Chapter 5: Calibrating ^{14}C ages to sidereal years and* vice versa *with a Microsoft Excel™ spreadsheet.* In this chapter I introduce a Microsoft Excel spreadsheet to quickly calibrate radiocarbon and 'real' ages.

5) *Chapter 6: Conclusions.* Here I will discuss the new insights that these analyses of speleothem palaeoclimate proxies offer for models of Quaternary palaeoclimate change.

6) *Chapter 7: Appendices.* Including sample collection and site descriptions; data collection techniques; data presentation; and computer programs used.

1.6. References

Adhémar, J. (1842). "Révolutions de la mer." Carilian-Goeury & V. Dalmont, Paris.

Allen, B. D., and Anderson, R. Y. (1993). Evidence from western North America for rapid shifts in climate during the Last Glacial Maximum. *Science* **260,** 1920-1923.

Andrews, J. T., and Tedesco, K. (1992). Detrital carbonate-rich sediments, northwestern Labrador Sea: Implications for ice-sheet dynamics and iceberg rafting (Heinrich) events in the North Atlantic. *Geology* **20,** 1087-1090.

Bard, E. (1988). Correction of accelerator mass spectrometry ^{14}C ages measured in planktonic foraminifera: Paloceanographic implications. *Paloceanogaphy* **3,** 635-645.

Bard, E., Arnold, M., Fairbanks, R. G., and Hamelin, B. (1993). ^{230}Th-^{234}U and ^{14}C ages obtained by mass spectrometry on corals. *Radiocarbon* **35,** 191-199.

Bard, E., Arnold, M., Mangerud, J., Paterne, M., Labeyrie, L., Duprat, J., Mélières, M.-A., Sønstegaard, E., and Duplessy, J.-C. (1994). The North

Atlantic atmosphere-sea surface ^{14}C gradient during the Younger Dryas climatic event. *Earth and Planetary Science Letters* **126,** 275-287.

Bard, E., Hamelin, B., Fairbanks, R. G., and Zindler, A. (1990). Calibration of the ^{14}C timescale over the past 30,000 years using mass spectrometric U-Th ages from Barbados corals. *Nature* **345,** 405-410.

Barnola, J. M., Raynaud, D., Korotkevich, Y. S., and Lorius, C. (1987). Vostok ice core provides 160,000-year record of atmospheric CO_2. *Nature* **329,** 408-414.

Barry, R. G., and Chorley, R. J. (1987). "Atmosphere, Weather and Climate." Methuen, London.

Becker, B., and Kromer, B. (1993). The continental tree-ring record – absolute chronology, ^{14}C calibration and climatic change at 11 ka. *Palaeogeography, Palaeoclimatology, Palaeoecology* **103,** 67-71.

Berger, A. (1978). Long-term variations of caloric insolation resulting from the Earth's orbital elements. *Quaternary Research* **9,** 139-167.

Berger, A. (1980). The Milankovitch astronomical theory of paleoclimate: a modern review. *Vistas in Astronomy* **24,** 103-122.

Berger, A. (1988). Milankovitch theory and climate. *Reviews of Geophysics* **26,** 624-657.

Berger, A., Tricot, C., Gallee, H., and Loutre, M. F. (1993). Water vapour, CO_2 and insolation over the last glacial-interglacial cycles. *Philosophical Transactions of the Royal Society of London, Series B* **341,** 253-261.

Berger, W. H. (1990). The Younger Dryas cold spell - a quest for causes. *Palaeogeography, Palaeoclimatology, Palaeoecology (Global and Planetary Change Section)* **89,** 219-237.

Birks, H. H., Lemdahl, G., Svendsen, J. I., and Landvik, J. Y. (1993). Palaeoecology of a late Allerod peat bed at Godoy, western Norway. *Journal of Quaternary Science* **8,** 147-159.

Bjorck, S., and Digerfeldt, G. (1991). Allerod-Younger Dryas sea level changes in southwestern Sweden and their relation to the Baltic ice lake development. *Boreas* **20,** 115-133.

Bond, G., Heinrich, H., Broecker, W. S., Labeyrie, L., McManus, J., Andrews, J., Huon, S., Janshik, R., Clasen, S., Simet, C., Tedesco, K., Klas, M., Bonani, G., and Ivy, S. (1992). Evidence for massive discharges of icebergs into the North Atlantic during the last glacial period. *Nature* **360,** 245-249.

Bowen, D. Q., Rose, J., McCabe, A. M., and Sutherland, D. G. (1986). Correlation of Quaternary glaciations in England, Ireland, Scotland and Wales. *Quaternary Science Reviews* **5**, 299-340.

Bradley, R. S. (1985). "Quaternary Palaeoclimate." Chapman & Hall.

Broecker, W. S. (1994). Massive iceberg discharges as triggers for global climate change. *Nature* **372**, 421-424.

Broecker, W. S., Andree, M., Wolfli, W., Oeschger, H., Bonani, G., Kennett, J., and Peteet, D. (1988). The chronology of the last deglaciation: implications to the cause of the Younger Dryas event. *Paleoceanography* **3**, 1-19.

Broecker, W. S., Bond, G., Klas, M., Bonani, G., and Wolfli, W. (1990). A salt oscillator in the glacial Atlantic? 1. The concept. *Paleoceanography* **5**, 469-477.

Broecker, W. S., Bond, G., Klas, M., Clark, E., and McManus, J. (1992). Origin of the Northern Atlantic's Heinrich events. *Climate Dynamics* **6**, 265-273.

Broecker, W. S., and Denton, G. H. (1989). The role of ocean-atmosphere reorganizations in glacial cycles. *Geochimica et Cosmochimica Acta* **53**, 2465-2501.

Broecker, W. S., and Denton, G. H. (1990). The role of ocean-atmosphere reorganizations in glacial cycles. *Quaternary Science Reviews* **9**, 305-341.

Broecker, W. S., and van Donk, J. (1970). Insolation changes, ice volumes, and the O^{18} record in deep-sea cores. *Reviews of Geophysics and Space Physics* **8**, 169-198.

Bryson, R. A., Wendland, W. M., Ives, J. D., and Andrews, J. T. (1969). Radiocarbon isochrones on the disintegration of the Laurentide ice sheet. *Arctic and Alpine Research* **1**, 1-14.

Büdel, J. (1982). "Climatic geomorphology." Princeton University Press, Princeton.

Carrion, J. S. (1992). A palaeoecological study in the western Mediterranean area. The Upper Pleistocene pollen record from Cova Beneito (Alicante, Spain). *Palaeogeography, Palaeoclimatology, Palaeoecology* **92**, Jan-14.

Chappell, J., and Shackleton, N. J. (1986). Oxygen isotopes and sea level. *Nature* **324**, 137-140.

Chappellaz, J., Blunier, T., Raynaud, D., Barnola, J. M., Schwander, J., and Stauffer, B. (1993). Synchronous changes in atmospheric CH_4 and Greenland climate between 40 and 8 kyr BP. *Nature* **366**, 443-445.

Clarke, R. J., and Tobias, P. V. (1995). Sterkfontein Member 2 foot bones of the oldest South African hominid. *Science* **269,** 521-524.

CLIMAP. (1976). The surface of the ice-age Earth. *Science* **191,** 1131-1137.

Cornu, S., Patzold, J., Bard, E., Meco, J., and Cuerda-Barcelo, J. (1993). Paleotemperature of the last interglacial period based on $\delta^{18}O$ of Strombus bubonius from the western Mediterranean Sea. *Palaeogeography, Palaeoclimatology, Palaeoecology* **103,** Jan-20.

Croll, J. (1875). "Climate and Time in their Geological Relations." Appleton, New York.

Crowley, T. J. (1989). Paleoclimate perspectives on a greenhouse warming. *In* "Climate and Geo-Sciences." (A. Berger, S. Schneider, and J. C. Duplessy, Eds.), pp. 179-207. Kluwer, Dordrecht.

Cuffey, K. M., Clow, G. D., Alley, R. B., Stuiver, M., Waddington, E. D., and Saltus, R. W. (1995). Large Arctic temperature change at the Wisconsin-Holocene glacial transition. *Scienc* **270,** 455-458.

Darwin, C. R. (1859). "The Origin of Species." John Murray, London.

Dawson, A. G. (1992). "Ice age Earth: Late Quaternary geology and climate." Routledge, London.

de Vernal, A., Hillaire-Marcel, C., and Bilodeau, G. (1996). Reduced meltwater outflow from the Laurentide ice margin during the Younger Dryas. *Nature* **381,** 774-777.

Denton, G. H., and Hendy, C. H. (1994). Younger Dryas age advance of Franz Josef glacier in the Southern alps of New Zealand. *Science* **264,** 1434-1436.

Denton, G. H., and Karlén, W. (1973). Holocene climatic variations - their pattern and possible cause. *Quaternary Research* **3,** 155-205.

Dickinson, R. E., and Cicerone, R. J. (1986). Future global warming from atmospheric trace gases. *Nature* **319,** 109-115.

Dodson, J. (1977). Late Quaternary Palaeoecology of Wyrie Swamp, Southeastern South Australia. *Quaternary Research* **8,** 97-114.

Eddy, J. A. (1977). Climate and the changing sun. *Climatic Change* **1,** 173-190.

Edwards, R. L., Beck, J. W., Burr, G. S., Donahue, D. J., Chappell, J. M. A., Bloom, A. J., Drufell, E. R. M., and Taylor, F. W. (1993). A large drop in atmospheric $^{14}C/^{12}C$ and reduced melting in the Younger Dryas, documented with ^{230}Th ages of corals. *Science* **260,** 962-968.

Emiliani, C. (1955). Pleistocene temperatures. *Journal of Geology* **63,** 538-578.

Feng, X., and Epstein, S. (1994). Climatic implications of an 8000-year hydrogen isotope time series from bristlecone pine trees. *Science* **265,** 1079-1081.

Gascoyne, M., Schwarcz, H. P., and Ford, D. C. (1980). A palaeotemperature record for the mid-Wisconsin in Vancouver Island. *Nature* **285,** 474-476.

Ghil, M. (1989). Deceptively-simple models of climate change. *In* "Climate and Geo-Sciences." (A. Berger, S. Schneider, and J. C. Duplessy, Eds.), pp. 211-240. Kluwer, Dordrecht.

Goede, A., Murray, P., and Harmon, R. (1978). Pleistocene man and megafauna in Tasmania: Dated evidence from cave sites. *The Artefact* **3,** 139-149.

Goslar, T., Kuc, T., Ralska-Jasiewiczowa, M., Rozanski, K., Arnold, M., Bard, E., van Geel, B., Mieczyslaw, F. P., Szeroczynska, K., Wicik, B., Wieckowski, K., and Walanus, A. (1993). High-resolution lacustrine record of the Late Glacial/Holocene transition in Central Europe. *Quaternary Science Reviews* **12,** 287-294.

Goudie, A. S. (1981). "The Human Impact on the Natural Environment." Blackwell, Oxford.

Gray, J. M., and Lowe, J. J. (1977). The Scottish Lateglacial environment: A synthesis. *In* "Studies in the Scottish Lateglacial Environment." (J. M. Gray, and J. J. Lowe, Eds.), Oxford.

Grootes, P. M., Stuiver, M., White, J. W. C., Johnsen, S., and Jouzel, J. (1993). Comparison of oxygen isotope records from the GISP2 and GRIP Greenland ice cores. *Nature* **366,** 552-554.

Haq, B. U., Berggren, W. A., and Van Couvering, J. A. (1977). Corrected age of the Pliocene/Pleistocene boundary. *Nature* **269,** 483-488.

Heijnis, H., Ruddock, J., and Coxon, P. (1993). A uranium-thorium dated Late Eemian or Early Midlandian organic deposit from near Kilfenora between Spa and Fenit, Co. Kerry, Ireland. *Journal of Quaternary Science* **8,** 31-43.

Heinrich, H. (1988). Origin and consequences of cyclic ice rafting in the Northeast Atlantic Ocean during the past 130,000 years. *Quaternary Research* **29,** 142-152.

Hughen, K. A., Overpeck, J. T., Peterson, L. C., and Trumbore, S. (1996). Rapid climate changes in the tropical Atlantic region during the last deglaciation. *Nature* **380,** 51-54.

Imbrie, J., and Imbrie, K. P. (1979). "Ice ages: Solving the mystery." Macmillan, London.

Imbrie, J., van Donk, J., and Kipp, N. G. (1973). Palaeoclimatic investigation of a Late Pleistocene Caribbean deep-sea core: Comparison of isotopic and faunal methods. *Quaternary Research* **3,** 10-38.

Jensen, K. (1938). Some west Baltic pollen diagrams. *Quartar* **1,** 124-139.

Johnson, R. G., and McClure, B. T. (1976). A model for Northern hemisphere continental ice sheet variation. *Quaternary Research* **6,** 325-353.

Jouzel, J., Lorius, C., Petit, J. R., Genthon, C., Narkov, N. I., Kotlyakov, V. M., and Petrov, V. M. (1987). Vostok ice core: a continuous isotope temperature record over the last climatic cycle (160,000 years). *Nature* **329,** 403-407.

Kennett, J. P., and Ingram, B. L. (1995). A 20,000-year record of ocean circulation and climate change from the Santa Barbara basin. *Nature* **377,** 510-514.

Koç Karpuz, N., and Jansen, E. (1992). A high-resolution diatom record of the last deglaciation from the SE Norwegian Sea: Documentation of rapid climate changes. *Paleoceanography* **7,** 499-520.

Kotilaninen, A. T., and Shackleton, N. J. (1995). Rapid climate variability in the North Pacific Ocean during the past 95,000 years. *Nature* **377,** 323-326.

Kudrass, H. R., Eirenkeuser, H., Vollbrecht, R., and Weiss, W. (1991). Global nature of the Younger Dryas cooling event inferred from oxygen isotope data from Sulu Sea cores. *Nature* **349,** 406-409.

Kuhry, P., Hooghiemstra, H., van Geel, B., and van der Hammen, T. (1993). The El Abra stadial in the eastern cordillera of Colombia (South America). *Quaternary Science reviews* **12,** 333-343.

Kukla, G. (1989). Long continental records of climate – an introduction. *Palaeogeography, Palaeoclimatology, Palaeoecology* **72,** 1-9.

Labeyrie, L. D., Duplessy, J.-C., Duprat, J., Juillet-Leclerc, A., Moyes, J., Michel, E., Kallel, N., and Shackleton, N. J. (1992). Changes in the vertical structure of the North Atlantic ocean between glacial and modern times. *Quaternary Science Reviews* **11,** 401-413.

Landsberg, H. E. (1980). Variable solar emissions, the "Maunder Minimum" and climatic temperature fluctuations. *Archiv Für Meteorologie, Geophysik und Bioklimatologie (B)* **28,** 181-191.

Laskar, J., and Robutel, P. (1993). The chaotic obliquity of the planets. *Nature* **361,** 608-612.

Lawson, T. J. (1983). The glaciation of the Assynt area. *In* "Quaternary Geomorphology of the Assynt Area, N.W. Scotland." (T. J. Lawson, Ed.), pp. 97-122. Privately published PhD thesis, Edinburgh.

Lehman, S. J., and Keigwin, L. D. (1992). Sudden changes in North Atlantic circulation during the last deglaciation. *Nature* **356,** 757-762.

Lotter, A. F. (1991). How long was the Younger Dryas? Preliminary evidence from annually laminated sediments of Soppensee (Switzerland). *Hydrobiologia* **214,** 53-57.

Lovelock, J. E. (1979). "Gaia: A New Look at Life on Earth." Oxford University Press, Oxford.

Manabe, S., and Stouffer, R. J. (1993). Century-scale effects of incrased atmospheric CO2 on the ocean-atmosphere system. *Nature* **364,** 215-218.

Mangerud, J. (1987). The Allerod/Younger Dryas boundary. *In* "Abrupt Climatic Change." (W. H. Berger, and L. D. Labeyrie, Eds.), pp. 163-171. Reidel, Dordrecht.

Mangerud, J., Andersen, S. T., Berglund, B. E., and Donner, J. J. (1974). Quaternary stratigraphy of Norden, a proposal for terminology and classification. *Boreas* **3,** 109-128.

Markgraf, V. (1993). Paleoenvironments and paleoclimates in Tierra del Fuego and southernmost Patagonia, South America. *Palaeogeography, Palaeoclimatology, Palaeoecology* **102,** 53-68.

Martinson, D. G., Pisias, N. G., Hays, J. D., Imbrie, J., Moore, T. C. J., and Shackleton, N. J. (1987). Age dating and the orbital theory of the Ice Ages: development of a high-resolution 0 to 300,000 year chronostratigraphy. *Quaternary Research* **27,** 1-29.

Mathewes, R. W. (1993). Evidence for Younger Dryas-age cooling on the North Pacific coast of America. *Quaternary Science Reviews* **12,** 321-331.

McDermott, F., Grun, R., Stringer, C. B., and Hawkesworth, C. J. (1993). Mass-spectrometric U-series dates for Israeli Neanderthal/early modern hominid sites. *Nature* **363,** 252-254.

Mercer, J. H. (1969). The Allerod oscillation: A European climatic anomaly? *Arctic and Alpine Research* **1,** 227-234.

Milankovitch, M. M. (1941). "Canon of Insolation and the Ice-Age problem." Köninglich Servische Akademie, Beograd.

Nairn, A. E. M. (1961). Descriptive palaeoclimatology, pp. 380. Interscience, New York.

Neftel, A., Oeschger, H., and Suess, H. E. (1981). Secular non-random variations of cosmogenic carbon-14 in the terrestrial atmosphere. *Earth and Planetary Science Letters* **56,** 127-147.

Nisbet, E. G. (1992). Sources of atmospheric CH_4 in early postglacial times. *Journal of Geophysical Research* **97,** 12859-12867.

Oerlemans, J. (1993). Evaluating the role of climate cooling in iceberg production and the Heinrich events. *Nature* **364,** 783-786.

Oeschger, H., Welten, M., Eicher, U., Moll, M., Riesen, T., Siegenthaler, U., and Wegmuller, S. (1980). ^{14}C and other parameters during the Younger Dryas cold phase. *Radiocarbon* **22,** 299-310.

Peltier, W. R. (1988). Global sea level and earth rotation. *Science* **240,** 895-901.

Peteet, D. (1995). Global Younger Dryas? *Quaternary International* **28,** 93-104.

Pittock, A. B. (1978). A critical look at long-term sun-weather relationships. *Reviews of geophysics and space physics* **16,** 400-420.

Pollard, D. (1982). A simple ice sheet model yields realistic 100 kyr glacial cycles. *Nature* **296,** 334-338.

Potts, R. (1996). Evolution and climate variability. *Science* **273,** 922-923.

Rahmstorf, S. (1994). Rapid climate transitions in a coupled ocean atmosphere model. *Nature* **372,** 82-85.

Roberts, M. B., Stringer, C. B., and Parfitt, S. A. (1994). A hominid tibia from middle Pleistocene sediments at Boxgrove, UK. *Nature* **369,** 311-313.

Roberts, N., Taieb, M., Barker, P., Damnati, B., Icole, M., and Williamson, D. (1993). Timing of the Younger Dryas event in East Africa from lake-level changes. *Nature* **366,** 146-148.

Rognon, P. (1987). Aridification and abrupt climatic events on the Saharan northern and southern margins, 20,000 yrBP to present. *In* "Abrupt Climatic Change." (W. H. Berger, and L. D. Labeyrie, Eds.), pp. 209-220. Reidel, Dordrecht.

Rossignol-Strick, M., Nesteroff, W., Olive, P. & Vergnaud-Grazzini, C. (1982). After the deluge: Mediterranean stagnation and sapropel formation. *Nature* **295,** 105-110.

Rozanski, K., and Dulinski, M. (1987). Deuterium content of European palaeowaters as inferred from isotopic composition of fluid inclusions trapped in carbonate cave deposits. *In* "Proceedings of the International symposium on the Use of Isotope Techniques in Water Resources Development." (IAEA, Ed.), pp. 565-578. IAEA, Vienna.

Ruddiman, W. F., and McIntyre, A. (1981). The North Atlantic Ocean during the last deglaciation. *Paleogeography, Paleoclimatology, Paleoecology* **35,** 145-214.

Sauer, C. O. (1956). The agency of man on the Earth. *In* "Man's Role in Changing the Face of the Earth." (W. L. Thomas, Ed.), pp. 49-69. The University of Chicago Press, Chicago.

Seibold, E., and Berger, W. H. (1982). "The Sea Floor." .

Sejrup, H. P., Haflidason, H., Kristenen, D. K., and Johnsen, S. J. (1995). Last interglacial and Holocene climatic development in the Norwegian Sea region: ocean front movements and ice-core data. *Journal of Quaternary Science* **10,** 385-390.

Shackleton, N. J., and Opdyke, N. D. (1973). Oxygen isotope and palaeomagnetic stratigraphy of Equatorial Pacific core V28-238: Oxygen isotope temperatures and ice volumes on a 10^5 year and 10^6 year scale. *Quaternary Research* **3,** 39-55.

Shopov, Y. Y., Ford, D. C., and Schwarcz, H. P. (1994). Luminescent microbanding in speleothems: High-resolution chronology and paleoclimate. *Geology* **22,** 407-410.

Sirocko, F., Sarnthein, M., Erlenkeuser, H., Lange, H., Arnold, M., and Duplessy, J. C. (1993). Century-scale events in monsoonal climate over the past 24,000 years. *Nature* **364,** 322-324.

Smith, A. G., and Goddard, I. C. (1991). A 12500 year record of vegetational history at Sluggan Bog, Co. Antrim, N. Ireland (incorporating a pollen zone scheme for the non-specialist). *New Phytologist* **118,** 167-187.

Stein, R., Nam, S.-I., Schubert, C., Vogt, C., Futterer, D., and Heinemeier, J. (1994). The last deglaciation event in the eastern central Arctic Ocean. *Science* **264,** 692-696.

Stuiver, M., Grootes, P. M., and Braziunas, T. F. (1995). The GISP2 $\delta^{18}O$ climate record of the past 16,500 years and the role of the sun, ocean, and volcanoes. *Quaternary Research* **44,** 341-354.

Stuiver, M., and Quay, P. D. (1980). Changes in atmospheric carbon-14 attributed to a variable sun. *Science* **207,** 11-19.

Stute, M., Forster, M., Frischkorn, H., Serejo, A., Clark, J. F., Schlosser, P., Broecker, W. S., and Bonani, G. (1995). Cooling of tropical Brazil (5°C) during the Last Glacial Maximum. *Science* **269,** 379-383.

Walker, I. R., Mott, R. J., and Smol, J. P. (1991). Allerød-Younger Dryas lake temperatures from midge fossils in Atlantic Canada. *Science* **253,** 1010-1012.

Walker, M. J. C., Bohncke, S. J. P., Coope, G. R., O'Connell, M., Usinger, H., and Verbruggen, C. (1994). The Devensian/Weichselian Late-glacial in northwest Europe (Ireland, Britain, north Belgium, The Netherlands, northwest Germany). *Journal of Quaternary Science* **9**, 109-118.

Warren, W. P. (1985). Stratigraphy. *In* "The Quaternary History of Ireland." (K. J. Edwards, and W. P. Warren, Eds.), pp. 39-65. Academic Press, London.

Weaver, A. J., and Hughes, T. M. C. (1994). Rapid interglacial climate fluctuations driven by North Atlanic ocean circulation. *Nature* **367**, 447-450.

White, T. D., Suwa, G., and Asfaw, B. (1994). Australopithecus ramidus, a new species of early hominid from Aramis, Ethiopia. *Nature* **371**, 306-312.

Wohlfarth, B. (1996). The chronology of the last termination: A review of radiocarbon-dated, high-resolution terrestrial stratigraphies. *Quaternary Science Reviews* **15**, 267-284.

Wright, H. E. J. (1989). The amphi-Atlantic distribution of the Younger Dryas paleoclimatic oscillation. *Quaternary Science Reviews* **8**, 295-306.

Yiou, F., Raisbeck, G. M., Bourles, D., Lorius, C., and Barkov, N. I. (1985). ^{10}Be in ice at Vostok Antarctica during the last climatic cycle. *Nature* **316**, 616-617.

Chapter 2: Palaeoclimate from the frequency of speleothem U-series ages

2.1. Introduction

Speleothems are useful palaeoclimatic proxies because they provide information on palaeotemperature, palaeoprecipitation and palaeovegetation. The simplest information about palaeoclimate that may be obtained from these secondary cave deposits is that when speleothems are growing it can be assumed that certain minimum climatic conditions exist outside a cave. Speleothems grow when limestone ($CaMg(CO_3)_2$) is deposited from an aqueous solution that outgasses CO_2, according to the reaction (Ford and Williams, 1989):

$$CaMg(CO_3)_2(s) + 2CO_2(g) + 2H_2O(aq) \Leftrightarrow Ca^{2+}(aq) + Mg^{2+}(aq) + 4HCO_3^-(aq)$$

Equation 2.1. The solution of limestone.

Speleothems cease formation when their drip-water freezes, as during glacial periods. Growth of speleothems may also halt when vegetation is sparse, because the excess CO_2 required for limestone dissolution and transport of calcite to a cave interior derives mainly from soil CO_2

formed by root respiration and microbial processes (Ford and Williams, 1989). Lack of vegetation may be a result of extreme cold or extreme hot climatic conditions (deserts), but periods of continued speleothem growth generally represent warm periods in the palaeoclimatic record. Therefore, the presence of actively growing speleothems indicates relatively wet conditions and the existence of plant life at the time of speleothem growth.

Several authors have attempted to examine Quaternary palaeoclimate changes recorded by the frequency distribution in time of speleothems dated by uranium-series (U-series) techniques, because speleothem growth is quite closely consequent on these climate conditions.

1) Thompon (1974), Harmon (1975, 1979), and Lauritzen (1991) inferred warm periods from a simple growth occurrence record of U-series dated speleothems. These authors presented their data graphically as growth periods against time (figure 2.1). This technique allows the reader to see quickly where periods of no speleothem growth exist. However, one problem with this method is that only small numbers of ages can be effectively represented on one chart and it is not possible statistically to incorporate age errors in the analysis.

2) The approach used by Gascoyne *et al.* (1983) and Goede *et al.* (1983) was to construct a frequency histogram of U-series dates falling within certain time intervals (figure 2.2). The frequency interval used in both these papers was 5000 years. This technique has the advantage that it is easy to recognise the periods in which large numbers of U-series ages exist. The main problem is there is no weighting of the ages based on the size of their age errors. All ages are given equal

weighting in the histogram, even though older U-series ages have larger absolute ages than younger ages. In addition,

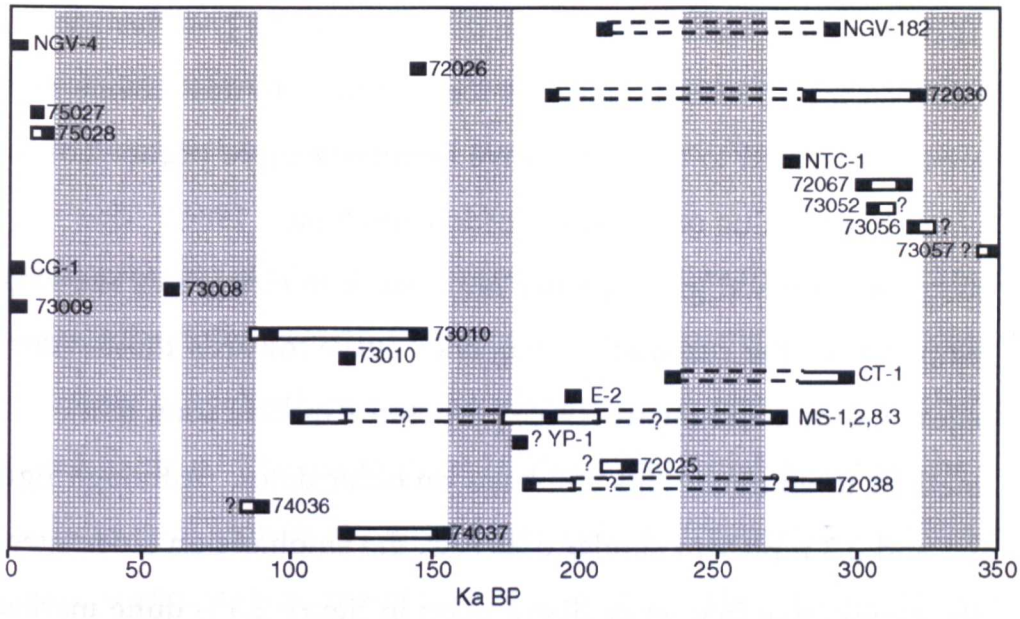

Figure 2.1. The growth periods of several Canadian speleothems, indicated as U-series dates (solid black boxes) joining sections of measured speleothem growth (solid lines) and inferred speleothem growth (dashed lines). Figure from Harmon (1979).

it is difficult to examine short-term palaeoclimate change where the histogram frequency interval is large.

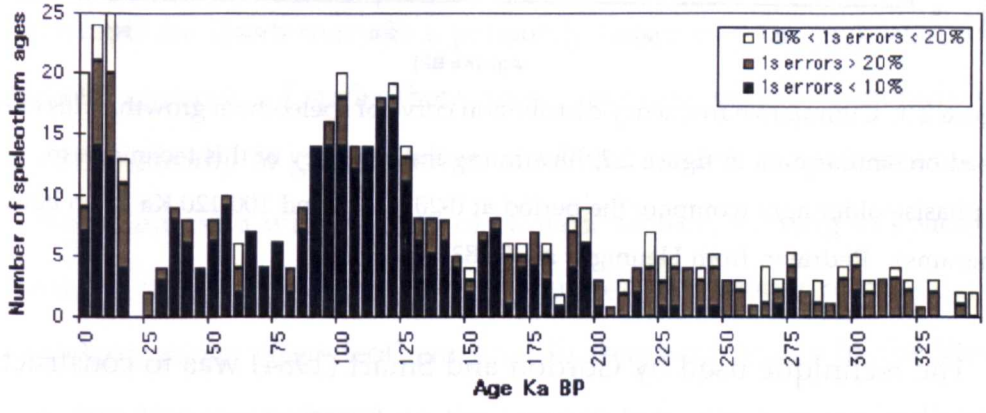

Figure 2.2. Frequency histogram of speleothems in 'region I', which corresponds to former glaciated regions, including N. America and central and northern Europe. Diagram redrawn from Hennig *et al.* (1983).

3) Hennig *et al.*, (1983) attempted to represent a database of U-series ages and to incorporate the varying absolute errors through time using an error-weighted cumulative frequency distribution curve. This technique sums uniform distributions of the U-series ages between the 1σ error boundaries for each age. In this scheme the total area contributed to the cumulative frequency curve (figure 2.3) is equal to the value of the age (Gordon and Smart, 1984). This simplistic method gives greater importance to older ages, skewing the emphasis of the cumulative frequency curve towards those older ages. Gordon and Smart (1984) proposed a modification to the method to eliminate this emphasis on older dates. Although figures 2.2 and 2.3 represent similar data sets, the emphasis on older ages in the cumulative frequency distribution in figure 2.3 is quite marked, as noted by Gordon & Smart (1984).

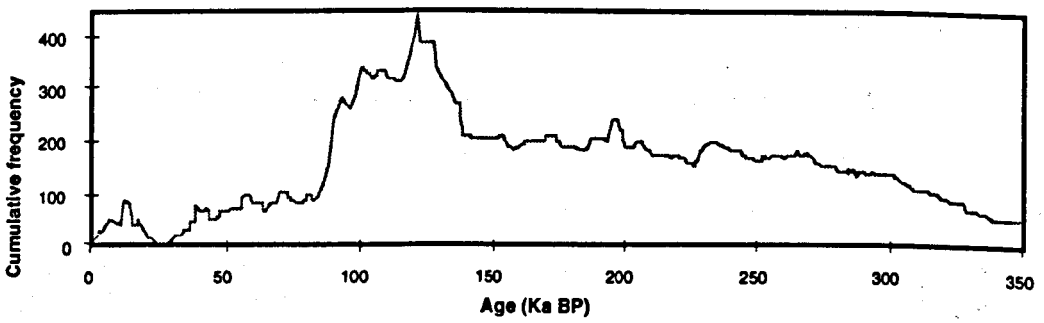

Figure 2.3. Cumulative frequency distribution curve of speleothem growth. This curve is based on similar data to figure 2.2, illustrating the tendency of this technique to emphasise older ages (compare the period at 0-20 Ka BP and 100-120 Ka BP in both diagrams). Redrawn from Hennig *et al.*, (1983).

4) The technique used by Gordon and Smart (1984) was to construct the cumulative frequency curve from normal curves representing the U-series ages and age errors. Further development of this method together with an enlargement of the database of U-series ages produced refined dates for palaeoclimatic events in Great Britain

(Gordon *et al.*, 1989) and north-west Europe (Baker *et al.*, 1993b). Note that Gordon & Smart (1984) and Baker *et al.* (1993b) assign a value of 1 to the area under each normal curve (at 1σ confidence limits), whereas the present work uses the values 0.68 and 0.95 to represent 1σ and 2σ confidence limits. Therefore, the normalised curves from those papers are not directly comparable with this work.

All four previous studies that have attempted to analyse palaeoclimate change from the growth frequency of speleothems have examined the database of speleothem U-series ages from the perspective of changes through time. The assumption made in these studies is that the frequency of growth of sampled speleothems (represented by U-series ages) is generally representative of Quaternary climate change. In fact, the location of limestone, caves, active speleothems and the location of laboratories dating speleothems with U-series techniques all have some bearing on the database of growth frequency. Despite some limited attempts to link the position of growing speleothems to the position of Quaternary ice-sheets (Baker *et al.*, 1993b), there have been few attempts to examine the distribution of speleothem U-series ages in space through the Quaternary Era, primarily because of the lack of a suitable global coverage of speleothem ages. This (as-yet unconsidered) analysis is theoretically of great interest, since the growth of speleothems is dependent on a wide variety of climatic factors, varying in space (global climate zones) and time (climate change). The majority of interpretations of speleothem growth frequency made in the literature to date has concentrated on the temperature effect on speleothem activity. However, it has been shown that temperature is only one of the limiting factors in speleothem growth (Baker and Smart, 1995). It is suggested that a complete cessation of speleothem growth reflects

increased aridity (hot or cold). Aridity is a function of temperature and moisture availability. When moisture for calcite dissolution is unavailable in a geographical region due to cold conditions (freezing) or dry conditions (lack of rainfall), speleothems will cease to grow. If changing climate restricts plant growth, soil CO_2 levels may fall below a level at which CO_2 is available to form carbonic acid for limestone solution. If climate conditions already permit speleothem growth, an increased number of speleothems will begin growth if more water is available and increased levels of vegetation increase soil CO_2 levels (Baker and Smart, 1995).

To evaluate any possible link between palaeoclimate and the spatial and temporal distribution of speleothem ages, a large database of published speleothem ages for worldwide caves was compiled and compared to other proxies for palaeoclimate during the Quaternary. However, the database of speleothem U-series ages may not be representative of global conditions during the Quaternary because it contains few analyses from the tropics and none from the continents of Africa, South America or Antarctica. It may be expected that caves occur in the majority of limestone regions (figure 2.4) and speleothem growth can be expected in the majority of limestone caves. Thus, it may be argued that the patchy global coverage of speleothems in the present database suggests it is not entirely representative of global palaeoclimate conditions. Regional studies are of interest because of the variety of local palaeoclimatic responses to global change as a result of Milankovitch forcing (see 1.3).

2.2. Methods

Almost 1,500 speleothem ages were compiled from published literature and the data filtered for reliability and standardised, before analysis for palaeoclimate signals in time and space. The details of each stage in this procedure are given below.

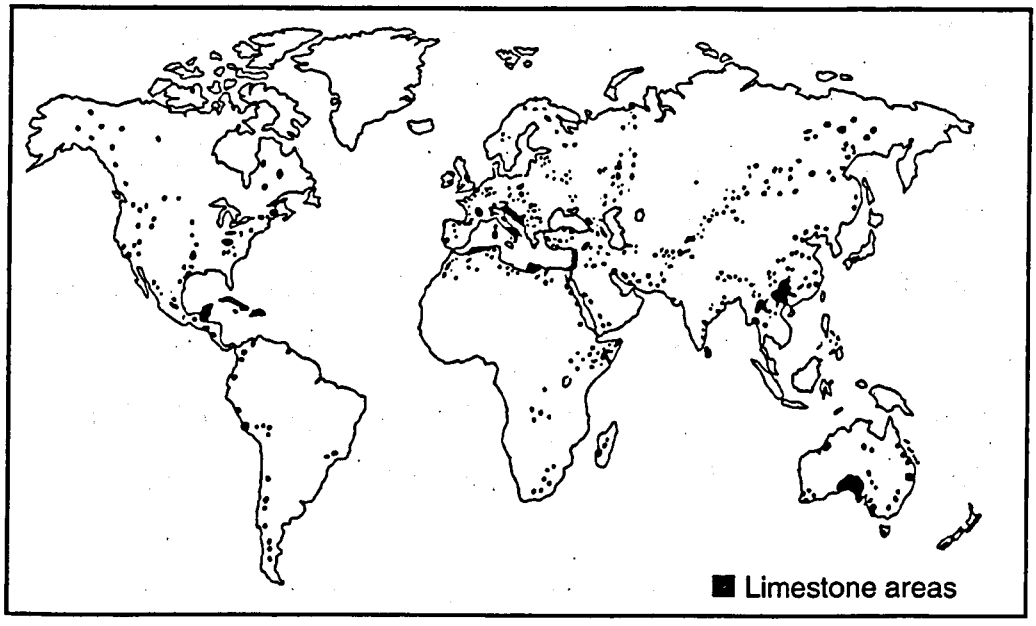

Figure 2.4. Major global outcrops of limestone. Figure redrawn from Jakucs (1977).

2.2.1. Data compilation and consolidation

Although U-series ages on speleothems have been published since 1965 (Cherdyntsev *et al.*, 1965), aspects of the calculations of the U-series ages from isotopic data have varied to a certain degree. The main possible procedural differences between various published U-series ages are the decay constants used for ^{238}U and ^{230}Th. These have been re-determined more recently than the publication date of some of the papers included in the present compilation. To eliminate this possible source of error, the ages were recalculated using the original isotopic data and the most recent published decay constants (Jaffey *et al.*, 1971; Meadows *et al.*, 1980). Ages published without a complete set of

isotopic ratios – (($^{230}Th/^{232}Th$), ($^{234}U/^{238}U$) and ($^{235}U/^{238}U$)) – could not be recalculated, and were discarded. In most cases the data were available to the original author, but not published (e.g. Hennig (1983)).

Isotopic data were compiled from published papers and available research theses. For this work 1441 speleothem ages were compiled from 22 different countries, on all continents except Antarctica, Africa and South America. Australasia provided 131 ages; 219 came from North America; 8 from Eastern Europe; 94 from Asia and 34 from the Caribbean; and the remainder were from Western Europe. The lack of data from Africa reflects the limited extent of cavernous limestone on that continent (figure 2.4) and the small number of cave scientists working in that region. The majority of papers are published in the English language, but papers examined here were also published

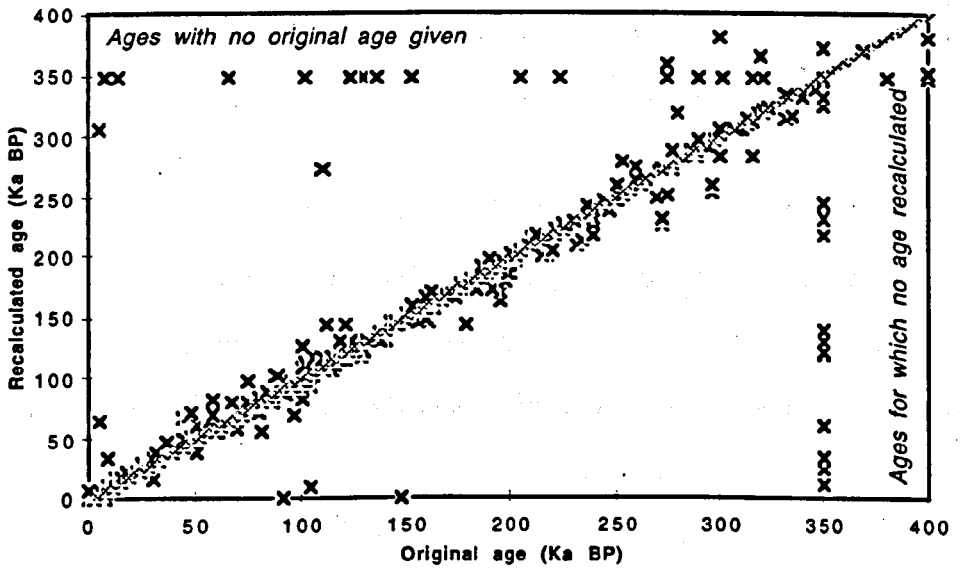

Figure 2.5. A comparison of U-series ages published with ages recalculated from published isotopic data using a single set of decay constants. Outliers on vertical and horizontal extremes of the diagram are those ages for which there is either no original information or insufficient information to recalculate an age.

in Chinese, Russian, French, German, Spanish and Portuguese. The published ages were filtered by published sample number to eliminate identical duplicate analyses.

2.2.2. Age recalculation (macro)

The data were entered on a Microsoft Excel spreadsheet to recalculate the ages. This spreadsheet includes the analysis code; cave name and location; longitude and latitude; isotopic data, including ($^{230}Th/^{234}U$), ($^{230}Th/^{232}Th$), ($^{234}U/^{238}U$) and ^{238}U concentration; the published age; and age error. The ages were recalculated using an Excel 4 macro. Ages are quoted in thousand year (kyr) units, as thousand years before present (Ka BP). To ensure equal treatment of all data, the ages were recalculated using just one set of decay constants (Jaffey *et al.*, 1971; Meadows *et al.*, 1980).

The recalculated ages may differ from the original published ages (figure 2.5) for the following reasons:

i) The original calculation process used by individual authors was not as accurate as that used in the Excel spreadsheet used here.

ii) Decay constants used in the original calculation of the ages were different to those used to recalculate the ages.

iii) The published data includes misprints or errors.

iv) Isotopic or procedural correction techniques were used to obtain the U-series age, but this was not indicated in the published work.

2.2.3. Filtering for valid ages

Certain ages were excluded from the compilation under the following criteria:

i) The effective upper limit of the U-series technique is approximately 5 ^{230}Th half-lives, or 350 Ka BP. One hundred and thirty-eight recalculated ages older than 350 Ka BP were excluded.

ii) Ten recalculated ages were younger than 0 Ka BP, perhaps due to analytical errors in the original isotopic analysis. Although in the original papers some authors use isotopic or procedural corrections to correct these erroneous analyses, the uncertain and variable nature of these corrections means these analyses were ignored in this compilation. Recalculated ages of less than 0 Ka BP were not corrected and are excluded from this compilation.

iii) Analyses of speleothems in which the matrix contains significant detrital ^{230}Th can produce erroneously old ages. Detrital ^{230}Th increases the apparent age of the speleothem sample because any ^{230}Th present in detrital material was not formed by *in situ* radiogenic decay of ^{234}U (non-authigenic ^{230}Th). An arbitrary exclusion limit of (^{230}Th/^{232}Th) < 20 is adopted by most authors as an indication of possible non-authigenic ^{230}Th in speleothem samples. Schemes for the calculation of U-series ages when the speleothem is detritally contaminated are available (Ku and Liang, 1984; Przybylowicz *et al.*, 1991; Schwarcz and Latham, 1989), although few such ages have been published because the data are difficult to interpret (Kaufman, 1993). In this work the (^{230}Th/^{232}Th) value below which possibly contaminated ages were excluded was also set at 20.

iv) A further exclusion criterion that applies solely to flowstone ages is the possibility of relocation of uranium within the deposit as seepage water passes over the upper layers of the flowstone (Schwarcz and Latham, 1984). Although this is a concern in most published studies, some flowstones have yielded acceptable

analyses (Falgueres and de Lumley, 1992). In general flowstone ages were accepted if the ($^{234}U/^{238}U$) ratio was ≤ 1.5.

Using these exclusion criteria, 1008 U-series ages were retained in the compilation for further analysis. For completeness, a large (>600) compilation of ages from the laboratory of Hennig (Hennig *et al.*, 1983) was added to this database, giving a total of >1600 ages. These latter ages could not be recalculated as no raw isotopic data were available. However, in preparing his compilation, Hennig only included data that satisfy the exclusion criteria for acceptable U-series ages in the present compilation. The majority of ages from Hennig's work are from caves in Germany and Spain.

2.2.4. Normalising U-series ages through time (macro & graphs)

To represent fully a U-series age in a stacked distribution some account must be taken of the age error. The technique used here is a modified version of that published by Baker *et al.* (1993b). After the U-series ages had been recalculated, the ages were distributed as normal curves on a continuous distribution. Using this technique each published U-series age x and its error σ are distributed as a normal curve with mean x and standard deviation σ. The area under each curve represents the probability that the age is correct. Thus, if a 1σ age error is assumed for each analysis, the area under the normal curve represents 68% confidence that the age is that value (figure 2.6). With a 2σ error, the area under the curve represents 95% confidence that the age is that value (figure 2.7).

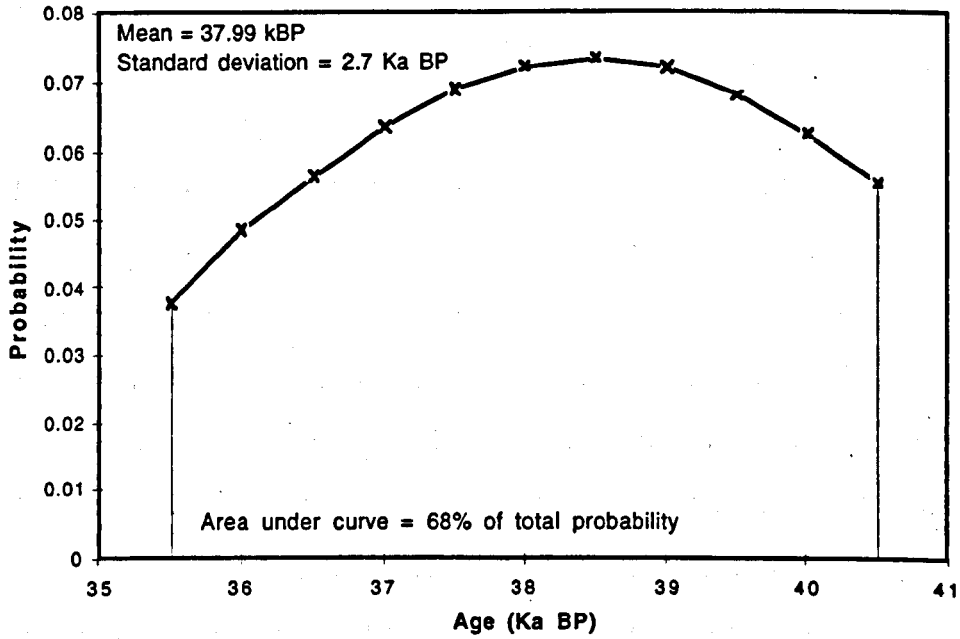

Figure 2.6. Example of a U-series age, normalised to a 1σ distribution. The skewing of the normal curve reflects the distribution over a fixed 500 year interval.

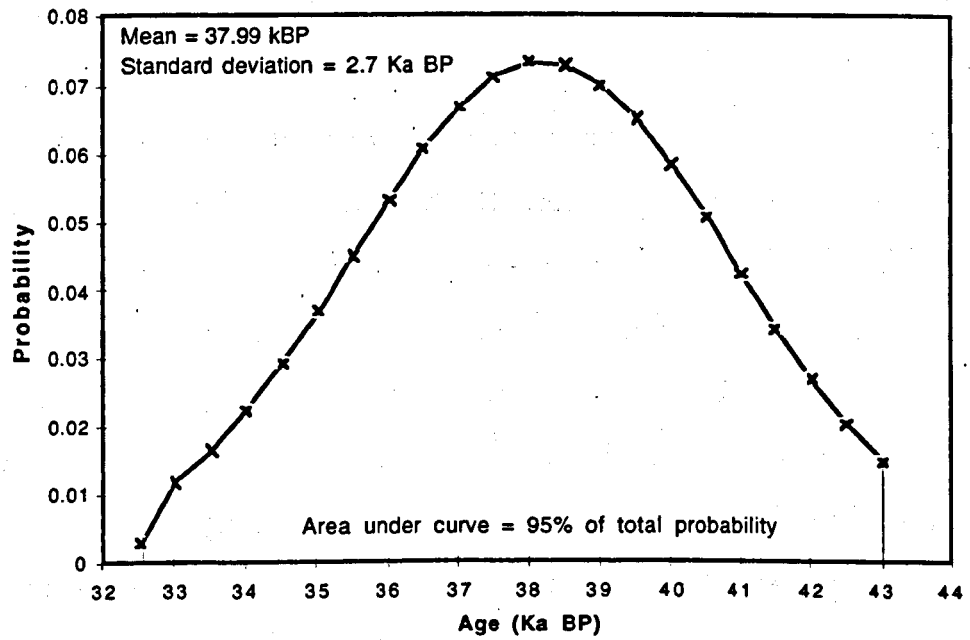

Figure 2.7. Example of a U-series age normalised to a 2σ distribution. The skewing is less marked by comparison with figure 2.6 due to the larger spread of the age over time. Note that the most skewing errors in the distribution will be eliminated in cases where large numbers of ages are normalised.

2.2.5. Plotting normal curves in time (macro and graphs)

The normalised ages are distributed over a continuous distribution from present-day (0 Ka BP) to 350 Ka BP (the limit of the technique) using a frequency interval of 500 years (e.g. figure 2.8). The advantage of this technique is that the age error is incorporated as part of the distribution (Gordon *et al.*, 1989). The result is a stacked, normalised frequency (SNF) curve that represents the age frequency of more than 1600 speleothem U-series ages (figure 2.12).

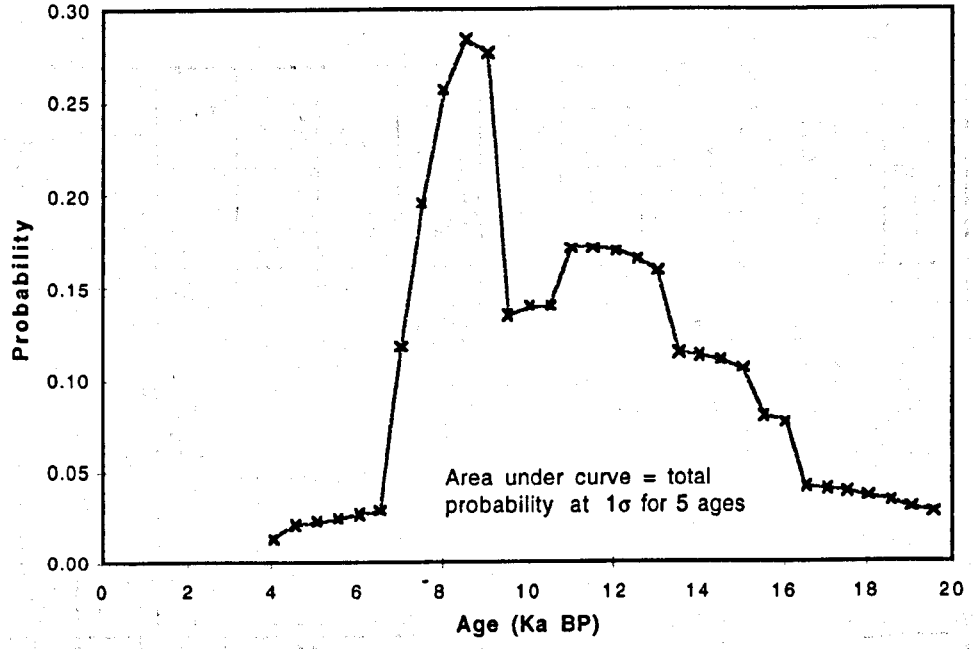

Figure 2.8. Five U-series ages normalised and stacked as a "stacked, normalised function".

2.2.6. Statistical testing of the significance of the distribution

A test of the robustness of the normalised distribution is to remove a certain number of the U-series ages to evaluate the persistence of any trend in the speleothem age data. Twenty percent of the speleothem ages were randomly removed 18 times using an Excel 4 macro and the remaining ages normalised to examine whether the individual peaks and troughs of the SNF curve persisted.

2.2.7. Plotting ages in space (macro and diagrams)

Although the U-series age distribution in time is represented by the SNF curve, it is difficult to visualise the geographical distribution of the ages without a map of their locations. The latitude and longitude of the caves from which each speleothem was sampled were determined from various maps. The ages from the database from 174 caves were located in space using this information. The longitude and latitude data were placed in a database with the recalculated U-series ages and

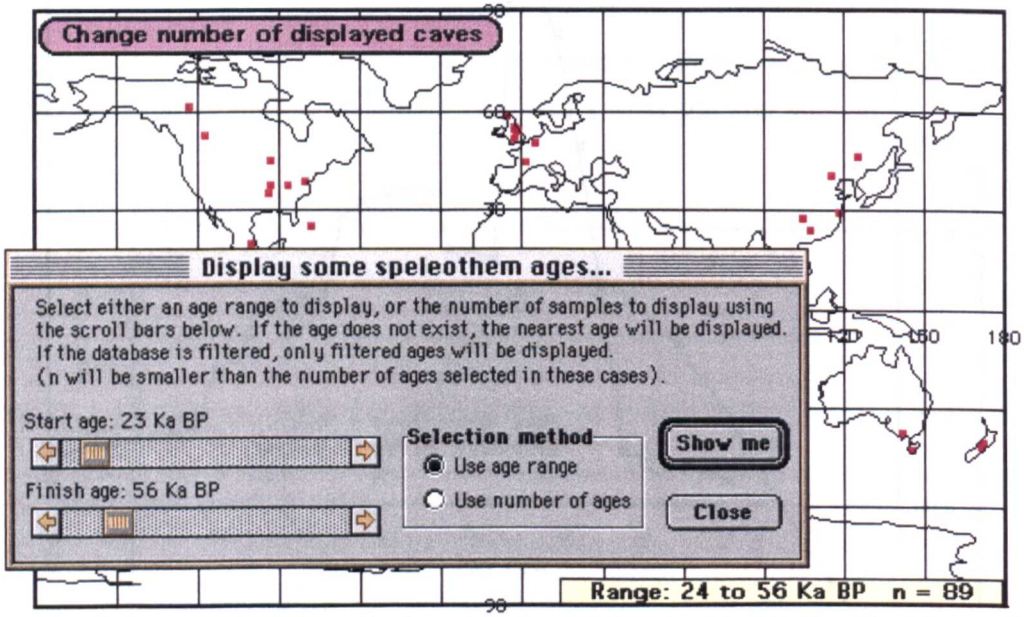

Figure 2.10. Dialog box from the Excel 5 worksheet to control the age range of dated speleothems displayed on the map. The start and finish ages are selected with the slider bars and the "Show me" button pressed to display those ages. Where an age cannot be found for the selected start or finish ages, the next age towards the centre of the distribution is displayed. Hence, on the map the range is indicated as 24 to 56 Ka BP although the sliders indicate the user actually requested a display of 23 to 56 Ka BP. The number of valid ages falling between the selected ages is displayed as "n = 89" in this example. The actual number of locations displayed may be smaller, since each cave may contain more than one dated speleothem.

an Excel 5 Visual Basic (VB) procedure written to interrogate the database from a world map display. The VB procedure permits the

selection of a period to display (figure 2.10). Alternatively, a number of speleothem ages from a particular start date may be selected (figure 2.11). For example, to examine the speleothem U-series ages available between the ages of 20 Ka BP and 28 Ka BP those ages are selected in the modal dialogue box using slider controls and the "Show me" button pressed. Used in conjunction with figure 2.13 – the age-distribution of U-series ages – the database permits an examination of the frequency and geographical location of published U-series ages.

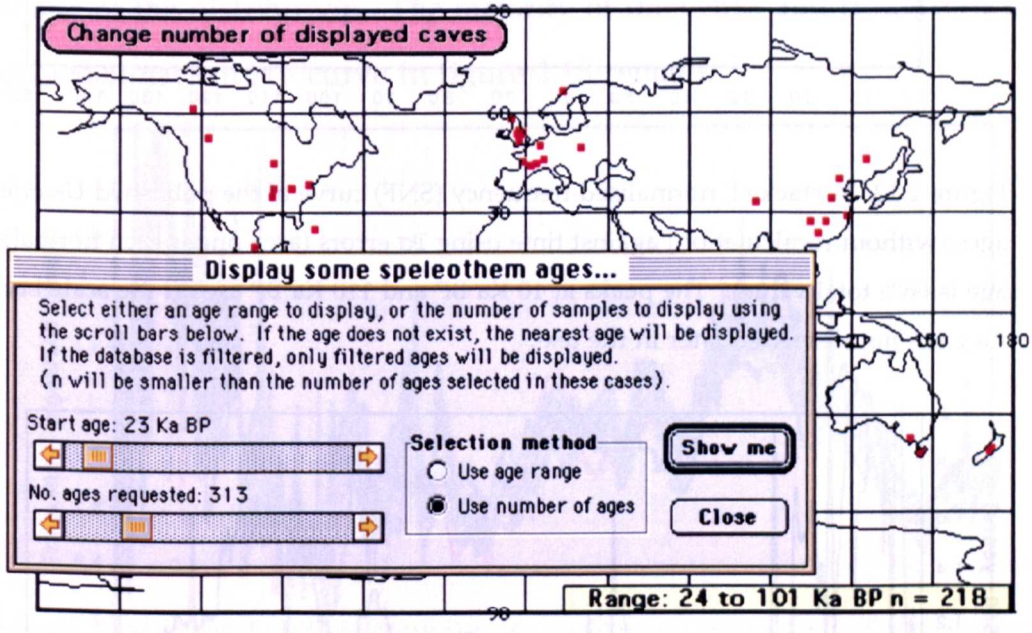

Figure 2.11. Dialog box from the Excel 5 worksheet to control the number of dated speleothems displayed on the map. The start age and number of U-series ages to display are selected with the slider bars and the "Show me" button pressed to display those ages. Note that although 313 ages were requested for display, only 218 ("n = 218") are shown. This feature indicates the number of U-series ages filtered out by the software for the reasons in point 2.2.3 above.

2.3. Results

A SNF curve of the published ages (before recalculation) is shown here for comparison (figure 2.12). The full recalculated set of U-series ages is also presented here for comparison (figure 2.13) with the datasets with ages randomly removed (figure 2.14).

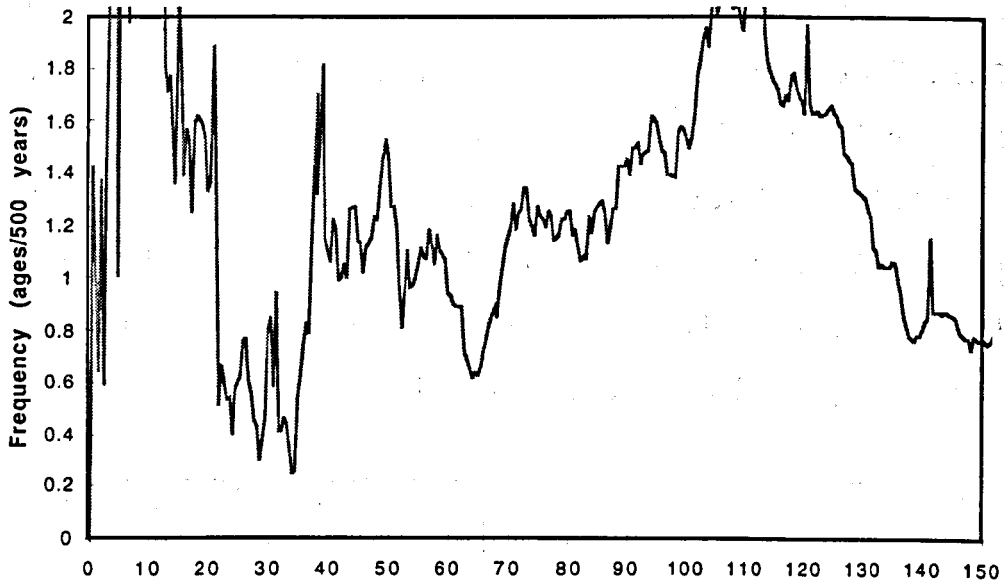

Figure 2.12. A stacked, normalised frequency (SNF) curve of the published U-series ages (without recalculation) against time using 1σ errors (area under each normalised age is 68% total value). The peaks at 10 Ka BP and 110 Ka BP are off the scale because they are not discussed later in the text.

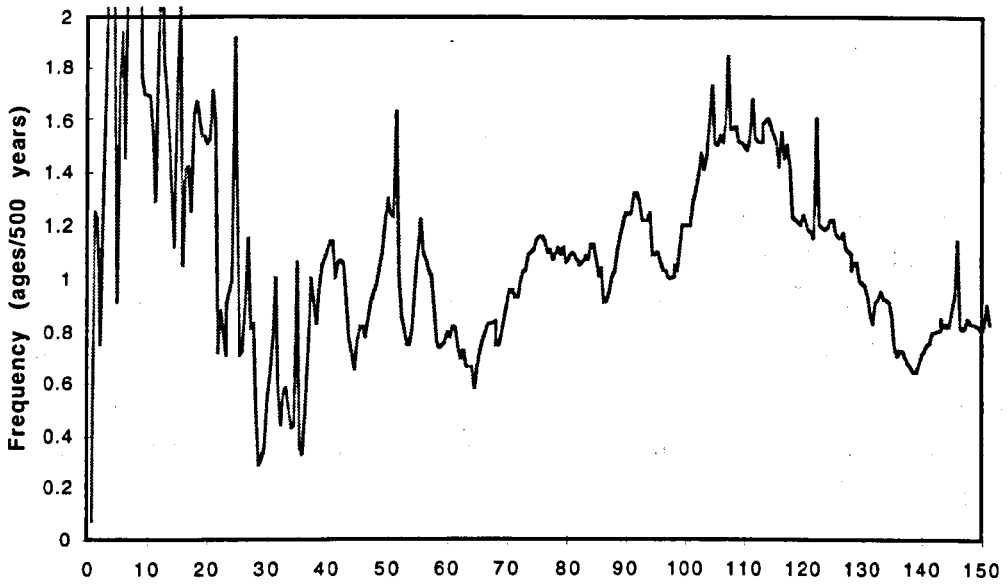

Figure 2.13. SNF curve of the recalculated U-series ages against time using 1σ errors (area under each normalised age is 68% total value).

2.3.1. Testing the SNF curve for significance

A certain number of the normalised ages were eliminated at random a number of times to test for the significance of the SNF distribution. Eighteen SNF curves were constructed and 20% of the ages were eliminated at random to test the robustness of the distribution.

Figure 2.14 shows how removing 20% of the total speleothems from the overall distribution at random 18 times has little effect on the overall shape of the distribution. The majority of the peaks and troughs of the palaeoclimate proxy curve in figure 2.13 remain.

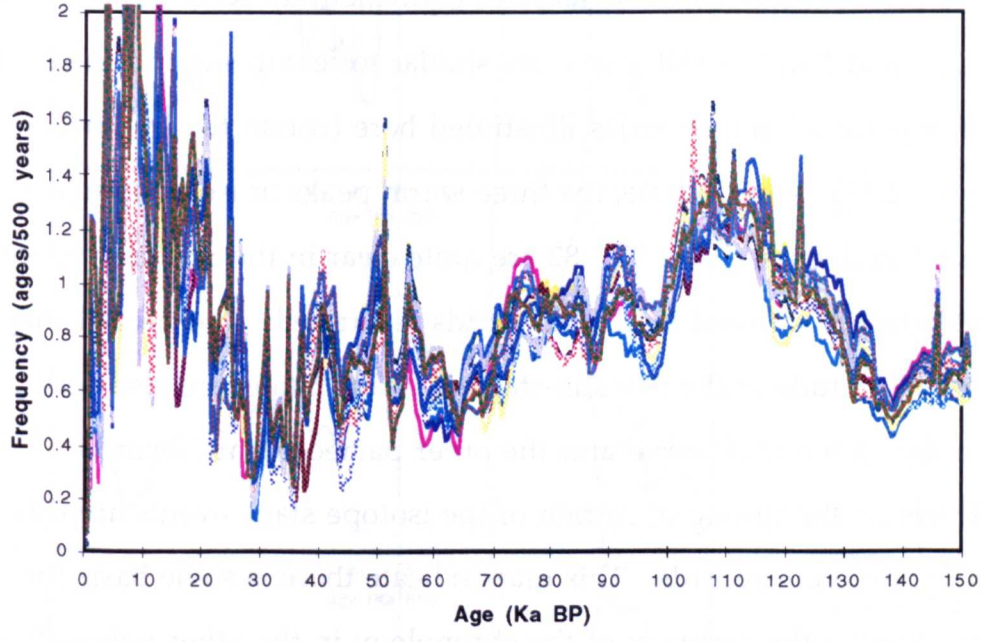

Figure 2.14. SNF curve of 18 identical speleothem databases, from which 20% of the ages were removed at random. The majority of the major peaks and troughs in the distribution persist despite the random removal of ages.

2.3.2. The SNF curve and Quaternary palaeoclimate change

The SNF curve was compared with other palaeoclimate proxies, including the V28-238 $\delta^{18}O$ record (Sancetta *et al.*, 1973) and a stacked normalised $\delta^{18}O$ record from a variety of deep-sea cores (Martinson *et al.*, 1987) to examine the usefulness of the SNF curve as a proxy for Quaternary

palaeoclimate events. As can be seen from figure 2.15, the SNF curve closely approximates those quantitative estimates of palaeotemperature in both magnitude and age. Few major events in global palaeoclimatic reconstructions are established unequivocally in time. However, a well-dated feature of all palaeoclimate reconstructions is the timing of the Last Glacial Maximum (LGM). The LGM ice extent in Europe was between 18 and 20 Ka BP (Lundqvist, 1986), and is given the age of 20 Ka BP in this work.

These similarities are most noticeable in the period prior to 30 Ka BP (10 kyrs before the LGM). The features equivalent to oxygen isotope stages 2, 3, 4 and 5 in the SNF curve are similar to features found in certain other palaeoclimate proxies illustrated here (connected by lines in figure 2.15). For example, the three warm peaks of isotope stage 3 found in deep-sea core V23-82 are quite clear in the SNF curve, whilst cold stage 4 is found in all the records illustrated. The overall shape and magnitude of the five sub-stages of stage 5 (a-e) are also very similar in the SNF curve and the other palaeoclimate records. However, the timing of certain of the isotope stage events are different in the different records. This may indicate there is some basis for questioning the accuracy of the chronology in the other palaeoclimate records, because the SNF curve is based on frequency of U-series ages and is more likely to be temporally accurate. The most intriguing example of this difference in the timing of certain palaeoclimate events is the timing of isotope stage 6 (the penultimate glacial). The boundary between stage 6 and stage 5e is generally placed at 128 Ka BP, although recent evidence from a U-Th TIMS dated $\delta^{18}O$ record (Devils Hole,

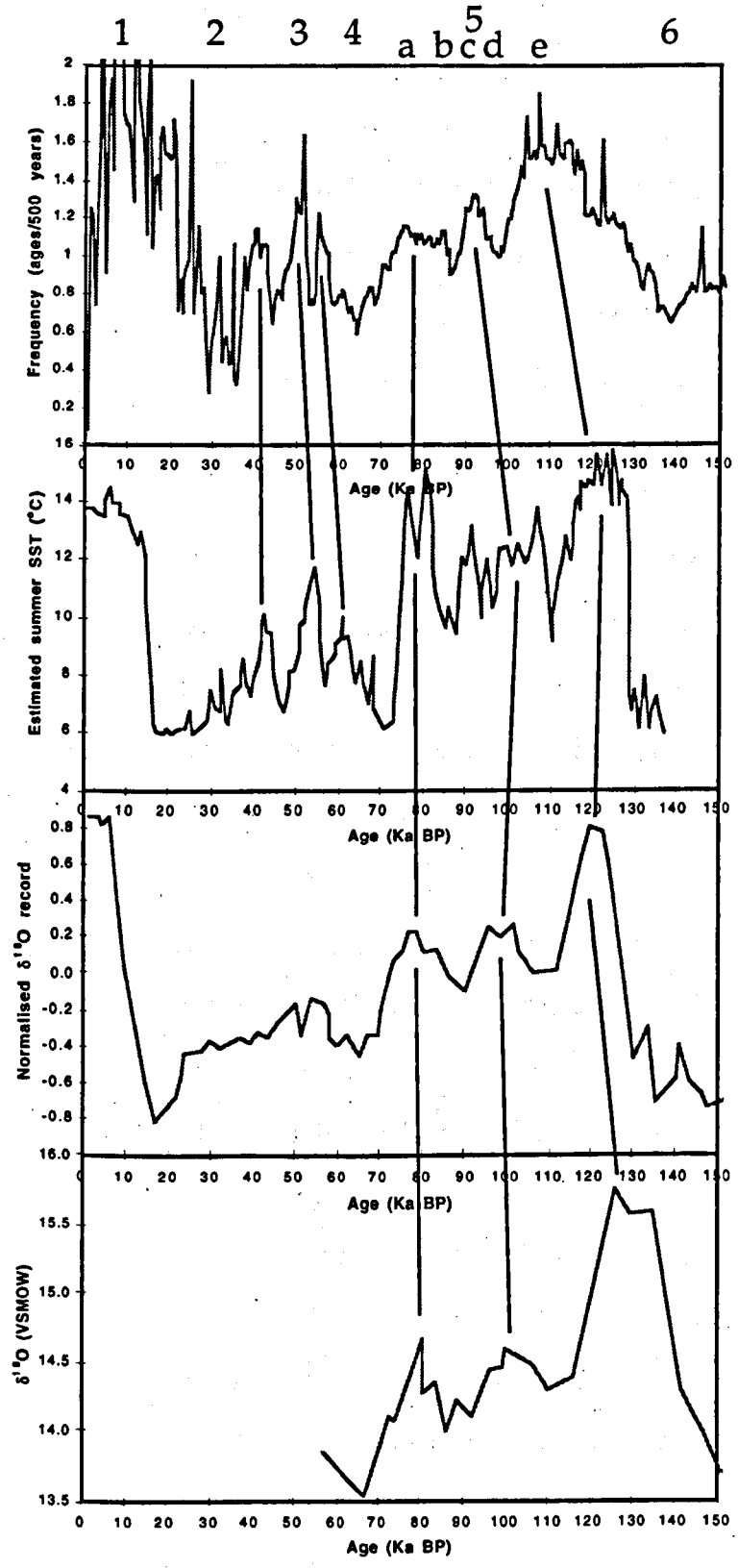

Figure 2.15. The SNF curve and several palaeoclimate proxies. Top panel is the SNF curve with isotope stages 1-6 marked; 2nd panel shows estimated summer sea-surface temperature (SST) in core V23-82 from the North Atlantic ocean, with a chronology based on the ages of ash layers (Sancetta *et al.*, 1973); the 3rd panel is a stacked normalised $\delta^{18}O$ record for various global deep-sea records, chronology by orbital tuning (Martinson *et al.*, 1987; Pisias *et al.*, 1984); the 4th panel is $\delta^{18}O$ record for the Devils Hole calcite, chronology by U-Th TIMS ages on calcite (Ludwig *et al.*, 1992).

panel 4 in figure 2.15) revised the age for this transition to 140 Ka BP (Ludwig *et al.*, 1992; Winograd and Coplen, 1989; Winograd *et al.*, 1992). Debate on the veracity of this new age for the stage 6/stage 5e transition has not been resolved (Gallup *et al.*, 1994; Ludwig *et al.*, 1993; Shackleton, 1993). Further evidence for an earlier 6/5e transition is recorded in Alaskan tephra deposits (Begét, 1996). On first appearances (figure 2.13), the SNF distribution appears to provide supporting evidence for an older transition, with increased numbers of dated speleothems after 140 Ka BP. However, this may reflect a tailing effect of the normalisation technique or a possible two-step deglaciation. To examine whether the implied older age for the termination of the penultimate glacial is 'real' or an artefact of the normalisation technique it is necessary to investigate the geographical location of the active speleothems at that point in time.

2.3.3. The SNF curve and global location of active speleothems during selected palaeoclimate events

To examine the geographical distribution of active speleothems during isotope stage 6/5e (penultimate glacial/last interglacial) transition; isotope stage 4; isotope stage 3; and isotope stage 2 (LGM/Holocene transition) the data were plotted on a world map.

2.3.3.1. The penultimate glacial/interglacial transition

To investigate whether the SNF curve reflects the standard age for the stage 6/5e transition (128 Ka BP) or the alternative chronology suggested by the Devils Hole Alaskan tephra record (140 Ka BP), the number of speleothems active in 10 kyr periods around this point were examined. The compiled speleothem U-series data were plotted on a map of the world for intervals between 130 and 140 Ka BP, 140 and 150

Ka BP and 150 and 160 Ka BP. In a random distribution of ages it would be expected that all intervals would have similar numbers of dated speleothems. In addition, the tailing from the peak at 128 Ka BP into 150 Ka BP evident in figure 2.13 may reflect large age errors associated with the last interglacial after 128 Ka BP. However, if the distribution of ages actually reflects active growth of speleothems in the four age ranges, the timing of those growing speleothems may indicate whether an age of 140 Ka BP for the termination of the penultimate glacial is possible.

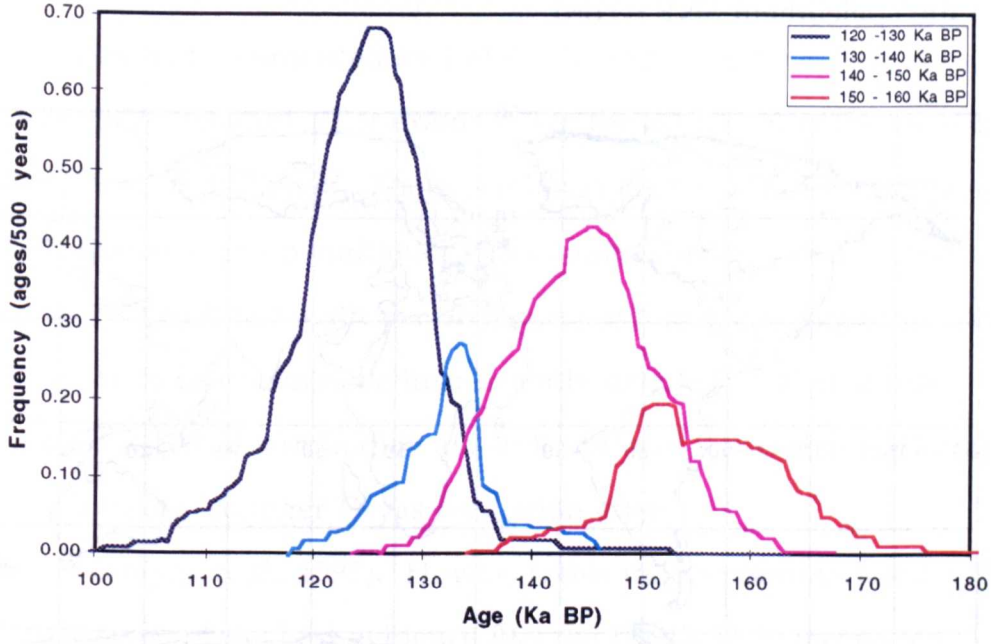

Figure 2.16. The location of caves with active speleothem between the ages of 120-130 KA BP, 130 Ka BP-140 Ka BP, 140-150 Ka BP and 150-160 Ka BP The normalised curves presented here show two major peaks of active speleothems, one in the 140-150 Ka BP period and one in the 120-130 Ka BP period. These curves are summed to illustrate individual periods in figure 2.13.

The frequency distribution of speleothem ages in the four 10 kyr periods examined here is not uniform. The largest peak is the 120-130 Ka BP period, which is an expected result of the interglacial warming after the stage 6/5e transition at 128 Ka BP. Between 130 and 140 Ka BP, only 7

speleothem ages are found in the filtered database. By contrast, between 140 and 150 Ka BP there are 21 speleothem ages, and between 150 and 160 Ka BP there are some 10 active speleothems (figure 2.16). As there are more speleothems ages during the period 140 to 150 Ka BP, the SNF curve accurately reflects the distribution of speleothem ages and is not a tailing artefact of the technique of normalisation. By the time of stage 5e, when warm conditions existed in most localities, the number of dated speleothems has greatly increased, with 49 speleothem ages found between the ages of 120 and 130 Ka BP. Figure 2.16 illustrates the double-peaked nature of this isotope stage 6/5e transition in the speleothem SNF record.

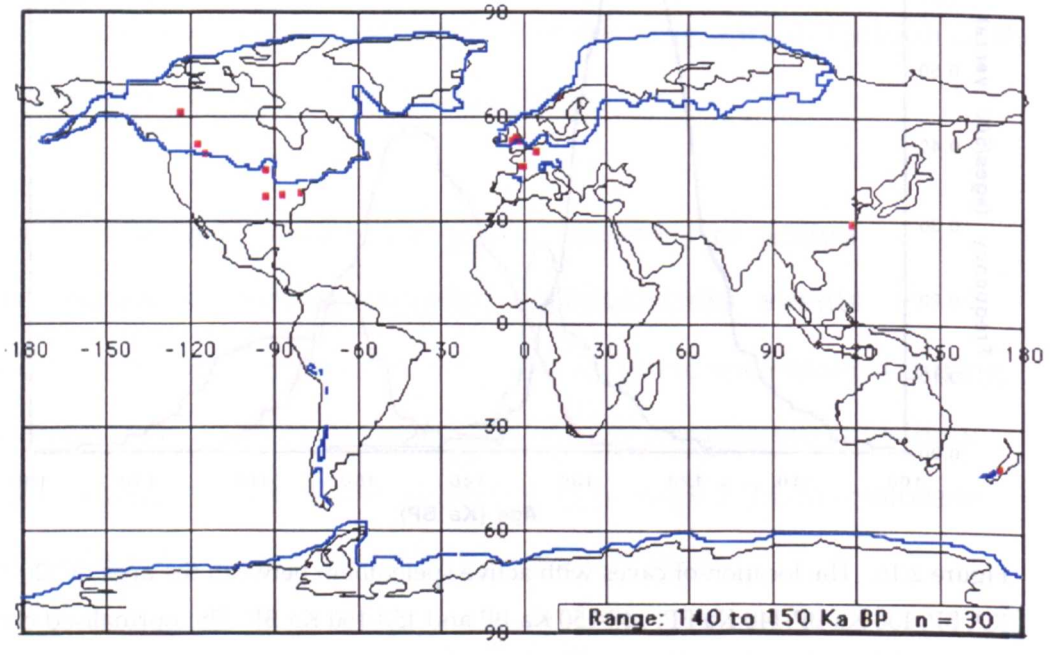

Figure 2.17. The location of speleothems dated by U-series from 140-150 Ka BP Note the speleothems growing in northern Norway and northern Canada, where ice sheets should have been present during the maximum penultimate glaciation. The ice sheet margins in the figure are derived from a variety of publications and are LGM ice-sheets. It is generally supposed that the penultimate glaciation was more extensive than the LGM (Nairn, 1961), so the extent of the ice sheets reconstructed here is probably a minimum estimate.

Although this evidence may reflect the time that speleothems *started* to grow, rather than the number of active speleothems *per se*, this is strong evidence for either a short-lived warm and wet period at 140-150 Ka BP (two-step deglaciation) or an early commencement of climatic amelioration following a maximum penultimate glaciation at 150-160 Ka BP. Figure 2.17 shows the geographical location of U-series dated speleothems during the period 140 to 150 Ka BP, and indicates that some caves were underneath the inferred position of the maximum penultimate glacial ice sheets (more extensive than the LGM ice sheets) in the British Isles, northern Norway and northern Canada. This evidence implies that widespread melting of the penultimate glaciation ice-sheets had commenced by 140 Ka BP, exposing caves and allowing speleothems to grow. For example, see the active speleothems at 60°N in Norway and Canada. There is other evidence for a two-step deglaciation at the penultimate glacial (Seidenkrantz *et al.*, 1996). This evidence, combined with the SNF curve information, suggests that the Devils Hole record may be insufficiently detailed to distinguish between a glacial termination at 140 Ka BP and a two-step deglaciation, similar to the Younger Dryas oscillation after the LGM (Polyak *et al.*, 1995). However, this independently-dated SNF data is some of the best evidence that the Devils Hole record may correctly identify the timing of an isotope stage 6/5e transition.

2.3.3.2. Cold isotope stage 4

Isotope stage 4 is a cold stage with global temperatures approaching the levels of the Last Glacial Maximum (LGM) (e.g. see panel 2 in figure 2.15). In figure 2.15, isotope stage 4 is placed at 63 Ka BP in the SNF record (1st panel), whereas the maximum cold of stage 4 is at 70 Ka BP, 65 Ka BP and 67 Ka BP in V23-82, the orbitally tuned record, and the

Devils Hole record respectively. The younger age for isotope stage 4 in the U-series age distribution may reflect the greater precision of that chronology. The age for stage 4 in the Devils Hole record is based on just two U-series ages, which are in the wrong chronological order (Ludwig *et al.*, 1992), and so that published age for isotope stage 4 may not be reliable.

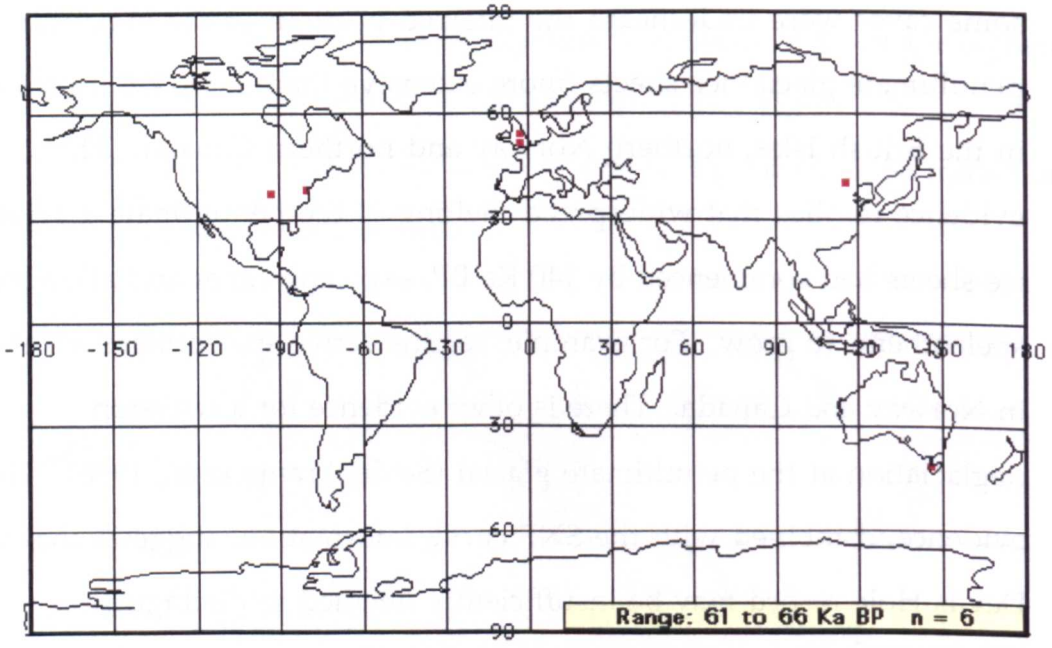

Figure 2.18. The location of caves with active speleothems between the ages of 61 and 66 Ka BP Total number of speleothem ages is 6.

Four of the active speleothems in the period 61-66 Ka BP are found in caves situated between the 45° parallels (figure 2.18). The remaining two are from Ibbeth Peril cave (Yorkshire) (Gascoyne *et al.*, 1983) and G.B. Cave (Mendips) (Atkinson *et al.*, 1978), dated to 61 Ka BP and 63 Ka BP respectively. This small number of speleothem ages may either reflect the presence of ice above caves in the rest of the world, or perhaps the lack of moisture or vegetation on most continents. The first explanation is more likely, given the strength of the stage 4 event in palaeoclimate records which reflect global ice volume (for example, see panel 3 in figure 2.15).

2.3.3.3. Warm isotope stage 3

Three periods of increased numbers of dated speleothems are found in the SNF distribution during isotope stage 3. The central point of the three periods date to 40 Ka BP, 50 Ka BP and 56 Ka BP (figure 2.15). The 50 Ka BP event in the SNF record is the strongest of the three, and has a similar relative magnitude to the central of the three events in isotope stage 3 in the V23-82 record (figure 2.15). The caves from which the dated speleothems were taken are in geographically varied locations. From 39 to 41 Ka BP (figure 2.20) five of the eight speleothem ages are found in low-latitude (between 45°N and 45°S) caves (China and the USA). During the period from 49 to 51 Ka BP (figure 2.21) seven out of the ten dated speleothems also come from caves in low latitudes (China, the Bahamas and Mexico). In the 55 to 57 Ka BP period (figure 2.22) the caves represented are predominantly in the high latitudes – a single exception in the five ages is from a cave in the eastern USA,

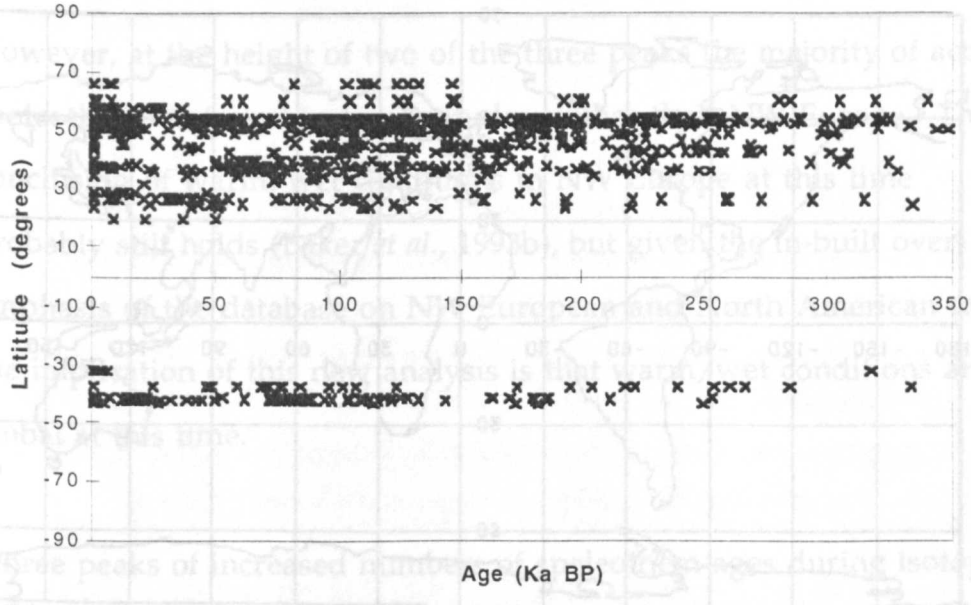

Figure 2.19. The latitudes of caves with dated speleothems from 0-350 Ka BP.

although it must be borne in mind that the majority of the caves sampled are from high latitudes (figure 2.19), which may make the data less representative.

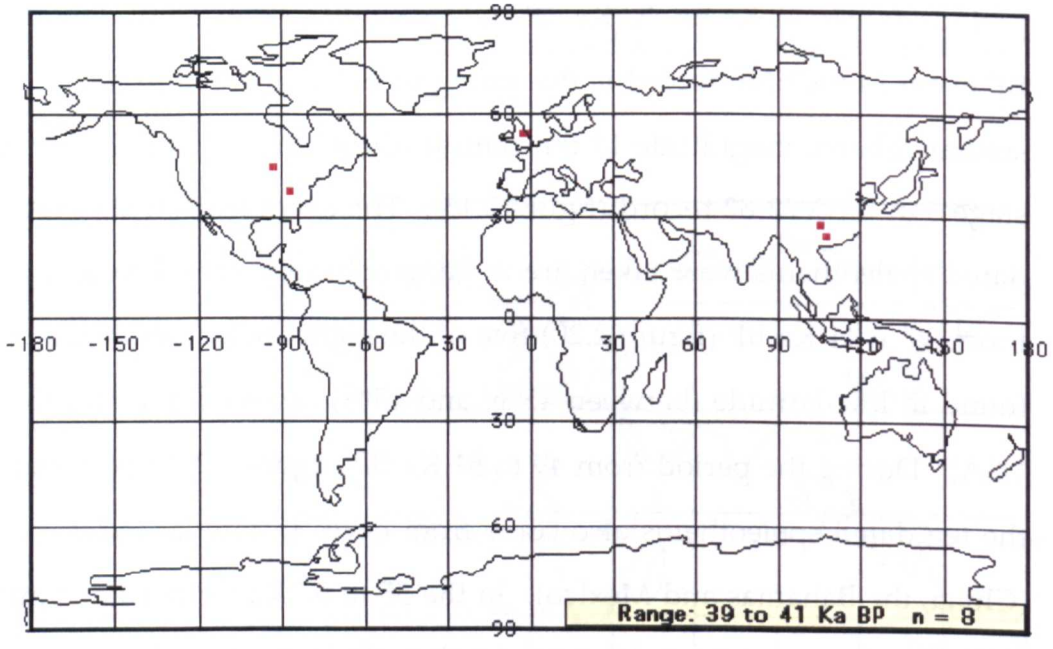

Figure 2.20. Cave sites with U-series dated speleothems for the period 39 to 41 Ka BP Countries with active speleothems include China (4), the USA (2) and England (2).

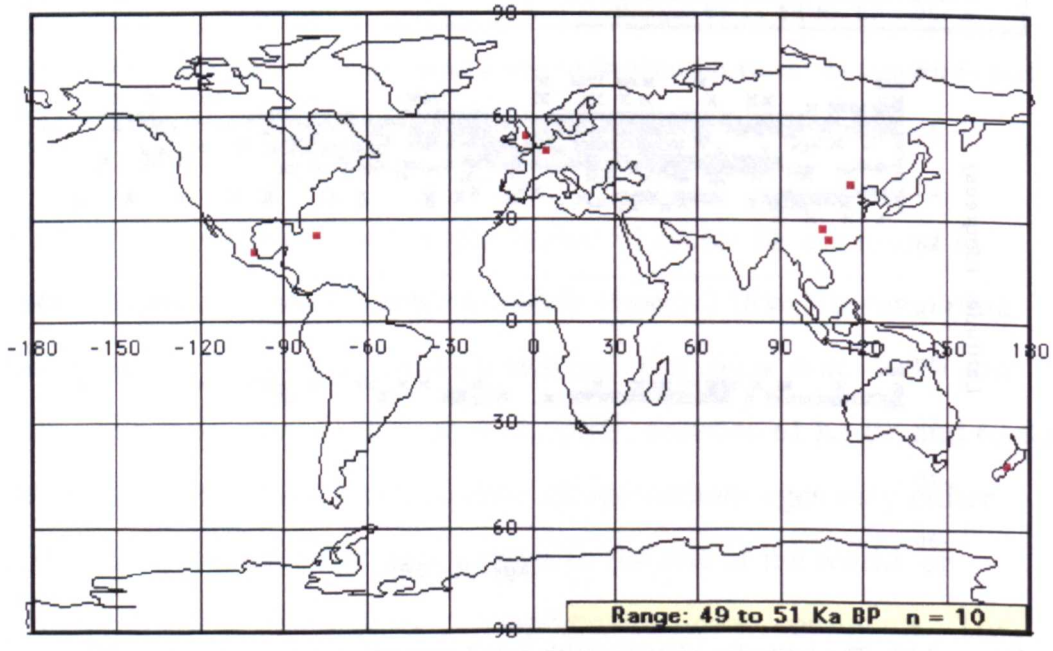

Figure 2.21. Cave sites with U-series dated speleothems for the period 49 to 51 Ka BP Countries with active speleothems include New Zealand, China (4), the Bahamas, England, Mexico (2) and Belgium.

The interpretation previously placed on three peaks (40, 49 and 60 Ka BP) of speleothem ages during isotope stage 3 by Baker *et al.* (1993b) was that they represent warm and/or wet conditions in Northwest Europe.

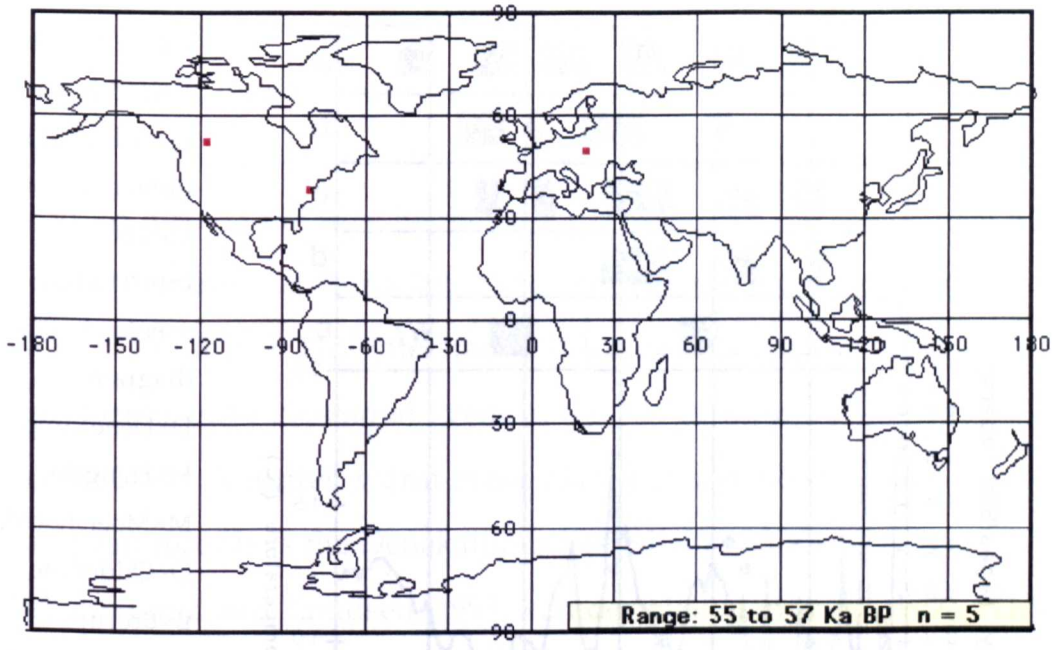

Figure 2.22. Cave sites with U-series dated speleothems for the period 55 to 57 Ka BP Countries with active speleothems include Canada, the USA and Czechoslovakia.

However, at the height of two of the three peaks the majority of active speleothems is found in low latitudes, rather than NW Europe. The conclusion of warm/wet conditions in NW Europe at this time probably still holds (Baker *et al.*, 1993b), but given the in-built over-emphasis of the database on NW European and North American caves, the implication of this new analysis is that warm/wet conditions are global at this time.

The three peaks of increased numbers of speleothem ages during isotope stage 3 may correspond to a warmer phase in Britain, termed the Upton Warren (UW) interstadial (*sensu lato*) complex (Coope, 1977). There is a great deal of discussion in the literature concerning the nature and timing of the individual events of this interstadial complex in a variety

of global locations. In Britain the UW interstadial complex is divided into three parts (figure 2.23), termed the Upton Warren, Chelford and Wretton interstadials (Shotton, 1986). In Europe, these periods may

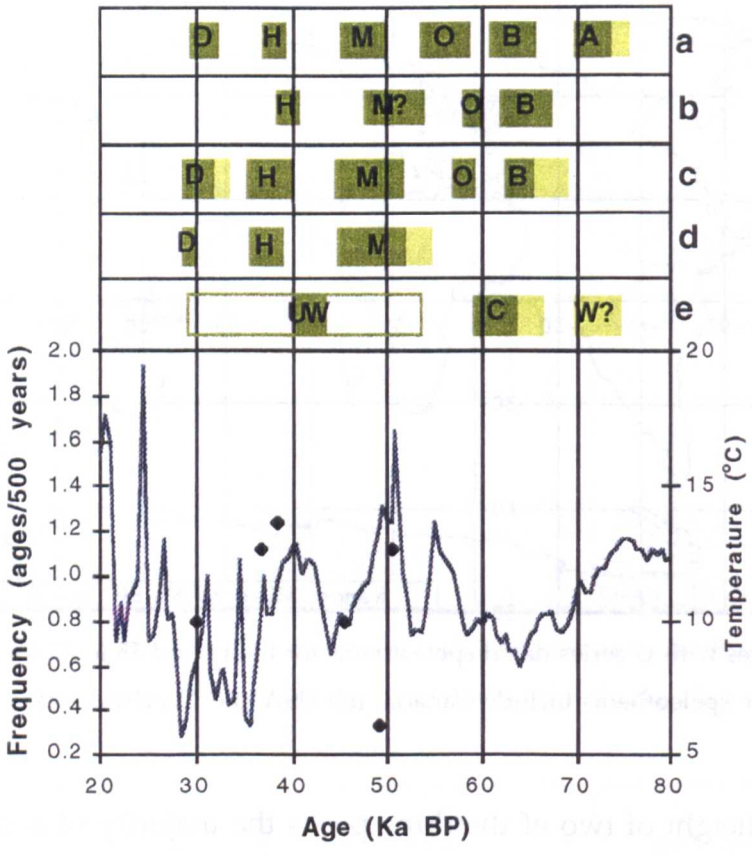

Figure 2.23. Isotope stage 3 in the SNF record, with the timing of North European interstadial events. In this diagram, D=Denekamp, H=Hengelo, M=Moershoofd, O=Odderade, B=Brörup, A=Amersfoort, UW=Upton Warren *sensu stricto* (dark shading), *sensu lato* (outline), C=Chelford and W=Wretton. Part a shows the standard six European interstadials in isotope stage 3 (Lundqvist, 1986; Vandenberghe, 1992). Part b indicates interstadials found near Eerbeek, Netherlands (van der Meer *et al.*, 1984). Part c is an interpretation of earlier work in the Netherlands by van der Hamman *et al.* (1967). Part d details work undertaken by Kolstrup & Wijmstra (1977), also in the Netherlands and part e represents British interstadials of the period (Shotton, 1986). The bottom graph is the SNF curve, 20–80 Ka BP. Also plotted (♦) on the bottom graph are mean July temperature estimates for the Netherlands (Kolstrup and Wijmstra, 1977). The light shading areas indicate possible age ranges unconfirmed by dating.

correspond to the Hengelo, Odderade/Brörup and Amersfoot interstadials respectively (Lundqvist, 1986). In addition, there is (temporally) equivocal evidence for 6 separate interstadials in North European isotope stage 3 (Lundqvist, 1986), making it difficult to assign

definite names to each feature in the SNF curve. The Chelford interstadial is estimated to date to 60.1 Ka BP and the Upton Warren interstadial *sensu stricto* is placed at 41.9 Ka BP by ^{14}C dating (Worsley, 1980). However, there is some evidence that the Chelford warm period is much older, and may be equivalent to isotope stage 5 in age (Rendell *et al.*, 1991). Given the imprecision of ^{14}C dates at this age, the Upton Warren interstadial *sensu stricto* may be the 40 Ka BP event and the Chelford interstadial may be the 56 Ka BP event in the speleothem SNF record. The event at 50 Ka BP in the SNF record corresponds to no event in the British UW interstadial complex, but may be equivalent to the Moershoofd interstadial event in the North European record (figure 2.23). A further warm event placed in isotope stage 3 in North European records is the Denekamp interstadial at 30 Ka BP (Seidenkrantz and Knudsen, 1993; van der Hamman *et al.*, 1967). This event was not as warm as the previous interstadials in the UW complex, and for example, is represented by grass tundra conditions in Poland (Krzyszkowski *et al.*, 1993). In the V23-82 core, this period is seen as a small return to warmer conditions (30 Ka BP) during the general cooling to the maximum glacial. The SNF record also contains this short-lived interstadial event, centred around 30 Ka BP (figure 2.15).

The Chelford interstadial was an event which did not approach full interglacial warm temperatures (West, 1968), and it is interesting to note that the peak of speleothem ages at 56 Ka BP is smaller than both the middle peak of ages at 50 Ka BP and the peak of ages at the last interglacial at 110 Ka BP (figure 2.13).

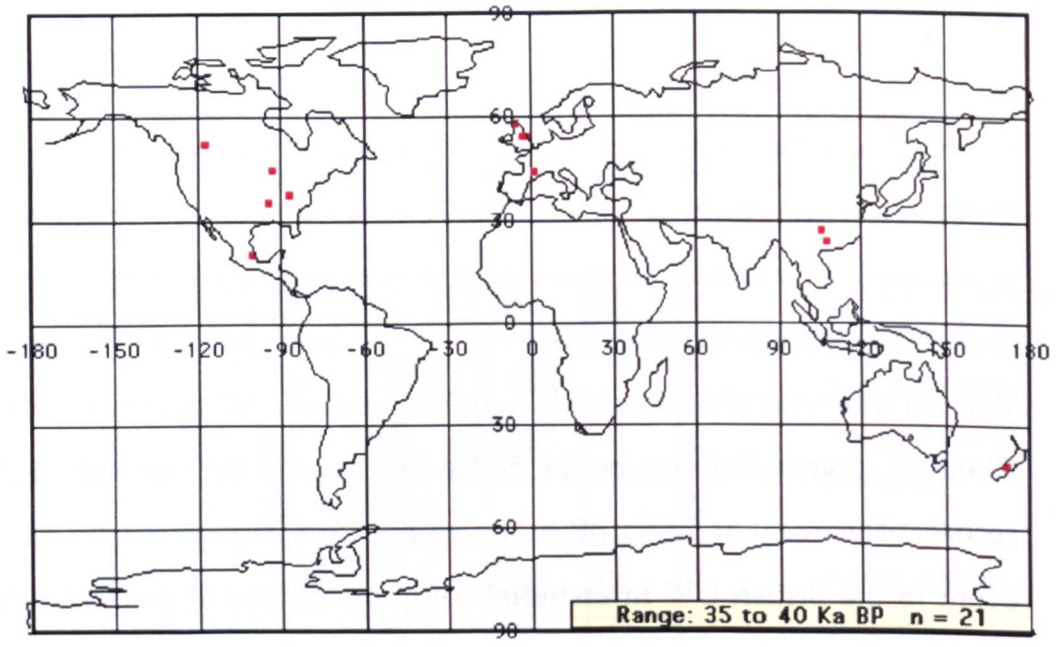

Figure 2.24. Cave sites with U-series dated speleothems for the period 35 to 40 Ka BP Countries with speleothem ages include Canada, the USA and Czechoslovakia, where ice sheets may have been present during the maximum penultimate glaciation.

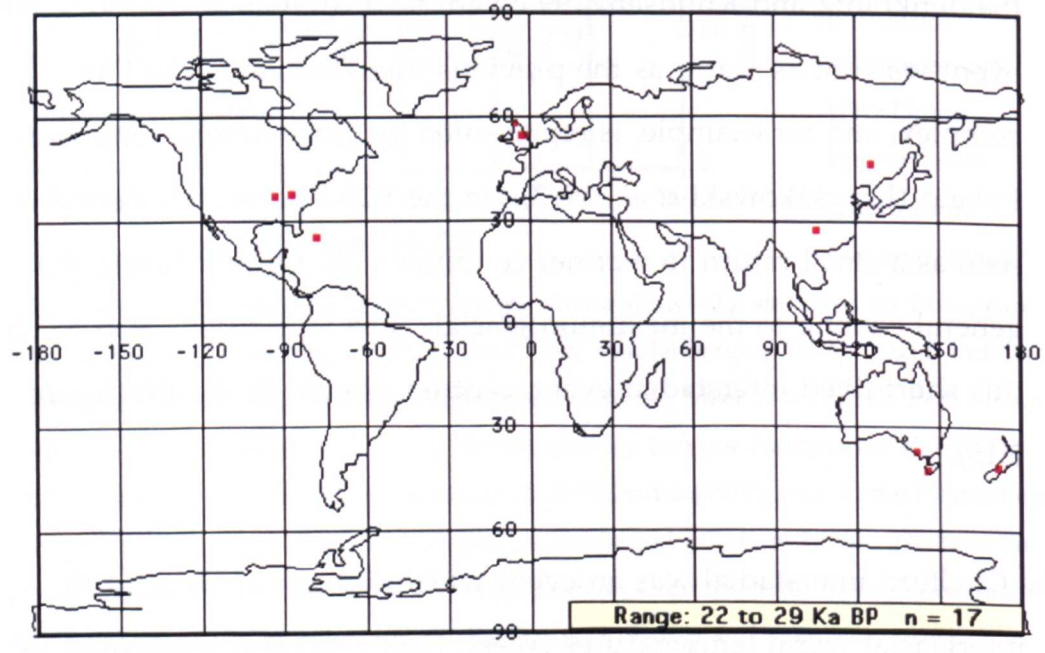

Figure 2.25. Cave sites with U-series dated speleothems for the period 22 to 29 Ka BP

2.3.3.4. Isotope stage 2 – the Last Glacial Maximum

Immediately prior to the penultimate glaciation, dated speleothems in Canada, the British Isles and northern Norway are found underneath the position of the maximum ice sheet at 140-150 Ka BP (section 2.3.3.1).

In a similar manner, dated speleothems are found immediately prior (35-40 Ka BP) to the Last Glacial Maximum underneath the position of the LGM ice sheets (figure 2.24) in Canada and the British Isles, indicating the ice was not there at that time.

During the period leading up to the LGM there are several caves with active speleothems in geographical locations where it might be expected that none would grow (figure 2.25). For example, in the north of Scotland several active speleothems have been dated at 26 Ka BP (Baker *et al.*, 1993a). This appears to suggest that the northern British ice sheet had not yet advanced sufficiently to cover this cave site and restrict speleothem growth. As Denmark was also free of ice until a similar time during isotope stage 2 (Lundqvist, 1986), this evidence may indicate a rapid expansion in ice volume from 25 Ka BP to the LGM at 20 Ka BP. Apart from one further active speleothem in Yorkshire during this period, the majority of the rest of the speleothem ages are from lower latitudes in both hemispheres. An important point about the SNF distribution in figure 2.15 at this time is that the large peaks in frequency partly reflect the greater precision of these ages. It is for this reason that no analysis of variations in the SNF distribution during the Late Glacial and Holocene are attempted here.

2.4. Conclusions

The aim of this chapter was to evaluate the temporal and spatial distribution of U-series dated speleothems and their relationship to palaeoclimate change. The main conclusions of this evaluation are:

1) Both the magnitude and location of palaeoclimate events in the SNF curve are strongly similar to those events in other palaeoclimate proxies (figure 2.15). In addition, the age control on the SNF distribution is more precise than that for other proxies (particularly those dated with radiocarbon techniques – see Chapter 5), because it is based on the frequency of an independent chronological technique. For this reason, the chronological control on (undateable) palaeoclimate proxies such as deep-sea core $\delta^{18}O$ records may need to be revised to take into account this new information.

2) Relationships between the geographical location of U-series dated speleothems and global Quaternary palaeoclimate change are revealing. For example, speleothems dated by U-series are found underneath the LGM position of the North American and British ice sheets between 35 and 40 Ka BP, which is 15-20 kyrs prior to the reconstructed LGM extent of the ice at 20 Ka BP. Although it was stated earlier that the LGM extent *sensu stricto* lasted from 20 Ka BP to 18 Ka BP, the normalised $\delta^{18}O$ record (3rd panel, figure 2.15), reflecting global ice volume, indicates the maximum extent of the ice sheets lasted approximately 7 kyrs (15-22 Ka BP) around the LGM. Thus, the presence of speleothems underneath the later position of the extensive North American and British LGM ice sheets may indicate the minimum position of ice sheets forming over the 15-20 kyrs prior to the LGM. Intriguingly, the last 'warm' summer SST in North Atlantic ocean core V23-82 (panel 2, figure 2.15) is also found just prior to 40 Ka BP.

3) Dated speleothems are also found beneath the position of the penultimate glacial ice sheets 15 kyrs before the maximum glacial

extent. However, it is difficult to establish a chronology of ice advance, speleothem activity and ice retreat for this event because the timing and duration of the penultimate glacial maximum are poorly constrained in other palaeoclimate records. One explanation may be that the first peak in speleothem ages at 140-150 Ka BP represents a 'false start' to deglaciation, followed by a period of 10 kyrs or more of further glacial conditions. The Devils Hole record militates against this interpretation, as it reveals no return to glacial climate in the period 130-140 Ka BP. Instead, the 'double peak' in speleothem frequency at this earlier glacial/interglacial transition, taken with the Devils Hole palaeoclimate record, may indicate an earlier amelioration of global climate after the penultimate glacial than previously recognised.

4) There may be some cause for concern when examining this data set because it does not include speleothem ages from all continents. The sampling of U-series ages in the compilation reflects to some extent the location of U-series laboratories and the field sites of their researchers. Climatic conditions are certainly a factor in speleothem growth (Baker and Smart, 1995), and global climatic conditions were very different during the Quaternary (CLIMAP, 1976), but inferring climatic conditions beyond available water and CO_2 from the presence of active speleothems may be a step too far.

5) The strong link between the location of dated speleothems during the Last Glacial Maximum and the distance to ice sheet margins is perhaps an indication of climatic control on the geographical location of dated speleothems. The details of geographical location of dated speleothems during the Quaternary requires further development.

6) The importance of geographical location when examining speleothem growth during the Quaternary is emphasised by the double-peaked termination of the penultimate glacial (isotope stage 6/5e) when two peaks of speleothem growth at 140-150 Ka BP and 120-130 Ka BP may indicate two periods of glacial termination. The presence of active speleothems beneath the previously assumed position of the maximum ice sheets before 140 Ka BP indicates the Devils Hole record (Ludwig *et al.*, 1992; Winograd *et al.*, 1992) cannot be dismissed as a valid record of the termination of the penultimate glaciation.

2.5. References

Atkinson, T. C., Smart, P. L., Harmon, R. S., and Waltham, A. C. (1978). Palaeoclimatic and geomorphic implications of $^{230}Th/^{234}U$ dates on speleothems from Britain. *Nature* **272,** 24-28.

Baker, A., and Smart, P. L. (1995). Recent flowstone growth rates: Field measurement in comparison to theoretical predictions. *Chemical Geology* **122,** 121-128.

Baker, A., Smart, P. L., Edwards, R. L., and Richards, D. A. (1993a). Annual growth banding in a cave stalagmite. *Nature* **364,** 518-520.

Baker, A., Smart, P. L., and Ford, D. C. (1993b). Northwest European palaeoclimate as indicated by growth frequency variations of secondary calcite deposits. *Palaeogeography, Palaeoclimatology, Palaeoecology* **100,** 291-301.

Begét, J. E. (1996). Tephrochronology and paleoclimatology of the Last Interglacial–Glacial cycle recorded in Alaskan loess deposits. *Quaternary International* **34-36,** 121-126.

Cherdyntsev, V. V., Kazachevskiy, I. V., and Kuz'mina, Y. A. (1965). Dating of Pleistocene carbonate formations by the thorium and uranium isotopes. *Geochemistry International* **2,** 794-801.

CLIMAP. (1976). The surface of the ice-age Earth. *Science* **191,** 1131-1137.

Coope, G. R. (1977). Fossil coleopteran assemblages as sensitive indicators of climatic changes during the Devensian (Last) cold stage. *Proceedings of the Royal Society, Series B* **280,** 313-337.

Falgueres, C., and de Lumley, H. (1992). U-series dates for stalagmitic flowstone (Riss/Wurm interglaciation) at Grotte du Lazaret, Nice, France. *Quaternary Research* **38,** 227-233.

Ford, D. C., and Williams, P. W. (1989). "Karst Geomorphology and Hydrology." Chapman & Hall, London.

Gallup, C. D., Edwards, R. E., and Johnson, R. G. (1994). The timing of high sea levels over the past 200,000 years. *Science* **263,** 796-800.

Gascoyne, M., Schwarcz, H. P., and Ford, D. C. (1983). Uranium-series ages of speleothems from Northwest England: correlation with Quaternary climate. *Philosophical transactions of the Royal Society of London, Series B* **301,** 143-164.

Goede, A., and Harmon, R. S. (1983). Radiometric dating of Tasmanian speleothems - evidence of cave evolution and climatic change. *Journal of the Geological Society of Australia* **30,** 89-100.

Gordon, D., and Smart, P. L. (1984). Comments on Speleothems, Travertines and Paleoclimates by G.J. Hennig, Grun, R. & Brunnacker, K. *Quaternary Research* **22,** 144-147.

Gordon, D., Smart, P. L., Ford, D. C., Andrews, J. N., Atkinson, T. C., Rowe, P. J., and Christopher, N. S. J. (1989). Dating of late Pleistocene interglacial and interstadial periods in the United Kingdom from speleothem growth frequency. *Quaternary Research* **31,** 14-26.

Harmon, R. S. (1979). U-series dating of speleothems and a glacial chronology for western North America. *National Speleological Society Bulletin* **41,** 102-104.

Harmon, R. S., Thompson, P., Schwarcz, H. P., and Ford, D. C. (1975). Uranium-series dating of speleothems. *National Speleological Society Bulletin* **37,** 21-33.

Hennig, G. J., Grun, R., and Brunnacker, K. (1983). Speleothems, travertines and paleoclimates. *Quaternary Research* **20,** 1-29.

Jaffey, A. H., Flynn, K. F., Glendenin, L. E., Bentley, W. C., and Essling, A. M. (1971). Precision measurement of half-lives and specific activities of ^{235}U and ^{238}U. *Chemical Review* **4,** 1889-1906.

Jakucs, L. (1977). "Morphogenetics of Karst Regions." Hilger, Bristol.

Kaufman, A. (1993). An evaluation of several methods for determining $^{230}Th/^{238}U$ ages in impure carbonates. *Geochimica et Cosmochimica Acta* **57,** 2303-2317.

Kolstrup, E., and Wijmstra, T. A. (1977). A playnological investigation of the Moershoofd, Hengelo, and Denekamp interstadials in the Netherlands. *Geologie en Mijnbouw* **56,** 85-102.

Krzyszkowski, D., Balwierz, Z., and Pyszynski, W. (1993). Aspects of Weichselian Middle Pleniglacial stratigraphy and vegetation in central Poland. *Geologie en Mijnbouw* **72,** 131-142.

Ku, T.-L., and Liang, Z.-C. (1984). The dating of impure carbonates with decay-series isotopes. *Nuclear instruments and methods in physics research* **223,** 563-571.

Lauritzen, S.-E. (1991). Uranium series dating of speleothems: A glacial chronology for Nordland, Norway, for the last 600 ka. *Striae* **34,** 127-133.

Ludwig, K. R., Simmons, K. R., Szabo, B. J., Winograd, I. J., Landwehr, J. M., Riggs, A. C., and Hoffman, R. J. (1992). Mass-spectrometric ^{230}Th-^{234}U-^{238}U dating of the Devils Hole calcite vein. *Science* **258,** 284-287.

Ludwig, K. R., Simmons, K. R., Winograd, I. J., Szabo, B. J., Landwehr, J. M., and Riggs, A. C. (1993). Last interglacial in Devils Hole - reply. *Nature* **362,** 596.

Lundqvist, J. (1986). Stratigraphy of the central area of the Scandinavian glaciation. *Quaternary Science Reviews* **5,** 251-268.

Martinson, D. G., Pisias, N. G., Hays, J. D., Imbrie, J., Moore, T. C. J., and Shackleton, N. J. (1987). Age dating and the orbital theory of the Ice Ages: development of a high-resolution 0 to 300,000 year chronostratigraphy. *Quaternary Research* **27,** 1-29.

Meadows, J. W., Armani, R. J., Callis, E. L., and Essling, A. M. (1980). Half-life of ^{230}Th. *Physical Review C* **22,** 750-754.

Nairn, A. E. M. (1961). Descriptive palaeoclimatology, pp. 380. Interscience, New York.

Pisias, N. G., Martinson, D. G., Moore, T. C. J., Shackleton, N. J., Prell, W., Hays, J., and Boden, G. (1984). High resolution stratigraphic correlation of benthic oxygen isotopic records spanning the last 300,000 years. *Marine Geology* **56,** 119-136.

Polyak, L., Lehman, S. J., Gataullin, V., and Jull, A. J. T. (1995). Two-step deglaciation of the southeastern Barents Sea. *Geology* **23,** 567-571.

Przybylowicz, W., Schwarcz, H. P., and Latham, A. G. (1991). Dirty calcites: 2. Uranium-series dating of artificial calcite-detritus mixtures. *Chemical Geology (Isotope Geoscience Section)* **86,** 161-178.

Rendell, H., Worsley, P., Green, F., and Parks, D. (1991). Thermoluminescence dating of the Chelford Interstadial. *Earth and Planetary Science Letters* **103,** 182-189.

Sancetta, C., Imbrie, J., and Kipp, N. G. (1973). Climatic record of the past 130,000 years in North Atlantic deep-sea core V23-82: Correlation with the terrestrial record. *Quaternary Research* **3,** 110-116.

Schwarcz, H. P., and Latham, A. G. (1984). Uranium-series age determination of travertines from the site of Vertesszollos, Hungary. *Journal of Archaeological Science* **11,** 327-336.

Schwarcz, H. P., and Latham, A. G. (1989). Dirty calcites: Uranium-series dating of contaminated calcite using leachates alone. *Chemical Geology* **80,** 35-43.

Seidenkrantz, M. S., Bornmalm, L., Johnsen, S. J., Knudsen, K. L., Kuijpers, A., Lauritzen, S.-E., Leroy, S. A. G., Mergeai, I., Schweger, C., and van Vliet, L. B. (1996). Two-step deglaciation at the oxygen isotope stage 6/5e transition; the Zeifen-Kattegat climate oscillation. *Quaternary Science Reviews* **15,** 63-75.

Seidenkrantz, M. S., and Knudsen, K. L. (1993). Middle Weichselian to Holocene palaeoecology in the eastern Kattegat, Scandinavia: foraminifera, ostracods and ^{14}C measurements. *Boreas* **22,** 299-310.

Shackleton, N. J. (1993). Last interglacial and Devil's Hole. *Nature* **362,** 596.

Shotton, F. W. (1986). Glaciations in the United Kingdom. *Quaternary Science Reviews* **5,** 293-297.

Thompson, P., Schwarcz, H. P., and Ford, D. C. (1974). Continental Pleistocene climatic variations from speleothem age and isotopic data. *Science* **184,** 893-895.

van der Hamman, T., Maarleveld, G. C., Vogel, J. C., and Zagwijn, W. H. (1967). Stratigraphy, climatic succession and radiocarbon dating of the last glacial in the Netherlands. *Geologie en Mijnbouw* **46,** 79-95.

van der Meer, J. J. M., Slotboom, R. T., and de Vires-Bruynsteen, I. M. E. (1984). Lithology and palynology of Weichselian alluvial fan deposits near Eerbeek, The Netherlands. *Boreas* **13,** 393-402.

Vandenberghe, J. (1992). Geomorphology and climate of the cool oxygen isotope stage 3 in comparison with the cold stages 2 and 4 in The Netherlands. *Zeitschrift für Geomorphologie, N.F. Suppl.* **86,** 65-75.

West, R. G. (1968). "Pleistocene Geology and Biology." Longman, London.

Winograd, I. J., and Coplen, T. B. (1989). Great Basin calcite vein and the Pleistocene time scale - response. *Science* **246,** 262-263.

Winograd, I. J., Coplen, T. B., Landwehr, J. M., Riggs, A. C., Ludwig, K. R., Szabo, B. J., Kolesar, P. T., and Revesz, K. M. (1992). Continuous 500,000-year climate record from vein calcite in Devils Hole, Nevada. *Science* **258,** 255-260.

Worsley, P. (1980). Problems in radiocarbon dating the Chelford Interstadial of England. *In* "Timescales in Geomorphology." (R. A. Cullingford, D. A. Davidson, and J. Lewin, Eds.), pp. 289-304. John Wiley & Sons, Chichester.

Chapter 3: Reconstructing Irish palaeoclimate and environmental conditions during the Late Glacial from speleothems

3.1. Introduction

Many current models of Late Glacial climate change have a common geographical focus – the North Atlantic ocean. Changes in oceanic circulation (Broecker *et al.*, 1990), atmospheric circulation (Broecker and Denton, 1990) and ice volume in the North Atlantic (Ruddiman and McIntyre, 1981) have been invoked in hypotheses explaining short-term changes in global climate during the transition between glacial and interglacial conditions. The island of Ireland occupies a central geographical position in the North Atlantic. Climate in present-day Ireland is dominated by warm surface water of the North Atlantic Drift (NAD). Without this 'heat-engine' providing both mild temperatures and reliable precipitation, the climate of the British Isles would probably be closer to that of the Canadian Maritime Provinces – less equable and subject to harsh winters (Barry and Chorley, 1987). NAD is driven by oceanic processes north of the British Isles, where cool, dense, north-bound salty water sinks from the surface of the Atlantic to form a deep south-bound current returning to the Caribbean. This North

Atlantic Deep Water (NADW) formation appears to be a dominant process in the global ocean-atmosphere system (Broecker and Denton, 1989), and is responsible for much more than simple climate amelioration in the British Isles. For example, without transport of warm water to the North Atlantic there would be less reinforcement of Rossby waves (the long waves of atmospheric circulation) by differential heating and atmospheric circulation would be weakened (Barry and Chorley, 1987). NAD maintains the equable annual temperature of the British Isles and means that the British Isles are some 16°C warmer in winter than the latitudinal average (Barry and Chorley, 1987).

Data from the last 20,000 years show there have been several instances when the site of NADW formation altered or NADW formation was weaker than the present-day (Rahmstorf, 1994). This period includes the termination of the Last Glacial Maximum (LGM) (Yu *et al.*, 1996) and transition to the Holocene, termed the Late Glacial. It is now understood that the Late Glacial was climatically exceptionally complicated, involving large-scale re-organisations of the ocean-atmosphere system (Broecker and Denton, 1990).

Here I examine palaeoclimate changes of the Late Glacial in Ireland through the geochemistry of speleothems. These secondary deposits form where percolating calcium carbonate ($CaCO_3$) saturated waters arrive in limestone caves and CO_2 de-gases from solution, depositing calcite ($CaCO_3$) in layers from the ceiling (stalactites), along walls (flowstone) or on the floor (stalagmites). Over time, calcite layers record changes in both cave environment and by implication, the environment outside the cave. In general, cave air temperature reflects

the mean annual temperature outside the cave (Ford and Williams, 1989), although there are exceptions to this rule in caves with large volumes (Cropley, 1965) or caves with strong air- (Nepstad and Pisarowicz, 1989) or stream-flow (Lange, 1954). Five palaeoclimate proxies are introduced for two caves in southern Ireland to reconstruct conditions in Ireland during the Late Glacial and Holocene periods.

3.2. The Irish Late Glacial and Holocene

The last glacial-interglacial transition in NW Europe is traditionally divided into the Oldest Dryas-, Bølling-, Older Dryas-, Allerød-, Younger Dryas-, and Preboreal on a chronostratigraphic basis (Mangerud *et al.*, 1974; Wohlfarth, 1996). These terms have some local equivalents in the British Isles, and the relationship between the main (originally Scandanavian) NW European terms and local equivalents is presented here (table 3.1).

Climate period	Event	British name	European name		Stage
Littletonian		Flandrian	Holocene	W	1
	Nahanaghan	Loch Lomond	Younger Dryas	S	
	Woodgrange	Windermere	Bølling-Allerød	IS	
	Glenavy	Dimlington	Weichselian	S	
Midlandian		Devensian	Weichselian	C	2

Table 3.1. Irish palaeoclimate periods and Late Glacial climate events with British and European equivalents. W denotes a warm period; C, cool period; IS, interstadial; S, stadial.

Irish Late Glacial palaeoclimatic change has been studied mainly through pollen analyses from a variety of sites (Andrieu *et al.*, 1994; Barnosky, 1988; Edwards and Warren, 1985; Smith and Goddard, 1991; Walker *et al.*, 1994) and from a examination of moraines (Bowen *et al.*, 1986).

According to Bowen *et al.* (1986), Jessen (1949) divided the Irish Late Glacial into three periods of Older *Salix herbacea;* Late Glacial birch; and Younger *Salix herbacea.* Watts (1985) suggested that this scheme was too simplistic and proposed a non-formal sequence of events outlined in figure 3.1. The most fundamental division of the Late Glacial period in Ireland is made between a "Late Glacial Interstadial" (13.0–11.0 ^{14}C Ka BP) and the "Younger Dryas Stadial" (11.0–10.0 ^{14}C Ka BP) (Walker *et al.,* 1994). Figure 3.1 shows that several further divisions of Irish Late Glacial palaeoclimate may be made.

Prior to 13.0 ^{14}C Ka BP (15.4 Ka $BP_{cal.}$ [calibrated years]) the mean July temperature was below 7°C and extensive periglacial activity with skeletal soils and permafrost limited vegetation to an *Artemisia*-Gramineae assemblage. Climate amelioration after 13.0 ^{14}C Ka BP permitted soil development in a more stable landscape and low scrub and heathland vegetation communities resulted, developing into a *Juniperus* or *Juniperus-Empetrum* assemblage by 12.0 ^{14}C Ka BP (14.0 Ka $BP_{cal.}$). This early phase of the Late Glacial interstadial is termed the Bølling in European records, but forms an early part of the Woodgrange interstadial complex in Ireland (table 3.1). The Irish equivalent of the Allerød (the late Woodgrange) is characterised by a deteriorating environment with discontinuous permafrost, causing itermittent periods of soil erosion. The vegetation has changed to open grassland with *Helianthemum* by this time. At 11.0 ^{14}C Ka BP (12.9 Ka $BP_{cal.}$) the climate deteriorates rapidly, causing destruction of the interstadial soil and mineral inwash in lakes. Tundra and low alpine scrub vegetation develops, with *Rumex* and *Artemisia* characterising pollen assemblages, and small cirque glaciers are found above 350m. Extensive permafrost features are found in the landscape, including

pingos, ice-wedges, involutions, solifluction, protalus ramparts and rock glaciers (Coxon, in press). The cirque moraines at Lough Nahanagan, County Wicklow, give the name to the Irish Younger Dryas equivalent event – the Nahanagan Stadial, dated between 11.0 and 10.5 ^{14}C Ka BP (12.9 – 12.4 Ka BP$_{cal.}$). Colhoun and Synge (1980) suggest the regional snowline was depressed by approximately 470m and Ireland was 7.2°C cooler during the YD than the present day (Bowen *et al.*, 1986). After 10.5 ^{14}C Ka BP, the climate ameliorated and soil stabilisation and development occurred, permitting open scrub, (and later open woodland), dominated by *Juniperus* and later also *Betula* (Coxon, in press).

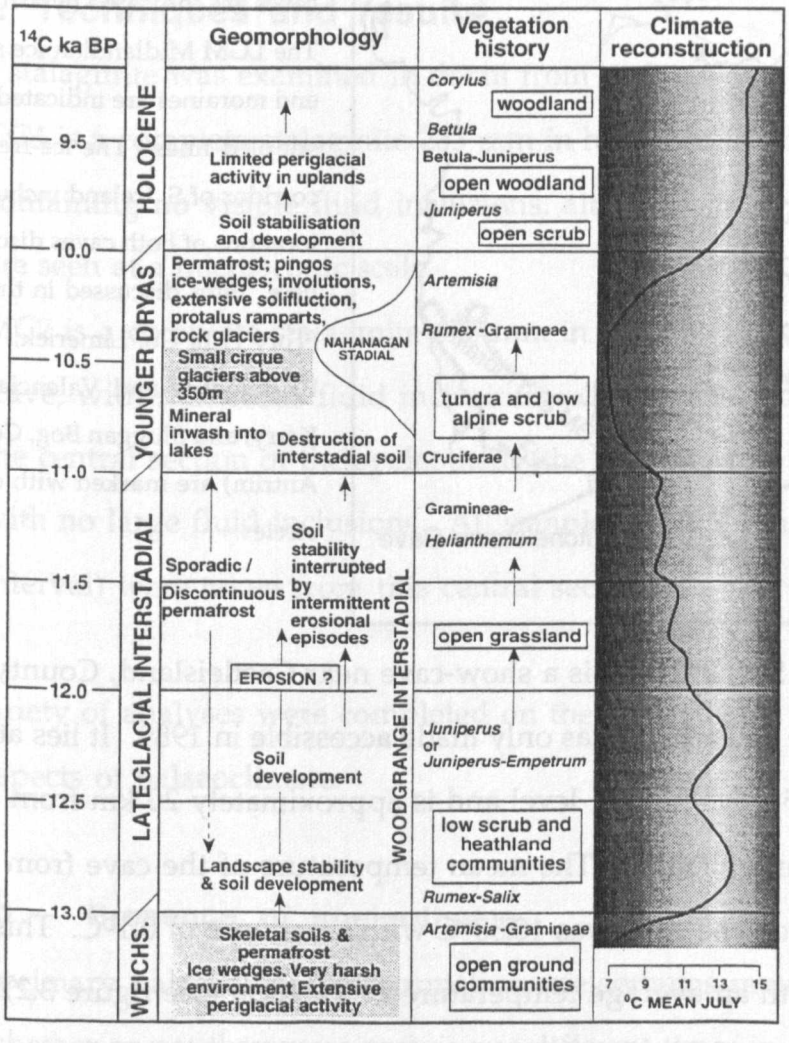

Figure 3.1. Events of the Irish Late Glacial, from Coxon (in press).

3.3. Sites and samples

Two cave sites were chosen in south-central and south-western Ireland to examine Irish palaeoclimate during the Late Glacial. Two sites were selected to examine the effect on speleothem geochemistry of distance from a precipitation source (the North Atlantic). The majority of studies examine a single speleothem record, possibly because of the work involved in analysing comprehensively more than one speleothem.

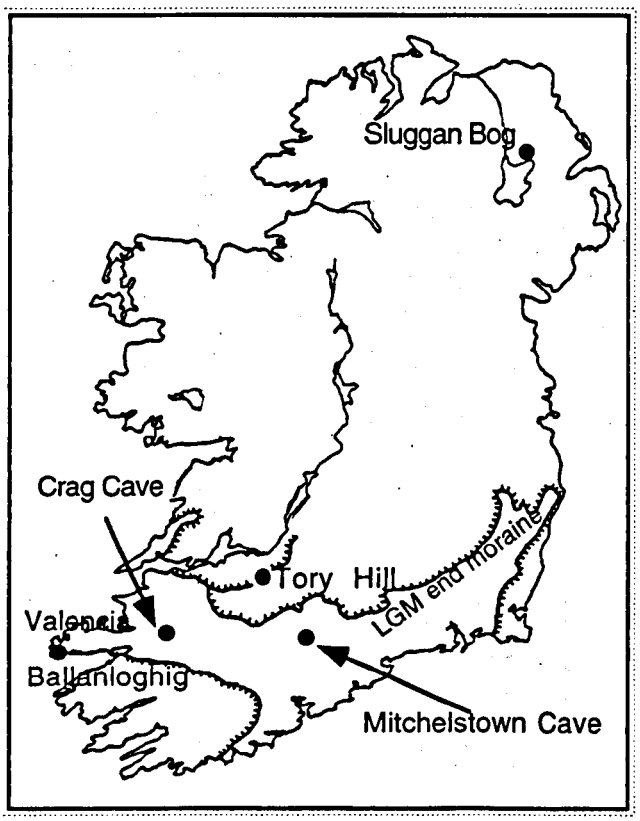

Figure 3.2. Map of Ireland showing sites discussed in the text. Crag and Mitchelstown caves are indicated by arrows. The LGM Midlandian ice sheet end moraines are indicated by stippled lines. The ice-free corridor of S. Ireland includes the locations of both caves discussed here. Sites discussed in the text (Tory Hill, Co. Limerick; Ballinloghig and Valencia, Co. Kerry; and Sluggan Bog, Co. Antrim) are marked with closed circles.

Crag Cave (52°15'N, 9°24'W) is a show-cave near Castleisland, County Kerry (figure 3.2) which was only made accessible in 1989. It lies at an altitude of 45 m above sea level and is approximately 20 km from the Atlantic ocean at Tralee. The mean temperature of the cave from March 1995 to June 1996 was 10.38°C with a variance of 0.1°C. This compares with an average temperature at Valencia (see figure 3.2) of 10.4°C for the same period. These data suggest the temperature in Crag

Cave is a good approximation of average temperature in Ireland at present and may have also been so in the past.

Mitchelstown Cave (52°18'N, 8°11'W) is also a show cave, near Mitchelstown, County Tipperary, lying at an altitude of 80 m, approximately 150 km from the Atlantic. No data are available on the temperature of Mitchelstown Cave during the year, but the cave is likely to approximate mean annual temperature in the same way as Crag Cave, particularly as Mitchelstown Cave contains no flowing stream.

3.4. Techniques and results

One stalagmite was examined in detail from each cave:

a) CC4 is a complete stalagmite 283 mm in height from Crag Cave, containing no visible fluid inclusions, although many fluid inclusions are seen at a microscopic scale.

b) MC2 is a complete stalagmite 638 mm in height, from Mitchelstown Cave, with numerous fluid inclusions in the calcite matrix, although the central section of the speleothem (the growing tip) is solid calcite with no large fluid inclusions. All samples (at a 5 mm sampling interval) were taken from this central section.

A variety of analyses were completed on the speleothems to examine aspects of palaeoclimate:

3.4.1. Presence of speleothems.

The primary palaeoclimatic information speleothems may provide is whether or not they were growing at different times in the past. Lack of calcite deposition may indicate insufficient dripwater as a result of

reduced rainfall – possibly due to glacial or periglacial conditions. Growth may also cease when the dripwater path is diverted or the speleothem is covered by sediment or water. Another growth-limiting factor is the availability of soil CO_2 which forms weak carbonic acid with rainwater and enhances limestone solution. Reductions in rainfall or partial pressure of soil CO_2 (pCO_2) may both inhibit speleothem growth and act as rate-limiting factors. Most soil CO_2 derives from plant respiration and bacterial decay, so a reduction in plant productivity may limit the number of active speleothems on a regional scale (Baker *et al.*, 1993b). Several authors have used the number of growing speleothems from several caves within a single region as a proxy indicator for Quaternary climate change (Atkinson *et al.*, 1986; Baker *et al.*, 1993b; Gascoyne, 1984). In a single speleothem, cessation of calcite deposition produces an hiatus in growth.

A total of 18 uranium-thorium thermal ionisation mass spectrometric (U/Th TIMS) ages were obtained on speleothem calcite using Finnigan MAT261 and MAT262 mass spectrometers equipped with pulse counting and retarding potential quadrupole (RPQ) and secondary electron multiplier (SEM) amplifiers (table 3.2). The samples were spiked either with a double spike system (^{229}Th and ^{235}U) or a single mixed spike ($^{229}Th/^{236}U$). Corrections were made in the single spike scheme for a small ^{238}U and ^{230}Th contributions from the spike.

Speleothem samples were dissolved using 7M nitric acid to limit mobilisation and loss of authigenic ^{230}Th from carbonate to detritus during solution. Total rather than selective solution means some samples have relatively low ($^{230}Th/^{232}Th$) (R_o) ratios because all detrital ^{232}Th is included in the solution. R_o is a reasonable indicator of

non-authigenic ^{230}Th (Ford *et al.*, 1972), but in MC2 young, low-U samples also contain less ^{230}Th than older, high-U calcite (table 3.3). All ages were also corrected for an assumed detrital contribution to total ^{230}Th (Kaufman, 1993) using a correction factor R_o for the detritus.

mm	^{238}U (µg/g)	error	$(^{234}U/^{238}U)$	error	$(^{230}Th/^{234}U)$	error	$(^{230}Th/^{232}Th)$	Age (yrs)	1σ err.
CC4									
0	1.9067	0.0123	0.9772	0.0012	0.1568	0.0027	13	18560	350
55	4.0634	0.0021	0.9800	0.0128	0.1251	0.0023	27	14540	290
80	3.6282	0.0056	0.9865	0.0028	0.1073	0.0004	175	12350	49
85	3.4331	0.0054	0.9853	0.0021	0.1064	0.0003	504	12240	37
100	4.3785	0.0093	0.9892	0.0027	0.1045	0.0003	889	12010	36
145	5.5026	0.0016	0.9740	0.0011	0.0991	0.0015	3522	11350	180
160	4.9215	0.0170	0.9729	0.0014	0.0902	0.0008	3479	10280	96
185	4.2673	0.0011	0.9997	0.0146	0.0848	0.0013	683	9637	150
205	3.0280	0.0024	0.9959	0.0112	0.0697	0.0010	1308	7857	120
288	2.5510	0.0040	0.9709	0.0003	0.0277	0.0002	65	3055	22
MC2									
10	0.1295	0.0000	1.0882	0.0011	0.1260	0.0029	15	14620	360
15	0.1490	0.0003	1.1434	0.0066	0.1146	0.0017	20	13200	210
92	0.1284	0.0002	1.1100	0.0061	0.1129	0.0011	17	13000	130
107	0.1300	0.0002	1.1010	0.0048	0.1092	0.0006	20	12550	73
143	0.1219	0.0002	1.1716	0.0079	0.1059	0.0009	18	12140	110
180	0.1076	0.0002	1.1513	0.0078	0.1045	0.0009	18	11980	110
195	0.0994	0.0001	1.1100	0.0044	0.1040	0.0012	31	11920	150
295	0.0995	0.0000	1.0878	0.0015	0.1019	0.0022	19	11670	270
522	0.0696	0.0001	1.0993	0.0039	0.0420	0.0018	11	4663	200

Table 3.2. U/Th isotopic data for Irish speleothems CC4 and MC2. Distance (column 1) is mean distance from the base of the speleothem to the centre of the calcite sampling site (maximum width 5 mm). Ages (column 9) are calculated with Larry Edwards' PC program Isoplot, producing ages correct to the nearest decade with 1σ errors. Ages produced by Isoplot were checked with a Microsoft Excel spreadsheet created at the Open University. Ages and age errors agree within the accuracy of the two methods.

A previously measured R_o of 0.67 for glacial sediments (Szabo *et al.*, 1982) was used since both caves are overlain by extensive glacial and glaciofluvial sediments derived from Irish LGM ice-sheets. In CC4 only three corrected ages differ from uncorrected ages by more than the 1σ age error using this R_o and only one age correction is larger than the 2σ

age error. As may be expected, the older and more detritally contaminated ages are those which require greatest correction. Corrected ages in MC2 are on average 3.5% younger than uncorrected ages, although the youngest age is shifted by 6.3% when corrected. However, when the speleothems are compared using uncorrected ages, there is very little difference in the position in time of major palaeoclimate events during the Late Glacial and Holocene in $\delta^{18}O$, $\delta^{13}C$ or luminescence intensity (LI) proxies. As MC2 ages need no correction, the close similarity through time of the timing of major events in the various palaeoclimate proxies in both speleothems suggests R_o is likely to be lower in this study than the value of 0.67 previously found for glacial till. However, at present there is no information on the actual R_o of detritus in these Irish speleothems. There is one exception to this generally close similarity in corrected and uncorrected ages through time – the corrected age for the base of CC4 is more similar to the interpolated age for the base of MC2 (17.63 Ka BP and 17.95 Ka BP). However, the start of speleothem growth in each cave may reflect small variations in local climate conditions.

Low ^{238}U (and hence low ^{230}Th) concentrations in MC2 samples make any ^{230}Th contribution to the analysis from laboratory contamination important. A typical concentration of ^{230}Th in the youngest MC2 samples (lowest likely ^{230}Th concentrations) is 0.25 picograms ^{230}Th, whilst blank analyses (estimated from the ^{232}Th blank, assuming a ($^{230}Th/^{232}Th$) ratio of 1.7 (Kaufman, 1993)) typically produce 0.01 picograms/gram ^{230}Th and often much lower values. ^{230}Th contents in CC4 are an order of magnitude greater and so the blank correction is negligible. The ^{238}U blank is typically 0.035 nanograms/gram, compared to a typical concentration of 200 nanograms/gram ^{238}U from

MC2 and 3000 nanograms/gram ^{238}U from CC4. Therefore, no ^{238}U blank correction was required for either data-set.

Age-distance curves were constructed by interpolating linearly between the uncorrected U/Th TIMS ages (figure 3.3). Six ages (out of 16) for CC4 and 3 (out of 12) for MC2 which appeared to be out of sequence due to possible errors in analysis were removed from the age-distance curves. In what follows, all palaeoclimatic proxies are plotted against time using these age–distance curves. Including those ages which are out of sequence has the effect of inverting certain sections of the time-distance relationship for the speleothems.

3.4.2. Growth rate

Speleothem growth rate varies as a result of several factors (table 3.2). The controlling factor is the volume of available water, since without soil water no solution can take place. However, other factors become important where soil water is available without restriction (Baker and Smart, 1995).

The volume of calcium carbonate ($CaCO_3$) which can be held in solution is dependent on soil pCO_2, temperature, soil water acidity and several other factors (Ford and Williams, 1989). Soil CO_2 derives from plant respiration and bacterial oxidation of organic matter. In addition, decaying plants produce organic acids and complexes which have the potential dramatically to boost calcium (Ca^{2+}) solution and hence speleothem growth rates.

The effect of changes in water film thickness on speleothem growth rates is almost as important as Ca^{2+} solution rates and varies according to volume of water arriving in a cave (Baker and Smart, 1995). $CaCO_3$

Variable	Mean	Growth rate change (mm yr^{-1})
Calcium concentration	2.00 mmol l^{-1}	+0.037
Water film thickness	0.08 mm	+0.025
Temperature	10°C	+0.018
CO_2 partial pressure	3 x 10^{-4} atm	+0.007

Table 3.3. Experimental reponse of speleothem growth rate to a 50% increase in variables involved in calcite solution in caves (Baker 1993). The most significant change in growth rate results from an increase in calcium concentration of the speleothem dripwater, followed by water film thickness (which reflects the volume of water arriving in the cave). Temperature changes are the third most important influence on speleothem growth at approximately half the importance of calcium concentration.

solubility theoretically should be depressed when cave temperature (which reflects long-term environmental temperature) increases (Bogli, 1980). However, the effect of increasing environmental temperature is actually to increase dissolved CO_2 in cave waters through increased microbial activity and increased CO_2 production by plants (Harmon *et al.*, 1975), leading to increased rates of $CaCO_3$ solution. Despite this, the temperature effect was shown by Baker and Smart (1995) to be of minor importance to changes in growth rate.

U/Th ages were integrated over distance on the speleothem to construct growth rates (figure 3.4). On average MC2 grew 4-5 times faster than CC4. At present, both Crag Cave and Mitchelstown Cave lie between the present-day 800 mm and 1200 mm mean annual water surplus isopleths (Culleton and Gardiner, 1985). Such data are not available for the Late Glacial, but the relative continentality of CC4 and MC2 was

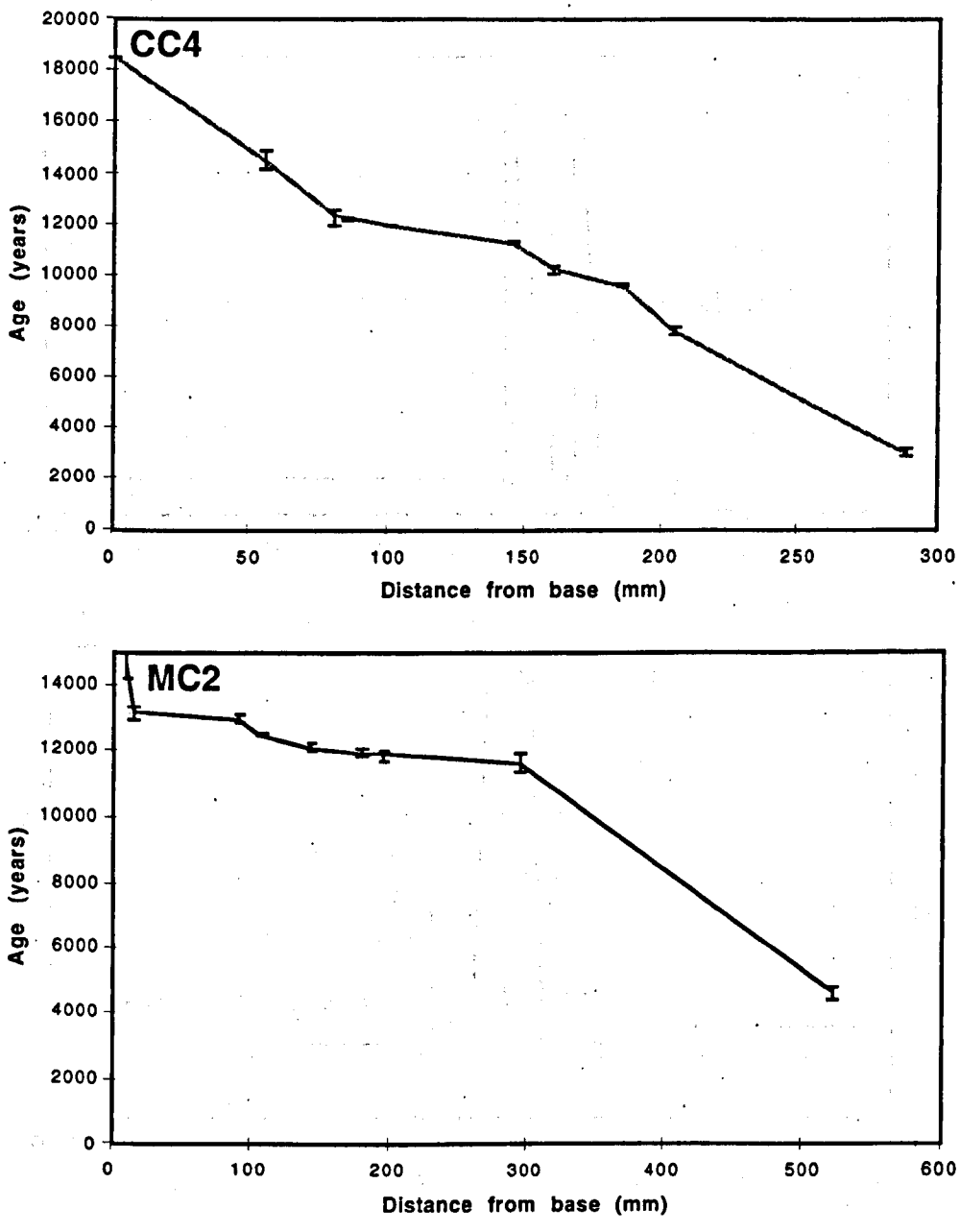

Figure 3.3. Age–distance curves for both Irish speleothems. The curves were constructed by plotting U/Th TIMS ages against distance from the base of the speleothem. Vertical error bars are 1σ age errors. Faster rates of growth are indicated where the curves are more horizontal.

probably similar. Therefore, it is almost certain that the faster growth rate of MC2 is not due to a greater volume of precipitation, although it may indicate a greater volume of water to the growing tip of the

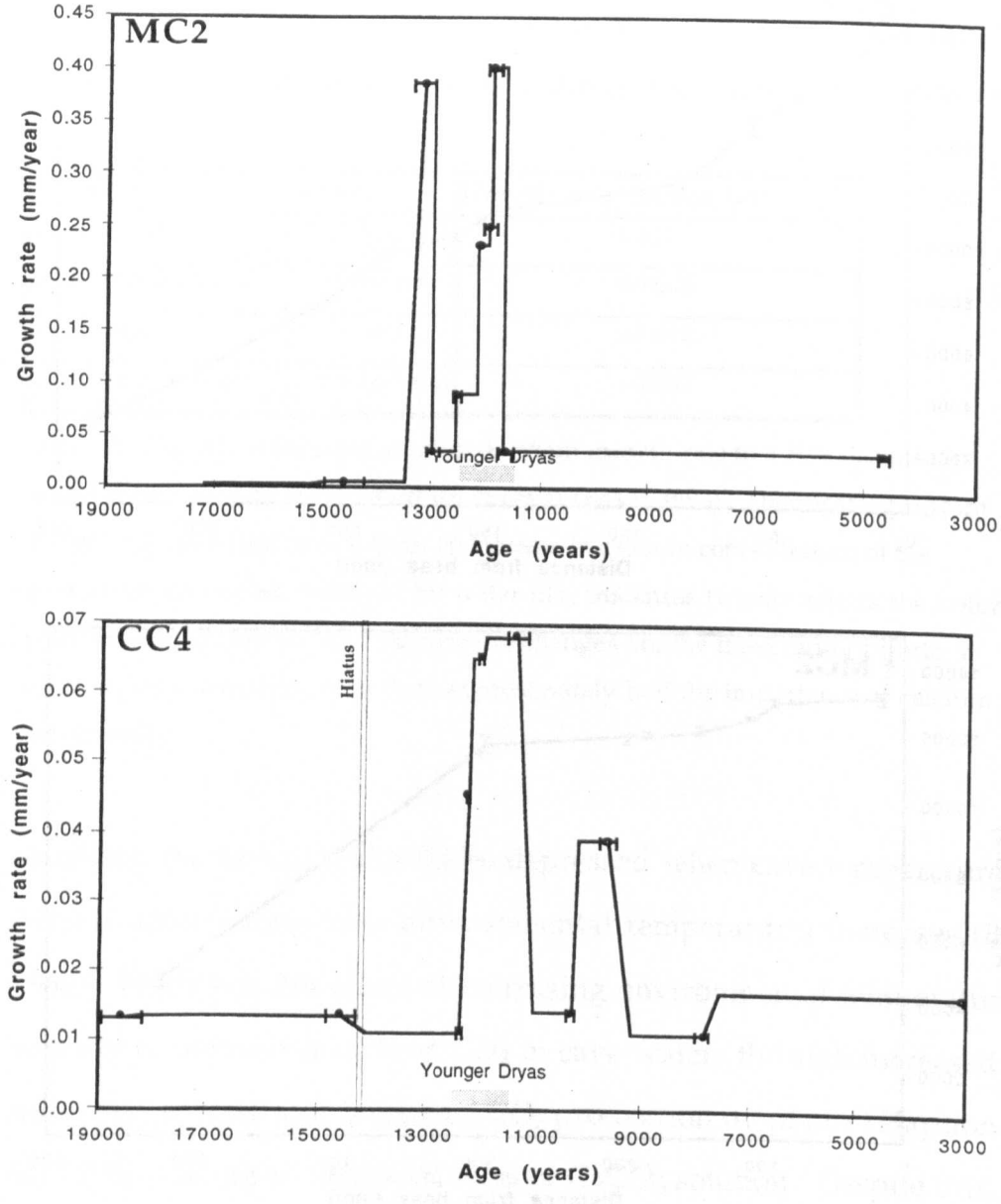

Figure 3.4. Speleothem growth rates for both speleothems. The growth rate curves were constructed by integrating age over distance. 1σ age errors are shown on each plot. The fastest rates of growth are 0.41 mm/year for MC2 and 0.68 mm/year for CC4, both during the second half of the Younger Dryas period (the YD is the stippled area on each graph).

speleothem or higher soil pCO_2 than at Crag Cave. Both speleothems grew most rapidly during the period from 12.4 to 11.5 Ka BP – the time of the Younger Dryas (YD), although it is not certain that MC2 did not

also continue to grow rapidly after the YD. Maximum rates of growth during the YD are 0.4 mm/year in MC2 and 0.068 mm/year in CC4, which represents a 10-fold and 5-fold increase in growth rate respectively, compared to the Holocene period. The average growth rate of MC2 is 6.5 times faster than CC4. CC4 also shows faster growth during the period from 10.3 to 9.2 Ka BP, a period which may coincide with the Boreal palaeoclimate event. In MC2, this event is probably missing due to insufficient U-series ages available. MC2 shows a significant increase in growth rate between 13.6 and 13.0 Ka BP, which may correspond to the Older Dryas event. This period in CC4 probably lies within a marked growth hiatus in the speleothem.

3.4.3. Oxygen isotopes

When a single cave is considered, oxygen isotope ratios in individual speleothems are influenced by several factors.

i) In caves with high humidity, $\delta^{18}O_s$ (speleothem) increases as cave temperature decreases (Emiliani, 1972) (equilibrium fractionation).

ii) As air temperature outside the cave decreases, $\delta^{18}O_p$ (precipitation, i.e. rainfall) becomes lighter and, because rainfall becomes cave dripwater, it also has a strong influence on $\delta^{18}O_s$ (Schwarcz and Harmon, 1976).

iii) An increase in global ice volume preferentially removes light ^{16}O into glaciers, meaning that a decrease in global temperatures leads to more positive $\delta^{18}O$ in the ocean sources of precipitation.

In most studies at high latitudes, cave temperature is the dominant influence on $\delta^{18}O_s$ (Goede *et al.*, 1986). In caves at low latitudes (Fischer *et al.*, 1996) and in some ocean-proximal settings (Gascoyne *et al.*, 1980) the precipitation effect may dominate. In a less humid cave environment, evaporation of dripwater on the speleothem may cause

mass-dependent fractionation (non-equilibrium, or kinetic, fractionation), limiting interpretation of $\delta^{18}O_s$ on the basis of temperature. A test for kinetic fractionation is to determine whether multiple analyses from a single layer of calcite on a speleothem show correlation between $\delta^{18}O$ and $\delta^{13}C$ (Hendy, 1971). Unfortunately, single layer sampling is procedurally difficult, and co-variation may be caused by inadvertant sampling across multiple layers.

Attempts have been made to reconstruct absolute palaeotemperatures from speleothem $\delta^{18}O$ and deuterium/hydrogen (δD) values of fluid trapped by contemporaneous calcite growth (Goede *et al.*, 1986). However, practical difficulties with the technique of extracting fluid inclusions from calcite have meant that reconstructing absolute cave palaeotemperatures from speleothems remains elusive. Despite this, the interpretation of relative temperature changes from speleothem $\delta^{18}O$ remains a valid technique with data of the kind presented here.

100 microgram samples of calcite from the speleothem growth axes were analysed using an Autocarb carousel attached to a VG Prism gas-source mass-spectrometer at Royal Holloway, University of London. Speleothem $\delta^{18}O$ and $\delta^{13}C$ was corrected to several calcite standards analysed at the same time, at an average of one standard to 9 samples (see table 3.4).

Standard	$\delta^{18}O$	1σ error	$\delta^{13}C$	1σ error	no. analyses
NBS-19	-1.783	0.035	1.886	0.035	17
RHBNC	-9.529	0.030	3.128	0.024	70
Coral	-3.285	0.160	0.045	0.060	29
SPA-1	-11.079	0.010	-7.717	0.008	3
PSU-1	-22.096	0.014	-3.892	0.014	2

Table 3.4. $\delta^{18}O$ and $\delta^{13}C$ analyses for calcite standards performed during this study.

Stable isotopes from a single layer of calcite were analysed for MC2 because of the possibility that the 'scatter' of $\delta^{18}O$ evident in that speleothem is due to mass-dependent fractionation. However, no evidence for mass-dependent fractionation was found over a distance of 65 mm (figure 3.5), although the value of such a test is limited by the difficulties of sampling coeval calcite layers.

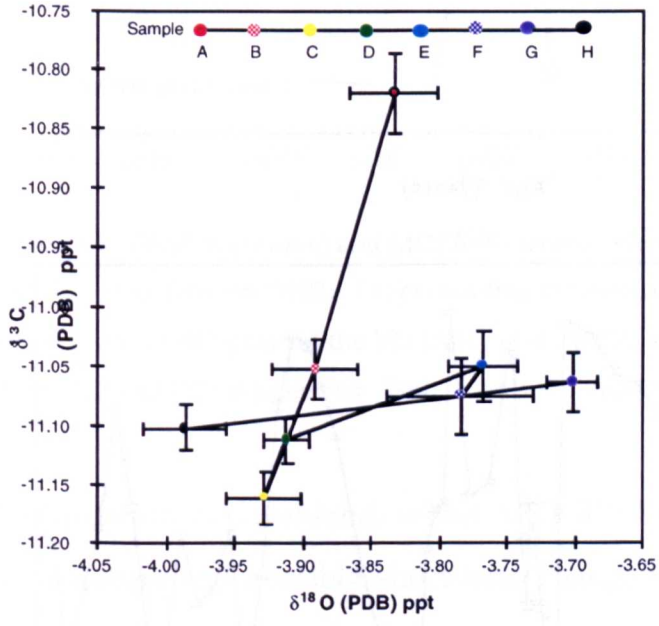

Figure 3.5. $\delta^{18}O$ plotted against $\delta^{13}C$ for a single layer (408 mm) of MC2. The correlation between $\delta^{18}O$ and $\delta^{13}C$ is not significant at the 90% level, indicating that kinetic fractionation effects were not important (Hendy, 1971).

3.3.3.1. MC2 $\delta^{18}O$

$\delta^{18}O$ in MC2 is much more scattered than CC4 (figure 3.6). This is probably due to the sampling regime: Samples were taken for stable isotope analysis at an interval of 5mm in both speleothems, but the faster average growth rate of MC2 means a single 1 mm sample may represent between 200 years and two year's calcite deposition. Thus, variations in $\delta^{18}O$ may be due to inter-annual variability or even seasonal effects. More positive $\delta^{18}O$ values at 18 Ka BP (when glacial conditions prevailed in Ireland), indicate the general trend in MC2 $\delta^{18}O$ represents changes in cave temperature. To confirm this, $\delta^{18}O$ from

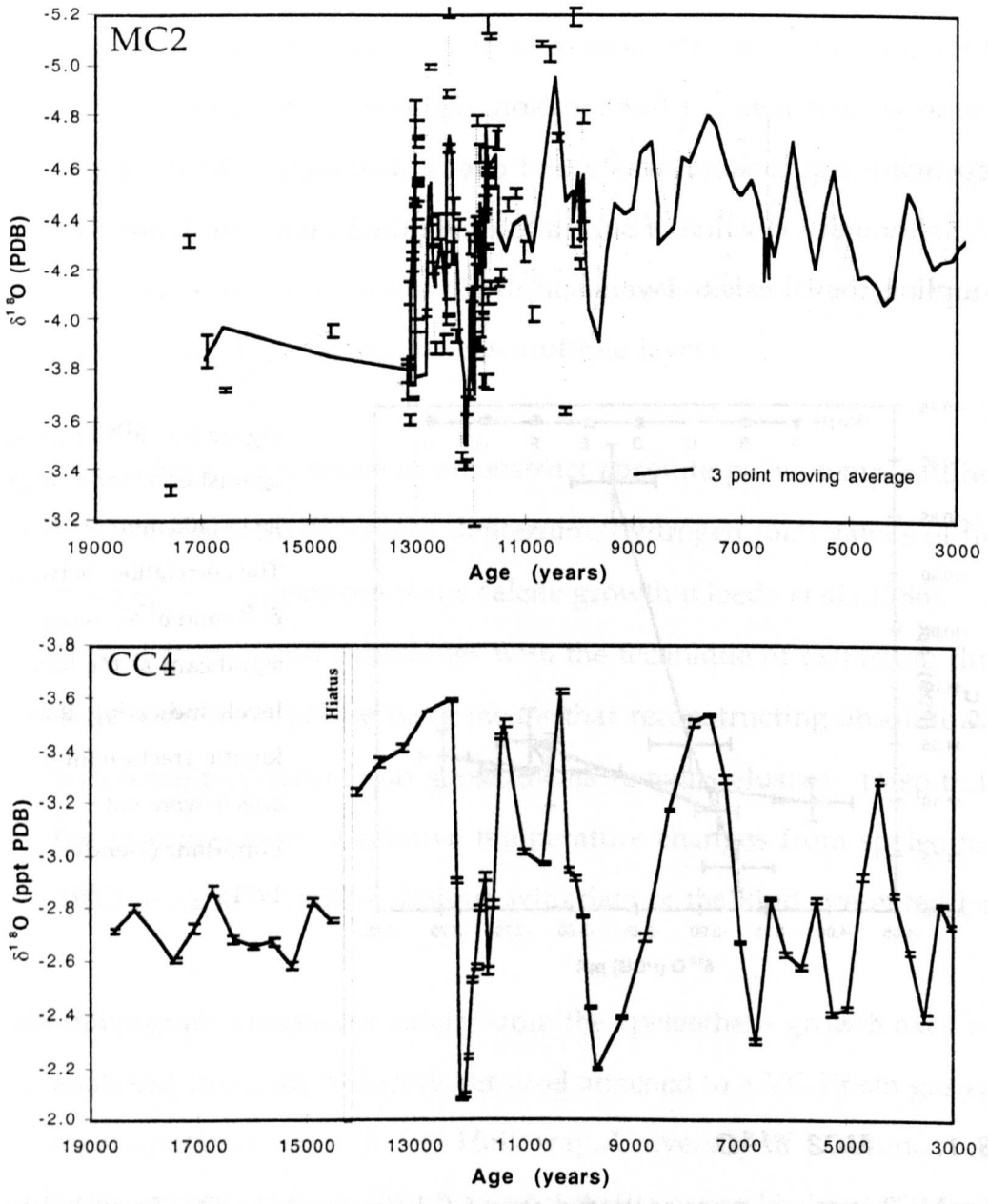

Figure 3.6. $\delta^{18}O$ records for both speleothems, plotted against time (ages from table 3.3). 1σ measurement errors are shown. $\delta^{18}O$ in MC2 is highly scattered (pecked line), probably because of the high rate of growth (see figure 3.4). To enable direct comparison with CC4 the MC2 curve has been smoothed with a simple 3-point moving average (solid line).

MC2 was compared to $\delta^{18}O$ records from the GRIP ice-core (figure 3.7) from Greenland (Alley *et al.*, 1993; Grootes *et al.*, 1993; Johnsen *et al.*, 1992). GRIP $\delta^{18}O$ represents the temperature of formation of

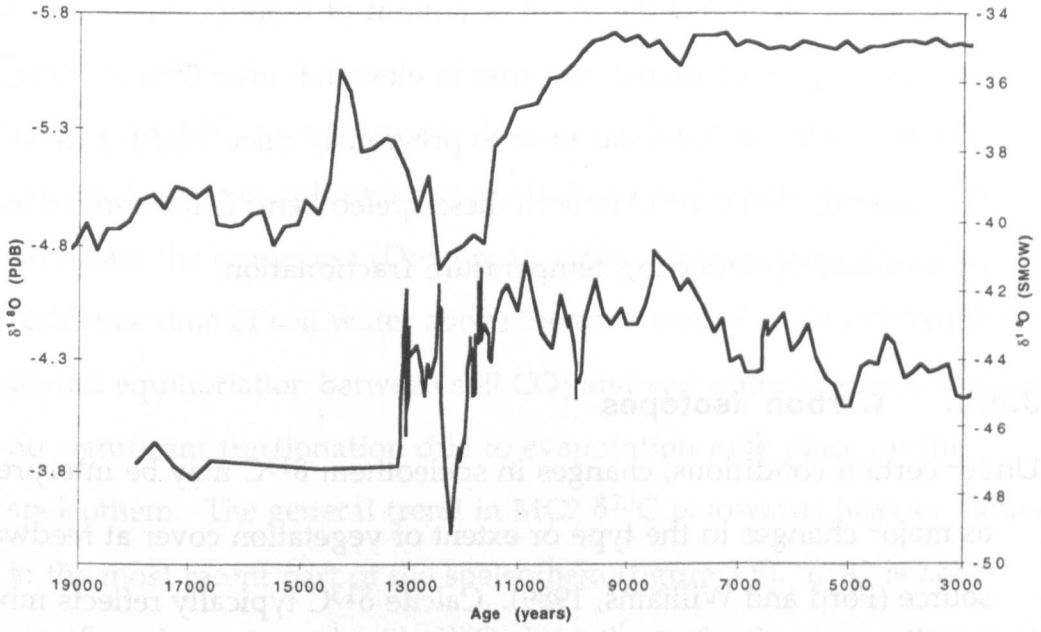

Figure 3.7. GRIP (top curve) and MC2 $\delta^{18}O$ records plotted against time using age data for GRIP from Johnsen (1992). Layer counting in Greenland ice cores may lead to age errors of 5% or 625 years at the YD (Alley *et al.*, 1993), and thus the chronology derived from MC2 and CC4 is preferred. Both records are smoothed with running means.

precipitation in Greenland, whilst MC2 $\delta^{18}O$ represents general cave temperature and possibly short-term change in precipitation $\delta^{18}O$ values. Thus, the close correlation displayed in figure 3.7 is not unexpected. The MC2 $\delta^{18}O$ data was smoothed with several filters to produce a curve allowing direct comparison with CC4 $\delta^{18}O$. The filter which appears to give the best signal to noise ratio is a three-point running mean.

3.3.3.2. CC4 $\delta^{18}O$

The CC4 $\delta^{18}O$ signal is much less variable than MC2 $\delta^{18}O$ (figure 3.6). This probably reflects the slower growth rate of CC4, such that $\delta^{18}O$ values are averaged over several years. On average a single 1 mm sample in CC4 represents 36 years growth, which is an average growth rate 6.5 times slower than MC2. The offset of $\delta^{18}O$ by 1.4‰ between the two

speleothem records is the result of rainout of more positive $\delta^{18}O$ as air masses progressed inland and rose in elevation over Ireland. This rate of $\delta^{18}O$ depletion is similar to rates previously calculated for ice sheets (Dansgaard, 1961). $\delta^{18}O$ in both these speleothems is interpreted as predominantly reflecting temperature fractionation.

3.4.4. Carbon isotopes

Under certain conditions, changes in speleothem $\delta^{13}C$ may be interpreted as major changes in the type or extent of vegetation cover at feedwater source (Ford and Williams, 1989). Calcite $\delta^{13}C$ typically reflects mixing between carbon derived from a carbonate rock source (where generally $\delta^{13}C = 0 \pm 5‰$ PDB) and from HCO_3^- ions in soil water ($\delta^{13}C$ = -16 to -24‰ PDB) (Ford and Williams, 1989). HCO_3^- ions derive mainly from soil CO_2 and the $\delta^{13}C$ of soil CO_2 where C3 plants dominate differs from $\delta^{13}C$ of soil CO_2 where C4 or CAM plants are predominant (Hendy, 1971). The optimum climatic conditions for most C4 plants are different to those for C3 plants (Teeri and Stowe, 1976), so in the right conditions $\delta^{13}C$ may also reflect palaeoclimate changes as the vegetation shifts from C3 to C4 dominated plant regimes (Talma and Vogel, 1992). However, since C4 plants (which favour warm, dry environments) are unlikely to have been present in Ireland during the Late Glacial, $\delta^{13}C$ in Irish speleothems probably reveals more about the way in which carbon is incorporated in the speleothems. Speleothem $\delta^{13}C$ values lie along a mixing line between $\delta^{13}C$ of soil CO_2 and $\delta^{13}C$ of the local limestone ($CaCO_3$). Thus, changes in local hydrological or palaeoclimatic conditions which permit one or other source to become more important will shift speleothem $\delta^{13}C$ values along this mixing line. A typical value assumed for this mixing ratio is 50% soil CO_2 and 50% $CaCO_3$ (Talma and Vogel, 1992).

3.3.4.1. MC2 $\delta^{13}C$

$\delta^{13}C$ values in MC2 vary between -11.3 and -9.1‰, compared to an expected range of values between -14.0 and -6.0‰ where C3 plants dominate the ecosystem (Dreybrodt, 1980). This indicates that the residence time of soil water above the cave was of sufficient length to permit equilibriation between soil CO_2 and soil water CO_2 and suggests no significant fractionation due to evaporation took place on the speleothem. The general trend in MC2 $\delta^{13}C$ is towards heavier values in the most recent part of the speleothem (figure 3.8). $\delta^{13}C$ is not significantly correlated with $\delta^{18}O$ along the speleothem growth axis at the 90% level of confidence. Subdividing the complete dataset reveals no subset of $\delta^{13}C$ values in which the relationship between $\delta^{18}O$ and $\delta^{13}C$ is statistically significant.

3.3.4.2. CC4 $\delta^{13}C$

$\delta^{13}C$ in CC4 varies between -10.8 and -7.7‰ and can be divided into two separate time periods (figure 3.8b). $\delta^{13}C$ varies inversely with $\delta^{18}O$ prior to the YD (figure 3.9), but after the YD the relationship is positive ($\delta^{18}O$ becomes more positive where $\delta^{13}C$ becomes more positive). Overall the correlation between $\delta^{18}O$ and $\delta^{13}C$ is not significant at the 90% level, but when the dataset is separated at the YD event both the older and younger periods show correlation between $\delta^{18}O$ and $\delta^{13}C$ significant at the 99% level. The magnitude of changes in $\delta^{13}C$ does not correspond to the magnitude of shifts in $\delta^{18}O$ through time, meaning there is unlikely to have been significant mass dependent fractionation due to kinetic effects.

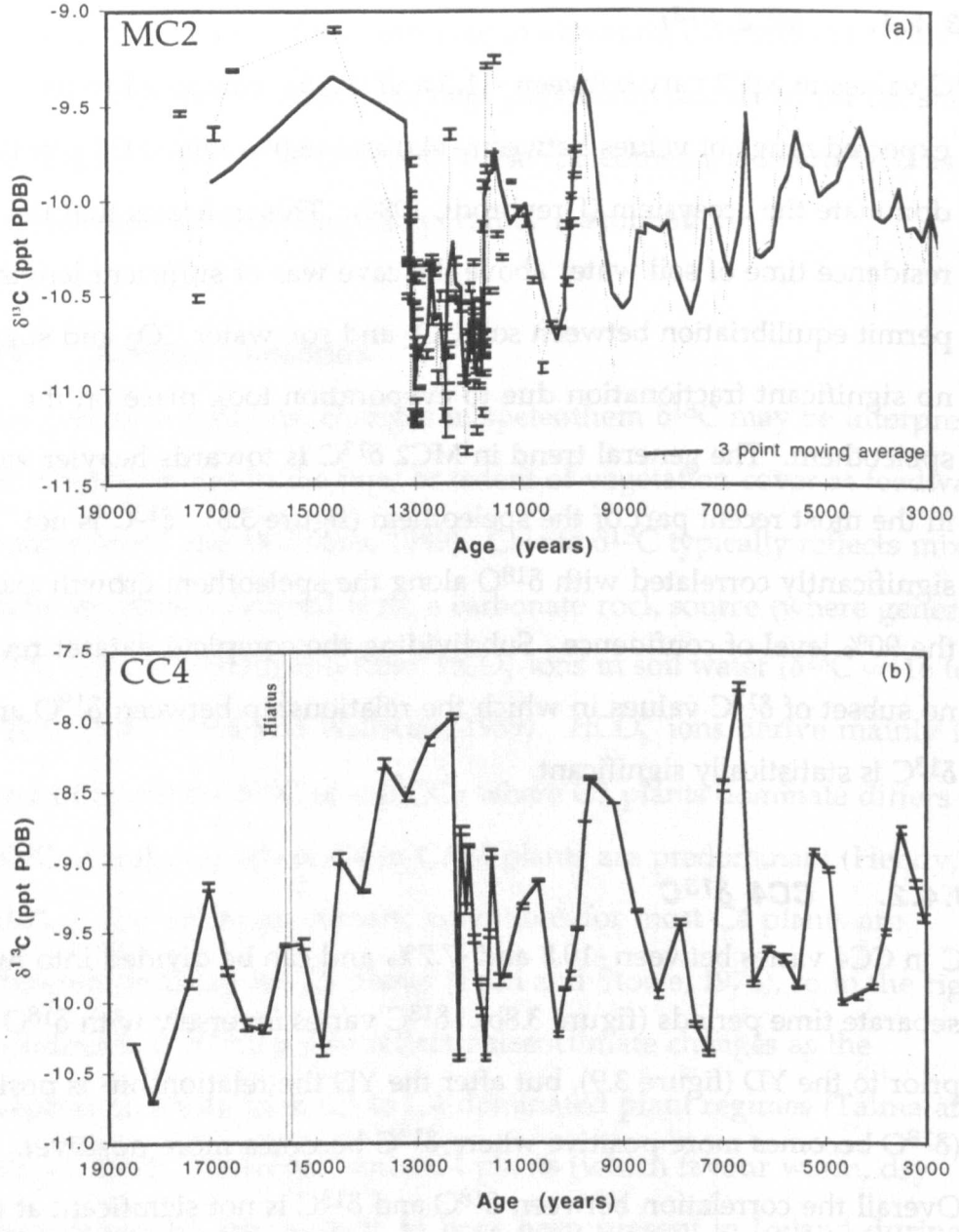

Figure 3.8. $\delta^{13}C$ records for both speleothems, plotted against time (ages from table 3.3). 1σ measurement errors are shown. $\delta^{13}C$ in MC2 is highly scattered, probably because of the high rate of growth (see figure 3.4). To enable direct comparison with CC4 the MC2 curve has been smoothed with a simple 3-point moving average (solid curve).

$\delta^{13}C$ in both speleothems is within the range expected for an ecosystem with predominantly C3 plants. $\delta^{13}C$ generally becomes more positive with time in both speleothems, with a linear increase in $\delta^{13}C$ from

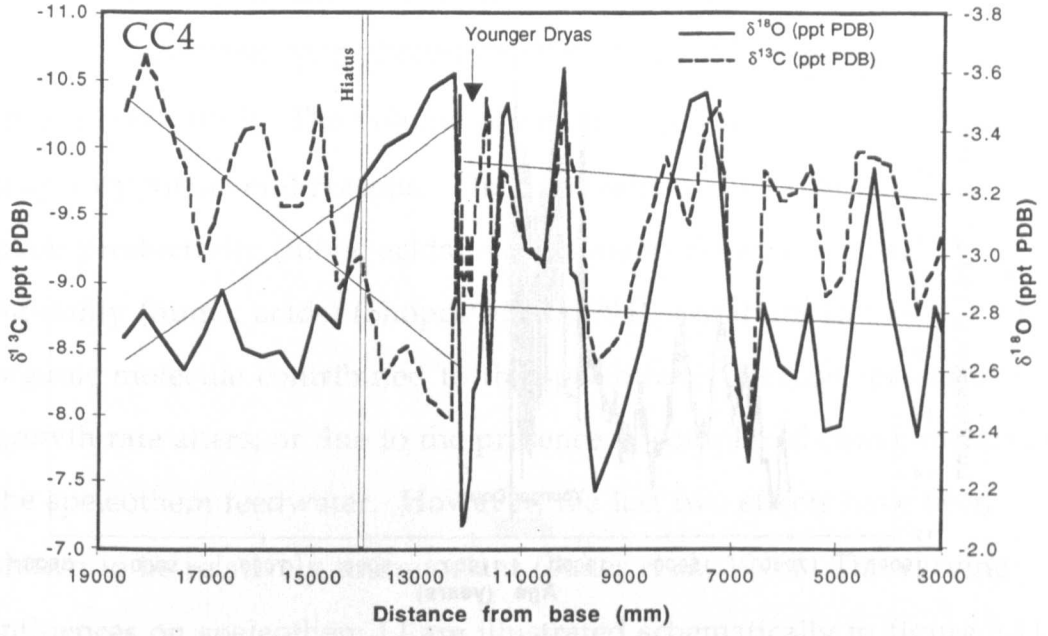

Figure 3.9. Graph of $\delta^{18}O$ and $\delta^{13}C$ in CC4 with four linear trendlines marked for $\delta^{18}O$ and $\delta^{13}C$ prior to the Younger Dryas (YD) and after the YD. The inverse relationship between $\delta^{18}O$ and $\delta^{13}C$ prior to the YD is marked by the two crossing trend lines and the positive relationship between $\delta^{18}O$ and $\delta^{13}C$ after the YD is marked by the two parallel trends.

19 Ka BP to 3 Ka BP of 0.3‰ CC4 and a linear increase of 0.6‰ in MC2. Within the Holocene period, MC2 $\delta^{13}C$ moves from -11.2‰ at the YD to -10.2‰ by 3 Ka BP. CC4 $\delta^{13}C$ shifts from -10.7‰ at the YD to -9.5‰ by 3 Ka BP. This may reflect stabilisation of the ecosystem such that decaying plant materials no longer contribute large volumes of carbon with negative values to speleothem $\delta^{13}C$. As carbon stable isotopes in speleothems reflect mixing between two carbon reservoirs, the difference in the range of speleothem $\delta^{13}C$ between MC2 and CC4 probably reflects changes in local conditions such as residence time of soil water. The CC4 $\delta^{13}C$ ratios are skewed more towards rock values than MC2, which may indicate a shorter residence time of speleothem feedwater in the soil horizon. The higher growth rates and higher luminescence intensity of MC2 also suggest that the influence of plants is greater on that speleothem.

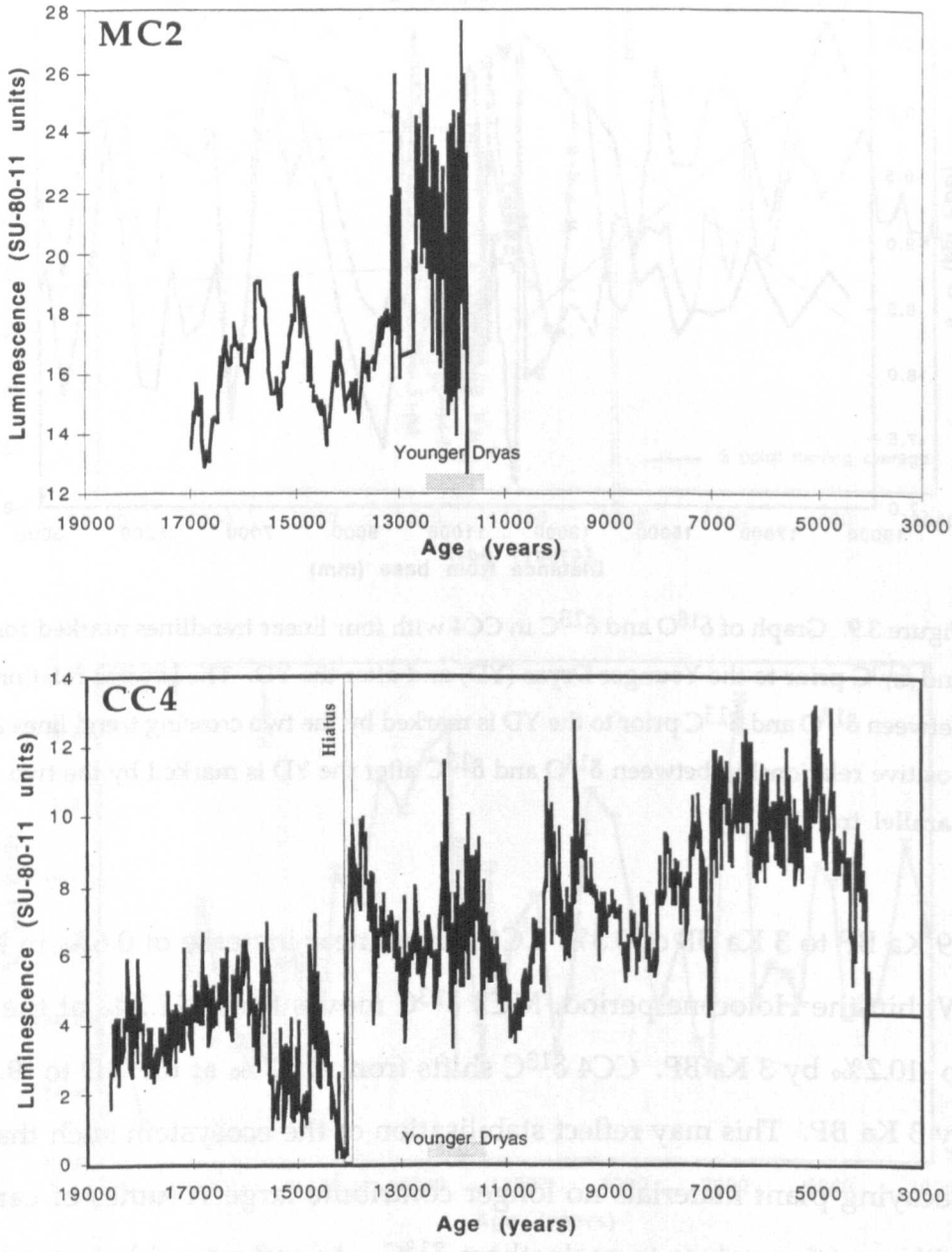

Figure 3.10. Luminescence records for both speleothems, plotted against time (ages from table 3.3). Units of measurement are by normalisation to a standard calcite (SU-80-11). No data is available after 11.8 Ka BP for MC2. The density of the data in both CC4 and MC2 at the Younger Dryas reflects the increase in growth rate at that point.

3.4.5. Luminescence spectra

When humic and fulvic acid molecules incorporated in calcite matrix are excited with ultraviolet (UV) light, the emission of photons in the blue-green part of the spectrum can be recorded (Shopov *et al.*, 1994).

Variations in speleothem luminescence intensity (LI) are determined by the volume and type of organic acids deposited in the speleothem (Baker *et al.*, 1996). The volume of organic acids incorporated in calcite may vary for several reasons. These include: Dilution effects; changing plant productivity (fulvic acids); variations in the rate of plant mortality (humic acids) (Shopov *et al.*, 1994); variations in the type of organic molecule contributed to the speleothem; because speleothem growth rate alters; or due to the presence of complexed heavy metals in the speleothem feedwater. However, the last two effects have been shown to be relatively unimportant (Baker *et al.*, 1996). The varying influences on speleothem LI are illustrated schematically in figure 3.11, where inputs are organic acids from dead or living plants, and water. These combine to form an 'organic solution' which is incorporated in the calcite matrix as a function of speleothem growth. Humic acids have more intense luminescent spectra (Senesi *et al.*, 1991), so a large increase in LI may indicate greater volumes of dead plants contributing organic material to the speleothem.

Both speleothems were excited with a laser at a wavelength of 325 nm using a spot size of 0.25 mm and the emission spectra measured at 480 nm. These wavelengths produce the best compromise in emission and excitation of a wide variety of organic molecules from different soil types (Senesi *et al.*, 1991). LI has been normalised to a standard unit (SU) for both CC4 and MC2, based on speleothem SU-80-11 from Assynt, Scotland (Baker *et al.*, 1993a). This allows LI curves from each speleothem to be compared directly. LI varies from 0-13 SU in CC4 and from 12.5-27.5 SU in MC2 during the Late Glacial. LI in MC2 (figure 3.10a) generally has values twice those of CC4 (figure 3.10b), which probably indicates a greater volume of organic acids dripping on the

speleothem. MC2 also grew at an average rate 5 times faster than the average rate for CC4, suggesting up to 10 times as much organic material arriving on MC2 as CC4.

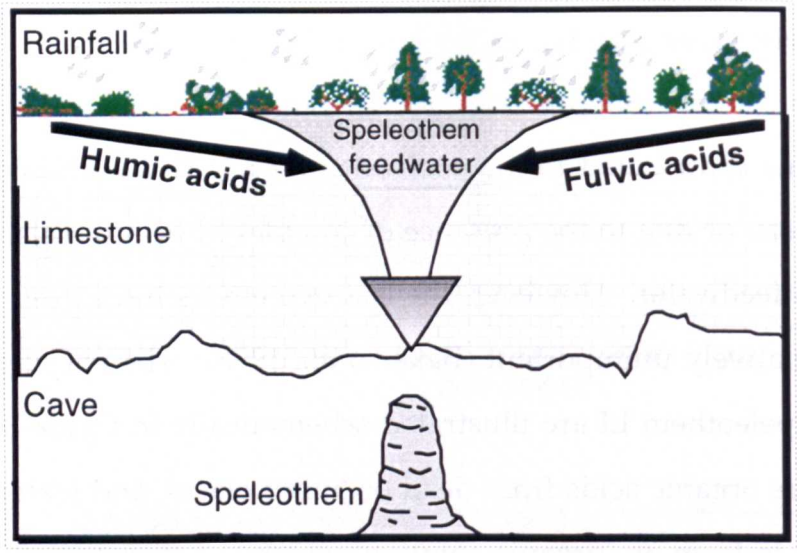

Figure 3.11. Schematic representation of the incorporation of humic and fulvic acids into the speleothem matrix. Living plants predominantly contribute fulvic acids, whilst decaying dead plants supply microbial mediated humic acids. These organic acids are transported from the soil to the cave by rainfall seeping through the soil. The same rainfall acts directly to dissolve and transport $CaCO_3$ to the speleothem. The total effect of the organic acids on speleothem luminescence intensity (LI) is governed initially by the volume of rainfall (and soil seepage water) available to transport the organic acids. Seepage water also dissolves heavy metals from local bedrocks and soil which have a minor effect on LI.

3.4.6. Other palaeoenvironmental information from speleothems

Other palaeoenvironmental information that may be derived from speleothems includes pollen trapped in the calcite matrix (Bastin, 1979); palaeomagnetic signals in the calcite (Latham *et al.*, 1979; Noel, 1990); and palaeoseismicity (Moser and Geyer, 1979). These are not considered further here.

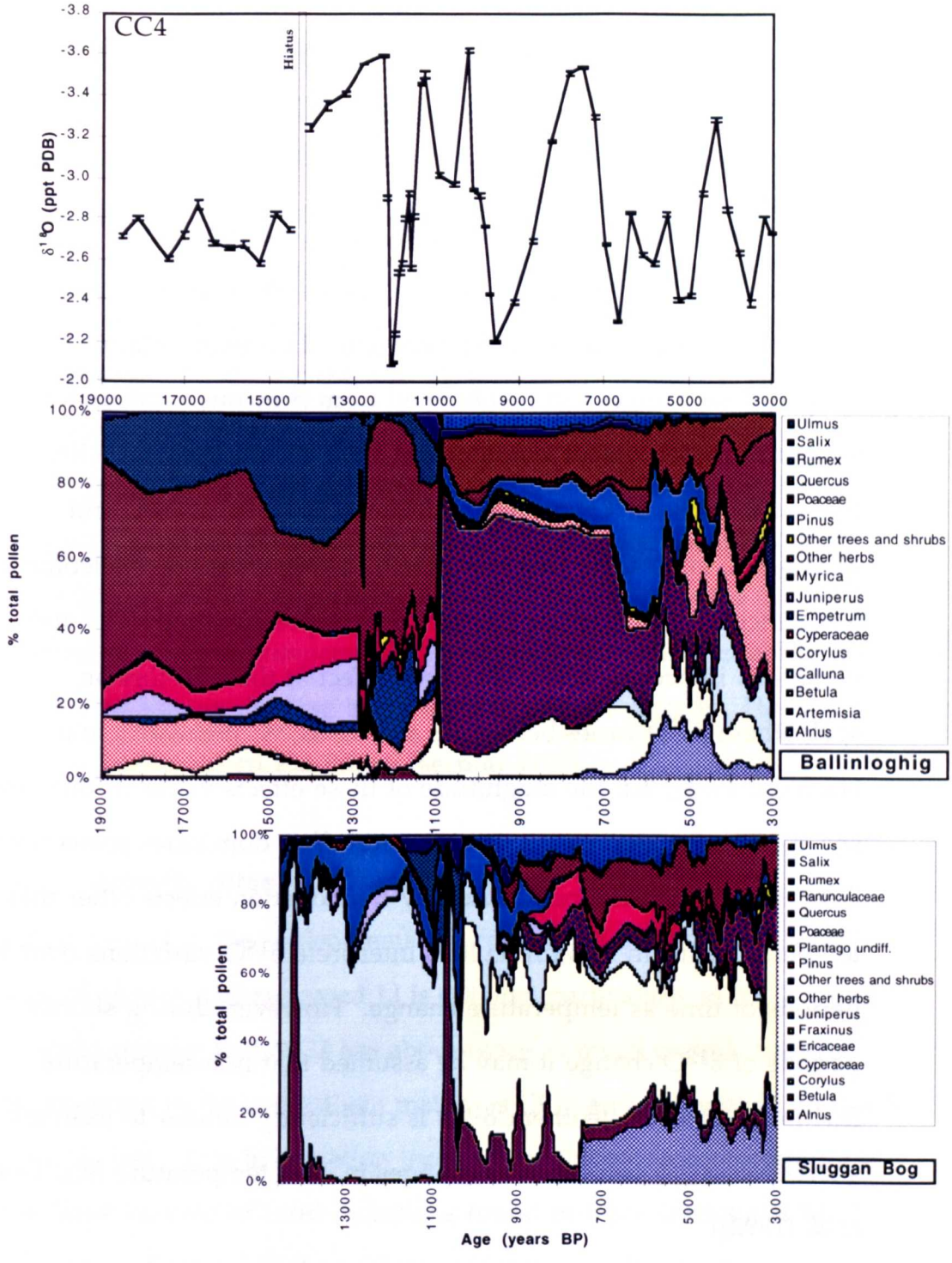

Figure 3.12. A comparison of CC4 stable isotope records with Irish pollen records. The top panel is the CC4 $\delta^{18}O$ record. The second panel is a pollen summary for Ballinloghig, Dingle Peninsula, County Kerry The third panel is a pollen summary for Sluggan Bog, County Antrim (see figure 3.2 for locations). Both pollen diagrams were originally dated with radiocarbon (^{14}C) techniques. Original ^{14}C ages have been converted to sidereal years using the spreadsheet described in Chapter 5.

3.5. Discussion

The nature of the relationships between several of the five data proxies are discussed below. A synthesis of the data follows.

3.5.1. Palaeotemperature during the Late Glacial

As the dataset does not include δD it is not possible to assign absolute palaeotemperatures to either speleothem. However, relative temperature changes can be obtained from previously calculated temperature-dependent fractionation rates for inorganic calcite. Inorganic calcite $\delta^{18}O$ typically shifts by -0.22‰ /°C at 20°C and -0.24‰ /°C at 10°C (O'Neil *et al.*, 1969). Other effects on speleothem $\delta^{18}O$, include temperature fractionation of precipitation $\delta^{18}O$ and variations in oceanic $\delta^{18}O$. The total effect of these factors on speleothem $\delta^{18}O$ varies between 0 and 0.3‰ /°C (Schwarcz and Harmon, 1976), but the magnitude of these effects varies in time and space. In most studies the temperature effect dominates speleothem $\delta^{18}O$, although variations caused by fractionation effects other than temperature mean it is difficult to interprete $\delta^{18}O$ variations over long periods of time as temperature change. However, during shorter periods of $\delta^{18}O$ change it may be assumed that non-temperature fractionation of speleothem $\delta^{18}O$ is sufficiently limited to examine short-term $\delta^{18}O$ variations as changes in cave temperature (e.g. Dorale *et al.* (1992)) .

The $\delta^{18}O$ change in the Irish speleothems at the YD is approximately 1.5‰ in CC4 and 1.4‰ in MC2, indicating a cooling of 5.8–6.3°C in southern Ireland at the height of the YD assuming no influence from variations in precipitation amount or ice-volume effects on $\delta^{18}O$. Beetle records suggest a July temperature decrease of 7°C (Coope and Lemdahl, 1995)

(figure 3.12c), whilst pollen records indicate a fall in average annual temperature of 6–7°C (Barnosky, 1988; Watts, 1985) and ELR estimates suggest 7.2°C of cooling (Colhoun and Synge, 1980). Thus, these estimates for speleothem palaeotemperature based on temperature-dependent fractionation in inorganic calcite are very similar to other palaeotemperature reconstructions for Ireland. The implication is that changes in precipitation and ice volume have little or no effect on speleothem $\delta^{18}O$ during the YD. However, it is likely that such variations were present during the Late Glacial and Holocene periods, which probably accounts for larger variations in $\delta^{18}O$ during those periods than might be expected from changes in temperature alone. For example, $\delta^{18}O$ changes during the Boreal period in CC4 (figure 3.6) intepreted solely as temperature change indicate cooling equal to the YD and this is not the case in most palaeoclimate records. However, see the discussion on the Boreal (section 3.6.7).

3.5.2. Growth rates and luminescence

At certain points in the speleothems the correlation between increased rates of growth and increased LI is striking, particularly in MC2. Also, LI levels suggest that MC2 has about twice as much organic material incorporated in the speleothem matrix as CC4, and on average grew 4-5 times as fast. This information leads to the following interpretations:

i) The large volume of fluid inclusions found in thick sections of MC2 probably indicates a higher volume of water arriving on that speleothem than CC4. As LI is also higher in MC2, the effect of the greater volumes of available soil water would appear to be to flush organic acids from the soil in greater concentrations (rather than to dilute the total amount of organic acids present), a situation also found

in experimental results by Baker et al. (1996). This general conclusion is supported by the following evidence:

a) Relatively low speleothem LI levels are found immediately following the LGM (18.5 – 14.8 Ka BP) when Andrieu *et al.* (1994) find cold–dry arid continental-type climate in Ireland, supporting this concentration hypothesis.

b) In the first part of the YD Andrieu *et al.* (1994) find very wet conditions in Ireland at a time when LI in both speleothems is very high.

ii) LI in speleothems is not controlled entirely by soil water volume, but relies to some extent on the nature of the organic acid being contributed to soil water. Fulvic acids from living vegetation may be up to 10 times as luminescent in speleothems as humic acids produced by decomposing organic material (Senesi *et al.*, 1991). Despite this wide difference in LI values between living and dead plants, it may be difficult to derive data on vegetation change in the British Isles from luminescence data alone due to the wide range and large overlap in LI for various kinds of fulvic and humic acids (Baker *et al.*, 1996).

Baker et al. (1996) find that the direct effect of speleothem growth rates on LI is unimportant, which suggests that concommitant increases in growth rate and LI are the result of changes in a third factor. The evidence that wet conditions prevailed during the first part of the YD may indicate that the mechanism controlling both growth rates and LI is the volume of water arriving in the cave.

3.5.3. Vegetation cover from luminescence intensity and $\delta^{13}C$

The correlation between LI and $\delta^{13}C$ in MC2 during the Late Glacial is significant at the 99% confidence level (figure 3.13). In CC4 the overall

correlation between these two variables is not significant. This is not unexpected since extreme variations in LI probably occur during major climate changes rather than during climatically stable periods. Thus, data points where $\delta^{18}O$ is less than -3.1‰ (a mid-range value) were excluded from the CC4 data set to examine only the result of extreme shifts in temperature on the two variables. When these points are excluded the correlation between LI and $\delta^{13}C$ in CC4 becomes significant at the 95% confidence level. During the YD for example, two peaks in LI are matched by two troughs of more negative $\delta^{13}C$ in MC2 (figures 3.8, 3.9 and 3.13).

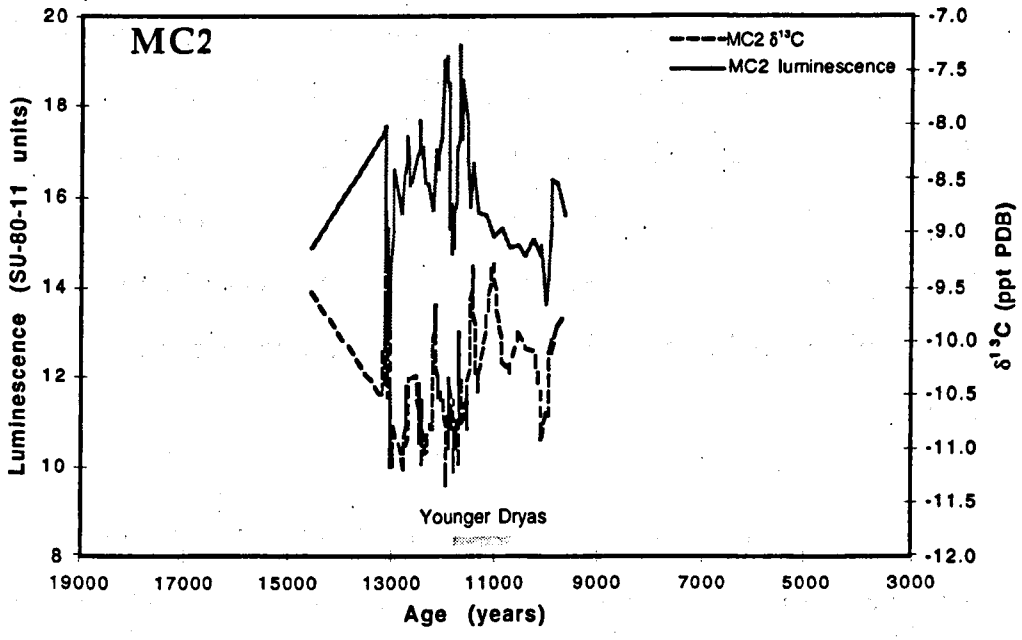

Figure 3.13. $\delta^{13}C$ and luminescence variation in MC2. The close correlation between the two proxies is evident from the way in which positive and negative excursions occur simultaneously in both records.

This co-variation of $\delta^{13}C$ and LI could be interpreted as the speleothem deriving more carbon from an organic source than from the host rock at the same time as more organic material or higher LI material is incorporated in the speleothem. Soil CO_2 includes both respired CO_2

and CO_2 from organic decay, making it difficult to distinguish the respective influences of humic or fulvic contributions in speleothem LI. In most soil horizons organic decay (humic acids) is the principal source of soil CO_2 (Ford and Williams, 1989).

An alternative interpretation is that an increase in the volume of organic material incorporated in the speleothem (increased LI) is sufficient to alter $\delta^{13}C$. However, the organic carbon contribution to $\delta^{13}C$ in the speleothem is swamped by large contributions from rock and soil CO_2 carbon reservoirs. In addition, organic residues in the calcite sample do not contribute to the $\delta^{13}C$ signal directly when the sample is dropped in acid for analysis of CO_2. Bacterial decomposition of decaying plant material increases soil CO_2 levels, and organic acids released by the decomposing material also boost limestone solubility (Ford and Williams, 1989). Thus, increased speleothem growth rates during the YD may be due either to increased soil CO_2 levels or increased volumes of organic acids in speleothem feedwater, or a combination of the two effects.

The favoured scenario for co-variation of LI, $\delta^{18}O$ and $\delta^{13}C$ during the YD is that rapid mean annual temperature cooling of approximately 6.5°C at the start of the cold event killed large numbers of plants, and so contributed a large volume of humic acids to the soil profile, which resulted in increased speleothem LI. The increased volume of organic acids and possibly increased pCO_2 from organic decomposition (indicated by more 'organic' speleothem $\delta^{13}C$ values) allowed limestone solution and speleothem growth rates to increase. A similar situation is found at the start of the Boreal period, although at the height of the Boreal another peak in LI is observed in CC4 – unmatched

by a concomitant peak in $\delta^{13}C$. More positive $\delta^{13}C$ and 'cold' $\delta^{18}O$ values might suggest less available organic material (climate conditions limiting plant production) in the Boreal, yet the speleothem was growing faster at this point. A possible source for the elevated LI is an increase in plant productivity (fulvic acids) and increased die-off of plants (humic acids) as several plant species attempt to outcompete one another in succession during the changing palaeoclimate conditions of the Boreal.

In MC2 the correlation between the rate of change of $\delta^{18}O$ and LI, which is significant at the 99% level of confidence (see earlier), provides some evidence to support a hypothesis of climate-controlled plant productivity affecting LI. The two factors which may be involved in this scenario are increased levels of fulvic acids from competing plant species and increased levels of humic acids from dying, 'out-competed' plants at any major change in climate which affects the regional plant community.

3.6. Synthesis

Ireland experienced a number of extreme palaeoclimatic changes during the Late Glacial. It has been shown here that the rate of these changes was rapid during the short Stadial known as the Younger Dryas and involved changes in temperature, plant productivity and biome type. Here the new findings are linked to other palaeoclimatic reconstructions in Ireland and the North Atlantic region. The standard European adjectives for Late Glacial palaeoclimate are used to describe the speleothem records.

3.6.1. Last Glacial Maximum – Bølling

At the Last Glacial Maximum (LGM –18.5 Ka BP) Midlandian ice-sheets covered virtually the whole of Ireland (figure 3.2), leaving an ice-free corridor between the Macgillycuddy's Reeks and the Wicklow mountains (Eyles and McCabe, 1989). Both caves are positioned within that ice-free corridor, although Crag Cave is much closer to the moderating influence of the North Atlantic ocean. At Tory Hill (Limerick), close to the LGM end-moraine, deposition of varved layers is estimated to begin at 17.3 Ka $BP_{(cal.)}$ (no published error) and records the first retreat of Midlandian ice (Andrieu *et al.*, 1994). However, the speleothems start growing at 18,560±350 BP (CC4) and 17,950±350 (MC2), suggesting either that a warm North Atlantic was providing sufficient moisture for speleothem growth even before ice retreat commenced, or that the ^{14}C age is in error. The cave at Mitchelstown is slightly closer to the Midlandian glacial limits, further from the Atlantic ocean, which may have delayed the growth of MC2 compared to CC4, although the available ages are not analytically distiguishable at the 1σ level.

The growth rate of CC4 was low during the Bølling-Allerød period. $\delta^{18}O$ indicates cold conditions, but not as cold as during the YD, suggesting seasonal bias towards summer $\delta^{18}O$ values, whilst speleothem LI is very low, indicating very low productivity in the ecosystem. Coleoptera (beetle) records indicate a continental climate in the British Isles with summer temperatures of 15°C and an annual temperature range of 30-35°C between 18.0 Ka $BP_{(cal.)}$ and 14.8 Ka $BP_{(cal.)}$, similar to the climate found today in north-west Siberia (Atkinson *et al.*, 1987). Further evidence for low ecosystem productivity in Ireland is found in very low pollen concentrations and high rates of erosion on the Dingle Peninsula before 16.5 Ka $BP_{(cal.)}$ (Barnosky, 1988). Gramineae (grasses)

in open ground communities dominate this period, in a very sparse *Pinus-Artemisia*-Gramineae pollen assemblage (Andrieu *et al.*, 1994), with bare soil predominant in the landscape (Watts, 1985). These published records detail a periglacial environment which may have permitted speleothem growth only in warmer summer months. This may explain the warmer $\delta^{18}O$ values during this period (figure 3.6), apparent in both speleothems – the speleothems did not grow in the cold winter, but only during the summer months – suggestive of periglacial conditions.

At ~18.0 Ka BP MC2 commenced growth as sufficient water and soil CO_2 became available for limestone solution. The MC2 $\delta^{18}O$ signal (figure 3.6) indicates cold temperatures until 13.2 Ka BP. LI is also lower at this point in MC2 than most of the rest of the record (figure 3.10). However, at 14.7 Ka BP the CC4 $\delta^{18}O$ record (figure 3.6) becomes more negative, suggesting warmer temperatures. At 14.2 Ka BP LI values in CC4 (figure 3.10) move from less than 1 to 8 in just 20 years, as plant productivity increases dramatically in the milder climate of the Bølling-Allerød. This period is the start of the *Rumex-Salix* pollen phase in Irish records – a substantial climatic amelioration into the Bølling (Andrieu *et al.*, 1994) also found in coleoptera records (Atkinson *et al.*, 1987).

3.6.2. Bølling

The Bølling is the first warm period in Europe after the LGM. It is traditionally viewed as a strong warm period from 15.4 Ka $BP_{(cal.)}$ to 13.0 Ka $BP_{(cal.)}$. The first part of this period in the speleothems does not show warm temperatures, but reflects a cold environment until 14.7 KaBP (in CC4, see above). The second stage (after 14.7 Ka BP)

involves rapid warming to temperatures close to the Allerød. The growth rate of MC2 increases at this point (figure 3.4), whilst LI increases from 18 to 26 (figure 3.10) and $\delta^{13}C$ also becomes more negative (figure 3.8). The hiatus in CC4 may obscure the first part of the Bølling period (figure 3.6). Andrieu *et al.* (1994) also subdivide the Bølling in Ireland into two periods with a *Rumex-Salix* zone earlier, followed by a zone of developing shrub taxa and *Juniperus* (figure 3.12), the two phases separated by a period when winter temperatures were colder.

3.6.3. Older Dryas/Intra-Allerød Cold Period

The Older Dryas (OD) is a very short period (200 years) of cold climate separating the Bølling and Allerød in some European records. (Watts, 1985) finds the Older Dryas as a phase of erosion at several sites in Ireland, possibly caused by lower temperatures and lower precipitation, ^{14}C dated to 14.0 – 13.8 Ka $BP_{(cal.)}$. Dust levels and $\delta^{18}O$ in Greenland ice-cores do reveal a short-lived cold event at this time, but the most extreme cold event in both GRIP and GISP2 during the Bølling-Allerød period (figure 3.7) commences at 13.1 Ka BP (Alley *et al.*, 1993; Stuiver *et al.*, 1995). A cold event is also found in MC2 at approximately 13.0 Ka BP (figure 3.6). At this time, the LI record for MC2 increases dramatically (figure 3.10a) and growth rate (figure 3.4a) rises to levels similar to the Younger Dryas, suggesting increased plant mortality. The event at 13.1 Ka BP is particularly strong in MC2 and GRIP, but a Younger Dryas precursor is also found in the Troll 3.1 record (Lehman and Keigwin, 1992). I designate the cold event at 13.1 Ka BP as the Intra-Allerød Cold Period (IACP) (Stuiver *et al.*, 1995).

In CC4, both the OD and the IACP events may lie within the hiatus. It is difficult to determine the duration of this hiatus as a large amount of detrital material lies in a lens within the calcite matrix at this point, which makes U/Th ages difficult to complete. Microscopic analysis reveals the detritus is composed of fine silts and mud transported by water and deposited in a low-energy environment. This may be evidence for a flood event in Crag Cave during the Bølling–Allerød transition. The possible cause of the flood is not clear: The stream in Crag Cave lies several metres below the location of CC4 and either a large volume of water entering the cave or some blockage at the exit of the stream would be required to dam the cave stream to cover CC4. The TIMS ages provides insufficient detail to distinguish changes in growth rate due to increased precipitation during this period. A large ice-sheet melt event in the region could have provided enough water to inundate CC4. Obviously, the largest melt event in this region was following the termination of the LGM. However, this is unlikely to be the flood event found in Crag Cave, given the growth of the speleothems prior to the hiatus.

3.6.4. Allerød

In the speleothem records, the Allerød period lies between 13.0 Ka BP and 12.4 Ka BP and shows warm conditions (from $\delta^{18}O$), with generally declining temperatures in MC2. At the same time LI is declining in both speleothems. $\delta^{13}C$ values in CC4 also become more positive, towards less organic values, probably indicating that this period was one of declining plant productivity. In pollen records the Allerød (Woodgrange) Interstadial in Ireland commences with birch woodland and becomes essentially treeless (figure 3.12) by the start of the YD (Smith and Goddard, 1991), suggesting gradually deteriorating climatic

conditions, also reflected in Greenland in GRIP (figure 3.7) and GISP2 $\delta^{18}O$ (Grootes *et al.*, 1993). In the British Isles the Allerød is marked by progressive soil deterioration, although in Ireland this occurs as isolated erosion events rather than continuous degradation (Walker *et al.*, 1994). Some continental records show an Intra-Allerød cold period (Oeschger *et al.*, 1980; Walker *et al.*, 1991), which is also found in the MC2 record as a short-lived return to cold conditions at the height of the Allerød (figure 3.6).

3.6.5. The Younger Dryas

In the speleothem records the Younger Dryas (Nahanagan) Stadial commences at 12.4 Ka BP and lasts 900 years (figure 3.14). The onset of the Stadial is relatively rapid, with cooling of up to 6.5°C taking place over 200 years (figure 3.14). $\delta^{18}O$ of lake sediments at Gerzensee in Switzerland (Oeschger *et al.*, 1980), Lake Gosciaz, Poland (Goslar *et al.*, 1993) and $\delta^{18}O$ in Greenland ice cores (Grootes *et al.*, 1993) show similar rates of temperature decline at the start of the YD. However, the data for Lake Gosciaz suggest a YD of 1,640 years duration, ending at 11.2 Ka BP, although there are large errors associated with these ages (up to 500 years) and the authors express some reservations about their dating of the YD event (Goslar *et al.*, 1993). From deep-sea core evidence (Broecker, 1994) and examination of the rates of palaeoclimate change during the YD, Swabey *et al.* (submitted) have suggested the main control on the form and strength of the Irish YD is the presence of icebergs in the North Altantic – the so-called Heinrich events (Heinrich, 1988).

As the YD commences, $\delta^{18}O$ shows rapid cooling (figure 3.6), LI peaks dramatically (figure 3.10) and $\delta^{13}C$ becomes more negative (soil CO_2

values) in both speleothems (figure 3.8). A secondary peak in LI, just after the maximum YD cold event in $\delta^{18}O$ (12.0 Ka BP) is also matched by a peak in $\delta^{13}C$, indicating further organic material arriving in the

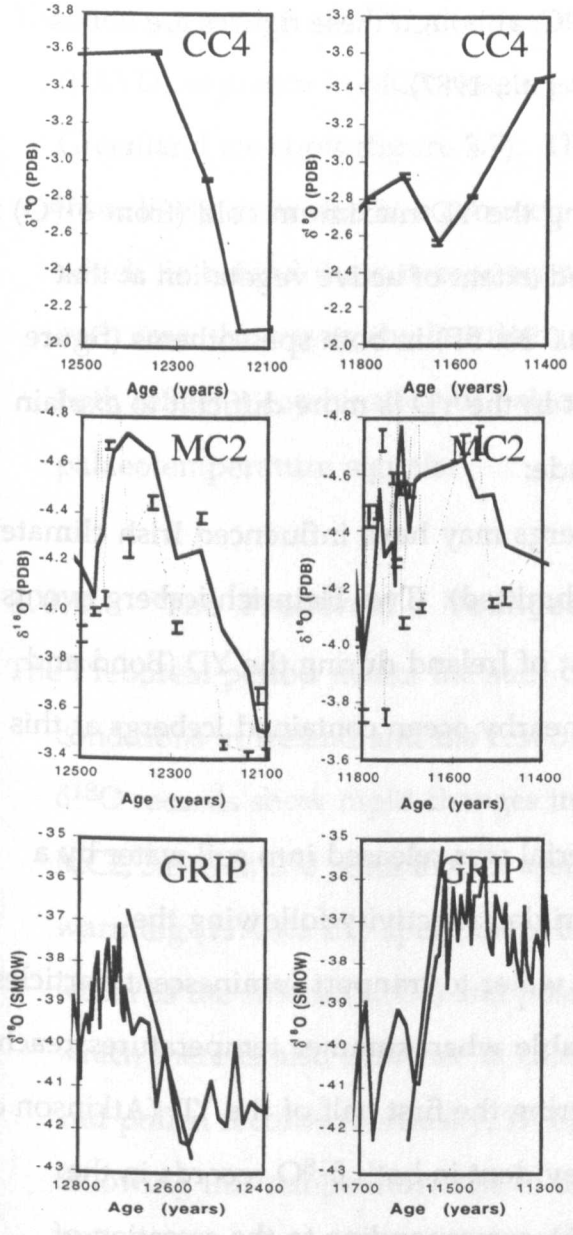

Figure 3.14. Rates of $\delta^{18}O$ change into and out of the Younger Dryas in CC4 (top panel), MC2 (middle panel) and the GRIP ice-core (bottom panel). Both speleothem $\delta^{18}O$ records place the YD transitions at the same position in time (12.5–12.1 Ka BP and 11.8–11.4 Ka BP). The GRIP ice-core $\delta^{18}O$ transitions are plotted at the position of the Allerød-YD and YD-Preboreal transitions designated by Johnsen et al. (1992) using their layer-counted dating. The discrepancy in age for the YD transitions between the ice-core and Irish speloethem records is approximately 300 years at the start and 100 years at the end of that event. However, the rate of cooling is similar in all three records. The rate of warming at the end of the YD is also similar in all three records, with MC2 warming slightly faster.

interior of both caves (figures 3.8 & 3.9). These synchronous changes in $\delta^{18}O$, $\delta^{13}C$ and LI probably indicate massive plant mortality at the start of the severe cold of the YD. The YD is marked by the spread of tundra vegetation in Irish pollen records, revealing a sharp decrease in temperature. Severe erosion also becomes common at the transition

from the Allerød to YD (Watts, 1985) and on the Dingle peninsula periglacial activity was renewed (Barnosky, 1988). Mean annual temperature in the British Isles probably declined to -5°C, whilst winter temperatures were -15°C to -20°C, although these figures are not as extreme as the LGM (Atkinson *et al.*, 1987).

The fall in LI immediately following the YD maximum cold (from $\delta^{18}O$) in CC4 probably records the limited extent of active vegetation at that point. The later peak in LI (~12.0 Ka BP) in both speleothems (figure 3.10) after the second cold event in the YD is more difficult to explain but two possible scenarios include:

i) More than one outburst of icebergs may have influenced Irish climate during the YD (Swabey *et al.* submitted). Two Heinrich iceberg events are found in deep-sea cores west of Ireland during the YD (Bond and Lotti, 1995), indicating that the nearby ocean contained icebergs at this time.

ii) A second influx of organic material was released into soil water by a melt event after a decline in periglacial activity following the maximum cold of the YD. Soil water to tranport luminescent particles to the speleothem is only available when summer temperatures reach 0°C, which seldom occurred during the first half of the YD (Atkinson *et al.*, 1987). Gradual warming is evident in both $\delta^{18}O$ records in the second half of the YD (figure 3.6), corresponding to the cessation of periglacial activity in Atkinson's reconstruction and gradual warming out of the YD in Camp Century, Dye 3 (Johnsen *et al.*, 1989) and GISP2 (Stuiver *et al.*, 1995) ice cores from Greenland (figure 3.14). However, evidence from both speleothem $\delta^{18}O$ records for a second cold event during the YD (figure 3.6) is difficult to reconcile with the warming

conditions needed for any decline in periglacial activity from warmer summer temperatures and the first scenario is preferred.

The general pattern of $\delta^{18}O$ changes in the Bølling-Allerød-Younger Dryas (BAYD) sequence in MC2 closely parallels changes in $\delta^{18}O$ of the Greenland ice-cores (figure 3.7). The similarity between these records is most likely to be due to a common control on $\delta^{18}O$. The processes which lie behind these two proxy records are unlikely to be identical in each case. However, the fact that any similarity exists at all suggests both reflect a combination of palaeoprecipitation and palaeotemperature signals.

3.6.6. The Preboreal / Youngest Dryas

The Preboreal period marks the start of warm Holocene (Littletonian) conditions in Ireland and the rest of Europe. At the end of the YD, both $\delta^{18}O$ records show rapid changes in temperature (4.7°C in 200 years in MC2, 3.8°C in 250 years in CC4 assuming -0.24‰/°C). At the end of this warming (11.4 Ka BP) speleothem $\delta^{18}O$ suggests temperatures at least as warm as the Allerød (CC4) and possibly warmer (MC2) (figure 3.6) for which there is also evidence in coleoptera (Coope and Lemdahl, 1995) and pollen records (Barnosky, 1988) (figure 3.12). Almost immediately following this temperature rise to the first part of the Preboreal (11.4 Ka BP) both speleothem records indicate a temperature decrease of ~2°C (CC4) by 11.3 Ka BP (figure 3.6). At the same time $\delta^{13}C$ in both speleothems shifts closer to rock values (0‰ PDB) and LI indicates less contribution from organic material in the speleothems (figure 3.8). Smith & Goddard (1991) find a *Betula* (birch) peak as evidence for a cooler period in the middle of the Preboreal and note that a similar event is found in global records from as far afield as Japan. This

Preboreal oscillation has now been noted from several records in Europe and has been assigned the name of "Youngest Dryas".

Warm conditions return at the end of the Preboreal in both speleothems (10.3 Ka BP) for a short period (figure 3.6). At this point, $\delta^{13}C$ and LI (figures 3.8 & 3.9) indicate more organic material in CC4, suggesting a more productive local ecosystem or increased precipitation to flush organic material into the cave. The latter situation may have been more likely as CC4 also shows an increase in growth rate at the end of the Preboreal period (figure 3.4). Pollen records also provide evidence for this, with a transition to wetter conditions marked by a deposit of reedswamp peat and a fall in *Betula* pollen in Co. Antrim (Smith and Goddard, 1991).

3.6.7. The Boreal

Although the Boreal is generally seen as a warm, dry period at the start of the Holocene in most palaeoclimate reconstructions, in some records it appears as a cool event. For example, δD values of kerogen from Austin Lake, Michigan indicate that cold temperatures persisted until 9.8 Ka $BP_{(cal.)}$ and a further cool period was experienced to 8.3 Ka $BP_{(cal.)}$ (Törnqvist and Bierkens, 1994). In CC4 $\delta^{18}O$ values close to those of the YD maximum cold are found during the Boreal, although the relative shift in MC2 $\delta^{18}O$ is only half as great (figure 3.6). As the magnitude of the Boreal event is not experienced in other palaeoclimate records, CC4 may be recording some other influence on $\delta^{18}O$, such as changes in the source ocean $\delta^{18}O$ value, or a precipitation effect (see 3.6.8). In both speleothems, the trend in $\delta^{13}C$ is towards less organic values at the start of the Boreal (figure 3.8). At the height of the Boreal both $\delta^{18}O$ records show cooler temperatures when $\delta^{13}C$ indicates

a less organic-rich source. However, LI in CC4 peaks at a value of 12 at this point, a value not reached again until the Climatic Optimum (5 Ka BP). This is contrary to the rest of the CC4 record, where $\delta^{13}C$ closely parallels changes in LI. The MC2 LI record ends just before the Boreal (figure 3.10).

In Irish pollen records a *Corylus* (hazel) peak is found at 10.3 Ka $BP_{(cal.)}$ (Watts, 1985), but by 10.1 Ka $BP_{(cal.)}$ records in Co. Antrim show a decline in *Corylus* and general diversification of the ecosystem with invasion by forest trees (Smith and Goddard, 1991). The unusual feature of this point in Irish palaeoecology is the variety of forest species colonising the landscape in quick succession. *Pinus* (pine), *Quercus* (oak), *Ulmus* (elm), *Corylus*, *Betula* and *Salix* (willow) are all represented in low diversity pollen sequences, indicating the dominance of forest species. In some cores *Quercus* dominates, whilst *Ulmus* and *Pinus* are more important elsewhere (Watts, 1985). In the Dingle peninsula *Pinus* (37%) and *Alnus* (alder) (18%) are the most important trees, but *Betula*, *Corylus*, *Quercus*, *Ilex* (holly), and *Hedera* (ivy) also feature (Barnosky, 1988). At 10.0 Ka BP Smith & Goddard (1991) find 80% arboreal pollen in their Sluggan core (figure 3.12).

This rapidly developing vegetational succession implies massive mortality of forest species as more capable species become established. The effect on LI would be high contributions from more luminescent fulvic acids as each stage of the succession attempts to 'out-compete' both the previous phase and the next phase in the succession, and contributions from humic acids from dying trees which have been out-competed – in fact higher LI is found in CC4 at this point. The start of the Boreal also marks the last period of high growth rate in CC4, which may be due to

high levels of organic acids (from high plant mortality) available for limestone solution. This is similar to the situation found during the YD. These two events suggest that increased LI and increased growth rate in speleothems reflect a common factor of increased organic acids in the soil from decaying plants, killed by climatic stress.

3.6.8. The Holocene

Interpretation of the speleothem data after the Boreal is difficult because of the small number of U/Th ages. There appears to be general agreement between the two speleothem $\delta^{18}O$ records in magnitude and location of climatic events. There are some relatively large $\delta^{18}O$ variations in both records. By contrast, $\delta^{18}O$ records from the polar ice caps exhibit little variation after the end of the YD (figure 3.7), but speleothem $\delta^{18}O$ varies for different reasons. Speleothem $\delta^{18}O$ variations during the Holocene may reflect a precipitation amount effect (Gascoyne *et al.*, 1980), long-term changes in precipitation $\delta^{18}O$ due to changes in continentality (Dansgaard, 1961), or an ice volume effect as sea level recovered during the Holocene (Andrews *et al.*, 1973). Thus, it may not be possible to interpret the relative long-term speleothem $\delta^{18}O$ variations solely in terms of temperature. However, many other proxy records show significant palaeoclimatic variation during the Holocene. For example, the Holocene in δD of Californian bristlecone pines commences with warming out of the Boreal to a climatic optimum around 7.6 Ka $BP_{(cal.)}$ (Feng and Epstein, 1994) when temperature may have been 2°C warmer than present day (Huntley and Prentice, 1988), followed by a slow decline in temperature to the present day (Huntley, 1990).

3.7. Conclusions

1) Rapid, major shifts in Irish palaeoclimate are recorded over the last 18,000 years from speleothem palaeo-proxies.
2) Changes in cave temperature, source of carbon and luminescent molecules all reflect climate forcing in Ireland during this period, with the dominant agent probably being North Atlantic oceanic circulation (Swabey and others, submitted).
3) Warming out of the Last Glacial Maximum commenced at ~18.0 Ka BP in Ireland permitting speleothem growth, although this warming was slow and characterised by a lack of productivity in the ecosystem.
4) The IACP is placed at 13.1 Ka BP as a cool period of ~200 years.
5) The shape of the BAYD cycle in Ireland is similar to the BAYD cycle in the GRIP and GISP2 ice records, suggesting a common control on Late Glacial palaeoclimate. The Younger Dryas event in Ireland was a cooling of approximately 6.5°C over 200 years, commencing at 12.4 Ka BP. Other work has suggested this cooling may be initiated by the presence of icebergs in the North Atlantic (cf. Swabey *et al.* submitted).
6) The age of the YD is confirmed by U-Th dating as 12.4 Ka BP to 11.5 Ka BP, from both speleothem $\delta^{18}O$ records.
7) The Boreal period was a strong cooling event in Ireland, although the present shortage of U/Th dates mean the duration of this event is poorly constrained. Evidence for rapid vegetational succession in pollen cores may indicate competing plants increased fulvic acid concentrations (and speleothem LI) at this point.
8) Palaeoclimate variations in the Holocene may be synchronous in both speleothem records, although the shortage of U/Th ages during this period limits interpretation of this data for the present.
9) The nature of links between $\delta^{13}C$, $\delta^{18}O$, growth rate and luminescence need further examination, given the observed correlations between

these four variables at certain times of the Late Glacial period in Ireland. It may be concluded that speleothem LI may be controlled by plant mortality in periods of rapid palaeoclimate change, and by plant productivity during more quiescent periods.

Coxon,P. (in press) Pleistocene Climate Change: the evidence from Irish sequences. in Sweeney J., (ed.) Ireland and Global Environmental Change Royal Irish Academy. Dublin

3.8. References

Alley, R. B., Meese, D. A., Shuman, C. A., Gow, A. J., Taylor, K. C., Grootes, P. M., White, J. W. C., Ram, M., Waddington, E. D., Mayewski, P. A., and Zielinski, G. A. (1993). Abrupt increase in Greenland snow accumulation at the end of the Younger Dryas event. *Nature* **362,** 527-529.

Andrews, J. T., King, C. A. M., and Stuiver, M. (1973). Holocene sea level changes, Cumberland coast, Northwest England: eustatic and glacio-isostatic movements. *Geologie en Mijnbouw* **52,** 1-12.

Andrieu, V., Huang, C. C., O'Connell, M., and Paus, A. (1994). Lateglacial vegetation and environment in Ireland: First results from four western sites. *Quaternary Science Reviews* **12,** 681-705.

Atkinson, T. C., Briffa, K. R., and Coope, G. R. (1987). Seasonal temperatures in Britain during the past 22,000 years, reconstructed using beetle remains. *Nature* **325,** 587-592.

Atkinson, T. C., Lawson, T. J., Smart, P. L., Harmon, R. S., and Hess, J. W. (1986). New data on speleothem deposition and palaeoclimate in Britain over the last forty thousand years. *Journal of Quaternary Science* **1,** 67-72.

Baker, A., Barnes, W. L., and Smart, P. L. (1996). Speleothem luminescence intensity and spectral characteristics: Signal calibration and a record of palaeovegetation change. *Chemical Geology* **2026.**

Baker, A., and Smart, P. L. (1995). Recent flowstone growth rates: Field measurement in comparison to theoretical predictions. *Chemical Geology* **122,** 121-128.

Baker, A., Smart, P. L., Edwards, R. L., and Richards, D. A. (1993a). Annual growth banding in a cave stalagmite. *Nature* **364,** 518-520.

Baker, A., Smart, P. L., and Ford, D. C. (1993b). Northwest European palaeoclimate as indicated by growth frequency variations of secondary calcite deposits. *Palaeogeography, Palaeoclimatology, Palaeoecology* **100,** 291-301.

Barnosky, C. W. (1988). A Late-Glacial and Post-Glacial pollen record from the Dingle Peninsula, County Kerry. *Proceedings of the Royal Irish Academy* **88B,** 23-37.

Barry, R. G., and Chorley, R. J. (1987). "Atmosphere, Weather and Climate." Methuen, London.

Bastin, B. (1979). L'analyse pollinique des stalagmites: une nouvelle possibilite d'approche des fluctuations climatiques du Quaternaire. *Annales de la Societe Geologique de Belgique* **101,** 13-19.

Bogli, A. (1980). "Karst hydrology and physical speleology." Springer, Berlin.

Bond, G. C., and Lotti, R. (1995). Iceberg discharges into the North Atlantic on millenial time scales during the last glaciation. *Science* **267,** 1005-1010.

Bowen, D. Q., Rose, J., McCabe, A. M., and Sutherland, D. G. (1986). Correlation of Quaternary glaciations in England, Ireland, Scotland and Wales. *Quaternary Science Reviews* **5,** 299-340.

Broecker, W. S. (1994). Massive iceberg discharges as triggers for global climate change. *Nature* **372,** 421-424.

Broecker, W. S., Bond, G., Klas, M., Bonani, G., and Wolfli, W. (1990). A salt oscillator in the glacial Atlantic? 1. The concept. *Paleoceanography* **5,** 469-477.

Broecker, W. S., and Denton, G. H. (1989). The role of ocean-atmosphere reorganizations in glacial cycles. *Geochimica et Cosmochimica Acta* **53,** 2465-2501.

Broecker, W. S., and Denton, G. H. (1990). The role of ocean-atmosphere reorganizations in glacial cycles. *Quaternary Science Reviews* **9,** 305-341.

Colhoun, E. A., and Synge, F. M. (1980). The cirque moraines at Lough Nahanagan, County Wicklow, Ireland. *Proceedings of the Royal Irish Academy* **80B,** 25-45.

Coope, G. R., and Lemdahl, G. (1995). Regional differences in the Lateglacial climate of northern Europe based on coleopteran analysis. *Journal of Quaternary Science* **10,** 391-395.

Cropley, J. B. (1965). Influence of surface conditions on temperatures in large cave systems. *Bulletin of the National Speleological Society* **27,** 1-Oct.

Culleton, E. B., and Gardiner, M. J. (1985). Soil formation. *In* "The Quaternary History of Ireland." (K. J. Edwards, and W. P. Warren, Eds.), pp. 133-153. Academic Press, London.

Dansgaard, W. (1961). The isotopic composition of natural waters with special reference to the Greenland ice cap. *Meddr Grønland* **165,** 1-120.

Dorale, J. A., González, L. A., Reagan, M. K., Pickett, D. A., Murrell, M. T., and Baker, R. G. (1992). A high-resolution record of Holocene climate change in speleothem calcite from Cold Water Cave, Northeast Iowa. *Science* **258,** 1626-1630.

Dreybrodt, W. (1980). Deposition of calcite from thin films of calcarious solutions and the growht of speleothems. *Chemical Geology* **29,** 89-105.

Edwards, K. J., and Warren, W. P. (1985). "The Quaternary History of Ireland." Academic Press, London.

Emiliani, C. (1972). Quaternary paleotemperatures and the duration of the high temperature interval. *Science* **178,** 398-401.

Eyles, N., and McCabe, A. M. (1989). The late Devensian (<22,000 BP) Irish sea basin: the sedimentary record of a collapsed ice sheet margin. *Quaternary Science Reviews* **8,** 307-351.

Feng, X., and Epstein, S. (1994). Climatic implications of an 8000-year hydrogen isotope time series from bristlecone pine trees. *Science* **265,** 1079-1081.

Fischer, M. J., Gale, S. J., Heijnis, H., and Drysdale, R. N. (1996). Low latitude speleothems and palaeoclimate reconstruction. *In* "Climate Change: The Karst Record." (S.-E. Lauritzen, Ed.), pp. 196. Karst Waters Institute, Inc., Charles Town.

Ford, D. C., Thompson, P., and Schwarcz, H. P. (1972). Dating cave calcite deposits by the uranium disequilibrium method: Some preliminary results from Crowsnest Pass, Alberta. *In* "Research Methods in Pleistocene Geomorphology." (E. Yatsu, and A. Falconer, Eds.), pp. 247-255. D-81. Geo Abstracts, Norwich.

Ford, D. C., and Williams, P. W. (1989). "Karst Geomorphology and Hydrology." Chapman & Hall, London.

Gascoyne, M. (1984). Twenty years of uranium-series dating of cave calcites. *Studies in Speleology* **5,** 15-30.

Gascoyne, M., Schwarcz, H. P., and Ford, D. C. (1980). A palaeotemperature record for the mid-Wisconsin in Vancouver Island. *Nature* **285**, 474-476.

Goede, A., Green, D. C., and Harmon, R. S. (1986). Late Pleistocene palaeotemperature record from a Tasmanian speleothem. *Australian Journal of Earth Sciences* **33**, 333-342.

Goslar, T., Kuc, T., Ralska-Jasiewiczowa, M., Rozanski, K., Arnold, M., Bard, E., van Geel, B., Mieczyslaw, F. P., Szeroczynska, K., Wicik, B., Wieckowski, K., and Walanus, A. (1993). High-resolution lacustrine record of the Late Glacial/Holocene transition in Central Europe. *Quaternary Science Reviews* **12**, 287-294.

Grootes, P. M., Stuiver, M., White, J. W. C., Johnsen, S., and Jouzel, J. (1993). Comparison of oxygen isotope records from the GISP2 and GRIP Greenland ice cores. *Nature* **366**, 552-554.

Harmon, R. S., White, W. B., Drake, J. J., and Hess, J. W. (1975). Regional hydrochemistry of North American carbonate terrains. *Water Resources Research* **11**, 963.

Heinrich, H. (1988). Origin and consequences of cyclic ice rafting in the Northeast Atlantic Ocean during the past 130,000 years. *Quaternary Research* **29**, 142-152.

Hendy, C. H. (1971). The isotopic geochemistry of speleothems-I. The calculation of the effects of different modes of formation on the isotopic composition of speleothems and their applicability as palaeoclimatic indicators. *Geochimica et Cosmochimica Acta* **35**, 801-824.

Huntley, B. (1990). European vegetation hisotry: palaeovegetation maps from pollen data – 13 000 yr BP to present. *Journal of Quaternary Science* **5**, 103-122.

Huntley, B., and Prentice, I. C. (1988). July temperatures in Europe from pollen data, 6000 years before present. *Science* **241**, 687-690.

Johnsen, S. J., Clausen, H. B., Dansgaard, W., Fuhrer, K., Gundestrup, N., Hammer, C. U., Iversen, P., Jouzel, J., Stauffer, B., and Steffensen, J. P. (1992). Irregular glacial interstadials recorded in a new Greenland ice core. *Nature* **359**, 311-313.

Johnsen, S. J., Dansgaard, W., and White, J. W. C. (1989). The origin of Arctic precipitation under present and glacial conditions. *Tellus* **41**, 452-468.

Kaufman, A. (1993). An evaluation of several methods for determining $^{230}Th/^{238}U$ ages in impure carbonates. *Geochimica et Cosmochimica Acta* **57**, 2303-2317.

Lange, A. (1954). Rock temperature distributions underground, part 1. *Cave Studies* **1,** 21-25.

Latham, A. G., Schwarcz, H. P., Ford, D. C., and Pearce, G. W. (1979). Palaeomagnetism of stalagmite deposits. *Nature* **280,** 383-385.

Lehman, S. J., and Keigwin, L. D. (1992). Sudden changes in North Atlantic circulation during the last deglaciation. *Nature* **356,** 757-762.

Mangerud, J., Andersen, S. T., Berglund, B. E., and Donner, J. J. (1974). Quaternary stratigraphy of Norden, a proposal for terminology and classification. *Boreas* **3,** 109-128.

Moser, M., and Geyer, M. (1979). Seismospelaologic-Erdbebenzerstorungen in Hohlen am Beispiel des Gaislochs bei Oberfellendorf (Oberfranken, Bayern). *Die Hohle* **4,** 89-102.

Nepstad, J., and Pisarowicz, J. (1989). Wind Cave, South Dakota: Temperature and humidity variations. *National Speleological Society Bulletin* **51,** 125-128.

Noel, M. (1990). Palaeomagnetic and archaeomagnetic studies in the caves of Guangxi. *Cave Science* **17,** 73-76.

O'Neil, J. R., Clayton, R. N., and Mayeda, T. (1969). Oxygen isotope fractionation in divalent metal carbonates. *Journal of Chemical Physics* **51,** 5547-5558.

Oeschger, H., Welten, M., Eicher, U., Moll, M., Riesen, T., Siegenthaler, U., and Wegmuller, S. (1980). ^{14}C and other parameters during the Younger Dryas cold phase. *Radiocarbon* **22,** 299-310.

Rahmstorf, S. (1994). Rapid climate transitions in a coupled ocean atmosphere model. *Nature* **372,** 82-85.

Ruddiman, W. F., and McIntyre, A. (1981). The North Atlantic Ocean during the last deglaciation. *Paleogeography, Paleoclimatology, Paleoecology* **35,** 145-214.

Schwarcz, H. P., and Harmon, R. S. (1976). Stable isotope studies of fluid inclusions in speleothems and their paleoclimatic significance. *Geochimica et Cosmochimica Acta* **40,** 657-665.

Senesi, N., Miano, T. M., Provenzano, M. R., and Brunnett, G. (1991). Characterization, differentiation, and classification of humic substances by fluorescence spectroscopy. *Soil Science* **152,** 259-271.

Shopov, Y. Y., Ford, D. C., and Schwarcz, H. P. (1994). Luminescent microbanding in speleothems: High-resolution chronology and paleoclimate. *Geology* **22,** 407-410.

Smith, A. G., and Goddard, I. C. (1991). A 12500 year record of vegetational history at Sluggan Bog, Co. Antrim, N. Ireland (incorporating a pollen zone scheme for the non-specialist). *New Phytologist* **118**, 167-187.

Stuiver, M., Grootes, P. M., and Braziunas, T. F. (1995). The GISP2 $\delta^{18}O$ climate record of the past 16,500 years and the role of the sun, ocean, and volcanoes. *Quaternary Research* **44**, 341-354.

Szabo, B. J., Miller, G. H., Andrews, J. T., and Stuiver, M. (1982). Reply to comment on "Comparison of uranium-series, radiocarbon, and amino acid data from marine molluscs, Baffin Island, Arctic Canada. *Geology* **10**, 439-440.

Talma, A. S., and Vogel, J. C. (1992). Late Quaternary paleotemperatures derived from a speleothem from Cango Caves, Cape Province, South Africa. *Quaternary Research* **37**, 203-213.

Teeri, J. A., and Stowe, L. G. (1976). Climatic patterns and the distribution of C4 grasses in North America. *Oecologia* **23**, 1-Dec.

Törnqvist, T. E., and Bierkens, M. F. P. (1994). How smooth should curves by for calibrating radiocarbon ages? *Radiocarbon* **36**, 11-26.

Walker, I. R., Mott, R. J., and Smol, J. P. (1991). Allerød-Younger Dryas lake temperatures from midge fossils in Atlantic Canada. *Science* **253**, 1010-1012.

Walker, M. J. C., Bohncke, S. J. P., Coope, G. R., O'Connell, M., Usinger, H., and Verbruggen, C. (1994). The Devensian/Weichselian Late-glacial in northwest Europe (Ireland, Britain, north Belgium, The Netherlands, northwest Germany). *Journal of Quaternary Science* **9**, 109-118.

Watts, W. A. (1985). Quaternary vegetation cycles. *In* "The Quaternary History of Ireland." (K. J. Edwards, and W. P. Warren, Eds.), pp. 155-185. Academic Press, London.

Wohlfarth, B. (1996). The chronology of the last termination: A review of radiocarbon-dated, high-resolution terrestrial stratigraphies. *Quaternary Science Reviews* **15**, 267-284.

Yu, E.-F., Francois, R., and Bacon, M. P. (1996). Similar rates of modern and last-glacial ocean thermohaline circulation inferred from radiochemical data. *Nature* **379**, 689-694.

Chapter 4: Speleothems date the Younger Dryas: U-Th ages from the Late Glacial in Ireland

For the first time, the Younger Dryas (YD) and other Late Glacial palaeoclimatic events have been detected in two independent high-resolution stalagmite $\delta^{18}O$ time-series records. Uranium-Thorium dating of the stalagmite calcite by thermal ionisation mass spectrometry (TIMS) places the YD between 12,550± 73 and 11,350± 180 years Before Present (BP). The Late Glacial $\delta^{18}O$ variations provide a robust record of regional palaeoclimate because two stalagmites from cave systems some 100 km apart exhibit coherent variations for 3,000 years. Key features of both records include a moderate cooling rate at the start of the YD and slow interrupted warming following the coldest period of the YD. The latter coincides with the timing of iceberg outbursts in the N. Atlantic during the YD, suggesting that sub-Milankovitch climate oscillations like the YD may be driven by atmosphere-cryosphere variations, rather than changes in ocean circulation.

It remains frustratingly difficult to establish accurate chronologies of past climate events (Bard *et al.*, 1993), and there is considerable interest in

the age of the Younger Dryas (Broecker *et al.*, 1988; Denton and Hendy, 1994). Although estimated error limits for ice core ages can be as low as ± 70 years at 11.5 ky (Johnsen *et al.*, 1992) more conservative estimates suggest errors of ± 250 and ± 625 at the beginning and end of the Younger Dryas (Alley *et al.*, 1993). Similarly, recalibration of the radiocarbon timescale using U-Th ages on corals and tree-ring chronologies has shown that ^{14}C ages during the Younger Dryas period are subject to large systematic errors (Bard *et al.*, 1993), and one ^{14}C age may be equivalent to as many as seven different 'real' ages (Stuiver and Reimer, 1993). Here I report new TIMS U-Th ages on two speleothem $\delta^{18}O$ records from caves in SW Ireland, which provide a new absolute age for the Younger Dryas, and further insights into the causes of sub-Milankovitch palaeoclimate oscillations.

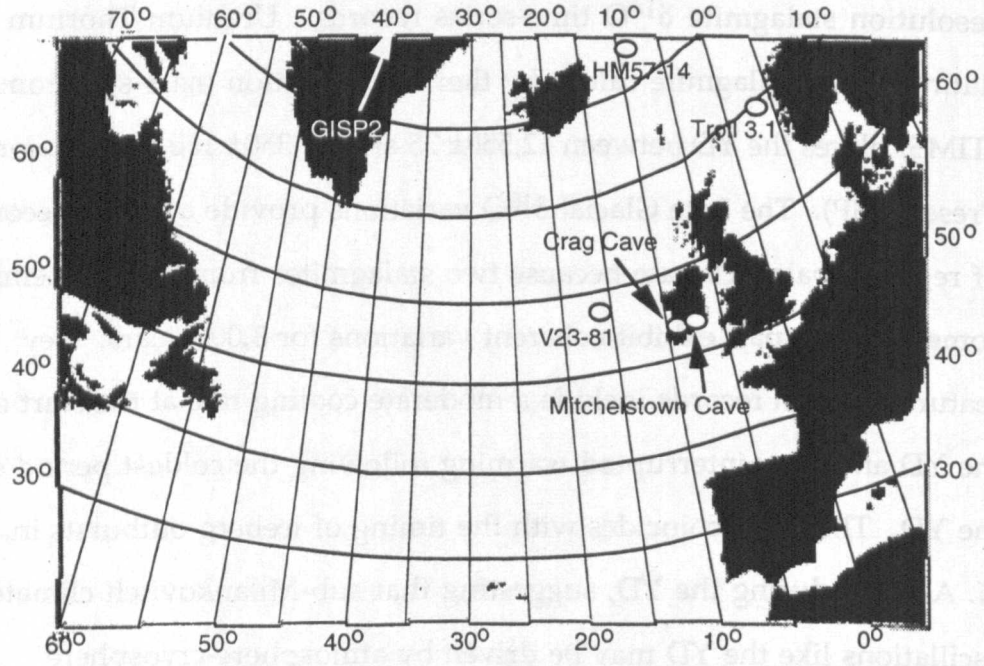

Figure 4.1. Map of the N. Atlantic region showing the location of the two cave sites in S.W. Ireland, Summit core GISP2 and the deep-sea drill sites discussed in the text.

Oxygen isotope, electrical conductivity and chemical data from the Greenland ice cores (Grootes *et al.*, 1993; Mayewski *et al.*, 1993), together

with recent detailed studies on selected N. Atlantic sediment cores (Bond *et al.*, 1993) have revealed unexpectedly large climatic oscillations during the last glacial and subsequent deglaciation (Koç Karpuz and Jansen, 1992; Ruddiman and McIntyre, 1973). These sub-Milankovitch oscillations apparently involve large-scale reorganisations of the cryosphere, atmosphere and oceans (Broecker and Denton, 1990), although the driving mechanism remains poorly understood. For example, key palaeoclimate records (e.g. N. Atlantic sea surface temperatures inferred from *N. Pachyderma* s. abundances) have poor time resolution, are difficult to date precisely and/or may be affected by bioturbation (Lehman and Keigwin, 1992). Speleothems (cave calcites) by contrast, offer the possibility of precisely dated high-resolution records of terrestrial palaeoclimate (Atkinson *et al.*, 1986; Baker *et al.*, 1993). In this study, oxygen isotope ($\delta^{18}O$) data (figure 4.2 are presented for two U-Th dated stalagmites (CC4 and MC2) obtained respectively from Crag and Mitchelstown Caves in S.W. Ireland (figure 4.1). The cave sites were chosen for their proximity to the N. Atlantic ocean and their sensitivity to events in the N. Atlantic – a key region because many models have ascribed sub-Milankovitch climatic changes to variations in the thermohaline circulation pattern of this ocean (Berger and Vincent, 1986; Broecker *et al.*, 1990). The stalagmites grew during the Late Glacial and early Holocene, and both include the Younger Dryas (YD), a relatively brief return to near-glacial conditions previously placed some 12,890-11,650 years ago (Stuiver *et al.*, 1995). Ten U-Th TIMS ages were obtained for CC4 and 9 ages for MC2 (table 4.1), including nine ages from both speleothems during the YD. Precise dating of MC2 was hindered by its extremely low U abundance, a problem that is most acute in its younger (lower ^{230}Th) part. For this reason I focus here on the more coherent and well-dated Late Glacial

events while noting that several smaller less well dated $\delta^{18}O$ oscillations occur during the Holocene (see chapter 3). Details of sampling intervals, analytical techniques and precision of $\delta^{18}O$ are given in the caption to figure 4.2.

Distance (mm)	^{238}U (µg/g)	error	$(^{234}U/^{238}U)$	error	$(^{230}Th/^{234}U)$	error	$(^{230}Th/^{232}Th)$	Age (years)	1σ error
CC4									
0	1.9067	0.0123	0.9772	0.0012	0.1568	0.0027	13	18560	350
55	4.0634	0.0021	0.9800	0.0128	0.1251	0.0023	27	14540	290
80	3.6282	0.0056	0.9865	0.0028	0.1073	0.0004	175	12350	49
85	3.4331	0.0054	0.9853	0.0021	0.1064	0.0003	504	12240	37
100	4.3785	0.0093	0.9892	0.0027	0.1045	0.0003	889	12010	36
145	5.5026	0.0016	0.9740	0.0011	0.0991	0.0015	3522	11350	180
160	4.9215	0.0170	0.9729	0.0014	0.0902	0.0008	3479	10280	96
185	4.2673	0.0011	0.9997	0.0146	0.0848	0.0013	683	9637	150
205	3.0280	0.0024	0.9959	0.0112	0.0697	0.0010	1308	7857	120
288	2.5510	0.0040	0.9709	0.0003	0.0277	0.0002	65	3055	22
MC2									
10	0.1295	0.0000	1.0882	0.0011	0.1260	0.0029	15	14620	360
15	0.1490	0.0003	1.1434	0.0066	0.1146	0.0017	20	13200	210
92	0.1284	0.0002	1.1100	0.0061	0.1129	0.0011	17	13000	130
107	0.1300	0.0002	1.1010	0.0048	0.1092	0.0006	20	12550	73
143	0.1219	0.0002	1.1716	0.0079	0.1059	0.0009	18	12140	110
180	0.1076	0.0002	1.1513	0.0078	0.1045	0.0009	18	11980	110
195	0.0994	0.0001	1.1100	0.0044	0.1040	0.0012	31	11920	150
295	0.0995	0.0000	1.0878	0.0015	0.1019	0.0022	19	11670	270
522	0.0696	0.0001	1.0993	0.0039	0.0420	0.0018	11	4663	200

Table 4.1. Mass-spectrometric U-series data and calculated ages for samples from speleothems CC4 and MC2 discussed in the text. Distance of samples is from the base of the speleothems. All errors are at the 1σ level. Decay constants: ^{234}U 2.8211×10^{-6}; ^{230}Th 9.1954×10^{-6}.

$\delta^{18}O$ varies from -2.1‰ to -3.6‰ in CC4 and -2.7‰ to -5.4‰ in MC2. $\delta^{18}O$ in MC2 is typically some 1.2‰ lighter than in CC4 (figure 4.2), an offset consistent with the c. 200m difference in elevation between the

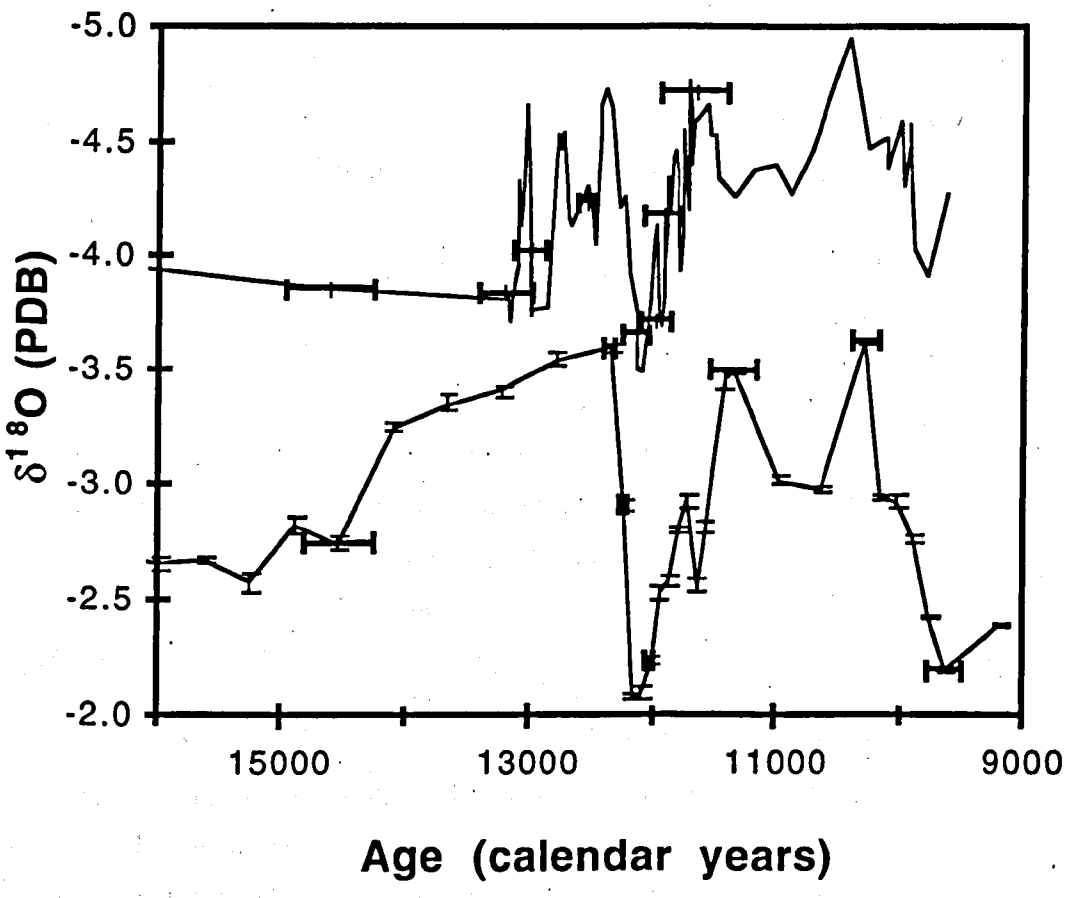

Figure 4.2. $\delta^{18}O$ records for MC2 (top) and CC4 (bottom). Samples for O isotope measurements were drilled initially at 5 mm intervals along the growth axes of both speleothems, and subsequently every 1mm over selected intervals. Thus, each O isotope measurement represents a time interval of <1 year to 40 years in MC2, and 11 to 58 years in CC4. Replicate analyses of an internal calcite standard indicate an external precision of ±0.1‰ for $\delta^{18}O$. U-Th TIMS ages are indicated at the sampling position with 1σ age errors. $\delta^{18}O$ is interpolated directly between U-Th ages. $\delta^{18}O$ in MC2 is smoothed with a simple 3 point moving average to eliminate high-frequency scatter.

two cave sites (Dansgaard, 1961). The most striking feature of both records is synchronous (within error) shifts in $\delta^{18}O$ during some 3,000 years (~ 13,000 to 10,000 years) of the Late Glacial. Lasting approximately 1,000 years, the YD is the largest $\delta^{18}O$ oscillation in both records, shifting by approximately 1.5‰ in CC4 and by 1.4‰ in MC2. A variety of published ages for the end of the YD is given here (table

4.2), together with the age for the same event from U-Th TIMS dating of the speleothems.

YD end (years BP)	Method	Comment
11640 ± 250*	GISP2 ice core, layer count	
11550 ± 70*	GRIP ice core, layer count	isotopic & other data
11700*	14C calibrated age	
11200-11500*	14C calibrated age	
11000-11700*	varve calibration of ^{14}C	also change in $\delta^{18}O$
>11300	tree-ring calibration of ^{14}C	
>10720 ± 150	Dye 3 ice core, Greenland	interpretation of data
10500-10800	varve calibration of ^{14}C	preliminary
10630	varve date for pollen change	
11500	average of entries marked *	mean age for YD termination
11350 ± 180	speleothem U-Th TIMS dated $\delta^{18}O$ record	termination age for this work

Table 4.2. The age of the termination of the YD from a variety of proxy records, after Alley *et al.* (1993). Most palaeoclimate proxies do not record the start of the YD with sufficient precision to make this information useful to present here. The ice-core records and some of the lake-varve records directly date climate events associated with the YD termination. U-Th years, tree-ring years, varve years and ice-core years as treated as equivalent timescales, although errors vary according to the technique used. The ^{14}C ages are calibrated using Bard's calibration technique.

In Ireland the well documented but poorly dated YD event (Andrieu *et al.*, 1994; Cwynar and Watts, 1989; Smith and Goddard, 1991) is characterised by a predominance of non-arboreal pollen in lake sediments, reflecting a sharp decrease in temperature (Barnosky, 1988). Lake sediments also record severe erosion at the Allerød–YD transition (Watts, 1985) and on the Dingle peninsula (S.W. Ireland) vegetation became sparse and periglacial activity was renewed (Barnosky, 1988). Coleoptera assemblages for this period indicate that mean annual temperatures in the British Isles declined to -5°C, whilst winter temperatures were -15°C to -20°C (Atkinson *et al.*, 1987).

Palaeotemperature estimates based on pollen from Irish sites suggest a decrease in mean annual temperatures of 6°C at the Allerød–YD transition (Edwards and Warren, 1985)and a change in mean July temperature of 7°C (Coope and Lemdahl, 1995; Walker *et al.*, 1994).

Unfortunately a quantitative palaeoclimatic interpretation of $\delta^{18}O$ in speleothem calcite is not straightforward. However, I am confident that $\delta^{18}O$ in the Irish speleothems represents cave temperature because:

(i) Calcite from single layers in MC2 exhibits no correlation between $\delta^{18}O$ and $\delta^{13}C$ (Hendy and Wilson, 1968).

(ii) $\delta^{18}O$ in the speleothem calcite analysed here is heavier during the Last Glacial termination, implying the temperature effect is dominant.

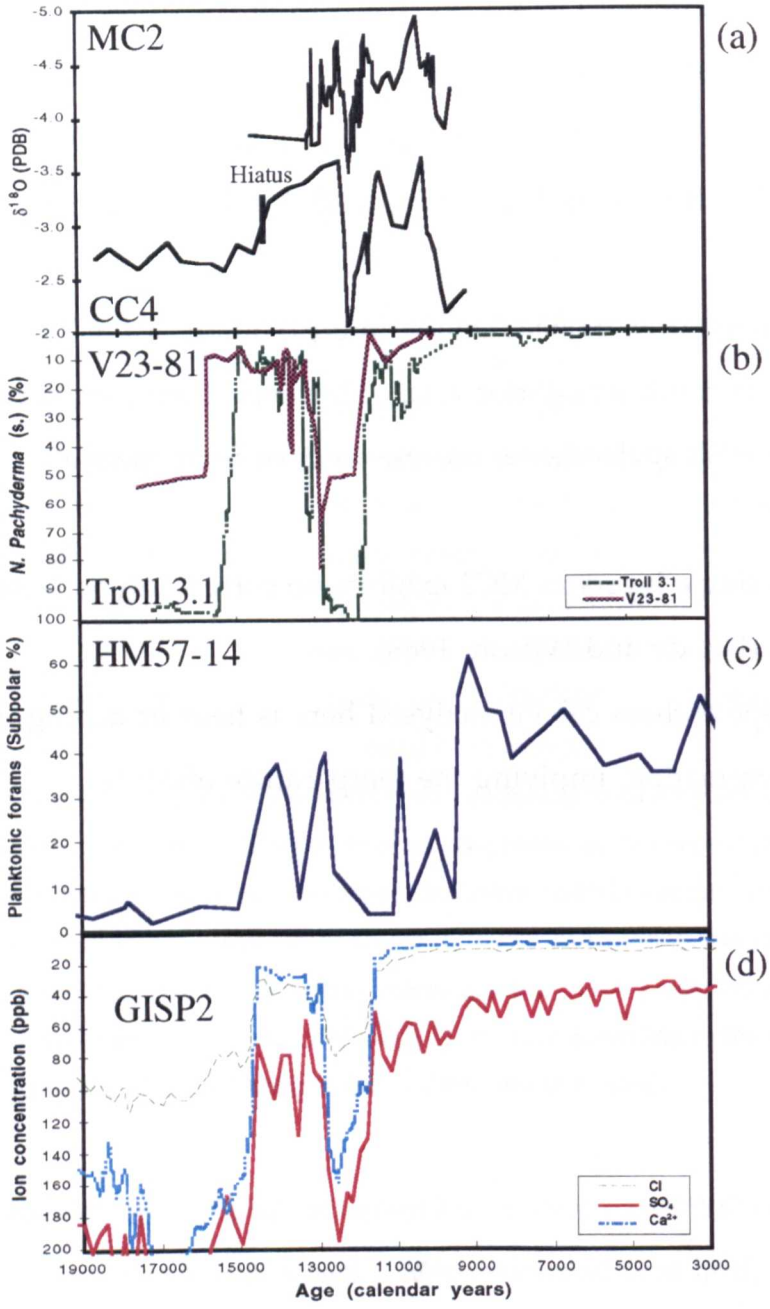

Figure 4.3. Various palaeoclimate proxy records compared to MC2 and CC4 $\delta^{18}O$. a) MC2 and CC4 $\delta^{18}O$ records to the same time scale as the rest of the figure. b) *N. Pachyderma* (s.) abundances in cores V23-81 (solid line) and Troll 3.1 (dashed line). Published radiocarbon ages have been converted to calender years using data contained in MacCalib 3.0 (Stuiver and Reimer, 1993). c) Subpolar planktonic forams in core HM57-14 (Sejrup *et al.*, 1995). d) Chloride (Cl), sulphate (SO_4) and calcium (Ca^{2+}) ion concentrations in ice-core GISP2 from Summit, Greenland. Dating is by layer counting (Mayewski *et al.*, 1993).

Finally, a temperature-dependent fractionation in CC4 and MC2 $\delta^{18}O$ of -0.23‰ and -0.25‰ per °C is inferred on the basis of the independent palaeoclimate proxy data (coleoptera and pollen) if $\delta^{18}O$ primarily reflects temperature change during the YD. This is similar to the range (-0.22‰/°C at 20°C and -0.24‰/°C at 10°C) calculated previously for temperature-dependent fractionation in speleothems (Gascoyne, 1992). On the basis of these independent estimates, both speleothem records indicate cooling at the onset of the YD of up to 6.3°C over 200 years. A similar rate of change is found in $\delta^{18}O$ records from deep-sea core Troll 3.1 (Lehman and Keigwin, 1992), V23-81 (Bond *et al.*, 1993), the GRIP and GISP2 ice cores (Grootes *et al.*, 1993) (figure 4.3), lake sediments at Gerzensee in Switzerland (Oeschger *et al.*, 1980) and Lake Gosciaz, Poland (Goslar *et al.*, 1993). However, the $\delta^{18}O$ of precipitation source waters may have been ~0.6‰ heavier in the Atlantic off Ireland during the YD (Jansen and Veum, 1990), so the total temperature-dependent $\delta^{18}O$ shift was probably closer to 2.0‰, suggesting cooling of 8–9°C at the YD in Ireland.

The speed of cooling at the start of the YD precludes Milankovitch insolation variations as the sole forcing factor (Overpeck *et al.*, 1989). Thus, changes in atmospheric or oceanic conditions seem to be the only plausible driving mechanism for such extreme and extensive shifts in Irish palaeoclimate. There is comprehensive evidence that N. Atlantic sea surface temperatures (SSTs), as recorded by the relative abundance of *N. Pachyderma* s. in deep-sea cores were significantly lower during the YD (Boyle and Rosener, 1990), although there is a paucity of well-dated oceanic cores which cover this time interval. Those that do (e.g. cores V23-81, Troll 3.1 and HM57-14, see figure 4.1) appear to have YD excursions with significantly different shapes. V23-

81 exhibits an asymmetric 'v' or 'saw-tooth' shape with a marked hiatus in the rate of warming following the YD, whereas cores Troll 3.1 and HM57-14 from further north in the Atlantic exhibit 'U-shape' patterns. Previously these differences were interpreted as the smoothing influence of bioturbation in V23-81 (Lehman and Keigwin, 1992), but our observation that the shape of the YD event in our speleothem records is similar to V23-81 indicates that both reflect SSTs in the eastern N. Atlantic. This in turn implies that recovery from the YD cooling was gradual and interrupted, occurring over a period of some 600 years. Cores Troll 3.1 and HM57-14 located in the northern N. Atlantic/Norwegian Sea on the other hand, are extremely sensitive to the flux of sub-polar planktonic foraminifera from the N. Atlantic in the Norwegian Current (Sejrup *et al.*, 1995), and so may represent a more regional palaeoclimate signal.

A significant recent discovery is that deep-sea cores from the Atlantic west of Ireland, including V23-81 (Bond and Lotti, 1995) contain detrital ice-rafted carbonate material derived from the Hudson Strait (Bond *et al.*, 1992) at the time of the YD – evidence for an iceberg outbreak event similar to the well-documented Heinrich events of the last glaciation (Heinrich, 1988). In our preferred model, an outburst of icebergs into the N. Atlantic would have driven the polar front southwards over the British Isles (Ruddiman and McIntyre, 1981), bringing expansion of the atmospheric polar cell (Kapsner *et al.*, 1995) and air-mass cooling, as recorded in the Irish speleothems. The two-step recovery following the YD documented here is also consistent with recently published data indicting two peaks in ice-rafted haematite-coated and basaltic glass grains west of Ireland during the YD (Bond and Lotti, 1995). Arguably such an ice-driven model is preferable to the alternative ocean-driven

model (Broecker *et al.*, 1990) because in the latter it is necessary to invoke an ad-hoc 'false restart' of NADW formation to acount for a two-stage YD recovery, for which no independent evidence exists.

Finally, variations with time in the concentrations of several trace elements in the Greenland ice cores, a proxy for the size of the atmospheric polar cell (Mayewski *et al.*, 1993) have a broadly 'v'-shape for the YD, and bear a striking resemblence to both speleothem $\delta^{18}O$ records (figure 4.3d). Significantly, recent studies of Pacific ocean sediments suggest that the size of the polar cell is also an important factor linking Heinrich events in the Pacific and Atlantic through atmospheric circulation (Kotilaninen and Shackleton, 1995; Thunell, 1995). These well-dated observations of the Late Glacial reinforce the notion that cryosphere-driven atmospheric reorganisations may be the key driving mechanism for sub-Milankovitch climate oscillations. More importantly, I provide internally-consistent ages from a continental setting for the age and duration of the intriguing Younger Dryas cold event.

References

Alley, R. B., Meese, D. A., Shuman, C. A., Gow, A. J., Taylor, K. C., Grootes, P. M., White, J. W. C., Ram, M., Waddington, E. D., Mayewski, P. A., and Zielinski, G. A. (1993). Abrupt increase in Greenland snow accumulation at the end of the Younger Dryas event. *Nature* **362**, 527-529.

Andrieu, V., Huang, C. C., O'Connell, M., and Paus, A. (1994). Lateglacial vegetation and environment in Ireland: First results from four western sites. *Quaternary Science Reviews* **12**, 681-705.

Atkinson, T. C., Briffa, K. R., and Coope, G. R. (1987). Seasonal temperatures in Britain during the past 22,000 years, reconstructed using beetle remains. *Nature* **325**, 587-592.

Atkinson, T. C., Lawson, T. J., Smart, P. L., Harmon, R. S., and Hess, J. W. (1986). New data on speleothem deposition and palaeoclimate in Britain over the last forty thousand years. *Journal of Quaternary Science* **1**, 67-72.

Baker, A., Smart, P. L., Edwards, R. L., and Richards, D. A. (1993). Annual growth banding in a cave stalagmite. *Nature* **364**, 518-520.

Bard, E., Arnold, M., Fairbanks, R. G., and Hamelin, B. (1993). ^{230}Th-^{234}U and ^{14}C ages obtained by mass spectrometry on corals. *Radiocarbon* **35**, 191-199.

Barnosky, C. W. (1988). A Late-Glacial and Post-Glacial pollen record from the Dingle Peninsula, County Kerry. *Proceedings of the Royal Irish Academy* **88B**, 23-37.

Berger, W. H., and Vincent, E. (1986). Sporadic shutdown of North Atlantic deep water production during the Glacial-Holocene transition? *Nature* **324**, 53-55.

Bond, G., Broecker, W. S., Johnsen, S., McManus, J., Labeyrie, L. D., Jouzel, J., and Bonani, G. (1993). Correlations between climate records from North Atlantic sediments and Greenland ice. *Nature* **365**, 143-147.

Bond, G., Heinrich, H., Broecker, W. S., Labeyrie, L., McManus, J., Andrews, J., Huon, S., Janshik, R., Clasen, S., Simet, C., Tedesco, K., Klas, M., Bonani, G., and Ivy, S. (1992). Evidence for massive discharges of icebergs into the North Atlantic during the last glacial period. *Nature* **360**, 245-249.

Bond, G. C., and Lotti, R. (1995). Iceberg discharges into the North Atlantic on millenial time scales during the last glaciation. *Science* **267**, 1005-1010.

Boyle, E. A., and Rosener, P. (1990). Further evidence for a link between Late Pleistocene North Atlantic surface temperatures and North Atlantic Deep-Water production. *Palaeogeography, Palaeoclimatology, Palaeoecology (Global and Planetary Change Section)* **89**, 113-124.

Broecker, W. S., Andree, M., Wolfli, W., Oeschger, H., Bonani, G., Kennett, J., and Peteet, D. (1988). The chronology of the last deglaciation: implications to the cause of the Younger Dryas event. *Paleoceanography* **3**, 1-19.

Broecker, W. S., Bond, G., Klas, M., Bonani, G., and Wolfli, W. (1990). A salt oscillator in the glacial Atlantic? 1. The concept. *Paleoceanography* **5**, 469-477.

Broecker, W. S., and Denton, G. H. (1990). The role of ocean-atmosphere reorganizations in glacial cycles. *Quaternary Science Reviews* **9**, 305-341.

Coope, G. R., and Lemdahl, G. (1995). Regional differences in the Lateglacial climate of northern Europe based on coleopteran analysis. *Journal of Quaternary Science* **10,** 391-395.

Cwynar, L. C., and Watts, W. A. (1989). Accelerator-mass spectrometry ages for Late-Glacial events at Ballybetagh, Ireland. *Quaternary Research* **31,** 377-380.

Dansgaard, W. (1961). The isotopic composition of natural waters with special reference to the Greenland ice cap. *Meddr Grønland* **165,** 1-120.

Denton, G. H., and Hendy, C. H. (1994). Younger Dryas age advance of Franz Josef glacier in the Southern alps of New Zealand. *Science* **264,** 1434-1436.

Edwards, K. J., and Warren, W. P. (1985). "The Quaternary History of Ireland." Academic Press, London.

Gascoyne, M. (1992). Palaeoclimate determination from cave calcite deposits. *Quaternary Science Reviews* **11,** 609-632.

Goslar, T., Kuc, T., Ralska-Jasiewiczowa, M., Rozanski, K., Arnold, M., Bard, E., van Geel, B., Mieczyslaw, F. P., Szeroczynska, K., Wicik, B., Wieckowski, K., and Walanus, A. (1993). High-resolution lacustrine record of the Late Glacial/Holocene transition in Central Europe. *Quaternary Science Reviews* **12,** 287-294.

Grootes, P. M., Stuiver, M., White, J. W. C., Johnsen, S., and Jouzel, J. (1993). Comparison of oxygen isotope records from the GISP2 and GRIP Greenland ice cores. *Nature* **366,** 552-554.

Heinrich, H. (1988). Origin and consequences of cyclic ice rafting in the Northeast Atlantic Ocean during the past 130,000 years. *Quaternary Research* **29,** 142-152.

Hendy, C. H., and Wilson, A. T. (1968). Palaeoclimatic data from speleothems. *Nature* **219,** 48-51.

Jansen, E., and Veum, T. (1990). Evidence for two-step deglaciation and its impact on North Atlantic deep-water circulation. *Nature* **343,** 612-616.

Johnsen, S. J., Clausen, H. B., Dansgaard, W., Fuhrer, K., Gundestrup, N., Hammer, C. U., Iversen, P., Jouzel, J., Stauffer, B., and Steffensen, J. P. (1992). Irregular glacial interstadials recorded in a new Greenland ice core. *Nature* **359,** 311-313.

Kapsner, W. R., Alley, R. B., Shuman, C. A., Anandakrishnan, S., and Grootes, P. M. (1995). Dominant influence of atmospheric circulation on snow accumulation in Greeland over the past 18,000 years. *Nature* **373,** 52-54.

Koç Karpuz, N., and Jansen, E. (1992). A high-resolution diatom record of the last deglaciation from the SE Norwegian Sea: Documentation of rapid climate changes. *Paleoceanography* **7**, 499-520.

Kotilaninen, A. T., and Shackleton, N. J. (1995). Rapid climate variability in the North Pacific Ocean during the past 95,000 years. *Nature* **377**, 323-326.

Lehman, S. J., and Keigwin, L. D. (1992). Sudden changes in North Atlantic circulation during the last deglaciation. *Nature* **356**, 757-762.

Mayewski, P. A., Meeker, L. D., Whitlow, S., Twickler, M. S., Morrison, M. C., Alley, R. B., Bloomfield, P., and Taylor, K. (1993). The atmosphere during the Younger Dryas. *Science* **261**, 195-197.

Oeschger, H., Welten, M., Eicher, U., Moll, M., Riesen, T., Siegenthaler, U., and Wegmuller, S. (1980). ^{14}C and other parameters during the Younger Dryas cold phase. *Radiocarbon* **22**, 299-310.

Overpeck, J. T., Peterson, L. C., Kipp, M., Imbrie, J., and Rind, D. (1989). Climate change in the circum-North Atlantic region during the last deglaciation. *Nature* **338**, 553-557.

Ruddiman, W. F., and McIntyre, A. (1973). Time-transgressive deglacial retreat of polar water from the North Atlantic. *Quaternary Research* **3**, 117-130.

Ruddiman, W. F., and McIntyre, A. (1981). The North Atlantic Ocean during the last deglaciation. *Paleogeography, Paleoclimatology, Paleoecology* **35**, 145-214.

Sejrup, H. P., Haflidason, H., Kristenen, D. K., and Johnsen, S. J. (1995). Last interglacial and Holocene climatic development in the Norwegian Sea region: ocean front movements and ice-core data. *Journal of Quaternary Science* **10**, 385-390.

Smith, A. G., and Goddard, I. C. (1991). A 12500 year record of vegetational history at Sluggan Bog, Co. Antrim, N. Ireland (incorporating a pollen zone scheme for the non-specialist). *New Phytologist* **118**, 167-187.

Stuiver, M., Grootes, P. M., and Braziunas, T. F. (1995). The GISP2 $\delta^{18}O$ climate record of the past 16,500 years and the role of the sun, ocean, and volcanoes. *Quaternary Research* **44**, 341-354.

Stuiver, M., and Reimer, P. J. (1993). Extended ^{14}C data base and revised Calib 3.0 ^{14}C age calibration program. *Radiocarbon* **35**, 215-230.

Thunell, R. C. M., P.G. (1995). Glacial climate instability in the Northeast Pacific Ocean. *Nature* **376**, 504-506.

Walker, M. J. C., Bohncke, S. J. P., Coope, G. R., O'Connell, M., Usinger, H., and Verbruggen, C. (1994). The Devensian/Weichselian Late-glacial in

northwest Europe (Ireland, Britain, north Belgium, The Netherlands, northwest Germany). *Journal of Quaternary Science* **9**, 109-118.

Watts, W. A. (1985). Quaternary vegetation cycles. *In* "The Quaternary History of Ireland." (K. J. Edwards, and W. P. Warren, Eds.), pp. 155-185. Academic Press, London.

Chapter 5: Calibrating radiocarbon ages to sidereal years and *vice versa* with a Microsoft Excel™ spreadsheet

5.1. Introduction

The dating of sediments and archaeological remains by measurement of the $^{14}C/^{12}C$ ($\Delta^{14}C$) ratio in carbon-based materials is a common tool in the geological sciences. Any material which incorporates fresh carbon into its structure also incorporates at that time a certain amount of radiocarbon (^{14}C) in a ratio determined by the current value of $\Delta^{14}C$ in the reservoir from which the carbon is derived. Thus, a sample from a marine environment will incorporate $\Delta^{14}C$ with a ratio similar to carbonate in local sea water, whilst plants and animals incorporate $\Delta^{14}C$ with a ratio similar to the carbon they respire (atmospheric CO_2) and consume (plant and animal carbon). A radiocarbon age is calculated by determining the present ratio of $\Delta^{14}C$ in a sample and comparing it to the $\Delta^{14}C$ ratio from the period during which carbon was included in the sample.

$$^{14}_{7}N+^{1}_{0}n\rightarrow^{14}_{6}C+^{1}_{1}H$$

Equation 5.1. Formation of radiocarbon (^{14}C) by bombardment of ^{14}N by neutrons.

Radiocarbon (^{14}C) is produced when ^{14}N is bombarded by neutrons produced by cosmic radiation at the outer edge of the atmosphere (equation 5.1). ^{14}C is oxidised to produce $^{14}CO_2$, and diffuses from the upper atmosphere to the rest of the atmospheric system and from the atmosphere to the oceans, lithosphere and biological systems (biosphere). Carbon enters the biosphere through respiration and consumption and is incorporated into all living plants and animals. In the geosphere, geological processes involving carbon (and hence ^{14}C) include the formation of limestone ($CaCO_3$) and other sediments (including organic material with carbon), and weathering of those rocks to release the carbon again (figure 5.1).

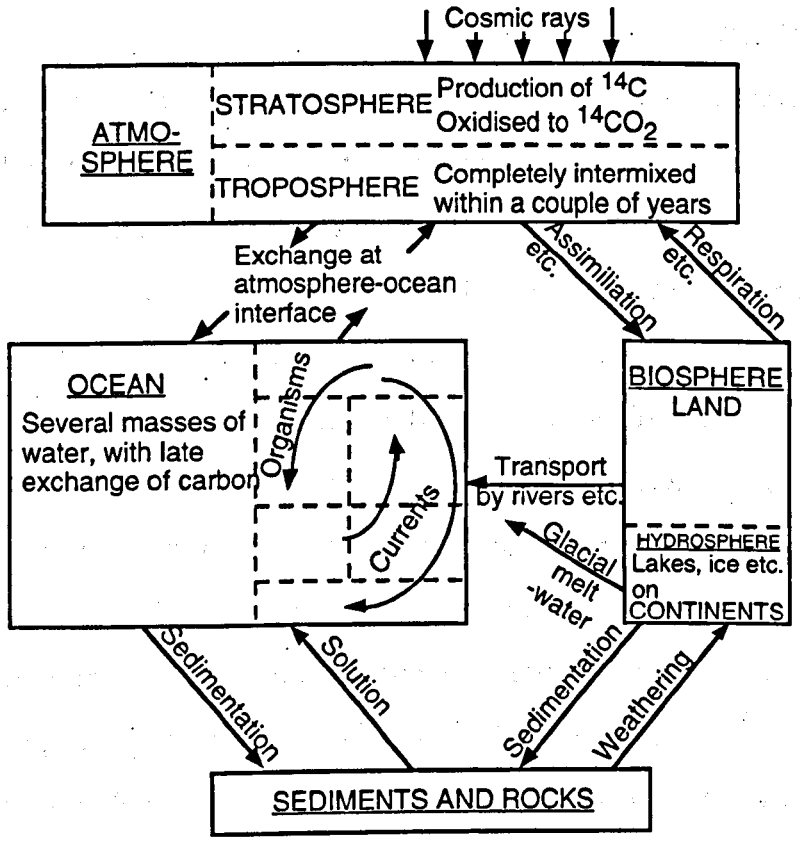

Figure 5.1. Carbon circulation in nature , redrawn from Bradley (1985).

^{14}C decays to ^{14}N through emission of a β particle (equation 5.2). The quantity of ^{14}C remaining is determined either by counting the number

of these β particles emitted by a sample as a proportion of the total carbon in the sample or by accellerator mass-spectrometry (AMS). The half-life of the ^{14}C isotope was originally determined to be 5,568 years (Libby, 1955), although the true half-life is now know to be 5,730 ± 30 years (Godwin, 1962). Radiocarbon ages are usually quoted with one of the two half-lives – usually the Libby half-life, although some publications may use the Godwin half-life.

$$^{14}_{6}C \rightarrow ^{14}_{7}N + \beta + neutrino$$

Equation 5.2. Decay of radiocarbon (^{14}C) by emission of a β particle to form ^{14}N.

For accurate radiocarbon dating to be possible, the assumption previously made in the literature was that total volume of global ^{14}C has remained constant – ^{14}C lost through radioactive decay is always balanced by ^{14}C produced by bombardment of ^{14}N by neutrons from cosmic rays in the upper atmosphere. In addition, it was assumed that incorporation of ^{14}C into carbon-based systems proceeded at a fixed rate. The discovery that radiocarbon years are not equivalent to sidereal (or calendar) years was made in 1958 (de Vries, 1958). It is now known that neither of these conditions presumed earlier actually hold, and there are four possible sources of error:

1) Production of ^{14}C in the upper atmosphere varies through time (Neftel *et al.*, 1981).
2) The mixing of ^{14}C with isotopically stable carbon alters the $\Delta^{14}C$ ratio in marine and atmospheric reservoirs, varies through time. Thus, assimilation of ^{14}C into organisms and carbonate sediments may vary in rate and/or volume through time.
3) The rate of transportation of ^{14}C within the ocean-atmosphere system and the incorporation of ^{14}C into marine sediments varies considerably through time, depending on oceanic circulation. The

mass of ^{14}C in marine sediments also varies with changes in the average mixing time of the ocean, although this appears to be a minor overall affect (Bard, 1988). Assimilation of the isotopes of carbon by an organism may also be at a different proportion to the atmospheric value (i.e. there is isotopic fractionation of the $^{14}C/^{12}C$ ratio) (Bradley, 1985).

4) Production of significant amounts of non-cosmogenic ^{14}C from atomic bomb detonations since 1950AD altered the volume of ^{14}C in carbon reservoirs (Rafter and Fergusson, 1957), whilst incorporation of ^{14}C-free carbon from the burning of fossil fuels during the industrial era has also changed global $\Delta^{14}C$ (Suess, 1955). These are man-made artefacts which are not relevant before 1945 in the case of post-bomb ages, and before the 19th century for excess ^{14}C-free carbon.

Little is known about variations in cosmic rays (source of error 1) through the period of the last 65,000 years (the effective limit of ^{14}C dating), since the main variations in cosmic rays derive from changes in the flux of galactic protons, solar-wind variations and the dipole movement of the earth and none of these are recorded unambiguously in geological records. Changes in the intensity of the Earth's magnetic field and/or changes in oceanic circulation are the most reasonable explanation for changes in $\Delta^{14}C$ through time (Bard *et al.*, 1990). When dating samples from marine settings the latter are extremely important (Bard, 1988). The effective technical upper age limit for counting β particles (due to extremely low signal/noise ratios) is about 10 ^{14}C half-lives, or 57,300 years. The upper limit for age determinations is approximately 100,000 years for AMS techniques. However, old ^{14}C ages (approaching 50,000 years) are susceptible to contamination by small quantities of modern carbon, and the ^{14}C ages appear to be

younger than is actually the case. For this reason, ages older than 25,000 years obtained by β counting are considered to be effectively infinite in age (Bradley, 1985) and AMS 14C ages may be inaccurate older than 45,000 years.

Material dated by radiocarbon techniques has significantly different calendar and radiocarbon age as a result of these variations in the production and incorporation of ^{14}C into carbon-based systems. Good evidence for the difference in age between the two time scales (figure 5.2) comes from the radiocarbon dating of tree rings (Becker, 1993; Becker and Kromer, 1986; Becker and Kromer, 1993). However, this technique suffers from error propagation from inaccuracies in annual ring-counting. This calibration may not be sufficiently reliable to form the sole basis for recalibration of the radiocarbon timescale.

However, comparison of ^{14}C and U-Th thermal ionisation mass spectrometry (TIMS) ages on corals from Barbados (Caribbean) and Mururoa (tropical Pacific) also reveals significant age discrepancies (figure 5.2) between the two chronometers (Bard *et al.*, 1993; Bard *et al.*, 1990). This is particularly noticeable at the Younger Dryas (YD) cold event during the transition from the last glacial maximum (LGM) to the present interglacial. Precise estimates of these discrepancies in independently-dated coral records has permitted the calibration curve for ^{14}C to be extended beyond the limit of dendrochronological records (figure 5.2). The recalibration of the radiocarbon time scale to sidereal (or calendar) years is important due to the increasing number of palaeo-records dated with this technique. The majority of new techniques for dating Quaternary events are based on sidereal time scales. These techniques include U-Th TIMS dating of corals (Edwards *et al.*, 1993),

speleothems (Richards *et al.*, 1994) and peat bogs (Heijnis *et al.*, 1993; Heijnis and van der Plicht, 1992), ^{36}Cl dating of surface exposure (Stone *et al.*, 1992), and $^{10}Be/^{26}Al$ dating of weathering rinds (Bierman *et al.*, 1995). A conversion of the radiocarbon time scale to a sidereal time scale, or *vice versa* is required to compare these results with geological or archaeological records dated by ^{14}C techniques.

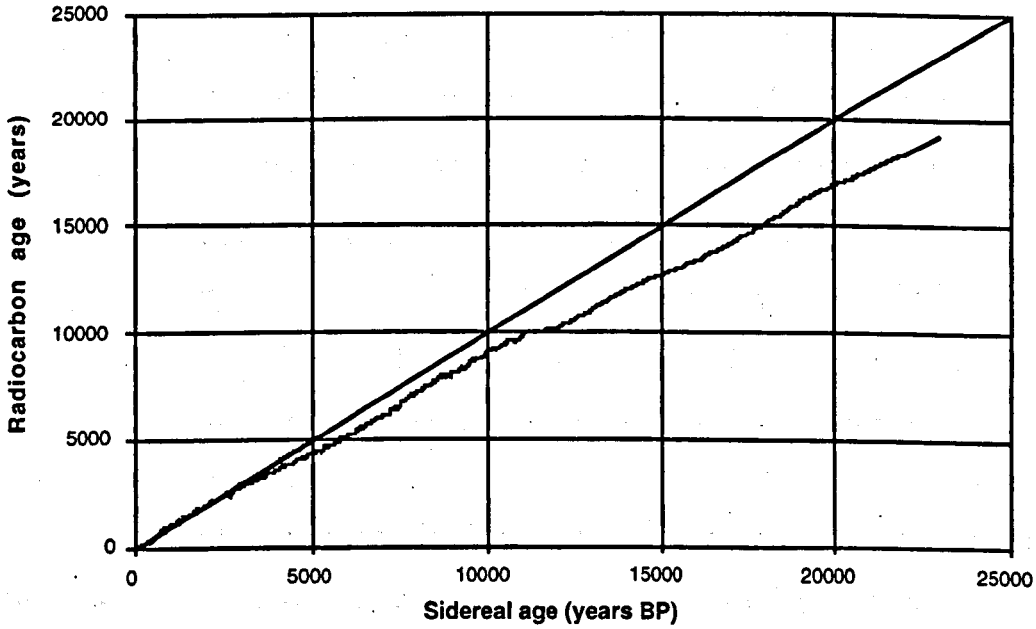

Figure 5.2. Atmospheric calibration data set for calibration of non-ocean based carbon. The straight line is a 1:1 relationship between radiocarbon years and sidereal years for comparison. The second curve shows the relationship between 'real' (calendar) years and radiocarbon years for the entire period of this calibration curve, derived from data in (Stuiver and Reimer, 1993) and (Bard *et al.*, 1993). The calibration data is based on dendrochronologies and U-Th/^{14}C dating of corals with a conversion for the ocean-atmosphere age difference. The apparent 'scatter' in the curve is actually small oscillations in the positive trend between 'real' and radiocarbon years (see figure 5.4). Note the plateau in radiocarbon age at approximately 10,000 ^{14}C years BP – the time of the younger boundary of the Younger Dryas.

In this chapter a Microsoft Excel™ spreadsheet "AgeCalib" – to convert between conventional radiocarbon (^{14}C) ages and sidereal or calendar (cal.) years and *vice versa* will be discussed. AgeCalib was written in Excel 4.0 macro language to overcome limitations of the specialized

software MacCalib (written in FORTRAN). AgeCalib software utilises calibration data originally published with MacCalib and (unlike MacCalib) it automates the calibration of more than one age in either direction. The new software introduced here is also much faster than MacCalib (see section 5.4 below). This software requires the spreadsheet program Microsoft Excel™ version 5 or later, operating on an IBM™-compatible or Macintosh™ computer.

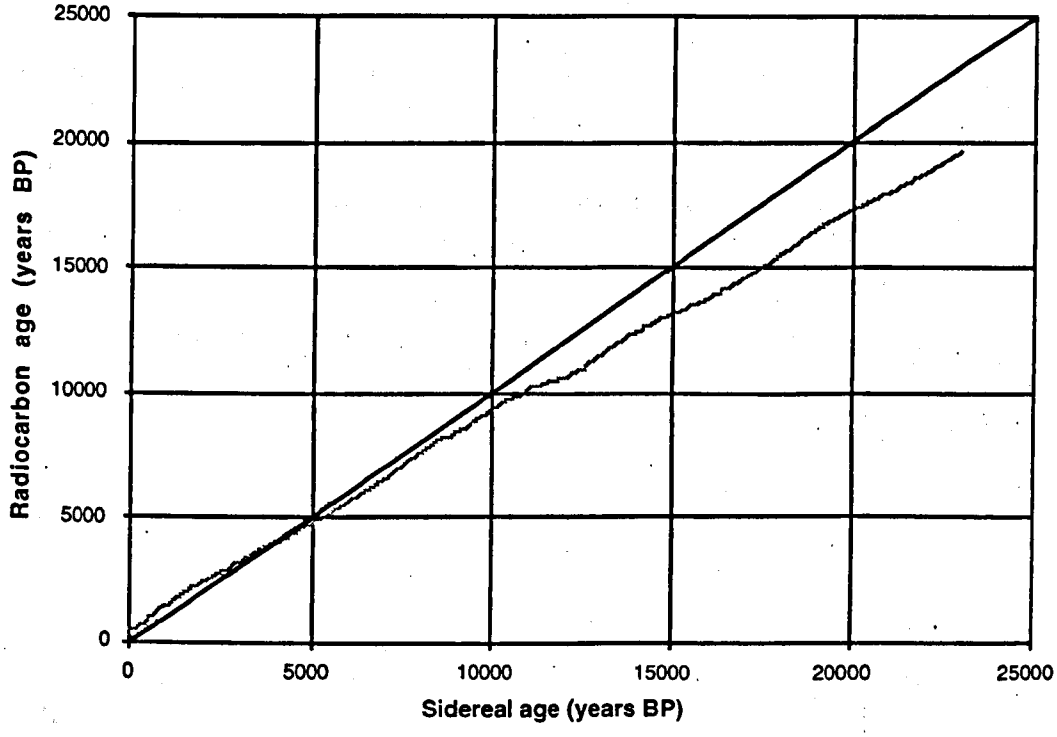

Figure 5.3. Marine calibration data set. The curve shows the relationship between 'real' years and radiocarbon years for the entire period of this calibration curve, derived from data in (Stuiver and Reimer, 1993) and (Bard *et al.*, 1993). The apparent 'scatter' in the curve is actually small oscillations in the positive trend between 'real' and radiocarbon years (see figure 5.4). The plateau at the YD is not as noticeable as in figure 5.2.

This chapter is to introduce the spreadsheet model and describe the operation of the spreadsheet. The spreadsheet model is included on disk 1 of the floppy disks which accompany this thesis. Calibration results obtained using MacCalib and AgeCalib are compared to

demonstrate the close similarity of results obtained with both programs. Errors in the ages obtained using each program are also discussed.

The AgeCalib spreadsheet is mouse-driven within a modified Excel environment. Automatic macro procedures executed when AgeCalib is first opened ensure user settings for the Excel program are retained. These settings are restored when AgeCalib is closed again. The spreadsheet allows simple entry of single ^{14}C or calendar ages in one cell on the display. The calibrated age is displayed immediately in the neighbouring cell. A series of ages may be calibrated when entered on an integral spreadsheet in the correct column. Ages may be placed on this "Multiple Ages" sheet following editing operations such as 'Copy and Paste' from other Excel spreadsheets, or from other programs with compatible data structures.

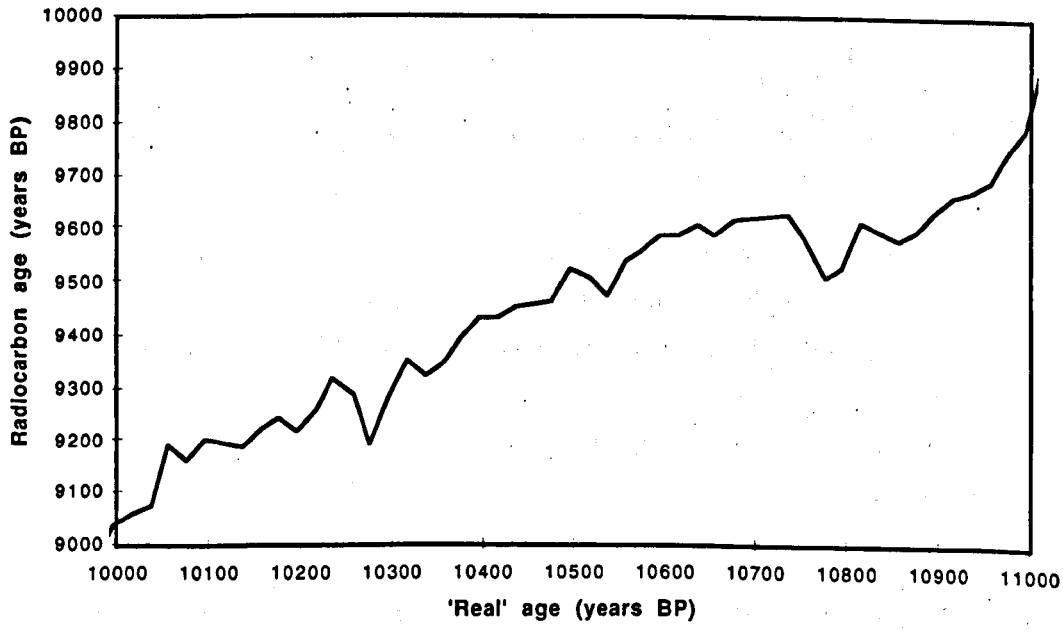

Figure 5.4. Relationship between 'real' (or calendar) years and radiocarbon years for the interval from 9,000 to 10,000 radiocarbon years BP. Note that one radiocarbon year may be equivalent to as many as four 'real' years during this period (e.g. 9,550 ^{14}C years).

5.2. Data

The ^{14}C data sets used for the AgeCalib program are derived from the data sets published with MacCalib. The MacCalib data sets have been combined and modified slightly (see below) to form two separate calibration curves for atmospheric (terrestrial) samples and marine samples.

2.1. Atmospheric data set

This data set is comprised of bidecadal ^{14}C calibration data from 0-11,390 cal BP (formally calibrated years Before Present, but actually years before 1950AD – the start of atomic bomb tests) based on averages of ^{14}C ages of tree-rings obtained by the Seattle, Heidelberg and Belfast laboratories (Becker, 1993; Becker and Kromer, 1993). A variety of dendrochronologies also dated by ^{14}C was obtained by the authors of MacCalib and corrected for variations in analysis between laboratories (Stuiver and Reimer, 1993). For ages older than 11,390 cal BP the data set is based on U-Th and ^{14}C ages of corals (Bard *et al.*, 1993; Bard *et al.*, 1990). The oldest point on the calibration curve is 19,262 ^{14}C years, which is equivalent to 22,950 calibrated years (figure 5.2). The dendrochronological data set from Stuiver and Reimer (1993) produces a calibration curve which does not have a constant rate of change through time. The calibration curve may be negative as well as positive (figure 5.4) due to variations in production (Bard, 1988) and uptake rates (Bard *et al.*, 1994) of ^{14}C, or possibly analytical errors in the measurement of the ages. For these reasons one radiocarbon age may be equivalent to more than one calendar age (figure 5.4). It has been shown that smoothed versions of the high-resolution calibration curves should be used where ^{14}C ages with large (>30 ^{14}C years) measurement errors, particularly organic deposits, are calibrated

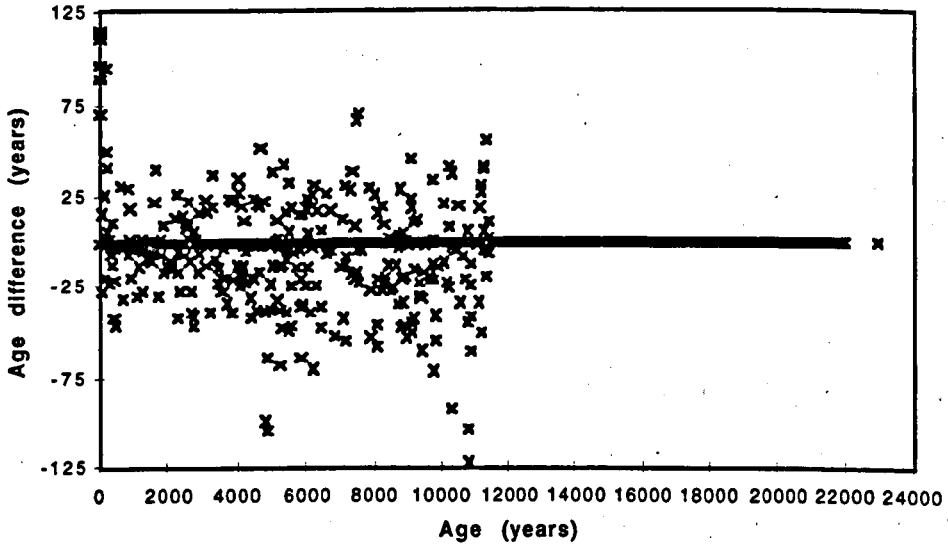

Figure 5.5. The difference between original atmospheric radiocarbon calibration curve (Stuiver and Reimer, 1993) and the smoothed atmospheric calibration curve. Note that ages older than 11.4 kBP fall on the x-axis because there is no difference between the original calibration curve and the smoothed calibration curve.

(Törnqvist and Bierkens, 1994). To make the calibration spreadsheet suitable for these situations and to avoid calculation problems on the spreadsheet which arise when the curve has negative excursions, the bidecadal data set was smoothed such that the gradient of the calibration curve remains positive and the difference between the original curve and the smoothed version is minimised (figures 5.5 & 5.6).

On average there is a -2.48 years age difference between the unsmoothed and smoothed calibration curves (whether negative or positive) with a standard deviation of 20.2 years. The actual difference between the original calibration curve and the smoothed calibration curve varies from 0 years to 115 years and -122 years. The quoted 2σ confidence errors for the unsmoothed calibration curve were plotted on the same

graph as the smoothed curve to ensure that the smoothed curve is representative. With approximately 40 exceptions, the smoothed

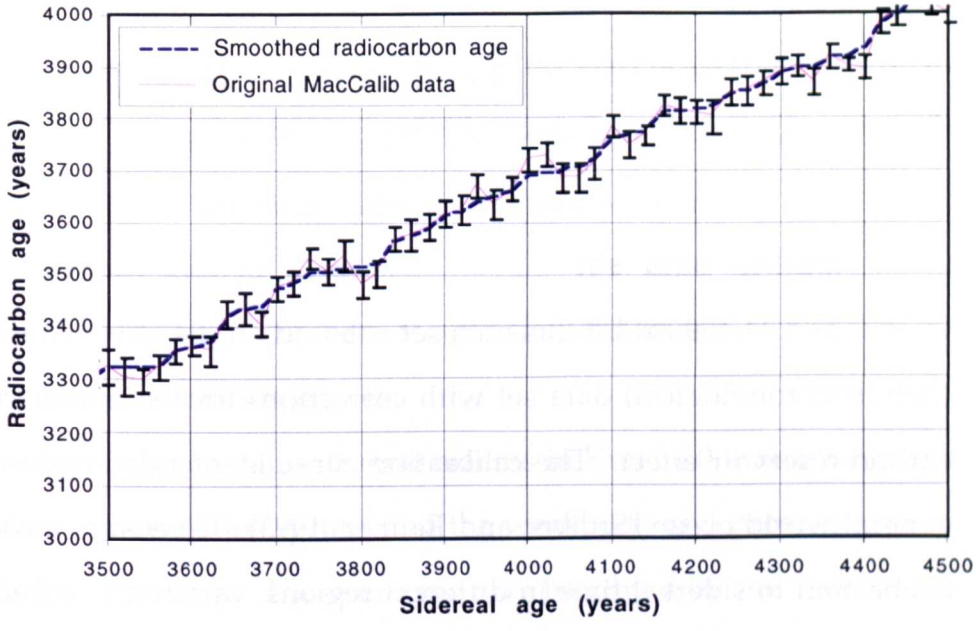

Figure 5.6. The original calibration data used for the atmospheric calibration data set, together with the smoothed calibration data used for this work. The error bars represent the 2σ (95%) confidence limits for the original calibration data (Stuiver and Reimer, 1993). The area of the diagram selected is intended to show certain sections of the calibration curve where the smoothed calibration curve may not fall within the 95% confidence limits of the original unsmoothed curve (see for example, the points before 3,700 calendar years BP).

calibration curve lies within these 95% confidence error bars over the period of the entire original calibration curve (figure 5.6). For ages older than 11,390 cal BP the data set is based on U/Th and ^{14}C dating of corals (Bard *et al.*, 1993; Bard *et al.*, 1990) because dendrochronologies do not extend past this time. Note that the interval of the calibration data is increased from 20 years to 50 years at this point. This second half of the data set is approximated by a smoothing spline with smoothing parameter = 4. Stuiver and Reimer inferred atmospheric ^{14}C ages from the marine data by deducting a 400 year reservoir age from the coral

data set, although it is known that the oceanic reservoir age is not constant through time (Bard *et al.*, 1994) or space (Kennett and Ingram, 1995). Linking the two sections of atmospheric calibration data in the original data set was accomplished by including a single point from the dendrochronological data set at 11,390 cal BP in the second section of the curve (Stuiver and Reimer, 1993).

2.2. Marine data set

Between 0 and 11,400 cal BP this data set is based on the atmospheric (dendrochronological) data set with corrections for variations in the carbon-reservoir effect. The calibration curve is intended for use with a general world ocean (Stuiver and Reimer, 1993). To ensure a correct calibration to sidereal time in different regions, variations caused by ^{14}C age differences between the world ocean and local oceans must be calculated. As the apparent age of modern shells can be as old as 750 years (Mangerud and Gulliksen, 1975) it is important to make this correction for each ocean location dated by ^{14}C techniques.

Each radiocarbon age in the marine calibration data set is equivalent to only one calendar age and therefore no smoothing was necessary for this data set. This feature of the marine data set may reflect the fact that approximately 85% of carbon in the ocean-atmosphere-biosphere reservoir lies in the deep ocean (Broecker and Peng, 1986), which has a slow turnover rate (Bard *et al.*, 1990). Thus, there is only a limited possibility of short-term variations in ^{14}C uptake by the oceans (ocean ventilation) (Keir, 1983; Shackleton *et al.*, 1988). From 11,400 cal BP to 21,950 cal BP the calibration curve is based on U/Th and ^{14}C dating of corals (figure 5.3) as in the atmospheric data set (figure 5.2). The two halves of the original data set were similarly connected by short linear

interpolation (Stuiver and Reimer, 1993). There is no difference between the oceanic and atmospheric calibration data sets >11,390 cal. BP.

5.3. The AgeCalib spreadsheet

AgeCalib.xlw is a Microsoft Excel™ version 0 workbook approximately 210 kilobytes in size which includes three spreadsheets:

i) For calibrating individual ages.

ii) For calibrating large numbers of ages simultaneously.

iii) For editing calibration curves.

The workbook also contains several macros in Excel 4.0 macro language for data manipulation, protecting the workbook and providing some limited on-line help. These macros may be edited by the user who is competent in Excel 4.0 macro language.

AgeCalib requires a computer (Macintosh or IBM-compatible) which is capable of running Excel 0. For Macintosh the requirements are generally System 7.0 or above and 8Mb RAM. For IBM-compatible the requirements are Windows 3.1 or later and 8Mb RAM. A minimum of a 68020 processor is recommended for Macintosh computers and a minimum of a 386DX processor is recommended for IBM-compatible computers. AgeCalib will operate particularly effectively on Power Macintosh or Pentium computers. Although AgeCalib may be used on either platform without requiring file conversion, the different system fonts used by each computer platform means it is preferable to use a dedicated version available at:

http://exodus.open.ac.uk/earth/indiv_home_pages/s_swabey.html

3.1. Selecting calibration data sets

The program stores the two calibration data sets on a separate worksheet inside AgeCalib. The user may alternate between data sets by clicking with the mouse on the relevant button on the screen. An indication of which data set is currently selected is always visible on the screen. Although the data sets are protected with Excel cell protection, this may be turned off using the available button and new calibration data entered by the user. New calibration data entered on the calibration sheet in this way will be lost when the alternative data set is selected. A calibration data set may be altered permanently by editing the calibration data sets spreadsheet. This may be selected by choosing the title of the current data set – i.e. "Atmospheric data" or "Marine data" on either the calibration sheet or the multiple ages sheet.

3.2. Single age conversion

Single ages may be converted between ^{14}C years and calendar years by typing the known age into the relevant cell and pressing <RETURN> or <ENTER>. The equivalent age is then interpolated from known data points in the currently selected data set. When a new data set is selected ages must be recalculated to take into account the updated calibration data.

3.3. Multiple age conversion

Multiple ages may be calibrated in either direction by entering or pasting data into the relevant column on the 'Multiple ages' spreadsheet and pressing the correct button on the spreadsheet display. The user must answer a dialog box about the number of ages they wish to convert, although the macro will alert the user if no further data can be found. The calibrated ages will appear in the neighbouring column after a

short delay for calculation. There is no upper limit to the number of ages which may be converted, although the limit of rows on an Excel spreadsheet is presently 16384.

5.4. Comparison with MacCalib 3.0.3

A series of ages and age errors was calculated using both MacCalib 3.0.3 and AgeCalib with both the atmospheric and marine data sets to check the reliability of AgeCalib age calibrations (table 5.1). The time taken for the calibration was also noted. It was only possible to compare ages calibrated from ^{14}C to sidereal time scales, since MacCalib is unable to work in the other direction – from sidereal to ^{14}C ages.

MARINE Calibration

Age	error	MacCalib	+error	-error	AgeCalib	+error	-error	% similarity
10400	45	11499	169	-111	11500	100	-74	100.01%
7429	38	7855	36	-55	7856	34	-52	100.01%
3294	32	3119	48	-46	3118	51	-49	99.97%
16526	128	19001	177	-157	19002	136	-127	100.01%
1004	21	561	45	-14	561	42	-13	100.08%
4239	31	4341	43	-60	4342	42	-58	100.03%
6467	40	6924	62	-46	6925	59	-45	100.01%
12891	52	14635	174	-165	14636	76	-74	100.00%
7449	112	7878	75	-135	7879	73	-135	100.01%
13928	161	16199	230	-238	16200	209	-218	100.01%
9277	93	9931	67	-71	9932	63	-69	100.01%
1251	19	771	22	-25	771	20	-20	100.06%
17218	173	19843	312	-278	19844	248	-235	100.01%
6492	28	6964	34	-48	6965	31	-45	100.01%
8155	71	8554	113	-72	8555	103	-69	100.01%
11346	109	12866	115	-115	12867	102	-103	100.01%
12163	145	13712	203	-185	13713	169	-165	100.01%
963	11	537	9	-10	537	6	-6	99.94%
18511	120	21625	221	-226	21626	153	-153	100.00%
Average % similarity for the two calibration schemes:								100.01%

Table 5.1. Random radiocarbon ages calibrated to the sidereal time scale using both MacCalib and AgeCalib with the marine data set. The "% similarity" is defined as MacCalib age/AgeCalib age x 100%.

4.1. Ages

When using the marine data set from MacCalib (table 5.1), the two programs produce almost identical calibrated ages, as the marine data set was not smoothed for use in AgeCalib. However, when the atmospheric data set is used (table 5.2) ages calibrated using AgeCalib are slightly different to those calibrated with MacCalib. In certain cases

ATMOSPHERIC Calibration

Age	error	MacCalib	+error	-error	AgeCalib	+error	-error	% similarity
10400	45	12298	96	-112	12299	57	-62	100.01%
7429	38	8167	134	-34	8168	24	-33	100.01%
3294	32	3475	85	-8	3475	25	-9	99.99%
16526	128	19455	225	-197	19456	165	-155	100.01%
1004	21	929	7	-7	929	6	-6	99.97%
4239	31	4830	7	-99	4813	21	-29	99.64%
6467	40	7378	8	-95	7378	9	-85	100.00%
12891	52	15261	152	-171	15262	85	-84	100.00%
7449	112	8175	164	-54	8176	162	-55	100.02%
13928	161	16705	212	-217	16706	193	-198	100.01%
9277	93	10251	113	-204	10238	122	-161	99.87%
1251	19	1171	53	-7	1171	7	-7	100.02%
17218	173	20425	317	-314	20426	248	-254	100.01%
6492	28	7383	5	-85	7384	5	-9	100.01%
8155	71	8997	215	-12	8998	206	-12	100.01%
11346	109	13254	136	-121	13255	114	-110	100.01%
12163	145	14193	234	-213	14194	189	-179	100.01%
963	11	915	6	-115	914	6	-6	99.93%
18511	120	out of range			22111	134	-134	
Average % similarity for the two calibration schemes:								**99.97%**

Table 5.2. Random radiocarbon ages calibrated to the sidereal time scale using both MacCalib and AgeCalib with the atmospheric data set. The "% similarity" is defined as MacCalib age/AgeCalib age x 100%.

the difference in calibrated ages is even larger than the 2σ error associated with each point on the calibration curve (for example, see figure 5.6 between the ages of 4,350 and 4,450 cal. BP). This is a result of the curve-fit applied to calibration data in AgeCalib to ensure the trend on the atmospheric data set calibration curve remains positive. However, there are so few cases where this is true (approximately 40

cases in the entire curve) that, in effect, there is no difference between the two programs' calibration curves for either data set.

4.2. Age errors

In MacCalib, age errors are calculated by determining either the intercept and age range, or by using a Gaussian age distribution generated from a probability distribution. Using AgeCalib the age errors are obtained by:

i) Determining the calibrated ages at the boundaries of the 1σ or 2σ age error distribution and calibrating those ages. For example, to determine the ^{14}C age and error distribution of a 'real' age of 12,305 ± 234 years three calibrations to radiocarbon years would be required – 12,305 years (age), 12,539 years (+ error) and 12,071 years (– error).

ii) Using the relative error for the age. For example, if the relative error for the ^{14}C age is 8%, assuming that the relative error for the calibrated age should also be 8%. This would only be true if the relationship between real age and radiocarbon age was 1:1, but the approximation is a realistic one.

Both these methods closely approximate a Gaussian distribution of age errors on the selected calibration data set. The user should note that MacCalib incorporates errors associated with the calibration curve into the quoted age errors, which is also reflected in AgeCalib calculations because both use the same calibration data. Age errors in AgeCalib are similar to those determined using MacCalib when calculating young ages using method i). However, errors for older ages obtained using this method with AgeCalib may underestimate the errors obtained using MacCalib by 67-90% (see table 5.1) due to the different techniques used to calculate age errors. The relative age error (method ii) is a better reflection of the actual age distribution, although the distribution

of the age along the calibration curve is incorrect due to variations in the gradient of that curve through time (figure 5.2). In reality, age errors are not symmetrical because the gradient of the calibration curve changes.

Given the large number of variables to consider (see introduction to this chapter) when calibrating the age error for radiocarbon ages, the second method of determining the calibrated age error is preferred as most accurately reflecting the error statistic.

4.3. Speed of operation

AgeCalib outperforms MacCalib in all aspects of entering data and calibrating ages. When each program is already running, the time required to enter a single ^{14}C age and obtain a calibrated age is approximately 45 seconds using MacCalib and under 2 seconds using AgeCalib on a Macintosh IIci. This performance differential holds even when calibrating multiple ages. 20 ages were calibrated in a little over 8 minutes using minimum information settings in MacCalib and in approximately 25 seconds using AgeCalib. (Multiple age calibration is faster than single age calibration using AgeCalib as the software does not re-draw the display.) This is a significant difference when users may require to calibrate hundreds of ^{14}C-dated time-series data points to a sidereal time scale.

5.5 Conclusions

AgeCalib is a powerful tool operated using a common spreadsheet package. It may be used equally on IBM-compatible and Macintosh platforms to calibrate ages efficiently between the sidereal and conventional

radiocarbon time scales. The software can calibrate ages in both directions with equal facility. The user may copy and paste data from other spreadsheets or applications into AgeCalib to calibrate multiple ages together. The user may also modify the calibration curve data if different data becomes available in the future. This feature also allows localised versions of AgeCalib to be constructed (e.g. for a local ocean calibration data set). Although AgeCalib lacks some of the finer details of the proprietary software 'MacCalib', the speed, ease of use and flexibility with which AgeCalib operates makes it a more useful tool in age calibrations between conventional ^{14}C ages and sidereal ages.

5.6. References

Bard, E. (1988). Correction of accelerator mass spectrometry ^{14}C ages measured in planktonic foraminifera: Paloceanographic implications. *Paloceanogaphy* **3**, 635-645.

Bard, E., Arnold, M., Fairbanks, R. G., and Hamelin, B. (1993). ^{230}Th-^{234}U and ^{14}C ages obtained by mass spectrometry on corals. *Radiocarbon* **35**, 191-199.

Bard, E., Arnold, M., Mangerud, J., Paterne, M., Labeyrie, L., Duprat, J., Mélières, M.-A., Sønstegaard, E., and Duplessy, J.-C. (1994). The North Atlantic atmosphere-sea surface ^{14}C gradient during the Younger Dryas climatic event. *Earth and Planetary Science Letters* **126**, 275-287.

Bard, E., Hamelin, B., Fairbanks, R. G., and Zindler, A. (1990). Calibration of the ^{14}C timescale over the past 30,000 years using mass spectrometric U-Th ages from Barbados corals. *Nature* **345**, 405-410.

Becker, B. (1993). A 11,000-year German oak and pine dendrochronology for radiocarbon calibration. *Radiocarbon* **35**, 201-213.

Becker, B., and Kromer, B. (1986). Extension of the Holocene dendrochronology by the Preboreal pine series, 8800 to 10,100 BP. *Radiocarbon* **28**, 961-967.

Becker, B., and Kromer, B. (1993). The continental tree-ring record – absolute chronology, ^{14}C calibration and climatic change at 11 ka. *Palaeogeography, Palaeoclimatology, Palaeoecology* **103**, 67-71.

Bierman, P. R., Gillespie, A. R., and Caffee, M. W. (1995). Cosmogenic ages for earthquake recurrence intervals and debris flow fan deposition, Owens Valley, California. *Science* **270,** 447-450.

Bradley, R. S. (1985). "Quaternary Palaeoclimate." Chapman & Hall.

Broecker, W. S., and Peng, T.-H. (1986). Carbon cycle: 1985 glacial to interglacial changes in the operation of the global carbon cycle. *Radiocarbon* **28,** 309-327.

de Vries, H. (1958). Variation in concentration of radiocarbon with time and location on Earth. *Koninklijke Nederlandse Akademie van Wetenschappen (B)* **61,** 1-9.

Edwards, R. L., Beck, J. W., Burr, G. S., Donahue, D. J., Chappell, J. M. A., Bloom, A. J., Drufell, E. R. M., and Taylor, F. W. (1993). A large drop in atmospheric $^{14}C/^{12}C$ and reduced melting in the Younger Dryas, documented with ^{230}Th ages of corals. *Science* **260,** 962-968.

Godwin, H. (1962). Half-life of radiocarbon. *Nature* **195,** 984.

Heijnis, H., Ruddock, J., and Coxon, P. (1993). A uranium-thorium dated Late Eemian or Early Midlandian organic deposit from near Kilfenora between Spa and Fenit, Co. Kerry, Ireland. *Journal of Quaternary Science* 8, 31-43.

Heijnis, H., and van der Plicht, J. (1992). Uranium/thorium dating of Late Pleistocene peat deposits in NW Europe, uranium/thorium isotope systematics and open-system behaviour of peat layers. *Chemical Geology (Isotope Geoscience Section)* **94,** 161-171.

Keir, R. S. (1983). Reduction of thermohaline circulation during deglaciation: The effect on atmospheric radiocarbon and CO_2. *Earth and Planetary Science Letters* **64,** 445-456.

Kennett, J. P., and Ingram, B. L. (1995). A 20,000-year record of ocean circulation and climate change from the Santa Barbara basin. *Nature* **377,** 510-514.

Libby, W. F. (1955). "Radiocarbon dating." University of Chicago Press, Chicago.

Mangerud, J., and Gulliksen, S. (1975). Apparent radiocarbon age of recent marine shells from Norway, Spitsbergen and Arctic Canada. *Quaternary Research* **5,** 263-274.

Neftel, A., Oeschger, H., and Suess, H. E. (1981). Secular non-random variations of cosmogenic carbon-14 in the terrestrial atmosphere. *Earth and Planetary Science Letters* **56,** 127-147.

Rafter, T. A., and Fergusson, G. J. (1957). Atom bomb effect - recent increase of carbon-14 content of the atmosphere and biosphere. *Science* **126,** 566-578.

Richards, D. A., Smart, P. L., and Edwards, R. L. (1994). Maximum sea levels for the last glacial period from U-series ages of submerged speleothems. *Nature* **367,** 357-360.

Shackleton, N. J., Duplessy, J.-C., Arnold, M., Maurice, P., Hall, M. A., and Cartlidge, J. (1988). Radiocarbon age of last glacial Pacific deep water. *Nature* **335,** 708-711.

Stone, J. O. H., Allan, G. L., and Fifield, L. K. (1992). Dating surface exposure using cosmogenic chlorine-36. *In* "Fourth Australian Environmental Isotope Conference." (A. R. Chivas, T. H. Donnelly, A. G. J. Mower, and Z. Roksandic, Eds.), pp. 33-34. Australian National University, Canberra.

Stuiver, M., and Reimer, P. J. (1993). Extended ^{14}C data base and revised Calib 3.0 ^{14}C age calibration program. *Radiocarbon* **35,** 215-230.

Suess, H. E. (1955). Radiocarbon concentration in modern wood. *Science* **122,** 415-417.

Törnqvist, T. E., and Bierkens, M. F. P. (1994). How smooth should curves by for calibrating radiocarbon ages? *Radiocarbon* **36,** 11-26.

Chapter 6: Conclusions

Speleothems (cave calcite) provide many different proxy indicators for palaeoclimatic changes during the Quaternary era (Chapter 1). This thesis has shown that the number of speleothems which have been dated with U-Th techniques appears to be a good indicator of past climatic changes (Chapter 2). In addition, palaeoclimate change on relatively short timescales (as little as several decades) may be recorded in individual speleothem proxy records, including $\delta^{18}O$, $\delta^{13}C$, growth rate and luminescence intensity (Chapter 3). U-Th TIMS ages on speleothems for one such short-lived cold event during the Late Glacial – the Younger Dryas (Chapter 4), may help distinguish between several hypotheses for this event. U-Th TIMS dated proxy records on two speleothems from Ireland suggest atmosphere-cryosphere reorganisations may have been responsible for the Younger Dryas event. The necessity of providing a common timescale to examine short-lived palaeoclimate events is addressed in Chapter 5, where a new program for converting between radiocarbon and sidereal years is introduced. In this chapter the main conclusions of the other chapters are summarised.

6.1. Chapter 1: Introduction

On-going change is a feature of the Earth's climate system. The Quaternary is a relatively recent period of geological time (1.65 Ma to the present) during which climate change occured at regular intervals. The predominantly cold global climate conditions of the Quaternary (glacials) were periodically interrupted by warm stages (interglacials). These palaeoclimate changes are the result of cyclic changes in the orbital parameters of the Earth around the sun – the Milankovitch variations. Global climate does not respond in a linear fashion to variations in total insolation received. Up to 50% of the variation in global palaeoclimate during the Quaternary may have been caused by various feedbacks in the distribution of energy from the outer atmosphere to climate systems (Berger, 1988). Palaeoclimate changes occurring on timescales shorter than half the shortest period in the Milakovitch variations (i.e. shorter than 8,500 years) are sub-Milankovitch in nature. The importance of these short-term palaeoclimate changes is that they may provide analogues for the effects of any future man-made climate change. One example of these short-lived natural palaeoclimate changes is the Younger Dryas (YD) cold event during the transition from the Last Glacial Maximum (LGM). Various hypotheses for the origin of the YD were introduced for examination in later chapters.

6.2. Chapter 2: Palaeoclimate from the frequency of speleothem U-series ages

The active growth of speleothems suggests certain minimum climate conditions in the are of the cave, for example, sufficient water and CO_2 for limestone solution and speleothem deposition to occur. Several authors have attempted to use this to reconstruct palaeoclimate from

the number of available speleothem ages through time, on the grounds that the number of ages broadly reflects the number of actively growing speleothems (Gascoyne *et al.*, 1983; Goede and Harmon, 1983; Gordon *et al.*, 1989; Hennig *et al.*, 1983). The techniques used in these publications were examined and a slight modification proposed to the most recent (and statistically representative) technique of stacking normal curves of the ages (Baker *et al.*, 1993). For the first time, the database of published speleothem U-series ages was also examined from a geographical perspective. Examined with the normalisation technique, the database shows some evidence for an early transition from the penultimate glacial to the last interglacial at ~140 Ka BP. This age for the transition is similar to that found with the Devils Hole record (Ludwig *et al.*, 1992), and is in contrast to a number of other studies (Shackleton, 1993). The stacked, normalised frequency (SNF) curve gives an age of 63 Ka BP for the maximum cold period within isotope stage 4. Isotope stage 3 contains three periods of increased number of speleothems growing, at 40, 50 and 56 Ka BP. The dated speleothems in the stage 3 peaks are from low latitude caves, whereas other work has shown three peaks of increased speleothem growth at slightly different ages (40, 49 and 60 Ka BP) based on ages from high latitude caves (Baker *et al.*, 1993). The age of 26 Ka BP for several speleothems from Scotland may indicate glaciers had retreated in that region prior to the generally accepted global warming at 21-18 Ka BP. Generally, this chapter shows that the occurrence of growing speleothems is a strong proxy for global palaeoclimate and may preserve some record of geographical variations in palaeoclimate.

6.3. Chapter 3: Reconstructing Irish palaeoclimate and environmental conditions during the Late Glacial from speleothems

In the pivotal North Atlantic region Ireland occupies an important site for reconstructing palaeoclimate changes during the Late Glacial period. Speleothems offer several palaeoclimate proxy indicators and may be dated with U-Th thermal ionisation mass-spectrometry (TIMS) to provide absolute ages for palaeoclimate events. An examination of the start of growth, growth rate, oxygen isotopes, carbon isotopes and luminescence intensity in two speleothems from southern Ireland provides high-resolution records of rapid palaeoclimate changes in that region during the Late Glacial.

The proxies show that warming at the end of the Last Glacial Maximum (LGM) commenced at approximately 18 Ka BP. An Intra-Allerød Cold Period lasting around 200 years is noted to start at 13.1 Ka BP. Changes in speleothem palaeoclimate records during the Bølling/Allerød/Younger Dryas (BAYD) period parallel changes in other palaeoclimate records from the North Atlantic, including the GRIP and GISP2 ice core records.

The Younger Dryas (YD) cold event is dated at between 12.5 and 11.4 Ka BP in both speleothem records. Relative temperature changes during the YD were calculated from $\delta^{18}O$ using previous values of temperature-dependent $\delta^{18}O$ fractionation (Gascoyne, 1992). The temperature changes calculated for both speleothems agree well with previous determinations of temperature change during the YD in Ireland.

Coeval changes in growth rates, $\delta^{13}C$, luminescence intensity and $\delta^{18}O$ suggest some common control on these proxies. During the Late Glacial, and particularly during the YD, this common control may be climate change. The links between these proxy palaeoclimate indicators require further study. The dominant agent of palaeoclimatic variation during the YD is probably changes in North Atlantic ocean circulation.

The Boreal period is also a strong cooling event in Ireland, although a paucity of U-Th TIMS ages limits the interpretation from the speleothem records of any palaeoclimate changes during this period. There is some evidence from luminescence intensity and $\delta^{13}C$ records or a period of increased plant competition during the Boreal. A similar lack of U-Th TIMS ages during the Holocene precludes extensive interpretation of the data, although change appears to be broadly synchronous in both speleothem records.

6.4. Chapter 4: Speleothems date the Younger Dryas: U-Th ages from the Late Glacial in Ireland

$\delta^{18}O$ records for two speleothems from Ireland (CC4 and MC2) show the Younger Dryas (YD) started at 12,550 ± 73 and ended at 11,350 ± 180 years Before Present (BP). This is the first time internally consistent ages have been obtained for the YD event in a continental setting. Cooling into the YD proceeded moderately slowly and warming was interrupted by a short-lived reversal to cold conditions. Iceberg outbursts in the North Atlantic occur at the same time as the second cool period of the YD, which suggests that atmosphere-cryosphere interactions may be of greater importance than ocean circulation during this period.

6.5. Chapter 5: Calibrating ^{14}C ages to sidereal years and *vice versa* with a Microsoft Excel™ spreadsheet

A common tool for dating carbon-based material from the Quaternary is radiocarbon dating. Radiocarbon years are not directly equivalent to sidereal (calendar) years due to variations in radiocarbon production at the outer atmosphere and assimilation into carbon-based systems. The Microsoft Excel spreadsheet created for this thesis is a powerful means of rapidly converting between ^{14}C and calendar years and *vice versa*.

6.6. References

Baker, A., Smart, P. L., and Ford, D. C. (1993). Northwest European palaeoclimate as indicated by growth frequency variations of secondary calcite deposits. *Palaeogeography, Palaeoclimatology, Palaeoecology* **100,** 291-301.

Berger, A. (1988). Milankovitch theory and climate. *Reviews of Geophysics* **26,** 624-657.

Gascoyne, M. (1992). Palaeoclimate determination from cave calcite deposits. *Quaternary Science Reviews* **11,** 609-632.

Gascoyne, M., Schwarcz, H. P., and Ford, D. C. (1983). Uranium-series ages of speleothems from Northwest England: correlation with Quaternary climate. *Philosophical transactions of the Royal Society of London, Series B* **301,** 143-164.

Goede, A., and Harmon, R. S. (1983). Radiometric dating of Tasmanian speleothems - evidence of cave evolution and climatic change. *Journal of the Geological Society of Australia* **30,** 89-100.

Gordon, D., Smart, P. L., Ford, D. C., Andrews, J. N., Atkinson, T. C., Rowe, P. J., and Christopher, N. S. J. (1989). Dating of late Plesitocene interglacial and interstadial periods in the United Kingdom from speleothem growth frequency. *Quaternary Research* **31,** 14-26.

Hennig, G. J., Grun, R., and Brunnacker, K. (1983). Speleothems, travertines and paleoclimates. *Quaternary Research* **20,** Jan-29.

Ludwig, K. R., Simmons, K. R., Szabo, B. J., Winograd, I. J., Landwehr, J. M., Riggs, A. C., and Hoffman, R. J. (1992). Mass-spectrometric ^{230}Th-^{234}U-^{238}U dating of the Devils Hole calcite vein. *Science* **258,** 284-287.

Shackleton, N. J. (1993). Last interglacial and Devil's Hole. *Nature* **362,** 596.

Chapter 7: Appendices

7.1. Samples

Speleothem samples were obtained from cave sites in Ireland, Scotland, England, Spain and Portugal. In what follows the location and description of samples obtained during this project is noted by country.

7.1.1. Ireland

Caves sampled in Ireland included Crag Cave (County Kerry), Mitchelstown Cave (County Cork), Lisodigue Cave (County Kerry), White Father's Cave (County Fermanagh) and Marble Arch Cave.

7.1.1.1. Crag Cave

Crag Cave (52°15'N, 9°24'W) is a show-cave near Castleisland, County Kerry that was only made accessible in 1989. The cave entrance is at an altitude of 45 m and is approximately 20 km from the Atlantic ocean at Tralee. It is an active stream cave with stretches of abandoned passage above the main river. The total length of the cave is 3.81 km, of which 350 m is show cave. The mean temperature of the cave from March 1995 to June 1996 was 10.38°C ± 0.1°C. This compares with an average temperature at Valencia (Dingle Peninsula) of 10.4°C for the same period. These data suggest the temperature in Crag Cave is a good approximation of average temperature in south-west Ireland at present

and may have also been so in the past. Samples were obtained from the non-commercial section of the cave, away from the lights of the tourist trail.

Sample	Size (mm)	Cut	Luminescence	$\delta^{18}O/\delta^{13}C$	U/Th TIMS
CC1	10	Ø			
CC2	291	Ø			
CC3		✔		✔	
CC4	283	✔	✔	✔	✔

Table 7.1. Samples from Crag Cave. In the tables which follow this one, ✔ means the sample has been analysed using that procedure. Ø indicates a core was obtained using a 25 mm coring bit.

7.1.1.2. Mitchelstown Cave

Mitchelstown Cave (52°18'N, 8°11'W) is also a show cave, near Mitchelstown, County Tipperary, lying at an altitude of 80 m, approximately 150 km from the Atlantic. There is no data available on the temperature of Mitchelstown Cave through a single year, but the cave is likely to approximate mean annual temperature in the same way as Crag Cave, particularly as Mitchelstown Cave contains no flowing stream.

Sample	Size (mm)	Cut	Luminescence	$\delta^{18}O/\delta^{13}C$	U/Th TIMS
MC1	310	Ø			
MC2	638	✔	✔	✔	✔

Table 7.2. Samples from Mitchelstown Cave.

7.1.1.3. Lisodigue Cave

Lisodigue Cave (52°18'20"N, 9°48'30"W) is a small cave close to the coast at Townland, Lisodigue in County Kerry. The cave is a small (250 m of passages) complex system based on solutional joints. A small stream

flows through two of its chambers, and fossil shells are found in one chamber from a cave-in from outside (Coleman, 1950).

Sample	Size (mm)	Cut	Luminescence	$\delta^{18}O/\delta^{13}C$	U/Th TIMS
LC5	200	✔		✔	✔
LC6					
LC7					
LC8					

Table 7.3. Samples from Lisodigue Cave.

7.1.1.4. Marble Arch Cave

Marble Arch cave (54°20'N, 7°45'W) is a show cave in Northern Ireland, south of Enniskillen. A large stream flows through the cave.

Sample	Size (mm)	Cut	Luminescence	$\delta^{18}O/\delta^{13}C$	U/Th TIMS
MA1	220	Ø			

Table 7.4. Samples from Marble Arch Cave.

7.1.1.5. Whitefather's Cave

Whitefather's Cave is a stream cave which passes underneath the border between the Republic of Ireland and Northern Ireland near .

Sample	Size (mm)	Cut	Luminescence	$\delta^{18}O/\delta^{13}C$	U/Th TIMS
WF2A	178	✔			
WF2B	310				

Table 7.5. Samples from Whitefather's Cave.

7.1.2. Scotland

7.1.2.1. Cnoc nan Uamh Cave

Cnoc nan Uamh Cave is located in the Allt nan Uamh valley of the Assynt district of Scotland at NC262177 and an altitude of 180 m. Cave

temperature was 9.3°C in Beachbarrow chamber during fieldword, with a relative humidity of 99%. The temperature of the stream flowing through the first part of the cave was 6.5°C and the outside temperature 8.1°C. No large speleothems were removed due to the limited amount of decoration in this cave.

Sample	Size (mm)	Cut	Luminescence	$\delta^{18}O/\delta^{13}C$	U/Th TIMS
UNC6	20				
CNU1	>200				
CNU3	12				
CNU4	54				
CNU8	50				

Table 7.6. Samples from Cnoc nan Uamh Cave.

7.1.2.2. Uamh an Claonite Cave

Uamh an Claonite Cave is also located in the Assynt district at NC271167. The cave lies at an altitude of 320 metres, some 140 metres above Cnoc nan Uamh Cave. Cave temperature was 7.6°C during fieldwork, with a relative humidity of 99%. The temperature of the river that flows through the cave was 7.5°C, which implies that the river must flow for a long distance underground before reaching the cave, since lower down the valley the same river was 6.5°C. No samples were obtained as very few speleothems exist in this part of the cave.

Sample	Size (mm)	Cut	Luminescence	$\delta^{18}O/\delta^{13}C$	U/Th TIMS
UAC1	12				

Table 7.7. Samples from Uamh an Claonite Cave.

7.1.2.3. Smoo Cave

Smoo Cave (NC419672) is a sea cave near the town of Durness on the north Scottish coast. It has a large river flowing through it, although

despite the open nature of the cave relative humidity was 96% in an air temperature of 10.6°C on a ledge on the east side of the entrance chamber. One speleothem was removed from this ledge.

Sample	Size (mm)	Cut	Luminescence	$\delta^{18}O/\delta^{13}C$	U/Th TIMS
SC1	200				
SC2	250	✔			
SC3	140				
SC4	160				
SC5	170				

Table 7.8. Samples from Smoo Cave.

7.1.2.4. *Mushroom Cave*

Mushroom Cave is located at approximately NC378620 in the Assynt district, Scotland. It is formed in a limestone breccia rather than pure limestone and is small and constricted. No humidity measurements were taken. Two samples of the local rock were obtained and one whole speleothem.

Sample	Size (mm)	Cut	Luminescence	$\delta^{18}O/\delta^{13}C$	U/Th TIMS
MC1	12				
MC2	130				
MC3	45				
MC4	17				
MC5	110				

Table 7.9. Samples from Mushroom Cave.

7.1.3. England

7.1.3.1. *Link Pot, Yorkshire*

Sample	Size (mm)	Cut	Luminescence	$\delta^{18}O/\delta^{13}C$	U/Th TIMS
LINK1	>200				
LINK3	35				

Table 7.10. Samples from Link Pot.

Link Pot is part of the Easegill Caverns system in North Yorkshire.

7.1.3.2. Lancaster Hole, Yorkshire

Lancaster Hole is part of the Easegill caverns system. The speleothem was removed from the main streamway, where it had been deposited by a large flood event.

Sample	Size (mm)	Cut	Luminescence	$\delta^{18}O/\delta^{13}C$	U/Th TIMS
LH1	330	✔			

Table 7.11. Samples from Lancaster Hole.

7.1.3.3. St. Cuthbert's Swallet, Mendips

St. Cuthbert's Swallet is a swallow-hole with one narrow entrance. This sample was removed from a rubble pile in the entrance series where it appeared to have been moved around by fluvial action.

Sample	Size (mm)	Cut	Luminescence	$\delta^{18}O/\delta^{13}C$	U/Th TIMS
SCS-1	35				

Table 7.12. Samples from St. Cuthbert's Swallet Cave.

7.1.4. Spain

7.1.4.1. La Lastrilla Cave, Spain

La Lastrilla is a large river cave with two entrances (the sink and the resurgence). The samples were obtained from the resurgence end of the cave from a well-decorated chamber ('Sala de los gours') which had been heavily vandalized some time in the past. Several broken stalagmites (often in several pieces) where the 'stump' could be located in the chamber were removed. The 'Sala de los gours' is well above the large river which flows through the cave, and humidity in this

chamber was relatively high at 98%, with an air temperature of 13.5°C. The temperature of the river was 12.5°C during fieldwork in October 1994.

Sample	Size (mm)	Cut	Luminescence	$\delta^{18}O/\delta^{13}C$	U/Th TIMS
LL1	180				✔
LL4 A-E	810				
LL3 A-B	110				

Table 7.13. Samples from La Lastrilla Cave.

7.1.5. Portugal

7.1.5.1. Algar do Peno

Algar (shaft) do Peno is a recently discovered cave (1985) where a lift shaft has been built into the mountain to accommodate future tourist operations. It is an exceptionally well decorated cave, although the majority of its speleothems have been shattered by explosives used to blast the lift shaft. The central gallery is the largest cave gallery in Portugal (100,000 m^3). Two speleothems were sampled from this cave. One stalagmite was cored at the base of entrance ladders and a single broken stalactite was removed from the floor in the bottom of the main chamber ("Salle inferieure") (Thomas, 1985).

Sample	Size (mm)	Cut	Luminescence	$\delta^{18}O/\delta^{13}C$	U/Th TIMS
Peno1A-L	310	Ø			
Peno2	65				
Peno5	236				✔
Peno6	145				✔

Table 7.15. Samples from Algar do Peno.

7.1.5.2. Gruta Almonda

The cave is over 5.5 km in length and the largest cave in Portugal (Thomas, 1985). It is situated near the town of Almonda, which is 8 km NW of the large town of Torres Novas. Samples were taken from the ancient entrance to the Almonda system that is situated above the weir to the tanning factory just downstream of the resurgence. This site is an archaeological dig and as such is permanently closed. Samples were also obtained from the main Almonda cave system, which is entered near the new Torres Novas caving centre. Again, the entrance is closed and locked. Relative humidity in the cave was not measured.

Sample	Size (mm)	Cut	Luminescence	$\delta^{18}O/\delta^{13}C$	U/Th TIMS
AL1	110				
AL2	125				
AL3	95				
AL4	80				
AL5	220				
AL6	292				✔
AL7	35				
AL8	45				
AL9	85				
AL10	30				
AL11	130				
AL12	25				
AL13	80				
AL14	337				
AL15	265				
AL16A-G	160				
AL17	145				
AL18	130				
AL19	150				
AL20	320				

Table 7.14. Samples from Almonda Cave.

7.1.5.3. Gruta Papagaio

Papagaio is located on the southern side of the polje known as the Polje de Mira Minde. It is a severely vandalized cave with many decorations broken or missing. Some broken speleothems were removed.

Sample	Size (mm)	Cut	Luminescence	$\delta^{18}O/\delta^{13}C$	U/Th TIMS
PAPAG1	220				
PAPAG2	145				
PAPAG3	160				
PAPAG4	80				

Table 7.16. Samples from Gruta Papagaio.

7.1.5.4. Gruta Anacreal

Anacreal is located on the southern side of the polje known as the Polje de Mira Minde. The cave has been vandalized, although an extensive archaeological dig is in progress. One speleothem was sampled from beneath the false calcite floor.

Sample	Size (mm)	Cut	Luminescence	$\delta^{18}O/\delta^{13}C$	U/Th TIMS
ANAC1	80				
ANAC3	200	✔			✔

Table 7.17. Samples from Gruta Anacreal.

7.2. Analytical Methods

7.2.1. U-series ages

7.2.1.1. Theory

The uranium-thorium (U/Th) series of radiogenic isotopes is used to date geological material up to 350,000 years old (Harmon *et al.*, 1975), although 500,000 years is possible. The length of the half-life of ^{230}Th makes effective dating using this technique difficult beyond that point

as ^{230}Th has grown into equilibrium with ^{234}U (all materials older than 750,000 years have $^{230}Th/^{234}U = 1$) (Ivanovich and Harmon, 1982).

The U series of radiogenic isotopes has two natural parent isotopes, ^{238}U and ^{235}U, which decay through further radiogenic 'daughter' products to the stable products ^{206}Pb (lead) and ^{207}Pb respectively (fig. of decay series).

i) ^{238}U has a half-life (λ) of 4,469,000 years (4.469×10^9 years), meaning that half of the parent isotope will have decayed to the daughter ^{234}U ($\lambda = 2.48 \times 10^5$ years) in that time. The next daughter product is ^{230}Th ($\lambda = 7.52 \times 10^4$ years).

ii) The half-life of ^{235}U is 7.13×10^8 years and the daughter isotope is ^{231}Pa (protoactinium).

As the natural abundance of ^{238}U to ^{235}U is 137.88 : 1, the first decay series is the easiest to use when dating carbonates, which contain low levels of natural uranium (typically <3 ppm) (Ivanovich and Harmon, 1982). The technique of U/Th dating of carbonate material is made possible because Th is highly insoluble in water, whereas U is highly soluble in oxidized water. When speleothems are deposited from carbonate solutions they incorporate U from the host limestone, but bring no Th and so have no initial ^{230}Th. In this way the radiogenic 'clock' in a speleothem is reset by dissolution and deposition of calcite. The subsequent decay of U to its daughter products (eg ^{230}Th) at fixed rates in the freshly deposited speleothem allows the age to be determined from the isotopic ratios between parent and daughter isotopes (eg, the $^{230}Th/^{234}U$ ratio).

Uranium in limestone oxidises and forms complexed ions with bicarbonate waters as $UO_2(CO_3)_2^{2-}$ and $UO_2(CO_3)_3^{4-}$. ^{230}Th and ^{231}Pa are insoluble and are adsorbed by clay and other detrital particles following

limestone weathering and are not deposited in speleothem calcite. This predilection of ^{230}Th for bonding to detrital materials creates a major problem when the technique is used to date detrital-rich ('dirty') calcite. Thus, a speleothem incorporating large amounts of detrital material may contain ^{230}Th derived from sources other than *in situ* decay from ^{234}U (non-authigenic ^{230}Th). The addition of non-authigenic Th has the effect of making the sample appear older than is really the case. However, the detrital material also contains ^{232}Th (λ = 1.39 x 10^{10} years), which behaves chemically in the same way as ^{230}Th. It has been suggested that where ($^{232}Th/^{230}Th$) > 20 the samples are likely to contain little non-authigenic ^{230}Th. The value of 20 is a purely arbitrary number with no basis in investigation, but one that is generally accepted in the literature (Baker *et al.*, 1993; Harmon, 1979), although lower ratios have been used in some studies (Goede and Harmon, 1983). Some studies have alternatively used a criterion of 1% concentration of insoluble detrital material to exclude contaminated U/Th ages (Atkinson *et al.*, 1978). There are isochron techniques available to date material contaminated with detrital ^{230}Th (Luo and Ku, 1991), but they are complicated and time consuming, requiring between 6-10 analyses of one sample for a single age. It is far preferable to ensure samples for analysis are as clean as possible before starting chemistry. Some attempts have been made to avoid detrital ^{230}Th contamination in speleothems by performing mechanical separation of calcite, silicate and organic fractions in the dry sample. However, isotopic analysis of the separated fractions reveals high levels of partitioning of ^{230}Th between the different minerals and organic material in lake sediments – a situation that probably also applies in speleothems (Carsten Israelson, pers. comm.).

7.2.1.2. Techniques

All samples were prepared in geochemical clean laboratories. The environment of the laboratory is one of controlled temperature (21°C ± 0.2°C) and positive absolute-filtered air flow. Acid reagents were prepared using two separate methods. Quartz-distilled (QD) reagents were distilled in quartz vessels. This method of preparation produces the highest blank of the two techniques and these reagents were used solely for initial stages in cleaning reaction vessels. The higher quality reagents (TD) were prepared by distillation in Teflon vessels. Blank analyses for individual acids using the two preparation methods were 1.41 pg/g ^{238}U and 0.72 pg/g ^{232}Th for QD 6M HCl and 0.54 pg/g ^{238}U and 0.35 pg/g ^{232}Th for TD 6M HCl during this study (Mabs Johnston, pers. comm. 1996). Water used in lab procedures was purified using either the TD method or by reverse osmosis (RO).

The mechanical and chemical preparation of $CaCO_3$ samples for thermal ionisation mass spectrometry (TIMS) was by the following procedures:

1) The calcite was cut from the speleothem using a chisel, saw or drill. At this stage any obviously 'dirty' sections of calcite were removed with a brush and RO H_2O. Between 0.5 and 5 grams of calcite were ground using a pestle and mortar, which was cleaned with RO 6M HCl and RO H_2O after each sample had been crushed. The sample powder was weighed into a 60 ml clean Teflon beaker using a 5-figure balance in preparation for dissolution.
2) The calcite was dissolved in teflon-distilled (TD) HNO_3 acid until no further reaction was observed. To avoid sample spillage due to vigorous reaction between calcite and acid, the solution was first wetted with TD H_2O and TD 0.2M HNO_3 was added (initially drop-wise). When addition of TD 7M HNO_3 caused no further reaction

from the calcite, the solution was examined for any remaining detrital material. If detrital particles were visible, the sample was centrifuged at 4000 rpm for 15 minutes and the supernate decanted into a clean beaker. The supernate (and appropriate U and Th spikes) were left in the balance room to equilibrate to room conditions normally overnight.

3) The dissolution and weighing procedure is one of the greatest sources of error when U/Th dating is undertaken using aliquoted solutions. Extremely low U and Th concentrations mean that small changes in volume caused by spillage or evaporation of the supernate can have disproportionately large effects on the number of ions of each element that are eventually loaded into the mass spectrometer. However, the main error lies in incomplete dissolution, as Th has a high partition coefficient between solid and liquid phases. An incompletely dissolved sample will contain fewer Th atoms than expected and therefore appear to be younger than expected. A further source of error is evaporation following aliquoting, but before adding a spike. Once the spike is added any evaporation will take place in equal volume on the natural isotope and the spike material. In an attempt to limit weighing errors the balance was checked with a standard weight before and after weighing was undertaken and the balance was zeroed between each part of the procedure.

4) To avoid loss of supernate by evaporation and consequent measurement errors, the final technique was to weigh the spike bottle to determine directly the amount of spike added to a sample. Two spike systems were used:

a) A double spike system with separate spikes for Th and U, which requires aliquoting each sample. Two sub-samples (aliquots) were made of each carbonate sample. The first aliquot was used to analyse

U concentration (^{238}U), whilst the second aliquot was used to determine ^{230}Th and ^{232}Th concentration and the natural ($^{234}U/^{238}U$) ratio. Three passes on ion-exchange resin are necessary to separate the various fractions of U and Th:

The large aliquots were loaded on 2 ml quartz columns.

i) The columns were cleaned beforehand with two washes of TD 6M HCl and TD H_2O) and resin was dropped onto a porous teflon plug through RO H_2O (to ensure uniform packing).

ii) The resin was preconditioned for the sample with TD 7M HNO_3 and the sample loaded in a few millilitres of that acid.

iii) The sample was slowly added to the resin 2 ml at a time and then 3 x 2 mls of TD 7M HCl were added to wash the sample into the column.

iv) 1.5 mls of TD 6M HCl were added to start the removal of Th from the resin. The Th fraction was collected in small teflon bombs using 3.5 mls of TD 6M HCl.

v) The U fraction was removed from the resin using TD 1M HBr. The column was initially prepared with 1.5 mls of HBr and the fraction collected in teflon bombs using 3.5 mls of TD 1M HBr. These fractions are dried down under heat lamps and the U fraction (for $^{234}U/^{238}U$) measurement) loaded on double rhenium (Re) filaments.

vi) The Th fraction requires a further pass through resin to remove elements such as calcium (Ca), strontium (Sr) and rubidium (Rb), which may interfere with efficient ionisation of the sample in the mass spectrometer.

The Th fraction was eluted through a 0.5 ml plastic column (pipette tip), cleaned in a similar way to the larger columns. A few drops (approximately 0.2 mls) of TD 7M HNO_3 were placed on the sample-

spot in the teflon bomb; the bomb was sealed and left on a heat-tray to ensure all Th salts were re-dissolved.

vii) The resin was preconditioned with TD 7M HNO3 and the sample loaded on to the resin. The sample was washed into the resin with 3 resin volumes (RV) of TD 7M HNO_3.

viii) One RV of TD 6M HCl was introduced to initiate removal of Th, followed by a further 3 RV of TD 6M HCl, which were collected in a teflon bomb. The solution was dried down and loaded on double Re filaments.

ix) The small aliquots for U contents determination were loaded on 0.5 ml columns, using the same resin and cleaning techniques as the larger columns. The aliquots were evaporated to dryness under heat lamps and re-dissolved in a small amount of TD 7M HNO_3 (< 0.5 ml). The columns were preconditioned with two resin volumes of TD 7M HNO_3 and the sample loaded on to the column.

x) Three and a half RVs of TD 6M HCl were eluted, followed by 0.5 RV of TD 1M HBr. The U was collected in 3 RV of TD 1M HBr and dried under heat lamps. The U was loaded on single Re filaments for the VG Isomass mass-spectrometer or on double Re filaments for the MAT262 mass-spectrometer

b) A single spike system using a single spike of ^{236}U, where the sample is spiked without aliquoting, reducing possible weighing errors and eliminating inconsistent treatment of aliquots, which may occur with the double spike system. 58% of the samples analysed for this work were analysed using the double spike system. The separation on ion-exchange resin when using the single spike system is simplified to just one pass, yielding two fractions (U and Th). The ^{236}U spike is used to measure both $^{234}U/^{236}U$ and $^{235}U/^{236}U$ ratios in the mass-spectrometer and the original amount of ^{238}U present in the sample

can be calculated by assuming ($^{238}U/^{235}U$) = 137.88 – the natural ratio of uranium (with a small correction for ^{238}U present in the double spike).

Chemical separation of elements using the single spike system required only steps i) to v) in the description above. No clean-up of the Th fraction was required and there is no requirement for a second aliquot.

7.2.1.3. Loading on filaments

When Th and U had been separated on ion exchange columns they were loaded on rhenium (Re) filaments and placed in a thermal-ionisation mass-spectrometer (TIMS). In the mass-spectrometer, samples are evaporated by a low voltage, high amplitude current and simultaneously ionised by a high voltage, low amplitude current in the filament, whilst in a vacuum of at least 10^{-7} torr. The 10 kV high voltage between the source and the collector ends of the mass-spectrometer repels ions of U or Th from the filament source towards the collectors. These are directed by another filament (double filament system) or by the angle of the filament (single filament system) through a slit opposite the source into the flight tube magnetic field of the mass-spectrometer. At the far end of the flight tube the ions are counted with a retarding potential quadrupole or secondary electron multiplier amplifier used for low intensity ion beams.

Two filament loading schemes were used during this work (figure 7.1).

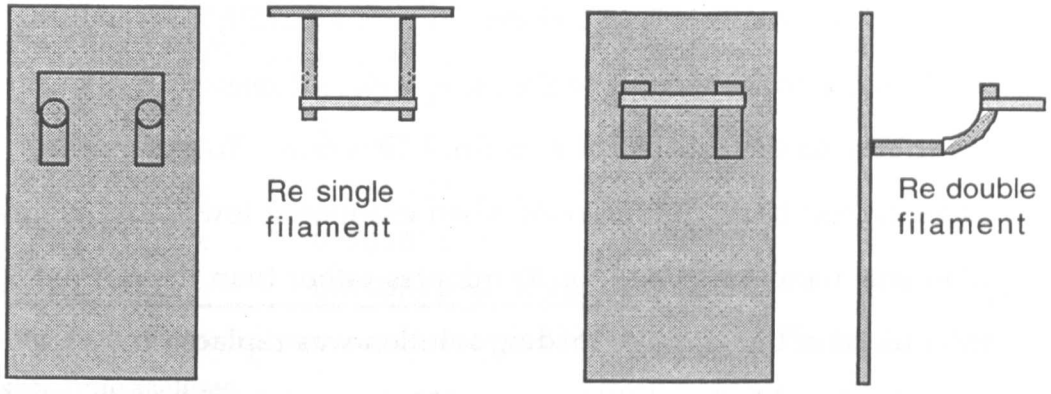

Figure 7.1. The two types of filaments used for loading samples in the mass spectrometer. The double filament is paired with another of identical configuration.

7.2.1.3.1. Double Re filaments

Double Re filaments are loaded with the sample on one graphite-coated filament (the evaporation filament). The second filament (ionisation filament) is used to ionize the ions emitted from the heated evaporation filament. This directs the stream of ions through the slit plate of the source chamber and into the flight tube of the mass spectrometer (figure y). The ionisation potential is such that only larger ion weights are directed into the flight tube – possible contaminants such as organic and graphite compounds do not ionize efficiently in this physical configuration. Those ions that are directed into the flight tube are separated by the magnet and quadrupole into heavier and lighter ions.

7.2.1.3.2. Single Re filaments

In the case of single Re filaments the sample is loaded on the single graphite-coated evaporation filament. This is placed in the source chamber of the mass spectrometer with the flat part of the filament directly facing the slit plate and flight tube. The advantage of this method over the double filament technique is that fewer ions are lost due to inefficient ionisation but the disadvantage is that hydrocarbon material may contribute to background mass spectra (Cohen and

O'Nions, 1991). This is of concern when measuring low-levels of ^{230}Th, since hydrocarbons of the same apparent mass as ^{230}Th may contribute to the number of measured Th atoms. To reduce hydrocarbon background levels when examining low ^{230}Th samples, filaments were outgassed for 30 minutes rather than the normal 5 minutes, and the graphite loading solution was replaced by 0.1 M phosphoric acid. In addition, mass 231 was monitored during each run to check for the presence of hydrocarbons.

7.2.1.4. Blanks

Blank measurements for acids used during sample preparation are given below (table 7.1).

Reagent	^{238}U pg/g	^{232}Th pg/g
RO H_2O	0.37	0.36
TD H_2O	0.26	0.43
QD 6M HCl	1.41	0.72
TD 6M HCl	0.54	0.35
QD 15M HNO_3	0.67	0.80
TD 15M HNO_3	0.71	0.45
TD 1M HBr	1.04	0.63

Table 7.18. Measured blank contributions for ^{238}U and ^{232}Th for acids used during this study. Certain measurements obtained over several analyses and are averaged (Mabs Johnston pers. comm. 1996).

Total procedure blanks were analysed in the same batch of chemistry as samples with similar volumes of acid added to the empty beaker. Smaller amounts of spike material were added to the empty beaker than is normal with samples to ensure the measured isotopic ratio did not exceed low. Completed blank analyses are given in the table below (table 7.19).

Sample	Name	^{238}U µg/g	^{230}Th ppb
5 6	Blank	0.00006927	1.3572E-05
7 6	Blank	0.00000202	0
8 1	Blank	0.00003147	3.1154E-05
9 0	Blank	0.00003827	0
9 0	Blank	0.06956310	5.2396E-05

Table 7.19. Blank analyses and the measured ^{238}U blank and ^{230}Th blank for total procedure analyses.

A typical blank for ^{238}U yields 38 pg. Blanks for ^{230}Th were measured directly and yield an average of 39 fg.

7.2.1.5. Standards

Two types of standard analysis were performed simultaneously with analysis of samples:

a) A standard calcite sample was analysed to check for repeatability between individual sets of samples. UEA calcite is a complete speleothem collected from GB cavern in the Mendip Hills, England, that has been crushed and homogenized. The mean age for five analyses of the UEA standard during this work (using TIMS techniques) was 57,598 ± 333 years which compares with a mean of 59,418 ± 3,975 years for the laboratory as a whole. However, removing an erroneously young age from the five analyses alters the mean age to 58,752 ± 244 years. UEA has also been analysed by the University of East Anglia (using alpha-spectrometry) where the mean age is 59,460 ± 2,320 years. Although the mean age from both laboratories is similar, the standard deviation of the age is better for the alpha-spectrometry analyses. This probably reflects the homogeneity of large sample sizes (up to 50 grams) used for alpha-spectrometry, compared to the hetrogeneity of smaller samples (approximately 1 gram) used in TIMS

analyses. This heterogenity of small samples is also reflected in the ^{238}U and ^{230}Th concentrations measured in each laboratory. The Open University finds 0.327 ± 0.028 ppm ^{238}U and 3.639 ± 0.798 pg/g ^{230}Th in standard UEA, compared to 0.345 ± 0.011 ppm ^{238}U and 4.114 ± 0.131 pg/g ^{230}Th at the University of East Anglia.

b) Standard solutions of known isotopic composition were analysed to check for repeatability between individual runs on the mass spectrometers. These standards were:

i) U112A, a standard U solution with a measured $^{234}U/^{238}U$ ratio of 5.277 ±0.002 E^{-5}. During this study, the mean $^{234}U/^{238}U$ ratio was 5.28E^{-5} with a mean error of 8.25E^{-8} and the mean $^{235}U/^{238}U$ ratio was 0.007271 with a mean error of 8.8E^{-6} (figures 7.2 and 7.3).

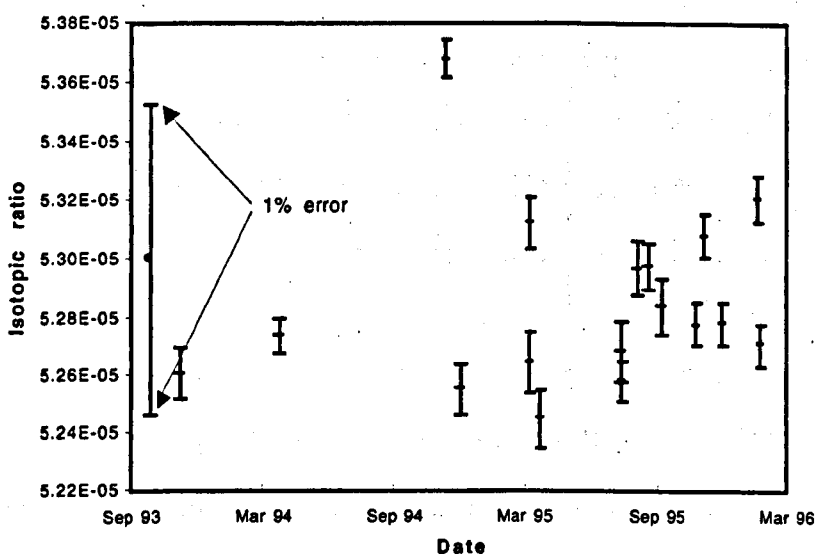

Figure 7.2. The $^{234}U/^{238}U$ ratios of standard solution U112A during the course of this study. Error bars are 1σ errors.

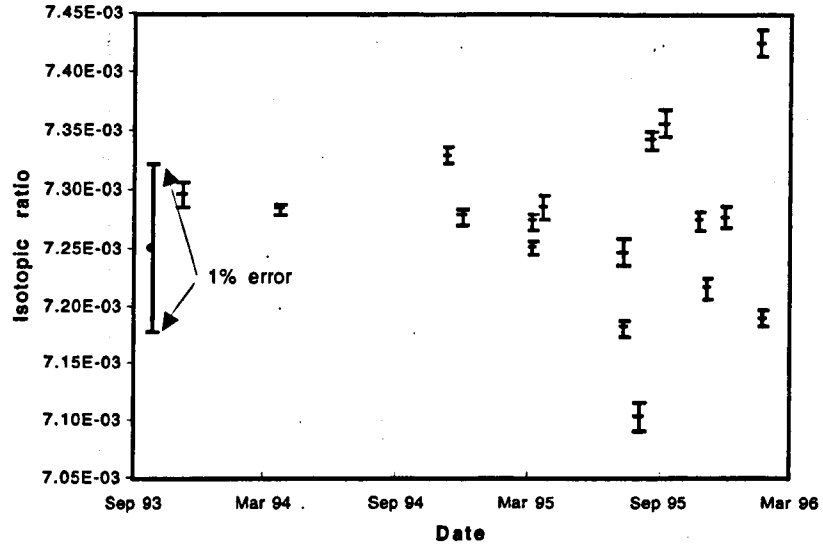

Figure 7.3. The $^{235}U/^{238}U$ ratios of standard solution U112A during the course of this study. Error bars are 1σ errors.

ii) Th mix, a standard Th solution with a measured $^{230}Th/^{229}Th$ ratio of 1.030875 ± 0.00151 and a $^{232}Th/^{229}Th$ ratio of 18.38827 ± 0.034045 during this study.

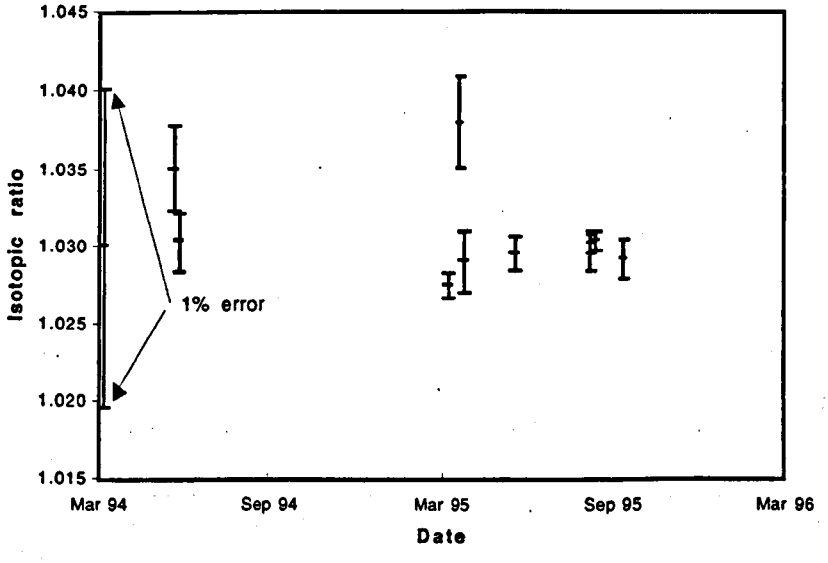

Figure 7.4. The $^{230}Th/^{229}Th$ ratios of standard solution Th mix during the course of this study. Error bars are 1σ errors.

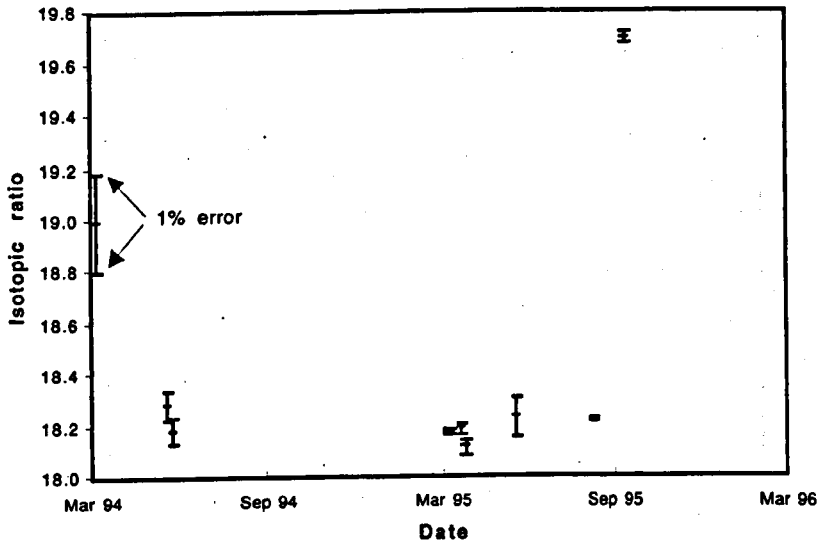

Figure 7.5. The $^{232}Th/^{229}Th$ ratios of standard solution Th mix during the course of this study. Error bars are 1σ errors.

iii) Th mix dil., a standard Th solution (a dilution of Th mix), with a measured $^{230}Th/^{229}Th$ ratio of 1.029345 ± 0.002281 and a $^{232}Th/^{229}Th$ ratio of 19.46756 ± 0.045604 during this study.

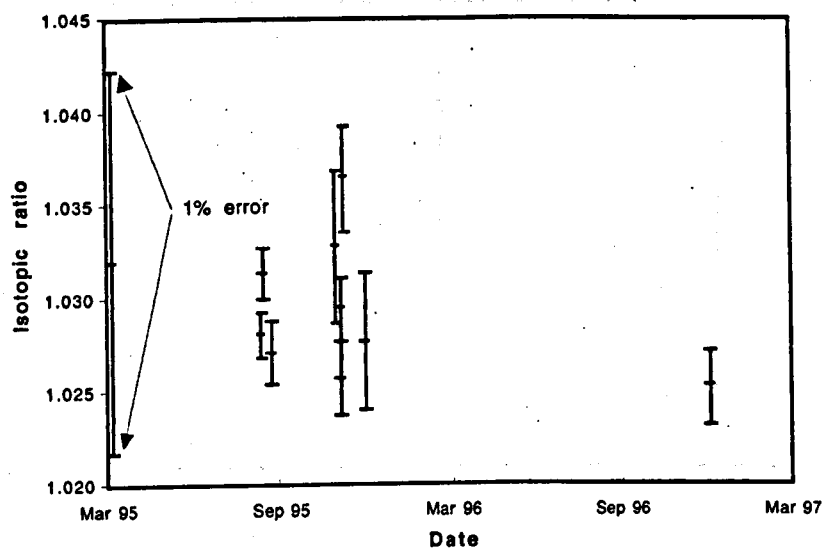

Figure 7.6. The $^{230}Th/^{229}Th$ ratios of standard solution Th mix dil during the course of this study. Error bars are 1σ errors.

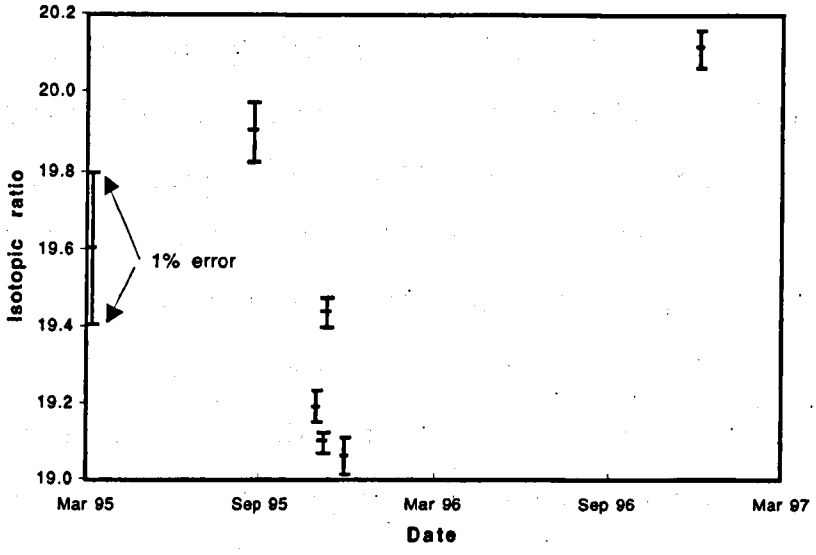

Figure 7.7. The $^{232}Th/^{229}Th$ ratios of standard solution Th mix dil during the course of this study. Error bars are 1σ errors.

7.2.1.5.1. Results

During the course of this work a total of 108 samples (including calcite standards) were prepared for analysis. For a variety of reasons some samples were not analysed on the mass-spectrometer. A total of 45 samples were run on the mass-spectrometer, yielding 30 'good' ages. A complete set of the data analysed during this project is given in Excel 5 format on disk 1 which accompanies this thesis.

7.2.2. Low-Th samples and mineral extraction techniques

Some speleothems have extremely low levels of ^{230}Th in the speleothem matrix, either because there is little ^{238}U in the host rock, or because the speleothem is recent in age. These samples cannot be dealt with using the techniques described above, and a further stage has to be introduced. The main problem is that large sample sizes required to obtain sufficient ^{230}Th atoms for a measureable beam on the mass spectrometer can only be dissolved in large volumes of 7M HNO_3. This volume of acid creates two problems during ion exchange:

i) The high volumes of acid (>100 ml) required to dissolve the sample may have a large blank associated with them (particularly important is the ^{230}Th blank), which may be larger than the total ^{230}Th in some samples examined in this thesis. The estimated procedure blank for 100 ml of TD 7M HNO_3 (made by mixing 15M HNO_3 with H_2O in equal quantities) is based on the ^{232}Th reagent blank. The measured blank contributions for these reagents obtained for table 7.1 are not multiplied by the total volume of acid used, since the majority of each ^{232}Th blank is from the filament and graphite used. 2 pg/g ^{232}Th is a typical filament blank, which suggets the total blank for each acid is negligible, since total procedure blanks are typically measured at 0.7 pg/g ^{232}Th. Assuming a worst-case scenario (the filament blank is larger than the acid blank) 2 pg/g ^{232}Th is equivalent to a total concentration of 1.8 E^{-17}/g ^{230}Th, which is 18 fg/g ^{230}Th in 100 ml of 7M HNO_3. This compares with an typical concentration of 590 fg ^{230}Th in the low-^{230}Th samples which require use of the Fe extraction method.

ii) When a smaller volume of acid is used, the adsorption of Th and U ions onto anionic exchange resin may be impaired by the presence of concentrated, high viscosity Ca^{2+} and Mg^{2+} solutions, despite the fact that these cationic solutions do not bind to the anionic resin (Cohen pers. comm.). Although this 'column overload' problem may be overcome by using a larger volume of anionic exchange resin in multiple columns, large volumes of resin also contribute to the ^{230}Th blank making the total procedure blank unacceptable. The high demand on lab equipment and consumables required to process large volumes of calcite also means using large volumes of acid is not viable. For example, large volumes of teflon-distilled (TD) reagents are required for dissolution and cleaning and extra-large teflon beakers needed to accommodate the sample during the analysis.

An alternative technique for obtaining Th and U sufficient for a good beam size on the mass spectrometer is to remove the Th and U ions from the calcium solution with a complexing agent. This was achieved by complexing Th and U with iron hydroxides. A $FeCl_2$ solution was added to the solution and $FeCl_2$ precipitate was formed by the addition of ammonia ($NH_4(OH)$) (Edwards *et al.*, 1986).

The method for this complexing was:

i) The calcite sample was dissolved *in toto* in 7M HNO_3, and placed in a large teflon beaker. Smaller volumes of acid (<50 ml) are required to dissolve the smaller sample sizes used in this technique, so reducing the blank contribution from the acid.

ii) A small amount (approx. 250µl) of iron chloride ($FeCl_2$) solution was initially introduced drop-wise into the 7M HNO_3 solution.

iii) The top of the beaker was covered with lab film and slow ammonia flow bubbled into the top of the solution to increase the pH of the solution. A magnetic stirrer system was used to agitate the solution during the ammonia flow. Further amounts of $FeCl_2$ were added during the ammonia flow. The addition of $FeCl_2$ is not necessary if the sample already contains some iron, although detrital iron may bring non-authigenic ^{230}Th, which alters the measured age.

iv) When ferric (brown) deposits were observed on the base and sides of the beaker the solution was removed from the ammonia flow and centrifuged at 4000 rpm for ten minutes and the supernate discarded.

v) The ferric deposit was then treated as a normal calcium sample would be (ie from point i) in the spike systems above).

7.2.2.1. Procedure blanks for the Fe extraction method

A total procedure blank for the $FeCl_2$ used to co-precipitate uranium and thorium in solution was examined to ensure a minimum amount of ^{230}Th and ^{238}U was contributed to samples. The blanks obtained were 0.26 fg/g ^{232}Th and 11.49 pg/g ^{238}U. Since the weight of $FeCl_2$ used to precipitate samples was usually less than 1g, the expected maximum contribution to measured ^{238}U and ^{230}Th levels in each sample would be 11.49 pg/g ^{238}U and 0.00024 fg/g ^{230}Th (assuming ($^{230}Th/^{232}Th$) in the $FeCl_2$ is 1.7). This compares with minimum concentrations of 0.02 μg/g ^{238}U and 0.03 fg/g ^{230}Th in speleothem samples (i.e. the blank contribution of $FeCl_2$ to the total procedure ^{230}Th is less than 1% total ^{230}Th). The technique of co-precipitation is used only with very low ^{238}U samples (i.e. also low ^{230}Th). These figures suggest that the effect on U/Th ages of blank-contributed ^{238}U is negligible and blank contributed ^{230}Th is likely to be only 1% of total ^{230}Th concentrations.

7.3. $\delta^{18}O$ and $\delta^{13}C$ stable isotopes

7.3.1. Theory

Stable isotopes of oxygen and carbon in speleothems are fractionated during phase shifts in limestone dissolution and deposition. When a phase shift takes place the heavier isotopes preferentially remain in the denser phase. Within a cave system the amount of fractionation may be determined by the temperature of the cave (equilibrium fractionation) or by a combination of the cave temperature and evaporation (kinetic fractionation). A test for the type of fractionation which has taken place is to determine whether trends in $\delta^{18}O$ and $\delta^{13}C$ are correlated along a single growth layer in a speleothem (Ford and Williams, 1989).

7.3.1.1. Techniques

100μg samples of calcite were obtained with a dental drill from cut faces of the speleothems. The samples were loaded in the autocarb preparation line of a VG Isomass mass spectrometer and dropped in an acid bath of 100% phosphoric acid. If necessary, the CO_2 produced was reduced in size with automatic bellows to ensure a sufficient quantity of gas molecules was delivered to the mass spectrometer.

7.3.1.2. Standards

Five different powder standards were analysed during this work (see table 7.20).

Standard	$\delta^{18}O$	1σ error	$\delta^{13}C$	1σ error	no. analyses
NBS-19	-1.783	0.035	1.886	0.035	17
RHBNC	-9.529	0.030	3.118	0.024	70
Coral	-3.285	0.160	0.045	0.060	29
SPA-1	-11.079	0.010	-7.717	0.008	3
PSU-1	-22.096	0.014	-3.892	0.014	2

Table 7.20. Powder calcite standards used during this work.

One standard was analysed for every 10 samples. Speleothem stable isotope data was corrected to long-term means for the laboratory for each run based on the measured value of the standards.

7.3.1.3. Results

A total number of 590 stable isotope analyses were completed during this project. The results from analyses of the speleothems examined are on disk 1 accompanying this thesis in Excel 5 format.

7.4. Luminescence intensity

7.4.1. Theory

A molecule in a high energy or excited state may relax to a lower energy state by emitting a photon (luminescing) (Baker *et al.*, 1996). Humic and fulvic acids (organic acids) and heavy metals luminesce in speleothem calcite when excited by ultra-violet (UV) light. Typically, two kinds of luminescence are measured:

1) Spectral characteristics of luminescence of a variety of organic molecules within the calcite. A wide variety of organic molecules exhibit slightly variant spectra of emission and excitation (Senesi *et al.*, 1991).
2) Overall luminescent intensity (LI) is influenced by several aspects of luminescent molecules in calcite. (Shopov *et al.*, 1994) proposed a division of these influences into six factors (in order of importance):

i) The concentration of humic and fulvic acids in the speleothem, affected by changes in the plant community above the cave and rate of organic decay.

ii) The discharge of water onto the speleothem from the limestone aquifer, with greater discharge diluting speleothem LI. (In fact it has been found that the opposite is the case: Increased discharge increases speleothem LI (Baker *et al.*, 1996)).

iii) Changes in speleothem growth rate, with a faster growing speleothem having lower LI if the contribution of luminescent material remains constant.

iv) The type of humic or fulvic acid being contributed to the speleothem at a given point in time, given the wide (and overlapping) range of LI values for each organic molecule. Fulvic acids are generally up to 20x more luminescent than humic acids (Baker *et al.*, 1996).

v) Luminescence decreases with depth in the aquifer as organic acids are filtered from the groundwater flow by varying pore sizes in the parent limestone. This is only a significant factor when comparisons are made between samples.

vi) The formation of complexed heavy metals with organic acids. This effect has been shown to be unimportant (Baker *et al.*, 1996) as calcium and magnesium ions dominate the complexing of organic acids in karst systems.

7.4.1.1. Techniques

The speleothem calcite was cut with a circular saw and polished to give a smooth surface and reduce backscatter from the laser. A UV laser (HeCd, 325 nm) was used to excite the luminescent molecules. The luminescence was collected with a focusing lens, selected at 480 nm with a spectrometer and detected with a photomultiplier. The spot size of the laser was approximately 250 µm. The speleothem was moved at a constant rate in front of the lens such that one measurement was made every 0.1 mm. Two parallel scans were made along the axis of each speleothem at a small distance apart to ensure reproducibility and the results averaged. The results were calibrated to a standard calcite taken from the speleothem SU-80-11 (Baker *et al.*, 1996).

7.4.1.2. Results

The LI data is available on disk 1 (MC2 data) and disk 2 (CC4 data) which accompanies this thesis in Excel 5 format.

7.5. Spreadsheets and macros

Several spreadsheet systems were developed during the course of this work. The computer program used to develop the spreadsheets was Microsoft Excel for the Macintosh, versions 4 and 5.

7.5.1. Linear interpolation

7.5.1.1. Description

The purpose of this macro is to interpolate one column of data to values based on another column of data. The example used in this work is placing palaeoclimatological data against time. Commonly, geological information is measured against distance from one end of a section, whether it is an ice core, a speleothem or a pollen core. In order to plot that section against time a limited number of absolute ages can be calculated and the intermediate points in the section interpolated to those ages. With large data sets the process of interpolation can be exceedingly time-consuming. A Microsoft Excel Add-In was written to simplify the task. An Excel Add-In is a file written in macro language (in this case Excel 4 macro language) and saved to disk as a read-only file. The Add-In may be activated using the Add-In manager in Microsoft Excel and will then be available at any time.

7.5.1.2. Theory

Where a continuous distribution has an associated continuous distribution with a limited number of known values the unknown values in the second distribution may be interpolated according to the formula:

$$\text{Unknown value} = \text{Relative position between values} \times \frac{\text{Interval between values}}{\text{Distance between values}}$$

Equation 7.1. Formula for interpolation of values.

This basic formula was adapated to a macro routine which checks on position within a table of known distance and unknown age data and interpolates between the known ages based on distance.

7.5.1.3. Results

Typically 2000 data points measured against distance can be interpolated to 10 ages in 2 minutes on a Macintosh IIci using Excel 5.0a. The Add-In (on disk 2 as "Interpol.xla") does require that the user place the cursor in the correct place in the spreadsheet, but will correctly check the start and end of each column of data.

7.5.2. U/Th TIMS age calculation spreadsheet

This spreadsheet allows the user to enter information on the sample, spike and isotopic ratio analysed for a carbonate or phosphate U/Th TIMS run and places it on a spreadsheet (on disk 1 as "U-Th Workbook"). The user also has the option to calculate an age for those data when the data are complete.

7.5.2.1. Theory

The calculation of a U/Th TIMS age requires information on the concentration of ^{238}U, ^{234}U and ^{230}Th in the sample, the decay constants of ^{238}U, ^{234}U and ^{230}Th and the activity ratios of ^{238}U, ^{234}U and ^{230}Th.

The information required to calculate an age is derived by weighing samples and spikes and analysing isotopic ratios of those samples and spikes on a mass-spectrometer. Once the activity ratios are known the age may be calculated by iteration in a spreadsheet. The spreadsheet is a

series of cells with data on sample size, spike weights and isotopic ratios. Further cells include formulae to calculate activity ratios and isotopic ratios of the various isotopes of interest.

7.5.3. Relative humidity calculation

7.5.3.1. Theory

Relative humidity is a measure of the saturation vapour pressure (e_s)in the air and is determined by comparing e_s at dew point with e_s at air temperature. In practice relative humidity is measured by determining the temperature of the air mass and the temperature of evaporation of the air mass. This is achieved using a wet bulb – dry bulb thermometer which is swung through the air. The relationship between the wet bulb and dry bulb measurements and saturation vapour pressure is not a direct one and table are required to determine the relative humidity of the air.

7.5.3.2. Spreadsheet for relative humidity calculation

A Microsoft Excel spreadsheet was written which determines the relative humidity of an air mass when the dry bulb and wet bulb temperatures are entered from a table of e_s values (on disk 2 as "Relative humidity workbook").

7.6. References

Atkinson, T. C., Smart, P. L., Harmon, R. S., and Waltham, A. C. (1978). Palaeoclimatic and geomorphic implications of $^{230}Th/^{234}U$ dates on speleothems from Britain. *Nature* **272**, 24-28.

Baker, A., Barnes, W. L., and Smart, P. L. (1996). Speleothem luminescence intensity and spectral characteristics: Signal calibration and a record of palaeovegetation change. *Chemical Geology* **2026**.

Baker, A., Smart, P. L., and Ford, D. C. (1993). Northwest European palaeoclimate as indicated by growth frequency variations of secondary

calcite deposits. *Palaeogeography, Palaeoclimatology, Palaeoecology* **100,** 291-301.

Cohen, A. S., and O'Nions, R. K. (1991). Precise determination of femtogram quantities of radium by thermal ionization mass spectrometry. *Analytical Chemistry* **63,** 2705-2708.

Coleman, J. C. (1950). Caves in the Tralee District. *Journals of the Cork Historical and Archaeological Society* **55,** 25-30.

Edwards, R. L., Chen, J. H., and Wasserburg, G. J. (1986). ^{238}U-^{234}U-^{230}Th-^{232}Th systematics and the precise measurement of time over the past 500,000 years. *Earth and Planetary Science Letters* **81,** 175-192.

Ford, D. C., and Williams, P. W. (1989). "Karst Geomorphology and Hydrology." Chapman & Hall, London.

Goede, A., and Harmon, R. S. (1983). Radiometric dating of Tasmanian speleothems - evidence of cave evolution and climatic change. *Journal of the Geological Society of Australia* **30,** 89-100.

Harmon, R. S. (1979). U-series dating of speleothems and a glacial chronology for western North America. *National Speleological Society Bulletin* **41,** 102-104.

Harmon, R. S., Thompson, P., Schwarcz, H. P., and Ford, D. C. (1975). Uranium-series dating of speleothems. *National Speleological Society Bulletin* **37,** 21-33.

Ivanovich, M., and Harmon, R. S. (1982). "Uranium Series Disequilibrium." Oxford University Press, Oxford.

Luo, S., and Ku, T.-L. (1991). U-series isochron dating: A generalized method employing total-sample dissolution. *Geochimica et Cosmochimica Acta* **55,** 555-564.

Senesi, N., Miano, T. M., Provenzano, M. R., and Brunnett, G. (1991). Characterization, differentiation, and classification of humic substances by fluorescence spectroscopy. *Soil Science* **152,** 259-271.

Shopov, Y. Y., Ford, D. C., and Schwarcz, H. P. (1994). Luminescent microbanding in speleothems: High-resolution chronology and paleoclimate. *Geology* **22,** 407-410.

Thomas, C. (1985). "Grottes et algares du Portugal." Lisboa, Eurograf.